INFORMATION TO USERS

This manuscript has been reproduced from the microfilm master. UMI films the text directly from the original or copy submitted. Thus, some thesis and dissertation copies are in typewriter face, while others may be from any type of computer printer.

The quality of this reproduction is dependent upon the quality of the copy submitted. Broken or indistinct print, colored or poor quality illustrations and photographs, print bleedthrough, substandard margins, and improper alignment can adversely affect reproduction.

In the unlikely event that the author did not send UMI a complete manuscript and there are missing pages, these will be noted. Also, if unauthorized copyright material had to be removed, a note will indicate the deletion.

Oversize materials (e.g., maps, drawings, charts) are reproduced by sectioning the original, beginning at the upper left-hand corner and continuing from left to right in equal sections with small overlaps.

Photographs included in the original manuscript have been reproduced xerographically in this copy. Higher quality 6" x 9" black and white photographic prints are available for any photographs or illustrations appearing in this copy for an additional charge. Contact UMI directly to order.

ProQuest Information and Learning
300 North Zeeb Road, Ann Arbor, MI 48106-1346 USA
800-521-0600

TWO- PHASE FLOW-INDUCED VIBRATIONS IN A HEATED TUBE BUNDLE

By

ALEJANDRO GIDI, P.Eng, M.Eng.

A Thesis
Submitted to the School of Graduate Studies
in Partial Fulfilment of the Requirements
for the Degree of
Doctor of Philosophy

McMaster University
©Copyright by Alejandro Gidi, July 1999

TWO- PHASE FLOW-INDUCED VIBRATIONS

IN A HEATED TUBE BUNDLE

Doctor of Philosophy 1999
(Mechanical Engineering)

McMaster University
Hamilton, Ontario

Title: Two-Phase Flow-Induced Vibrations in a Heated Tube Bundle

Author: Alejandro Gidi, P.Eng.
Master of Engineering (Mechanical), McMaster University.
Diploma in Mechanical Engineering, University of Chile.

Supervisors: Dr. David .S. Weaver
Dr. Ross L. Judd

Number of Pages: xiii, 255

Abstract

The U-bend region of nuclear steam generators tube bundles have suffered from two-phase cross flow induced vibrations. Tubes in this region have experienced high amplitude vibrations leading to catastrophic failures. Turbulent buffeting and fluidelastic instability have been identified as the main causes. Previous investigations have focused on flow regime and two-phase flow damping ratio. However, tube bundles in steam generators have vapour generated on the surface of the tubes, which might affect the flow regime, void fraction distribution, turbulence levels and tube-flow interaction, all of which have the potential to change the tube vibration response :

A cantilevered tube bundle made of electric cartridge heaters was built and tested in a Freon-11 flow loop. Tubes were arranged in a parallel triangular configuration with pitch to diameter ratio of 1.48. The bundle was exposed to two-phase cross flows consisting of different combinations of void from two sources, void generated upstream of the bundle and void generated at the surface of the tubes. Tube tip vibration response was measured optically and void fraction was measured by a gamma densitometry technique.

It was found that the ratio of tube vibration amplitude in the transverse direction was reduced by a factor of 8 for void fraction generated at the surface of the tubes only, when compared to the response observed under the upstream only void generation case. The main explanation for this effect is a reduction in the correlation length of the turbulent buffeting forcing function.Theoretical calculations of the tube vibration response due to turbulent buffeting under the same experimental conditions predicted a similar reduction in tube amplitude.

The void fraction for the fluidelastic instability threshold in the presence of tube bundle void fraction generation was higher than that for the upstream void fraction generation case. The first explanation of this difference is the level of turbulent buffeting forces to which the tube bundle is exposed. Increased values of turbulence will lower the void fraction for instability. The second explanation is related to the flow regime. In this study, it was clear that flow regime for bundle void generation was at all times bubbly and homogeneous, while the upstream void fraction generation cases showed a clear tendency to churn flow. A change in flow regime from bubbly to churn flow will produce the same effect as an increase in turbulence buffeting levels, and hence it seems difficult with the present knowledge to distinguish between the two causes. In as much as turbulence levels are related to flow regime, it is essential to have a clear knowledge of the flow regime in steam generators in order to predict the fluidelastic instability threshold of the tubes.

Acknowledgements

The author would like to gratefully thank the following people for their contribution to this investigation:

Ron Lodewyks, Joe Verhaeghe, Dave Schick, Gino Innocente (retired) for their technical help and advice.

Supervisors Dr. David Weaver and Dr. Ross Judd, for their constant guidance, continuous support, interest and endless encouragement of this investigation, without which, this work would not had been possible.

Paul Feenstra for his valuable help in the operation of the test loop and useful advice in the design of the experiments.

Anthony Robinson for the development of the optical vibrometer and Mike Bardeleben for his help in improving it.

The FIV group, for their positive comments during the group meetings, Vaidas Jakubauskas, Harland Mackenzie, Li Ming and Michael Morgenroth.

My wife Carmen for her positive and very long support. My sons, Pablo, Fernando, Claudio and Camilo, for their endless patience. I hope to share with them any rewards that may come from this work.

Table of Contents

Appendices

List of Figures

List of Tables

Nomenclature

V_p	-Pitch velocity	{m/s}
Φ	-Dimensionless power spectral density	
P/D	-Pitch over diameter ratio	
G_p	-Pitch mass flux	{kg/m^{2}s)
$\phi(f)$	-Spectral density of fluctuating force per unit length	{N^{2}s/m^2 }
ρ_w	-Water density	{kg/m^3}
D	-Tube diameter	{m}
f_R	-Reduced frequency (f D/Vp)	
f_a	-Tube natural frequency in air	{Hz}
U_c	-Critical pitch velocity for instability	{m/s}
f	-Tube natural vibration frequency	{Hz}
ρ	-Fluid density, subscript G for gas, L for liquid, H for mixture	{kg/m^3}
ζ	-Tube structural damping ratio	
m_T	-Total mass per tube unit length	
m_t	-Tube mass per tube unit length	
m_h	-Hydrodynamic mass per tube unit length	
C	-Constant in Connor's equation	
b	-Power exponent in Connor's equation	
Vr	-Reduced velocity V/fd	
$m/\rho D^2$	-Mass ratio	
$m\delta/\rho D^2$	-Mass damping parameter (MDP)	
δ	-Logarithmic decrement of damping ($2\pi\zeta$)	
ϕ_H	-Homogeneous equilibrium model void fraction	
G	-Mass Flux	{kg/m^{2}s}
A	-Cross section of the conduit	{m^2}
Q_L	-Liquid volumetric flow rate	{L/s}
Q_G	-Gas volumetric flow rate	{L/s}
V_U	-Upstream (Mean) flow velocity	{m/s}
x	-Quality	
u_G	-Gas velocity	{m/s}
u_L	-Liquid velocity	{m/s}
U_{GS}	-Superficial gas velocity parameter ($u_G (\rho_G / \rho_L)^{1/}$)	{m/s}
U_{LS}	- Liquid Superficial Velocity Parameter ($u_L (\mu_L \cdot \rho_L)^{1/2}$)	{(s^2/ m kg)$^{1/3}$}
μ_L	- Fluid dynamic viscosity	{kg/ms}
σ	- Liquid-Gas surface tension	{N/m}
Bo	-Boiling number (π q"/Gp λ)/(P/D-1)	
q"	-Heat flux at the tube surface	{kW/m^2 }
λ	-Heat of vaporization	{kJ/kg}

I	-Beam intensity	$\{W/m^2\}$
I_0	-Beam intensity at source	$\{W/m^2\}$
η	-Beam absortion constant	$\{m^2/kg\}$
x	-Distance penetrated by the beam	$\{m\}$
α	-Void fraction measured by gammadensitometry	
$\epsilon(\alpha)$	-Void fraction relative uncertainty.	
σ_{Ii}	-Standard deviation of gamma counts or voltage (Ii).	

CHAPTER 1

INTRODUCTION

1.1 General Description of Flow-Induced Vibrations

A demand for higher efficiency in both energy consumption and use of materials has forced engineering designers to build lighter mechanical structures and also to increase mass flow rates circulating within or around these structures. This is the case for aircraft wings, turbine shells, tube and shell heat exchangers, power transmission lines, centrifugal pumps, hydraulic gates and valves, metal expansion joints, nuclear fuel bundles, and nuclear steam generators among others. One of the consequences of this design approach has been the increase of fluid forces with respect to structural rigidity making these structures more prone to flow-induced vibrations.

Flow-induced vibrations have been found to be difficult to analyse in nature, due to the complex mechanisms of fluid structure interaction, in which fluid forces become affected by structural motion and vice versa. A complete and unified theory for predicting the behaviour of every case is not available. Modelling and experimentation have been the main methods of gaining knowledge and understanding in each problem.

The CANDU type of nuclear steam generators (NSG) have the primary objective of converting the thermal energy contained in the heavy water circulating through the nuclear reactor into steam. The steam at high pressure and temperature is directed to the turbine that drives the electric power generator. Figure 1.1 shows a schematic of the thermohydraulics system of a CANDU power plant unit. The heavy water coming from the calandria flows through the tube side of the steam generator, while feed water coming from the condenser flows through the generator shell side and gradually converts into steam as it flows upwards. The steam flow reaches the U-bend region. Then it is directed to the cyclones to remove the remaining water present in the flow before heading to the turbine.

To transfer the maximum amount of power, steam generators are designed to work at high mass flow rates flowing between tubes that are packed closely in the tube bundle to increase the heat transfer rate. The tube bundles feature long spans between the tube supports to minimize the pressure drop through the heat exchanger. All these requirements plus the presence of two-phase flow make the tubes in the NSGs very susceptible to flow-induced vibrations. This problem has proven to be a challenging case that has eluded simple solutions.

Nuclear steam generators suffer from single-phase cross flow-induced vibrations at the entrance of the heat exchanger tube bundle base, from single phase axial flow

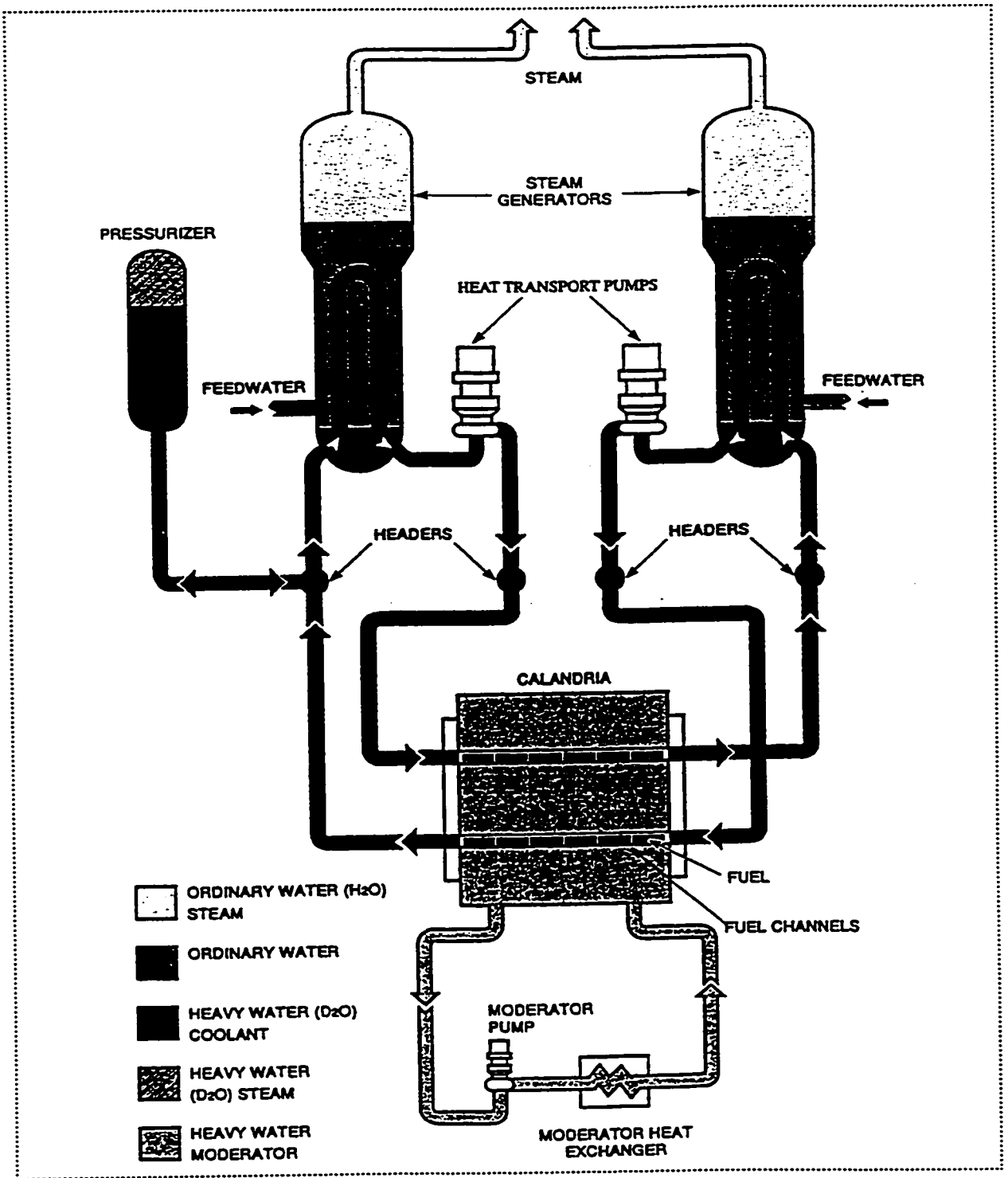

Figure 1.1 CANDU nuclear steam supply system.AECL Candu 6 technical outline, September 1995.

vibrations in the first (cold side) region of the vertical section of the tube bundle and from two-phase axial flow vibrations downstream (above) of this section. Most importantly, the tube bundles are susceptible to two-phase cross flow vibrations at the U-bend region of the bundle.

The section of the tubes comprising the U-bend region at the top of the tube bundle is also affected by nucleate boiling at its surface. It has been postulated (Weaver, 1992) that the presence of boiling at the surface of the tube could change the dynamic response of the tube vibration by changing the flow field around the tubes, the void fraction distribution and the bubble size or bubble size distribution, which could ultimately change the local flow regime conditions and the coupling phenomenon between the fluid forces and the tube motion.

Pettigrew et al (1989) argued that the tube conditions for instability are highly dependent on void fraction values and flow regime within the bundle. It is also possible that instability depends on void fraction distribution . Moreover, tube vibration due to turbulence response in the presence of two-phase flows has not been properly accounted for when using the homogeneous equilibrium model two-phase flow equations. However, despite the fact that all of the parameters mentioned in the previous paragraph may be affected by the nucleation of bubbles at the tube surface, there is no documented

information in the open literature of the possible consequences on the tube vibration response due to this effect.

The main objective of this study is to investigate the dynamic effects of tube surface boiling on the vibration response of tube arrays due to turbulent buffeting and fluid elastic instability produced by a two-phase Freon-11 cross-flow .

CHAPTER 2

FLOW-INDUCED VIBRATIONS IN TUBE ARRAYS

2.1 Introduction

Depending on the particular characteristics of the flow and the dynamic characteristics of the tube and the tube supports, there are four main mechanisms of flow-induced vibrations, turbulent buffeting, fluidelastic instability, Strouhal periodicity and acoustic resonance, which may be present in heat exchanger tube bundles. The first two mechanisms will be discussed in this chapter with extensive references for the interested reader. Special emphasis will be given to those cases with the presence of two-phase flows. Strouhal periodicity and acoustic resonance will not be addressed since they are not commonly encountered in two-phase cross flow situations in nuclear steam generators.

2.2 Turbulent Buffeting in Nuclear Steam Generators Tube Bundles

In the case of cross flow, turbulence-induced random vibrations resulting from turbulent buffeting produce a small tube vibration amplitude in tube arrays, due to small scale vorticity produced as the flow passes through the tube bundle. The level of turbulence is not constant within the bundle. As the flow goes into the bundle, the turbulence increases up to a steady state value, which is attained near the sixth row (Weaver & El-Kashlan, 1981).

In single phase flows, the level of vibration attributed to buffeting is a function of pitch velocity (Vp) or pitch mass flux, seen in figure 2.1.

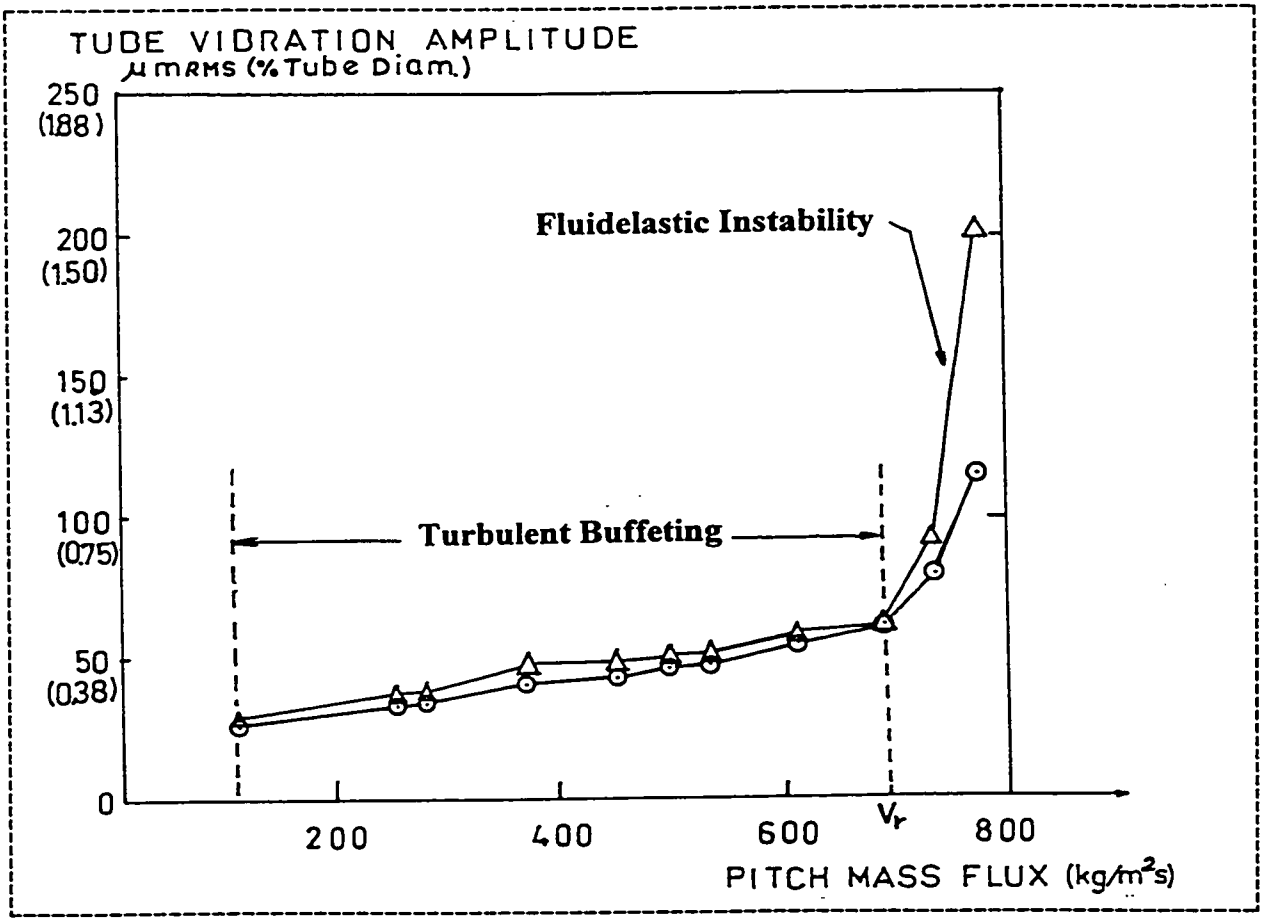

Fig 2.1Tube response due to turbulence and fluidelastic instability. Pettigrew et al.(1994) Triangles are for data in the lift direction and circles for drag direction

Although turbulence-induced random vibrations are usually of much smaller amplitude than those caused by other mechanisms, normally not exceeding 2-3% of the tube diameter, they are of great practical importance because they are always present whenever there is flow over a tube bundle. Through fretting wear at the tube supports, turbulent buffeting is capable of shortening the life span of the system.

Turbulent buffeting has been found to be different in single phase and in two-phase flows. In single phase, researchers have found that the dimensionless power spectral density Φ of the fluid forces (Taylor et al. 1988) collapsed to a single line in both lift and drag directions for reduced frequencies larger than 0.2, as the graphs presented in figure 2.2 (a) show. However, a similar correlation could not be found for the two-phase flow cases.

The dimensionless power spectral density Φ is defined as:

$$\Phi(f_R) = \frac{\phi(f)}{(1/2\ \rho_W V_P^2 D)^2} \frac{V_P}{D} \qquad 2.1$$

where $\phi(f)$ = spectral density of fluctuating force per unit length ($N^2 s/m^2$), ρ_W = density of the water (kg/m^3), V_P = reference gap velocity (pitch velocity)(m/s), D = tube diameter (m) and f_R = reduced frequency, defined as $f D/V_P$.

The non-dimensional power spectral density, Φ, shows a strong correlation with void fraction for both lift and drag directions and also for the two pitch to diameter ratios investigated (1.47 and 3.00). The graphs in figure 2.2 (b) show the experimental results for air-water cross flow and pitch to diameter ratio equal to 1.5. (Taylor et al. 1988).

There are two main factors to explain this anomaly. The first one is the difficulty of characterizing the two-phase flow mixture correctly. Its density, viscosity, and other

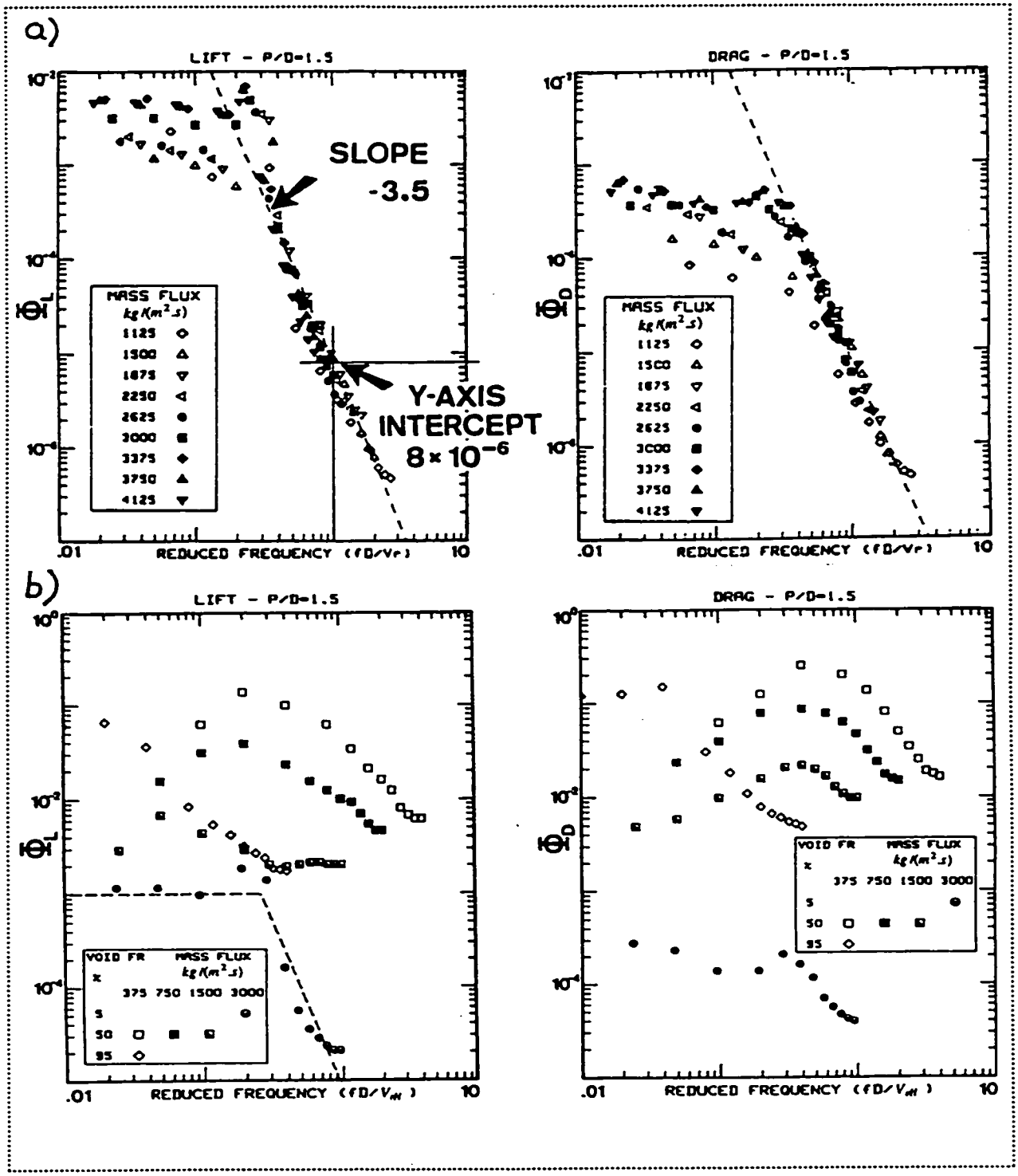

Fig.2.2 Dimensionless power spectral densities for tube rows subjected to a) water cross flow. b) air water cross flow. Taylor et al. 1988.

physical properties may not be correctly modelled by using the homogeneous equilibrium model equations, which assume that both phases are homogeneously distributed and travel at the same velocity.The second one is the fact that, the flow regime, which strongly affects the fluid properties and hence the tube vibration, has not been incorporated in the mathematical correlations.

In a more recent work (Yamaguchi et al.1993), tube bundles with in-line and staggered array configurations and pitch to diameter ratios of 1.31 to 1.42 were exposed to air-water cross flow. Based on the experimental evidence, the authors suggested that turbulence excitation forces are mainly the effect of rising water slugs and proposed a correlation that predicted the order of magnitude and distribution of the exciting forces reasonably well.

Papp and Chen (1994) proposed a numerical correlation to predict tube vibration response due to turbulence excitation in single phase and two-phase flows. The correlation is based on the assumption that tube response is proportional to pressure drop across the tube row, which is postulated from the conservation of energy of the flow-tube bundle system. The equations contain coefficients to account for tube array configuration, tube properties, mass flux, void fraction and mixture density. The predictions agree with experimental values extraordinarily well for the parallel triangular bundle geometry, but only reasonably well for the normal square geometry. Although a potentially useful tool for design purposes, the correlation does not address the important issue of flow regime

effect on tube vibration, nor does it address the tube surface boiling effect, which will affect the energy balance assumed in this work.

In an earlier study (Nakamura et al.1993), the researchers derived a numerical correlation to predict turbulence response, using a correlation length Lc, which is a measure of the phase angle among the turbulent forces along the tube axis. Their experimental study yielded results that needed correlation lengths of 300 mm for intermittent air-water flow. These results suggest the existence of slugs 300 mm long along the tube axis. Although, the authors did not indicate the length of the tube used in the study, the value seems rather large for tubes that were probably less than 1000 mm in total length. The study did not report any additional data that could be used in the numerical correlation to predict turbulent response in homogeneous (bubbly) flows.

At the present moment there is no completely reliable model that would predict levels of vibration in tube bundles for two-phase turbulent flows. The overall effect of tube surface boiling on force correlation length and flow regime also remains unclear.

2.3 Fluidelastic Instability

2.3.1 Fluidelastic Instability in Single Phase Flows

Fluidelastic instability is the most critical vibration excitation mechanism for tube bundles exposed to single and two-phase cross flows. When the design of the tube bundle in the steam generator fails to avoid tube instability, large vibration amplitudes will develop

at the midspan of the tubes. The graphs in figure 2.1 show the typical response of a tube exposed to single phase cross flow. Tubes vibrating under this condition are susceptible to fretting wear at the tube supports and also to clashing with the neighbouring tubes. When this situation occurs, the useful life of the steam generator is reduced dramatically, forcing the early shut down of the nuclear reactor.

Fluidelastic instability in single phase cross flow has been the subject of extensive investigation, by researchers such as Eisinger et al.(1995), Yetisir and Weaver (1993), Kaplunov and Makhutov (1992), Pettigrew and Taylor (1991), Granger (1991), Blevins (1990), Price at al. (1989), Teh and Goyder (1988), Andjelic and Popp (1988), Lever and Rzentkowski (1988), Weaver and Fitzpatrick (1988), Paidoussis and Price (1988), Price and Paidoussis (1987), Minakami and Ohtomi (1987), Scott and Weaver (1986), Axisa et al. (1986), Paidoussis et al.(1985, 1989), Weaver and Koyannakis (1983), Chen ,S.S. (1983,1984,1988), Lever and Weaver (1982), Paidoussis (1981), Weaver and El-kashlan (1981), Blevins et al.(1981), Chen and Jendrzejczyk (1981,1987), Weaver and Grover (1978), Grover and Weaver (1978) Southworth and Zdravkovich (1975), Hartlen (1974), Connors (1970). Despite all these efforts to elucidate the mechanism of fluidelastic instability in tube bundles, there is not a single universally accepted theory able to predict the instability for all the cases of pitch to diameter ratios P/D, bundle geometry configuration and mass damping parameter values that are encountered in steam generators. Nevertheless, it would be instructive to discuss two of the most important models to become

familiar with the basic concepts involved in this phenomenon. This is particularly important, considering that there is still a belief that the mechanism of instability is essentially the same for single phase and two-phase flows.

2.3.2 Displacement Mechanism

There are two main models of fluidelastic instability . The first model of fluidelastic instability is based on the displacement mechanism discussed by Blevins (1990). This model assumes that fluid forces are linear and react instantaneously with tube displacement. The position of the main tube and its neighbouring tubes define the flow pattern through the array, changing the fluid forces on the tubes. The equations of motion for each tube in both, streamwise and transverse directions are based on these principles. Under this theoretical framework, equation 2.2, which was first proposed by Connors (1970) arose. The equation is based on the following assumptions:

a) In every adjacent tube row, cylinders vibrate out of phase

b) The fluid forces produced, in the lift and drag directions, by the displacement of the cylinder in the same direction are negligible

c) The solution for the vibration amplitude is exponential in time

d) Damping ratios in lift and drag directions are equal

e) All cylinders have the same natural frequency in both the lift and drag directions and also among each other.

$$\frac{U_c}{f \cdot D} = C \left[\frac{2\pi\zeta m}{\rho D^2}\right]^{1/2} \qquad 2.2$$

where U_C = critical pitch velocity for instability, f = tube natural vibration frequency, D = cylinder diameter, ρ = fluid density, ζ = tube structural and fluid damping ratio, m = mass per unit length of cylinder including added mass.

The most important consequence of this model is that a single flexible tube in a rigid array would be always stable. However, experimental data obtained by Lever and Rzentkowski, (1988) and Pettigrew et al. (1989) indicate that for some tube arrays with particular configurations, this is not the case and that the tubes do become unstable.

Equation 2.3 is a slightly modified version of Connors' equation, which has been used in the design of tube bundles for nuclear steam generators.

$$\frac{U_c}{f \cdot D} = C \left[\frac{2\pi\zeta m}{\rho D^2}\right]^{b} \qquad 2.3$$

Different values of C and b have been presented since the inception of the equation. Connors (1970), advocated C=9.9, b=0.5 for a tube row and Pettigrew and Gorman (1978) recommended C=3.3 and b =0.5. A list of values that have been proposed can be found in Pettigrew and Taylor (1991). In general, it can be said that values of C and b will depend on

array geometry, pitch to diameter ratio and flow direction. Despite all efforts, no universal values for C and b have been found, suggesting that Connors' equation does not represent the fluidelastic instability phenomenon in its entire complexity.

2.3.3 Velocity Mechanism

The second model of fluidelastic instability is based on the velocity mechanism. This approach, which has been proposed by Lever and Weaver (1982) and by Paidoussis and Price (1988), overcomes the shortcoming of the displacement mechanism by which the fluid forces are assumed to respond instantaneously to a change in tube position. This model assumes that the main cause of instability is the time delay between the cylinder displacement and the change in fluid force.

The theory formulated by Lever and Weaver (1982) and a more recent version of the model formulated by Yetisir and Weaver (1993), treated the tubes as two-degree of freedom simple harmonic oscillators with the same natural frequency in orthogonal directions. The authors were able to solve the stability equations, which were defined in terms of the complex frequency ratio ω/ω_0 and mass ratio $m/\rho D^2$ as functions of reduced velocity V_r. The more recent version of the model also considered the effect of neighbouring tube motion. The theoretical predictions agreed very well with the experimental data for four standard tube array geometries. An important conclusion based on this model is that the single flexible tube in a rigid array model is not valid at high mass damping parameter

($m\ \delta/\rho D^2$) >100 if frequency is assumed a priori. In this situation, the instability is controlled by the stiffness associated with the motion of the neighbouring tubes.

A simple description of the fluidelastic instability mechanism has been given as follows. According to Pettigrew & Taylor, (1994), the fluid forces on one tube are affected by its motion and the motion of neighbouring tubes. Hence the fluid forces and tube motion are coupled. Fluidelastic instability is possible when the interaction between the motions of individual tubes produces fluid force components that are both proportional to tube displacement and in-phase with tube velocities. Instability occurs when, during one vibration cycle, the energy absorbed from the fluid forces exceeds the energy dissipated by the mechanism of damping. In such a case the vibration amplitude would increase without bound until non-linearities such as the presence of the other tubes or the clearance at the tube supports would limit its value.

2.3.4 Fluidelastic Instability in two-phase flows.

In two-phase flows, the existence of fluidelastic instability in tube bundles and steam generators is well documented by researchers such as Feenstra et al. (1996), Heilker & Vincent (1981, 1995), Pettigrew et al. (1994), Saito et al. (1994), Lian et al. (1992, 1994), Pettigrew et al. (1978, 1973, 1985, 1989, 1994), Pettigrew & Taylor, (1994), Nakamura et al. (1986, 1991,1992, 1993), Dam (1991), Gay et al. (1988), Goyder (1988), Nakamura & Fujita (1988), Taylor et al. (1988), Axisa et al. (1984), Remy (1982), Bates & Stewart

(1979), Pettigrew & Campagna (1980). Following a practical approach, nuclear steam generator designers have been using Connor's relationship (equation 2.3), to avoid the conditions which would yield instability of the tubes in bundles subjected to two-phase cross flows. This is mainly due to its simplicity and the lack of a better equation that would incorporate the effect of two-phase flows, despite the fact that this equation was derived for a much simpler case.

In order to use Connor's equation for tube bundles subjected to two-phase flows, some of the parameters such as damping ratio (ζ), fluid density ρ, and total mass per unit length m had to be modified to account for the presence of both gas and liquid phases. Up to the present, there is no general agreement among researchers in the field about the correct mathematical expressions for these parameters.

Fluidelastic instability in two-phase cross flows varies from the case of single phase. Most notably, void fraction has a strong effect on tube total damping ratio and flow regime transitions have an important effect in tube bundle vibration behaviour. It is not clear how these two effects can be incorporated into the equations for fluid elastic instability to correctly predict these phenomena.

2.4 Two-Phase Vertical Flows in Conduits and Tube Bundles

There seems to be a consensus among researchers in the field that further developments in the area of two-phase cross flow-induced vibrations in tube bundles would only be possible if the issues of two-phase flow properties, flow regime and void fraction distribution are properly addressed. In the following section, a brief description of these aspects and the basic concepts underlying them is presented.

2.4.1 Two-Phase Flow Equations

One of the most difficult tasks in working with two-phase flows is the correct characterization of the mixture. On one hand, physical properties such as density and viscosity are needed to define mass flux, and both mass flux and density are used to define the average velocity. On the other hand assumptions about phase distribution and phase velocities are needed to establish the equations needed to describe the flow characteristics. In this section, we will described the two principal models and the proper equations and concepts used in each one.

Homogeneous Equilibrium Model (HEM)

In this model, it is assumed that the two phases are in thermodynamic equilibrium. Therefore, temperature and pressure are the same for both the gas and the liquid phases. It is also assumed that the velocity of the two phases is the same so that there is no slip and that the phases are well mixed.

In a two-component flow, the definition of void fraction in accordance with this model is :

$$\phi_H = \frac{Q_G}{Q_G + Q_L} \qquad 2.4$$

where Q_G and Q_L are the volumetric flow rates of the gas and liquid phases respectively.

The density of the mixture is defined as :

$$\rho = \phi_H \rho_G + (1 - \phi_H) \rho_L \qquad 2.5$$

where ρ_G , and ρ_L are the densities of the respective gas and liquid phases.

The mass flux can then be defined as :

$$G = \frac{\rho_G Q_G + \rho_L Q_L}{A} \qquad 2.6$$

where A is the cross sectional area of the conduit.

The upstream and pitch flow velocities are defined as :

$$V_U = \frac{G}{\rho} \qquad 2.7$$

$$V_P = \frac{G}{\rho} \frac{P}{P - D} = V_U \frac{P}{P - D} \qquad 2.8$$

where P is the pitch (shortest distance between the tube centers regardless of direction) between tubes and D is the tube diameter.

The void fraction can be calculated as:

$$\phi_H = \frac{1}{1 + \frac{\rho_G}{\rho_L}\left(\frac{1}{\chi} - 1\right)} \qquad 2.9$$

where χ is the quality of the mixture, defined by :

$$\chi = \frac{h_{f2} - h_{f1} + \delta h}{h_{fg}} \qquad 2.10$$

where h_{f1} is the specific enthalpy of the liquid at the test section (after the heaters), h_{f2} is the specific enthalpy of the liquid at the inlet of the main heaters, δh is the increase in specific enthalpy of the liquid at the heaters and h_{fg} is the liquid enthalpy of vaporization.

One of the essential inadequacies of the HEM is the fact that very often both phases do not travel at the same velocity. Furthermore, there is some experimental evidence which indicates that the ratio between the gas and liquid velocities increases as the two-phase mixture passes through a tube bundle (Gidi et al.1996). Whalley (1987) pointed out in his book that HEM works reasonably well for ratios of liquid to gas density lower than 10 and

for mass fluxes higher than 2000 kg/m^{2}s. None of these conditions apply to nuclear steam generators or the majority of the experimental studies performed up to date. Under these circumstances, it is important to have theoretical tools that can better describe the actual characteristics present in a two-phase flow, so that a deeper understanding of the behaviour of this phenomenon can be achieved.

Separated Model.

In this model, the phases are assumed to travel at velocities that can be different (Whalley, 1987). Applying the continuity equation to both phases separately, the void fraction value can be calculated as follows:

$$\phi = \frac{1}{1 + \frac{u_G \rho_G}{u_L \rho_L} \left(\frac{1}{x} - 1\right)} \qquad 2.11$$

where u_G, and u_L are the velocities of the gas and liquid phase respectively. Usually the ratio u_G/u_L is called slip ratio and denoted by the symbol S. When true void fractions are measured, equation 2.11 is helpful in providing an estimation of the slip ratio S. Under the same flow conditions, slip ratios of up to S = 4.52 within the tube bundle and slip ratios of S = 3.0 in the open area upstream of the tube bundle were obtained by Gidi et al. (1996). The fluid was Freon-11 and flow conditions were Gp=250 kg/m^{2}s with HEM void

(upstream) of 79-83 %. This finding indicates that the gas accelerates with respect to the liquid when passing through the tube bundle. Until now, no clear explanation has been given for this effect nor its potential effects on tube vibration response.

Despite the fact that the separated model takes into account the fact that both phases do not travel at the same velocity, it is still based on the assumption that phases are not mixed but flow side by side in the same conduit. The true condition that phases can be homogeneously mixed and still travel at different velocities is hence not accommodated in either model. Due to its simplicity with respect to the numerical procedures, the HEM is used widely and until now has been accepted as the standard model.

2.4.2 Flow Regime Transitions

The main difficulty in dealing with two-phase flows is the fact that flows are not uniquely characterized by the void fraction value. Under the same void fraction value, different gas and liquid phase distributions will produce entirely different types of flows when considered in terms of flow properties such as pressure drop, and physical properties such as local density and local viscosity, etc. This issue becomes very important because there is some experimental evidence that shows that the vibrational response of tube bundles exposed to two-phase flows is extremely sensitive to the flow regime within the bundle (Pettigrew et al.1989). Classical fully developed flow patterns in upwards flow in a vertical conduit with increasing void fraction (or quality) value are depicted in figure 2.3.

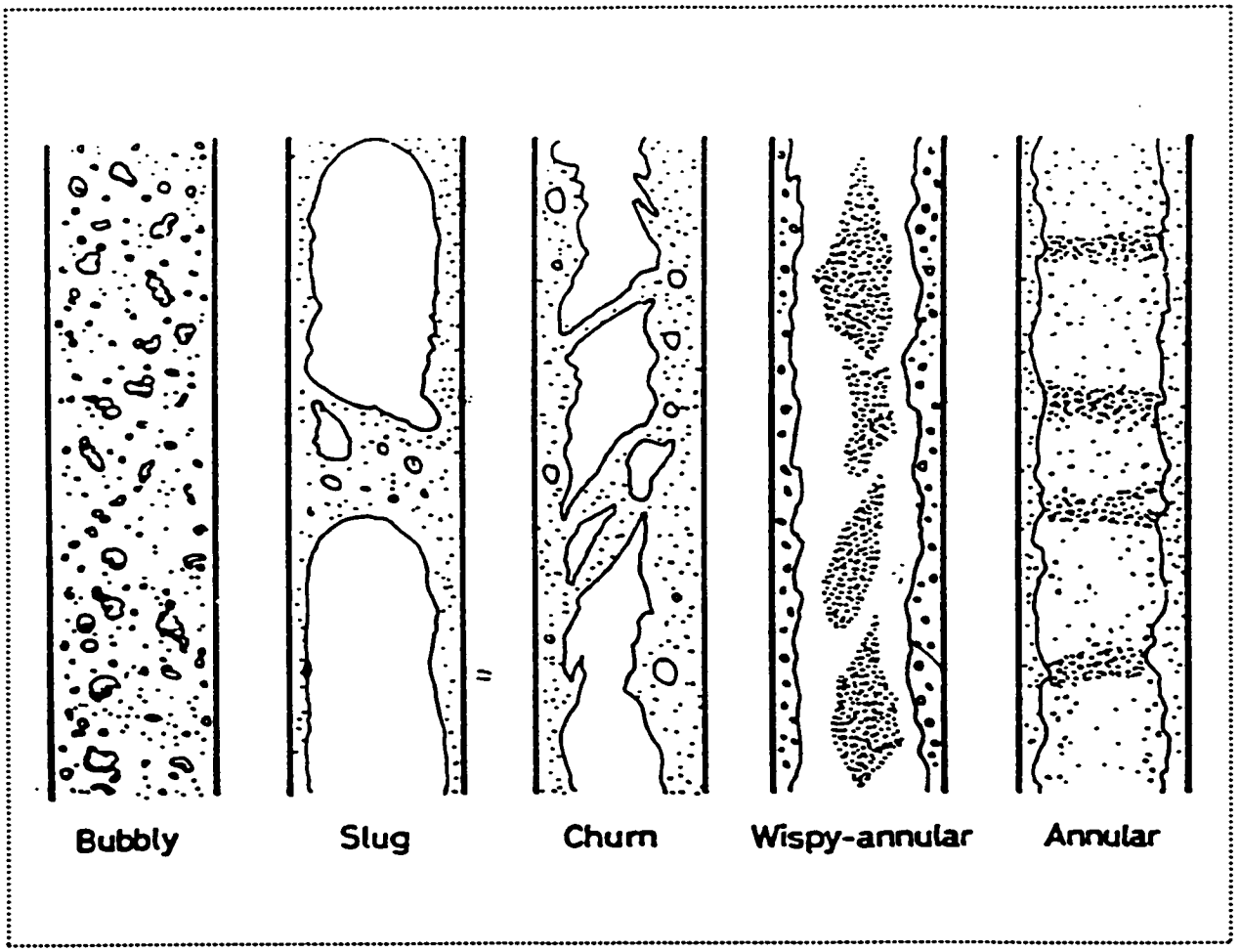

2.3 Flow patterns for vertical upward gas-liquid flows in a pipe.

For the purpose of studying two-phase flow tube vibrations, it is important to consider the first three flow regimes, which may be present at the upstream side of the tube bundle. In bubbly flow, the gas phase is distributed homogeneously in the liquid by discrete bubbles. When void fractions are low, the bubbles are small and tend to be spherical. As the void fraction increases, the bubbles tend to become more numerous, until coalescence of the bubbles occurs. It is not clear at what value of void fraction the flow will change to the

slug flow regime. A theoretical calculation based on equal size spherical bubbles in a quiescent fluid gives values between 52% and 72%, depending on the geometrical arrangement which determines how the bubbles are packed together (lattice, cubic, compact cubic or hexagonal). Slug flow is said to exist when the vapour bubbles are sufficiently large that they nearly occupy the entire cross section of the pipe, while a thin liquid film adheres to the wall around the vapour slug. The flow consists of alternately rising slugs of gas and liquid, whose size can vary considerably. The liquid slugs may also contain small vapour bubbles . Churn flow is somewhat similar to slug flow , but much more chaotic, frothy and disordered. The shape of the large bubbles is distorted and changes continuously as they move upwards. This flow pattern results from a breakdown of the well defined vapour bubbles in slug flow. In annular flow, a wavy liquid film forms at the pipe wall while a continuous gas phase occupies the core of the channel. Liquid droplets may become entrained in the core if the gas velocity is sufficient to detach them from the liquid film. This flow pattern is characteristic of high gas velocities.

As mentioned by Feenstra (1993), flow visualization of two-phase flows in Freon-11 gave no evidence of slug flow at the upstream edge of the bundle. He observed large vapour bubbles at 70% HEM void in the upstream flow. It is difficult to identify churn flow in the test section used in this study. It can be more appropriately said that churn flow will be assumed every time that bubbly flow is not present and that a chaotic motion of the gas phase is observed.

Flow Regime Transitions in Tube Bundles

This subject has become of importance since some investigators, Pettigrew et al. (1989), have found experimental evidence that would suggest that the fluidelastic instability in two-phase cross flow tube bundles is related to a flow regime transition from bubbly to churn flow. Despite this, there is limited information about the subject in the open literature. Flow pattern characterization is experimentally difficult due to the presence of the tubes, which are arranged in a compact geometry. However there are reasons to believe that flow regime may be different within a tube bank than in a open duct. The effect of the tubes on the gas phase distribution can be significant . In addition, bubble coalescence and bubble break down can also happen within the bank due to the impact of bubbles against the vibrating tubes. More questions arise when considering the effect of tube surface boiling on the flow regime transitions.

One of the few works in the area of flow regime transition in tube bundles was done by Grant & Chisholm (1979) who studied flow regime patterns on the shell side of a segmentally baffled shell and tube heat exchanger. Their 38 tube bundle was arranged in 11 rows and 4 columns. The tubes had a diameter of 19 mm and a pitch to diameter ratio of 1.25 forming a normal triangular array. The mixture was air and water and the test section was 483 mm long by 302 mm high by 130 mm wide. Three segmental baffles give four passes of the flow in the shell side, two upwards and two downwards. A window allowed for flow visualization. By observing the flow regime at different mass fluxes and void

fraction and different locations of the system, the authors were able to produce a map for each flow condition, flow perpendicular to the tubes (cross flow) and flow parallel to the tubes (parallel flow). Figure 2.4 shows the flow regime map with the transition lines between intermittent, bubbly and spray flows. The graph plots the Gas Superficial Velocity Parameter, defined as:

$$U_G^* \ (\rho_g/\rho_L)^{1/2} \qquad 2.12$$

versus the Liquid Superficial Velocity Parameter, which is defined as:

$$U_L^* \ (\rho_L \cdot \mu_L)^{1/3}/\sigma \qquad 2.13$$

where σ is the liquid-gas surface tension, μ_L is the fluid dynamic viscosity and U_G^* and U_L^* are defined as follows:

$$U_G^* = \frac{\chi \cdot G_P}{\rho_g} \qquad 2.14$$

$$U_L^* = (1 - \chi) \cdot G_P/\rho_L \qquad 2.15$$

Instability data from a number of investigations have been plotted on the figure.

Flow visualization data from Pettigrew et al. (1989) correspond with the predictions from the map somewhat, but only in a general trend as the map predicts intermittent flows

at lower void fraction values than the ones observed by Pettigrew. Flow observations from Feenstra (1993) corresponded only partially with the predictions from the map, some data points plotted in the bubbly flow region of the map corresponded with observed intermittent flow. In the following study, a more extended explanation about the ability of this map to predict flow regime in tube bundles will be presented.

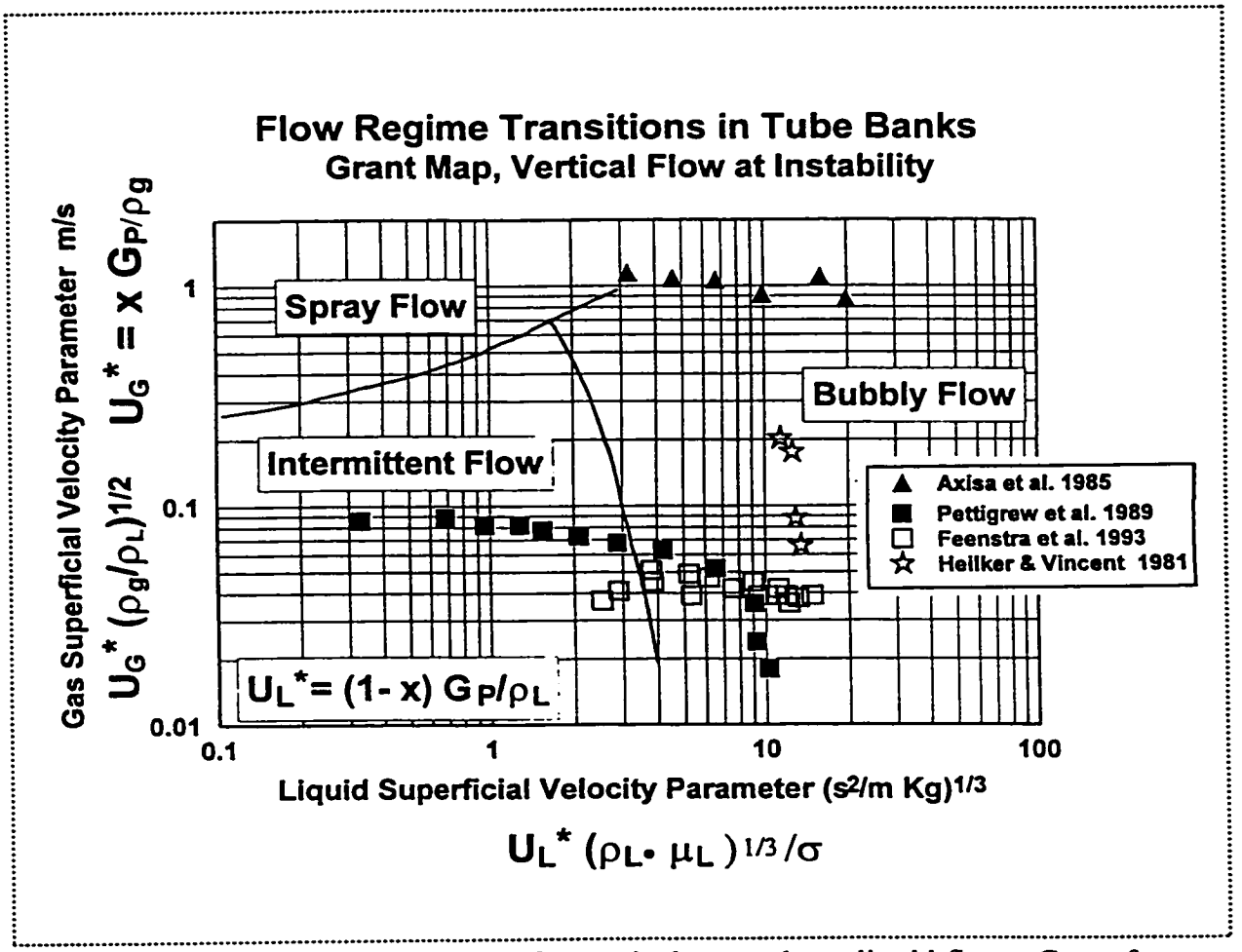

2.4 Flow pattern map in tube bundles for vertical upward gas-liquid flows, Grant & Chisholm 1979. Data have been plotted by A.Gidi

In a more recent work, Ulbrich and Mewes (1994), gathered a substantial part of all experimental flow regime data in the field and plotted them on different flow regime maps proposed by other investigators. They argued that of the four most important maps, the three maps, which were proposed by Grant and Murray (1972), Grant and Chisholm (1979) and Pettigrew et al. (1989) are practically identical and differ only in the coordinate system used. The fourth one is the map proposed by Taitel et al.(1980) for flow in a pipe . The authors found that when the data were plotted on the Grant and Murray map and also on the Taitel et al.(1980) map, none of them predicted the observed flow regime better than in 50% of the cases. This is a surprising revelation considering that the Grant and Murray map was specifically designed to be used in cross flow through tube bundles whereas the map proposed by Taitel et al.(1980) was intended to be used for flow in a vertical pipe.

Ulbrich and Mewes then obtained data in an air-water flow loop with a bundle of fifty tubes arranged in five columns and ten rows, using a square array configuration with pitch to diameter ratio of 1.5. The authors attributed the low prediction success of the previous maps to the fact that the flow regimes were identified by visual inspection, which is subject to the opinion of the investigator. In their work, the authors used the pressure drop and its standard deviation as a more scientific method for flow regime identification. Flow regime such as bubbly and dispersed regimes were characterized by a low standard deviation in the pressure measurements, whereas the intermittent regime had a pressure drop standard deviation at least twice as large.

A new flow regime map was proposed, wherein the flow regime corresponding to the authors' data were predicted correctly in 96.5 % of the cases. This is not surprising considering that the data and the map resulted from the same study. However, when the data from all the other authors were superimposed, the flow regimes were predicted correctly in 86.4% of the cases. Figure 2.5 shows the proposed map with all data points corresponding to bubbly flow.

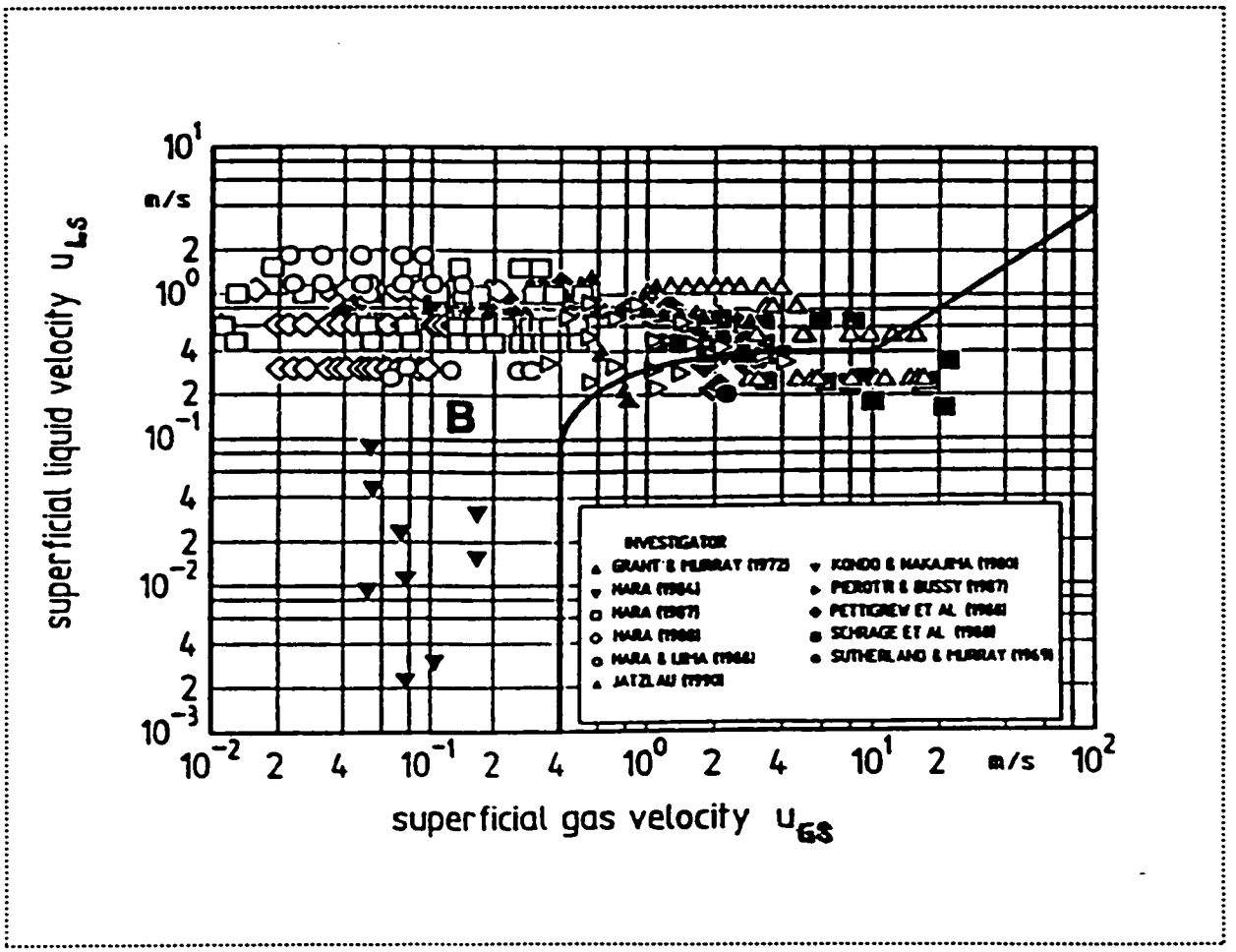

2.5 Flow pattern map in tube bundles for vertical upward gas-liquid flows, Ulbrich and Mewes (1994).

Tube Surface Boiling Effect in Flow Regime

Tube surface boiling phenomenon in the U-bend regions of tube bundles in nuclear steam generators and its effect on flow regime has not been considered by researchers in the field. It has been recognized that the flow regime is especially important for predicting two-phase damping ratios (Pettigrew et al.1994). Based on experimental evidence, it has been also suggested that tube vibration response is related to void fraction distribution in the vicinity of the tube (Pettigrew et al.1989). However, there is no information in the open literature about research conducted to investigate these aspects of flow-induced vibrations.

Tube surface boiling occurs homogeneously on the tube surface, and may ameliorate any potential void fraction distribution effects that may have occurred due to tube motion and flow interaction. This may, in turn, alter the added mass and damping ratio in the direction where void distribution has been affected. Flow regime may also be influenced by tube surface boiling. Such speculations have motivated the research reported in this thesis.

CHAPTER 3

EXPERIMENTAL MODEL DEVELOPMENT

Introduction

The design of the experimental model represented one of the biggest challenges to the completion of this investigation. This was a consequence of the various characteristics that the bundle had to meet, which in many instances seemed to be incompatible with one another. Particularly difficult were the following three: tube vibration requirements, with respect to frequency and low structural damping ratio, heating condition requirements and vibration measuring requirements. It was clear that heating conditions were not going to allow for the use of the optical vibration measuring technique used by Feenstra et al. (1996) due to the requirement that the tubes which were to be used had to be solid. This necessitated the invention of a new non-intrusive optical technique for measuring vibrations (Robinson et al.1995) which is described in detail in section 4.3.1. This condition also meant that a new system for fine frequency tuning the bundle had to be designed since the method used by Feenstra et al.(1996) of changing the length of each tube independently would not work in this case. The new bundle tuning system, based on mass addition to a chamber at the free end of the tube, is described in section 4.2.3.

The first approach to obtaining heated tubes involved the use of heat pipes, which would develop a heat flux at the tube surface sufficient to produce the boiling, necessary for the investigation. To assist in this approach, a computer code was developed in order to predict the performance of heat pipes based on different designs. Unfortunately, this attempt had to be abandoned after a year of work, during which time two approaches were attempted. The first was to purchase suitable heat pipes, but there was no heat pipe with the heat transfer performance and characteristics needed available on the market. One company, Noren Products Inc. from California offered one, which was purchased and tested, but the performance was not as claimed by the manufacturer and therefore not satisfactory for the purpose of this research. Interestingly, the performance was in agreement with the predictions given by the computer code. The second was to use the computer code to create a new heat pipe design, which would be capable of performing as required for the investigation. However, neither the off-campus company approached to manufacture the heat pipe nor the technicians in the Department of Mechanical Engineering could manufacture a prototype. Experience in this matter indicates that, for a heat pipe with the required performance, this advanced design required manufacturing capabilities beyond what was available. Details of the problems faced and experience obtained in this attempt along with the computer code that was developed are presented in Appendix E.

Concurrent with the attempt to obtain heat pipes, a search for tubes with internal electric heaters was undertaken. Initially, no electric heaters could be found available on the market with the necessary length for the experimental bundle. Nevertheless, by a fortunate coincidence, these tubular heaters just became available at the time the heat pipe attempt was abandoned. A description of these heaters is given in section 4.2.1 along with other details of the tube bundle.

The rest of this chapter is devoted to an explanation of how the dimensions, tube bundle characteristics, working fluid and scaling parameters were chosen to meet the modelling requirements of the phenomenon under investigation in this research.

Tube bundle design was based upon the same geometric configuration used by Feenstra et al.(1996). This approach to designing the test bundle saved time and effort by allowing the new bundle to be used in the existing test section. It also allowed both studies to be conducted concurrently simply by changing to the corresponding test bundle each time experiments were going to be performed. Otherwise, the test section would have had to be changed, something that would have required considerable more effort and time.

The tube bundle used in this study had to satisfy all the requirements of the previous tube bundle plus the additional ones associated with the necessity of producing the

tube surface boiling condition, something entirely new in this research field. The additional requirements introduced the condition that the tubes had to be electric cartridge heaters and few alternatives were presented by the manufacturer with respect to the choice of tube material and internal structure. Instead of using brass or copper, the tubes were made of Incoloy. As a consequence, the tube mounting conditions at the fixed end had to be met by means of a different fixture design than that used by Feenstra et al. (1996). These conditions were important because they determine the tube natural frequency and tube damping ratio, which are two parameters that demand values within a narrow range to properly reproduce the phenomena under investigation. The remainder of this chapter describes the main aspects of the process by which all the tube bundle requirements were achieved.

3.1 Tube Bundle Modelling

3.1.1 Tube Diameter, Tube Length and Tube Natural Frequency

It has been suggested, Pettigrew et al.(1989), that flow regime is one of the critical parameters in determining the instability threshold of a tube in a tube bundle exposed to two-phase-cross flow. The hypothesis suggests that tube instability is associated with the transition between bubbly flow and churn flow. Although this hypothesis has not yet been proven, it was considered that proper scaling of flow regime transition was important. A bibliographic search was performed to support the decision of previous investigations, such as that conducted by Feenstra et al. (1996) to use tubes 0.25 inch in diameter. Symolon

(1990), did an experimental study of flow regime transitions in a rod bundle in the presence of two-phase Freon-12 flow. One main conclusion of this study was that flow regime transitions from homogeneous bubbly flow to a more disorganized churn flow occurred at the same void fraction values when the results of a half scale model using Freon were compared with the results of a full scale model using steam-water. Not only the flow regime transition was correctly simulated but also the ratio between the gas phase and the liquid phase (slip ratio) velocities was appropriately simulated. Considering that nuclear steam generators bundles commonly use half inch diameter tubes, and following the conclusion of this previous study, it was found appropriate to use quarter inch diameter tubes.

Because of the desirability of being able to use the existing test section, the cantilevered section of the tubes was designed to be 0.3 metres (12 inch) long. This tube length resulted in a tube natural vibration frequency of about 38 Hz in air and 30 Hz when submerged in liquid Freon-11. This frequency is close to the value of 40 Hz, typical of the U-bend region of CANDU nuclear steam generator tube bundles.

3.1.2 Geometric Array Configuration, Pitch Ratio and Number of Tubes

The number of tubes in the bundle was determined by the pitch ratio, the geometric configuration, the flow capacity of the test rig main pump, and the flow simulation

requirements. With respect to the last requirement, the desirability of having at least six rows of tubes upstream of the monitoring tube was established in a study done by Weaver & El-Kashlan (1981) where this minimum number of rows was found to be necessary to study cross-flow induced vibrations in tube banks. Ten tubes arranged in three columns and seven rows were used. It was not possible to incorporate more columns due to limitations of the main pump flow capacity and also due to the desirability of being able to fit the tube bundle in the existing test section. Adding more columns would have increased the cross sectional area, reducing the mass flux through the tube bundle for the same total flow allowed by the pump. With the final design, maximum mass fluxes of 450-500 kg/m^2s were attainable in the test section. However, this value is in the lower half of the 100-1000 kg/m^2s range which has been used by other researchers. Tubes were arranged in a parallel triangular array with a pitch ratio of 1.48. This array geometry and pitch ratio are typical of those commonly encountered in nuclear steam generator tube bundles at the U-bend region. They are also typical of those commonly used in most of the important previous investigations.

3.1.3 Tube Fixing Conditions and Damping Ratio.

Tubes were arranged in a fixed-cantilevered condition. The cantilevered requirement was needed to obtain vibration amplitudes at the free end large enough to be clearly detected by the vibration measuring system and more importantly by visual inspection. The

vibration signal also had to be large with respect to the background signal coming from the rotating equipment present in the loop, which was being detected by the vibration measuring system. The fixed end support needed to comply with three basic conditions; first to hold the tubes firmly in place, secondly to allow the electric power coming from outside the test section to be connected to electric heater inside of each tube and thirdly to prevent Freon-11 leaking to the ambient. The design, which was based on a split plate concept whereby tubes were fixed in place by nylon ferrules located between the plates is fully described in section 4.2.

The total damping ratio of a cantilevered tube in a vacuum is controlled by two effects. First, some damping is due to the tube structure and hence the ability of the tube material to dissipate energy under a given deformation, and second, some frictional damping generated by the relative motion between the tube and its base support. The more rigidly the tubes are held at the base, the lower will be the total damping ratio of the tube. Theoretically, tubes being held very rigidly at the base will have the lowest damping ratio. Tubes at the U-bend region of a nuclear steam generator tube bundle typically have a damping ratio of about 0.2% for vibration amplitudes of about 2% of the tube diameter and frequency of vibration about 40 Hz. The damping ratio in air of the cartridge heaters was determined by the logarithmic decrement of damping technique and found to be between 0.2 to 0.4 %. Although this damping ratio range includes values larger than those found in

nuclear steam generators, it was not considered to be large enough to produced a significant difference in tube vibration response. The explanation is based on experimental evidence that indicates that the two-phase damping ratio, one of the components of the tube total in-flow damping ratio is in the order of 3% for a range of void fraction values in which the experimental results are significant, (Pettigrew et al.1994). Since the damping effect due to two-phase flow is much larger that the effect due to structural damping, the maximum difference of 0.2% in the tube damping ratio value was not considered to be of concern.

Since the main objective of this investigation was to find evidence in order to clarify whether or not the tube vibration behaviour would be affected by tube surface boiling, it was clear that anything else affecting tube vibration would be unwelcome. In this regard, it was found that when power was being dissipated by the tube heaters, the temperature of the split plate where the tubes were being held also increased, in particular around the Nylon ferrules which were used to fix the tubes in place on the mounting plate. It was found that this increase in temperature produced an increase in tube structural damping ratio, which obviously had the potential to affect tube vibration behaviour by reducing the vibration amplitude. To quantify the effect of temperature on tube damping ratio, a full study was performed (see Appendix A), which confirmed that this effect was problematic. Based on these results, and with the goal of eliminating this problem, modifications to the installation of the electrical system of the bundle were implemented. These consisted of positioning the

electrical box, which was bolted to the tube bundle base, further away from the fixing plate. In this way, a gap was created between the box and the base of the tubes, which enabled a convective flow of air to pass between the box and the base, thereby reducing the temperature of the region where the tubes where being held. This heat removal mechanism was enhanced by adding a forced air cooling flow by means of a fan. These changes were successful in maintaining this region close to ambient temperature, as confirmed by thermocouple measurements.

3.2 Two-Phase Flow Scaling Parameters

3.2.1 Working Fluid

Normal operating conditions on the shell side of a CANDU type nuclear steam generator are about 10 MP in pressure and 260 °C in temperature. Void fraction values at the U-bend region of the generator bundle are between 85% and 90%. The power required to generate a reasonable void fraction value of about 80% in a full scale tube array at laboratory conditions would exceed 1 MW. In addition, a flow loop designed to withstand this pressure and temperature would become extremely expensive to construct and operate. Costly equipment would also be needed to reject the heat from the working fluid in order to condense it. The few researchers who have used this approach in their investigations, include Axisa et al. (1985), and Nakamura el al. (1986, 1991).

The most common approach to modelling two-phase flows for vibration studies is to use air-water mixtures at atmospheric temperature and pressure. The main advantages of this solution are its affordable cost and its ability to accurately and independently control the air and water flows. This feature makes the calculation of void fraction value based on the homogeneous equilibrium model a simple task. Pettigrew et al. (1989), Axisa et al. (1984), Nakamura et al.(1982), Remy (1982), Heilker & Vincent (1981) have used this approach.

The disadvantages of this technique are that the gas-liquid density ratio, the viscosity ratio and the tube to fluid mass ratio are considerably different from those values present at nuclear steam generator operating conditions. Beside that, since air water is a two-component fluid, the mixture is not at thermodynamic equilibrium and hence there is no allowance for phase changes to occur between the liquid and the gas. In particular, bubble growth, vapour generation and bubble collapse cannot be reproduced with this type of model.

A compromised approach to modelling two-phase flow mixtures is to use a refrigerant such as Freon-11 (Feenstra et al. 1996) or Freon-22 (Pettigrew et al. 1994), as the working fluid combined with a scaled down model. Two main advantages of using Freon-11, the fluid used in this investigation, are the following:

* Power needed to produce the same void fraction in Freon-11 is 7.5% of that required in a steam-water investigation.

* Boiling temperature at atmospheric pressure is 23.6 °C, and hence operating pressure in the flow loop does not exceed 172 kPa (25 psi).

3.2.2 Scaling Parameters

In order to obtain a correct physical model, the following scaling parameters and physical properties have been considered to be important in this study. A brief analysis of their values in Freon-11 compared to the values in other investigations and steam generators conditions is presented in this section.

a) Reduced Velocity and Mass Damping Parameter

It is customary in this field that when instability data is plotted for comparison to data from other investigators, a reduced velocity (V_R) versus mass damping parameter (MDP) graph is used. Consequently, data should fall in the range where data from other studies have fallen. So far, Pettigrew et al.(1989) have covered the widest range for the mass damping parameter, presenting values ranging from 0.2 to 38. Pettigrew et al. (1994) found reduced velocity values between 1.79 to 3.28. Axisa et al. (1985), using a steam-water mixture, found even higher reduced velocity values for instability, in the range of 8.3. There is no precise method to predict the instability values for V_R and MDP in two-phase

flows, since the mechanism for fluidelastic instability is not yet completely understood. The approach taken in this study was to calculate these values using tube bundle dimensions and fluid physical properties along with some experimental data from Feenstra et al. (1996). Special care was taken to allow for the tube surface boiling phenomenon, covered in section 3.3, in which no previous experimental data existed.

Reduced velocity is calculated by the following equation :

$$V_r = \frac{V_P}{fD} \qquad 3.1$$

where V_P and f are pitch velocity and tube frequency at the instability threshold respectively and D is tube diameter. Pitch velocity can be calculated in accordance with:

$$V_P = \frac{G_P}{\rho_H} \qquad 3.2$$

where Gp is pitch mass flux and ρ_H is the Homogeneous Equilibrium Model (HEM) fluid mixture density.

Using tube diameter and frequency of vibration from the present investigation, along with mixture density and mass flux from Feenstra et al.(1996), estimated values for pitch velocity and reduced velocity were calculated as shown in Table 3.1, located at the end of

this chapter for the two extreme points in the instability range corresponding to mass fluxes of 98 and 478 kg/m^{2}s.

The mass damping parameter (MDP) is based on total tube damping ratio (ζ_t), total tube mass per unit length (m_T), HEM mixture density at instability (ρ_H) and tube diameter (D), as equation 3.3 shows:

$$MDP = 2\pi\zeta_t m_T / \rho_H D^2 \qquad 3.3$$

The total damping ratio is the summation of tube structural damping ratio and two-phase flow damping ratio. Since the two-phase flow damping ratio, which cannot be predicted, is the largest component, values from Feenstra et al.(1996) were used for the prediction of the two extreme instability points.

Total tube mass per unit length (m_T), including hydrodynamic mass (m_h), is a function of tube mass per unit length (m_t) and the ratio between frequency of vibration in-air (f_a) and in-flow (f), as shown in equation 3.4.

$$m_T = m_t + m_h = m_t + m_t[(f_a/f)^2 - 1] = m_t(f_a/f)^2 \qquad 3.4$$

Since instability points were not known at the design stage, they were taken from Feenstra et al.(1996), where total damping ratio and two-phase mixture density were used in the calculation of MDP, as shown in Table 3.1. Tube frequency in air, estimated in-flow tube frequency, and tube mass per unit length were taken from this study.

b) Mass Flux and Void Fraction

Normal values of mass flux at the U-bend region of a nuclear steam generator range between 800 to 1000 kg/m^{2}s. Pettigrew et al. (1989, 1994) used 28 to 775 kg/m^{2}s for their parallel triangular array studies. It is important not to use values over 1000 kg/m^{2}s since tube bundle vibration behaviour may be affected by phase slip phenomenon and non-uniformities in void fraction distribution, both of which are supposed to diminish as the mass flux increases.

In general, void fraction values in these studies should cover the full range from 0 to 100%, because experimental studies have shown, Pettigrew et al. (1989), that at low mass flux values (28-100 kg/m^{2}s) the void fraction for instability is in the range of 96 to 99 %. For the same study, instability occurred at 25% void fraction at high mass flux values (750 kg/m^{2}s). Feenstra et al. (1996), found instability to occur at void fraction of 86% at 89 kg/m^{2}s and 58% at 478 kg/m^{2}s.

c) Other Parameters

Although mass damping parameter and reduced velocity are important for comparison purposes, it is clear among researchers in the field that they do not uniquely define the tube vibration behaviour and instability. In an attempt to understand the mechanism by which fluid flow affects tube vibration, the following parameters have been identified and taken into account.

Pitch Ratio

The U- bend region of a tube bundle in a nuclear steam generator presents different values of pitch ratios, due to the variable spacing among tubes, which depends on the tube position within the bundle. Tubes at the centre have pitch ratios of about 1.3 , while tubes at the periphery have pitch ratios closer to 1.5. Since curvature radii for the tubes at the periphery are larger and tube supports are more widely spaced, these tubes are more prone to excitation by flow-induced vibrations. Consequently, most researchers (Feenstra et al.(1996), Pettigrew et al.(1989, 1994), Axisa et al.(1985)) have used pitch ratios between 1.4 and 1.5. A value of 1.49 was used in this investigation.

Mass Ratio

This parameter is important since it compares the total mass of the tube, including the hydrodynamics mass, with the mass of the two-phase mixture, per unit length. Light tubes in heavy fluids are more prone to vibrate, while heavy tubes in light fluids will be less

prone to vibrate. In a nuclear steam generator, different mass ratios are found in the U-bend region, due to the fact that void fraction increases as the flow passes from the centre of the bundle to the periphery at the top of the bundle. Higher void fraction means lower fluid density and hence higher mass ratio. For experimental purposes it is desirable to use values of mass ratio lower than the ones used in the steam generator, so that the tubes in the experiment will be more prone to vibrate under same flow conditions than the actual tubes. Mass ratios between 21 and 35 are found in steam generators. Values between 6 and 35 were used in this investigation. It corresponds to tubes at the periphery of the bundle, which are more prone to be excited by the flow.

Density Ratio

One of the biggest simplifications in dealing with two-phase flows is the assumption that both phases travel at the same speed. This assumption is the basis of the Homogeneous Equilibrium Model (HEM). However, there is experimental evidence, (Feenstra et al.(1993), Gidi et al.(1996), Symolon (1990)), that indicates that this is not the case. The ratio between the gas velocity and the liquid velocity, called the slip ratio, has been measured in these studies, with values found clearly in excess of unity. One of the explanations for this anomaly is associated with the difference in density between the bubbles and the liquid, where buoyancy forces act on the bubbles to make them move faster than the surrounding liquid. Since nuclear steam generators use steam-water at thermodynamic equilibrium,

density ratio tends to be low, at about 33. Some other investigations, for instance Pettigrew et al. (1989), used an air-water mixture, which gives a high density ratio of about 846. Refrigerant 11 (Freon-11) was used in this study, which has a density ratio of about 169. The closer the density ratio of the mixture in the experiment to the steam-water case, the more realistically the slip ratio will be modelled. Therefore, it is expected that the Freon-11 two-phase flow behaviour will be closer to the actual phenomenon. Values of density ratio for this and other investigations have been presented in Table 3.1

Kinematic Viscosity Ratio.

Fluid viscosity plays an important role in determining the viscous forces affecting the tube motion. Viscous damping ratio along with tube structural damping and two-phase flow damping ratio oppose the unbounded increase in tube vibration amplitude. Because of this, some attempts have been made to find a proper viscosity correlation for two-phase flows, based on the viscosities of the gas and liquid phases (McAdam, 1942). However, little success has been achieved in this regard. Values for kinematic viscosity ratio are shown in table 3.1

Bubble Size and Tube Bundle Geometrical Configuration

Bubbles have to travel through the tube gaps between the tubes in the tube bundle. This means that the bubble size to tube gap ratio and bubble size to tube diameter ratio should be two important parameters. In addition, flow regime is expected to be affected by bubble size and bubble size distribution. Although, it is clear that different bubble sizes for the same void fraction value may have an effect on flow regime and probably also in the void fraction distribution and flow field around the tubes, little effort has been dedicated to this issue.

Pettigrew and Knowles (1992), attempted to gain insight into the effect of bubble size on two-phase damping ratio, by changing the surface tension of the two-phase air-water mixture. However, no conclusive results were obtained since the correlation between surface tension and total damping ratio was strongly affected by the tube vibration frequency.

Symolon (1990) performed calculations to predict bubble size to tube diameter ratio for Freon and steam-water as a function of void fraction. It is interesting to note that the ratio values show a single peak at 40 % void fraction, with strong resemblance to the two-phase damping ratio versus void fraction curve obtained by Pettigrew et al. (1994).

Using air-water, Lian et al.(1994), found a connection between void fraction fluctuations in the vicinity of the tube and the local void fraction. They also found a similar correlation between the total damping ratio and the local void fraction. Their analysis suggested that energy transfer between the fluid flow and the tube is related to void fraction fluctuations, which they explained as a function of flow regime.

3.3 Tube Surface Boiling Modelling

3.3.1 Boiling Numbers in Tube Bundles and Nuclear Steam Generators.

As described in earlier chapters, the prime objective of this investigation was to measure tube vibration under the effect of tube surface boiling, thereby simulating more realistic tube bundle conditions at the U-bend region of a nuclear steam generator.

A numerical comparison between tube surface boiling in this study and in real steam generators was needed for a correct simulation process. The necessity arises from the fact that mass flux, heat flux and fluid properties are not the same in both cases. Consequently, a dimensionless number was required in order to achieve this modelling requirement. .

The dimensionless number that is appropriate for use in these cases is the boiling number Bo. The boiling number represents physically the ratio between the total power rejected from the tube per tube unit length to the total power needed to vaporize all the

flow contained in a cross section of dimension P-D (tube gap) per unit length parallel to the tube axis, as illustrated in figure 3.1.

The boiling number allows a comparison between the experimental case and the real one independent of mass flux, heat flux and fluid properties, in particular heat of vaporization. The definition is as follows :

$$Bo = \left(\frac{\pi\, q''}{Gp\ \lambda}\right) / \left(\frac{P}{D} - 1\right) \qquad 3.5$$

where q'' = heat flux at the tube surface in kW/m², λ = heat of vaporization of the fluid in kJ/kg, Gp = pitch mass flux kg/m²s, P/D = pitch to diameter ratio

Boiling number values Bo in the U-bend region of a typical nuclear steam generator, such as the Wolsung 2 station (Pettigrew, 1996), assuming Gp=1000 kg/m²s, and water-steam at 4.5 MPa and 450 K are $5.8 \cdot 10^{-4}$. Boiling number values Bo at the instability threshold for experiments in which void fraction was generated only in the tube bundle are $13.2 \cdot 10^{-4}$ for Gp= 420 kg/m ^{2}s and $8.7 \cdot 10^{-3}$ for Gp=250 kg/m ^{2}s.

Since boiling numbers in the nuclear steam generators are lower than the ones used in these experiments, the void fraction produced on the tube surface compared to the total

void fraction at the tube location should also be lower. Hence, the effects of boiling observed in these experiments are expected to be greater than those in steam generators.

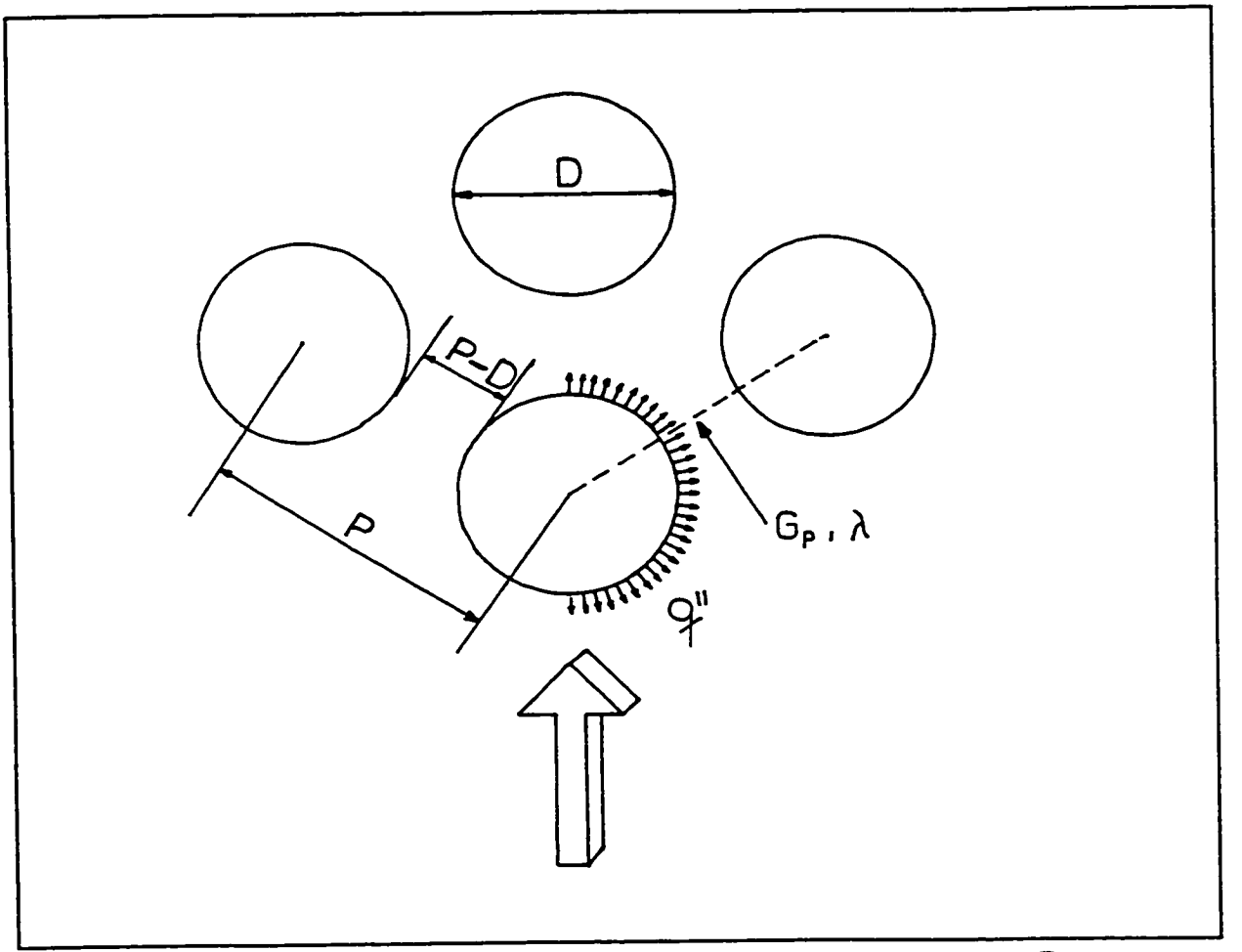

Fig. 3.1 Schematic to illustrate the physical meaning of the Boiling number Bo.

Parameter	Definition or simbol	Steam Generator	Pettigrew et al. (1989)	This study (estimated)
Temperature (°C)	T	260	22	40
Pressure (kPa)	P	4500	101	154
Mass damping (MDP)	$2\pi\zeta_T m_T/\rho_H D^2$	N/A	38.3-0.49	1.00-5.7
Reduced velocity (V_R)	Vp/f D	13-24	6.31-2.85	2.63-11.7
Mass flux (kg/m2s)	Gp	800-1000	28-750	90-424
Void fraction	α	0.82-0.90	0.99-0.25	0.95-0.25
Pitch ratio	P/D	1.3-1.5	1.47	1.488
Mass ratio	$m_T/\rho_H D^2$	21-35	209-3.9	35.8-5.5
Tube damping (air)	ζ(%)	0.16-0.45	0.2	0.2-0.4
Density ratio	ρ_L/ρ_G	34	833	132-180
Kinematic Viscosity ratio	ν_L/ν_G	0.17	0.07	0.19
Surface tension (N/m)	σ	0.0246	0.073	0.017
Boiling number	Bo	$5.8\ 10^{-4}$		$13.2\text{-}87.0\cdot10^{-4}$

Table 3.1 Summary of scaling parameters, physical properties and operating conditions for steam-water mixtures, air-water and Freon-11.

CHAPTER 4

EXPERIMENTAL TEST RIG

This chapter has been divided into four sections: Flow Loop Characteristics, Tube Bundle Design, Data Measurement Techniques and Experimental Procedures. Most of the emphasis in the chapter has been concentrated on recent changes in the test loop control and instrumentation and also on new techniques for the data acquisition procedures.

4.1 Flow Loop Characteristics

The description of the flow loop has been divided in three parts: Main Components, Instrumentation and Test Section.

4.1.1 Main Components

Figure 4.1 shows a schematic of the flow loop and its main components. The main pump (1) circulates the working fluid Freon-11 (Trichlorofluoromethane) through the piping in the flow loop. This pump is a gear type with a pumping capacity of 1.6 l/s, which is equivalent to a mass flow rate of $m = 2.4$ kg/s, corresponding to a mass flux $Gp=713$ kg/m^{2}s and a pitch velocity of $Vp = 0.48$ m/s through the test section (T) where the tube bundle is positioned. However, since some of the Freon flow is diverted from the main line

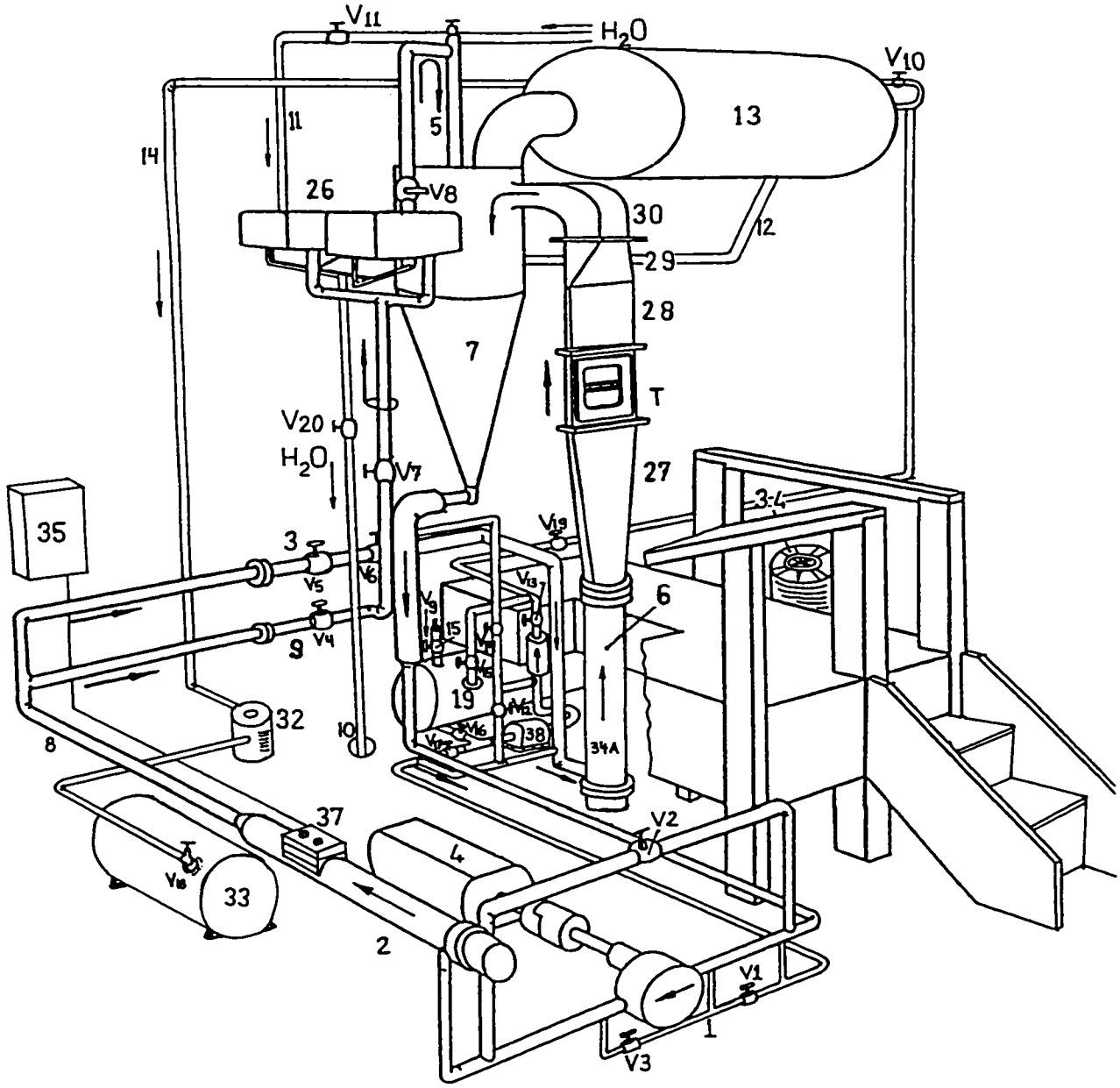

Figure 4.1 Flow loop.

(8) to the cooling line (9) for the purpose of condensing the Freon vapour, the maximum achievable mass flux in the test section is Gp= 472 kg/m^{2}s.

The maximum attainable speed of the pump is 1750 rpm, but a speed of only 1100 rpm was utilized due to the current limitation of the motor (4), which is 6.6 amperes for continuous operation.

After the main pump, the flow goes to the pre-heater (2) which was not used, and then branches to the main line (3) and the cooling line (9). The main line is a copper pipe 1.625 inches in diameter that runs to the main heaters located at the bottom part of the test column (6). The main heaters (34A) are comprised of tubular electric heating elements with a maximum nominal capacity of 48 kW, which are supplied by a Variac (34). However, under the present configuration, these heaters can only deliver up to 19.2 kW, which is enough to produce up to 99% void fraction values at the test section (upstream edge of the tube bundle) for the maximum mass flux allowed in the test section (472 kg/m^{2}s). For details of the heating element configuration see, Feenstra (1993).

Freon-11 is boiled during its passage through the main heaters, producing a two-phase flow mixture which moves upwards into the transition section (27). This section connects the 6 inch diameter steel pipe in which the heaters are installed to the test section (T) in which the tube bundle is positioned.

After passing through the test section, the two-phase flow goes into the straight section (28), the expansion section (29), and then the curved section (30), falling by gravitation into the condensation tank (7) where it is cooled down by the Freon flow (5) coming from the heat exchangers (26).

The Freon cooling line (9) is a 1.25 inch diameter copper pipe that runs to the tube side of the heat exchangers (26), where its temperature is decreased by the municipal water cooling flow on the shell side. In general, the cooling water supply (11) flow and temperature are adequate for most times of the year, but in the summer time and the two months after that , the warmer temperature of the water imposes some difficulties on running experiments at high mass fluxes (Gp over 400 kg/m^2s) and high void fraction values (Feenstra, 1993). The consequence is an increase in the operating pressure of the loop, which approaches the loop maximum operating pressure of 25 psig.

The Freon cooling flow enters into the condensation tank through a vertically positioned copper pipe containing numerous small orifices, in order to introduce a spray of cool Freon liquid into the Freon vapour coming from the test loop column. After the vapour is condensed, the Freon liquid flow returns to the main pump. The cooling water flow is directed to the drain (10) after passing through the heat exchangers.

The holding tank (19) is connected through piping to the bottom part of the loop column. A gear pump (38), located between the two is used to pump Freon-11 to and from the holding tank and the flow loop through the proper settings of the valves located in the piping (V12, V13,V14,V15,V16,V17,V19) . A filter (39) is also located in the return line from the loop to the holding tank to trap small particles which might be present in the fluid.

The expansion tank (13) located at the top of the test loop column is intended to assist the condensation tank in converting vapour into liquid, and to trap and contain non condensible gases, such as air, that may have found their way into the system. The expansion tank is connected to the condensation tank through a 0.5 inch diameter copper pipe (12) through which the liquid Freon returns by gravity. This tank is also connected to the vacuum system through a high pressure hose (14).

The vacuum pump (32) extracts gases from the expansion tank (13) and stores them in the pressure container (33). These gases are a mixture of air and Freon vapour. When the container reaches its maximum pressure, it is taken outdoors in the winter and allowed to cool down to the ambient temperature; in the summer, the container is submerged in an ice bath. Since the vapour pressure of Freon-11 below 10°C is very low compared to the air pressure at the same temperature and pressure, most of the Freon ends up in a liquid state. In this condition, the valve of the tank is opened slightly allowing the air to escape to the

atmosphere. Freon collected in the tank is pumped by gravity back into the holding tank through a hose connected to the chamber installed at its top (15).

The electrical controller (35) controls the electric power to the motor (4) of the main pump whose speed is controlled by a Variac rheostat (37).

The flow loop has 20 controlling valves, the function of which are described below

V1 & V3: Main pump by-pass valves used for flow loop drain.

V2 Main pump by-pass and air/vapour trapped release.

V4 Freon cooling flow.

V5 Freon main flow.

V6 Freon flow (main line) pressure drop regulation.

V7 Freon flow (cooling line) pressure drop regulation.

V8 Freon cooling flow between the heat exchangers and the condensation tank.

V9 Holding tank inlet for the addition of clean Freon.

V10 Vapour extraction from the expansion tank to the vacuum pump..

V11 Water cooling flow from the municipal pipe line.

V12 Isolation valve from the test loop to the charge pump .

V13 Freon filter isolation valve.

V14 Freon flow from charge pump to Freon cooling flow.

V15 Isolation valve from holding tank (inlet)

V16 Isolation valve from holding tank (outlet)

V17 Isolation valve between charge pump and main line.

V18 Vacuum system storage tank.

V19 Equalization pressure between holding tank and expansion tanks.

V20 Water cooling flow control valve.

4.1.2 Instrumentation

Thermocouples Location and Temperature Measurements

Table 4.1 lists the thermocouples in the flow loop that were used in this study.

Thermocouple. #	Type	Sensing parameter
1	E	Liquid Freon, downstream of bundle
2	E	Liquid Freon, downstream of main heaters
3	E	Brass at tube fixing plate.
4	E	Cooling water exit from heat exchangers
5	E	Liquid Freon, upstream of main heaters
6	E	Cooling water inlet to heat exchangers
7,8,9	E	Electric heaters, half power
10,11,12	E	Electric heaters, full power
B1	K	Most downstream tube core (mid span)
B7	K	Most upstream tube core (mid span)
		E= Chromel-Constantan, K= Chromel-Alumel

Table 4.1 Thermocouple locations in the test loop.

All type E thermocouples were monitored by a Philips PM8237A thirty channel temperature recorder. The recorder provided over-heating protection for the heaters (thermocouples 7 to 12) in the event of a dry out crisis. (Feenstra, 1993). The recorder precision is 0.01 mV, which is equivalent to 0.3°C for E type thermocouples (Feenstra, 1993, B7).

Temperature data from thermocouples 1, 2 and 5 were used to obtain the physical properties of the Freon-11 fluid and vapour for thermodynamic and flow calculations involving density, enthalpy, mass flux, quality and void fraction.

Thermocouple 3 was used to monitor the tube fixing region. The objective was to prevent high temperature in the region that might lead to a higher than normal tube structural damping ratio for those cases in which boiling was occurring at the tube surface (see Appendix A). Thermocouples 4 and 6 were used to perform heat rejection calculations, which were necessary to make changes in the cooling flow which required specific conditions of temperature and pressure to be obtained in the test section.

Two tubes, B1 and B7, located at the upstream and downstream edges of the tube bundle were equipped with thermocouples installed in the core at the mid span of the tubes. These thermocouples were intended to warn the loop operator about a possible tube burn-out due to boiling crisis. A typical value of the temperature at the mid-span core of tube B1 under full bundle power and Gp=250 kg/m^2 s was 80.7°C. For the same conditions temperature of the fluid was 41° C. This indicates that the thermal conductivity of the cartridge heating element was reasonably high.

Manometers and Pressure Gauges.

The flow loop U-tube manometers (U) and pressure gauges (P), which are an integral part of the measuring and control system are described below:

Sensor #	Type	Location	Measured Parameter
1	U	Freon-11 main line	Flow rate through test section
2	U	Freon secondary line	Flow rate through heat exchangers
3	U	Cooling water line	Water flow through heat exchangers
4	U	Test section	Gauge pressure of loop when out of operation
5	D(P)	Main & secondary lines	Duplication of 1 & 2
6	P	Test section	Pressure at operating conditions
7	P	Downstream of main Freon pump	Flow pressure
8	P	Upstream of main pump	Flow pressure
9	P	Vacuum tank	Freon storage tank pressure

Table 4.2 Manometers and pressure gauges.

4.1.3 Test Section

The test section (T) has an interior rectangular cross section 305 x 31.8 mm (12 x 1.25 inches). A more detailed schematic is shown in figure 4.2. The test section is constructed from aluminum plate 0.75" thick. The front and the back windows are glass

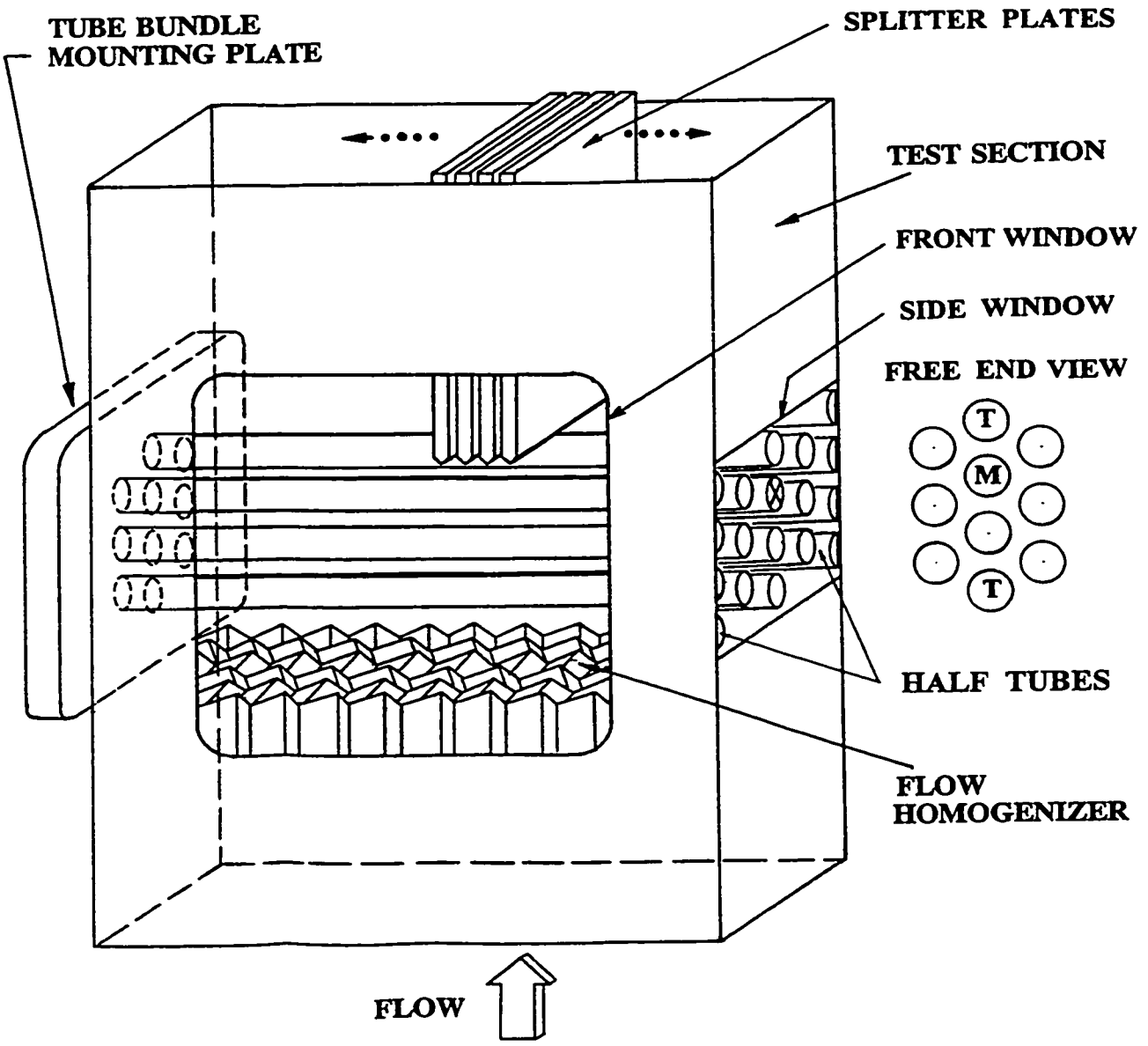

Figure 4.2 Test section

0.75 inch thick. The side window is used for flow visualization and tube vibration measuring purposes. Plates are installed upstream of the bundle with a particular geometry capable of homogenizing the void fraction distribution in the two-phase flow entering the test section. Downstream of the bundle, there are splitter plates 16.25 inch long intended to prevent a sudden decrease in the pressure drop after the bundle. The potential consequences of this effect are that the two-phase flow downstream of the bundle would produce unstable recirculation flows which would have an unpredictable effect on the fluid flow in the bundle and hence its vibrational response, (Feenstra, 1993, Appendix C).

The tube bundle is installed between the splitter plates and the flow homogenizer. A gap of 0.5 inch exists between the most upstream tube in the bundle and the homogenizer and a 0.25 inch gap exists between the most downstream tube in the bundle and the splitter plates.

There are 8 half tubes attached to the inside walls of the test section, four on each side of the bundle to maintain geometrical continuity of the tube array and prevent wall effects from influencing the fluid flow through the tube bundle (see also figure 5.5).

The tube bundle depicted in figure 4.3 was provided with a cooling system to prevent overheating of the region where the tubes (1) were attached to the fixing plate (2). The

objective was to maintain a temperature in that region that would not produce an increase in tube structural damping ratio as had been observed in a separate study of this investigation. The results of that study are reported in Appendix A. The cooling system was a fan installed to blow air in the gap (8) between the electrical box (5) and the fixing plate (2). In addition, a thermocouple identified as 3, in figure 4.4, was installed in the interior of the fixing plate in the vicinity of the monitored tube with the objective of obtaining temperature measurements at each trial.

4.2 Tube Bundle Design and Specifications

4.2.1 Main Components

The 10 solid tubes (1) depicted in figure 4.3 are arranged in a parallel triangular configuration with a pitch to diameter ratio P/D of 1.49. The fixing plate (2) is held against the test section through four screws (3). The fixing block (4) compresses the ferrules which hold the tubes in the fixing plate. The electric box (5) allows for the connection of electrical cables to the tubes through the connector (6). The rubber O ring (7) seals the fixing plate with respect to the test section.

Tubes were arranged in 7 rows and 3 columns. To be able to produce nucleate boiling at the tube surface and hence generate void fraction within the bundle, the tubes were actually electric cartridge heaters nominally 1/4 inch diameter by 13.25 inches long custom

made by Watlow Incorporated, St. Louis, Missouri, and purchased from Zesta Engineering Limited, Mississauga, Ontario.

The heaters had a nominal power rating of 650 W at 240 DC Volts with a maximum current rating of 2.7 Amperes. Two types of cartridge heaters were used in the bundle, the standard E13EX6A 9506 and the special SE1-3EX-167. Eight of the tubes were of the first type. The remaining two tubes, located in the most upstream and the most downstream positions in the central column of the test bundle, were of the second type, having a K type thermocouple installed at the midspan of the tube.

4.2.2 Fixed End Tube Design

Due to the fact that tubes were made of Incoloy 800, they could not be threaded or welded to the fixing block. Instead, a novel fixing system based on the use of ferrules was devised. Figure 4.4 shows the way in which the tubes were fixed with respect to the supporting plate . The fixing block (4) (detail A) had recesses machined in it to contain the nylon ferrules (1) by which each tube was fixed against the fixing plate (2) in order to compress the ferrules. Four screws (5) fixed the block against the plate. The fixing block was provided with slightly oversized holes to allow the tubes to vibrate in a cantilever fashion from their fixing point in the fixing plate (2). Thermocouple (3) was installed to monitor temperature at the tube fixing region. To confirm that the tubes would not remain

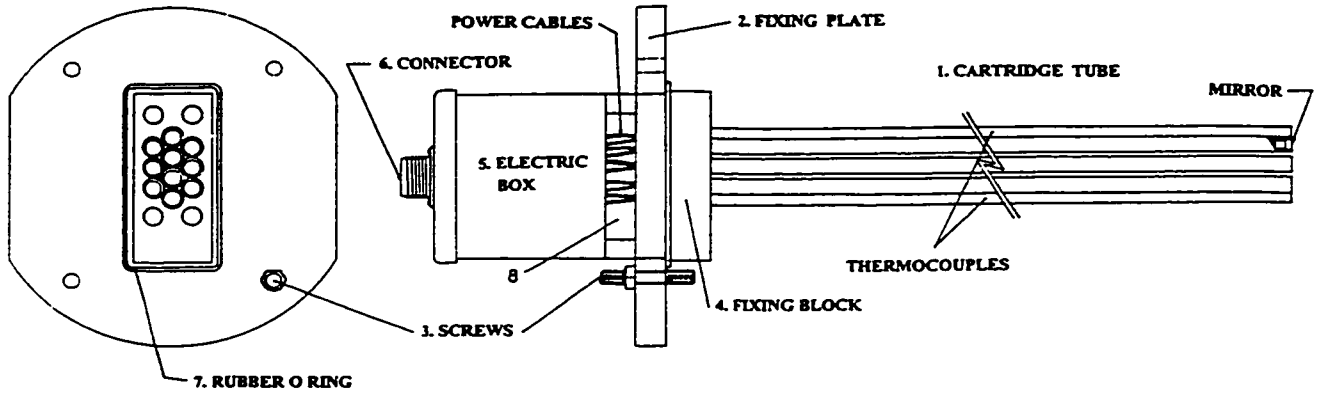

Figure 4.3 Tube bundle design

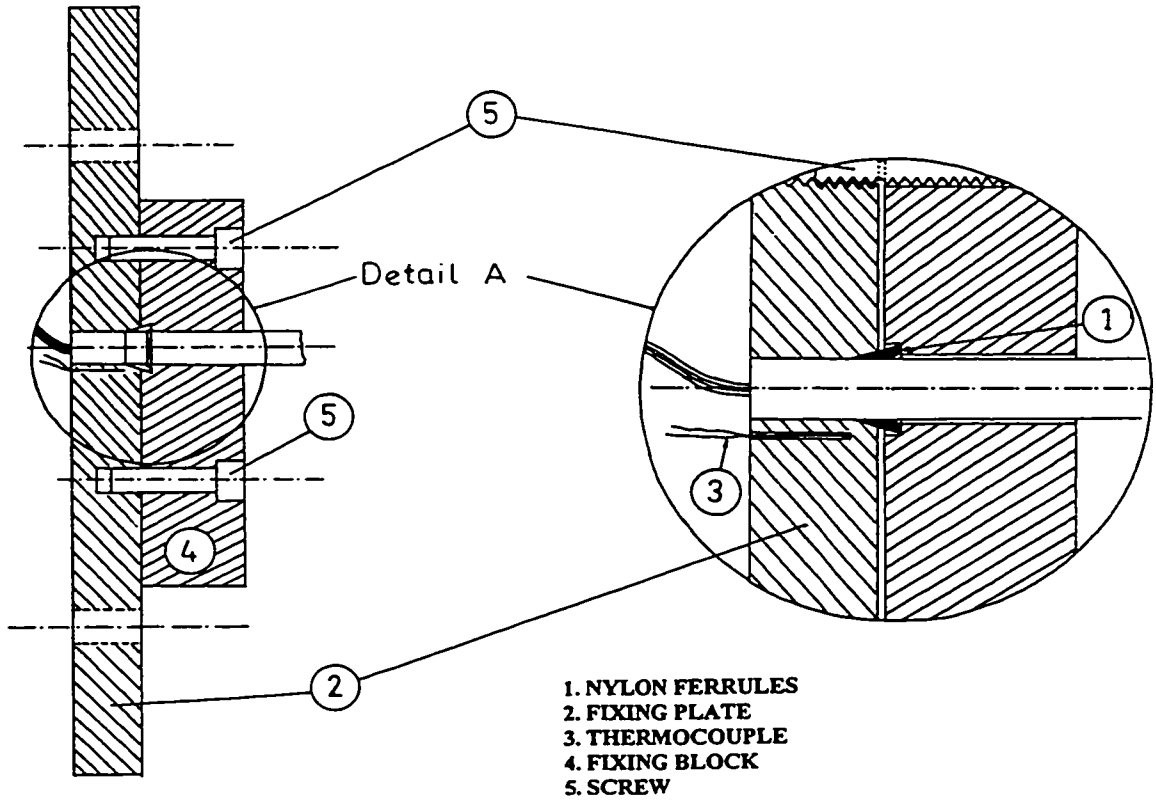

Figure 4.4 Tube fixed end design

in contact with the fixing block after the bundle was assembled and therefore affect their vibration response, a wire with the diameter equal to the gap dimension between the tube and the fixing block was inserted in each gap and moved circumferentially around the tube.

4.2.3 Free End Tube Design.

Because the tubes were solid, the tube vibration measurement technique had to be changed from that used by Feenstra (1993), (see also section 4.3.1 this thesis). The new design involved the inclusion of a mirror (4) at the free end of the tube and a fine frequency tuning mechanism based on weight addition at the tip of the tube. The tubes had a special design at the free end, which is depicted in figure 4.5. The solid cap (2), after being welded onto the tubular cartridge heater (1), was machined to obtain a fine finished surface and then drilled and tapped to accommodate the screws (3). The screws had the purpose of increasing the mass at the end of the tube and hence decreasing the natural frequency of the tube. The maximum natural frequency of the tube was achieved in the absence of any screw. The number of screws (one or two) in the chamber would produce a decrease in the tube natural frequency. In this way, it was possible to fine tune the full bundle within 1.3 % of the bundle frequency mean value.

The mirror (4), which was glued with epoxy into the cap, was a first surface mirror, 2 mm thick and 5 mm in diameter, purchased from Efton Science, Toronto.

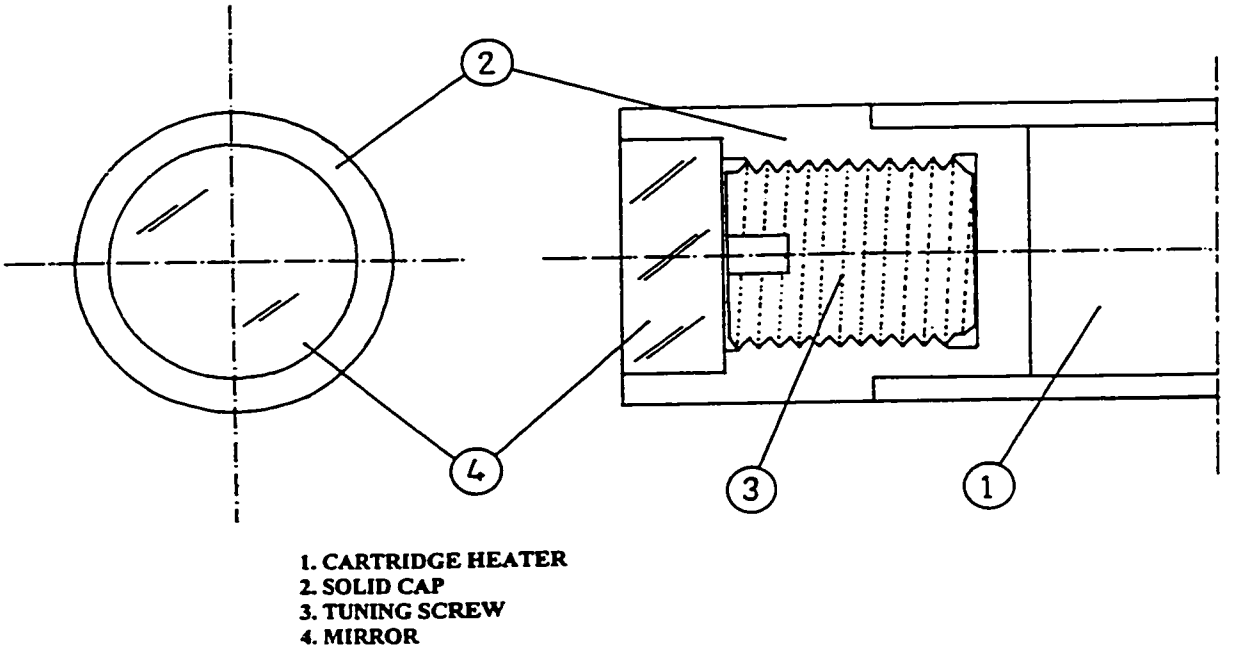

Figure 4.5 Tube free end design.

4.2.4 Tube Bundle Specifications

Tube bundle specifications are given in table 4.3. Most of the parameters included in the table are self-explanatory. In the case of the tube natural frequency, the unit cell has been defined as the 6 tubes surrounding the monitored tube and including the monitored tube.

Although all tubes were intended to be instrumented, due to travel limitations on the displacement of the optical vibrometer installed at the side window of the test section, only the tubes in the central column of the test bundle could be monitored in practice. In addition, tubes C2 and C4 (see figure 5.7) had to have their mirror replaced by a solid lead disc to reduce their natural frequencies to acceptable levels.

Tube bundle specifications	
Fixing conditions	Clamped-free (cantilever)
Geometry configuration	Parallel triangular
Number of tubes	10 (4 tubes instrumented)
Tube pitch	9.16 mm (0.361 “)
Tube diameter	6.17± 0.01 mm
Number of tube rows and columns	7 by 3
Tube length (total)	338.33 mm (13.32 in.)
Tube length (cantilevered)	325.63 mm (12.82 in.)
Tube material	Incoloy 800
Tube wall thickness	0.375 mm (0.015 in)
Tube mass per unit length	0.121 kg/m
Frequency in air (unit cell)	39.29 Hz ± 1.1%
Frequency in air (bundle)	39.50 Hz ± 1.3%
Frequency in Freon-11 (liquid)	29.25 Hz (monitored tube, B3)
Damping ratio in air	0.2-0.4% at 22°C and 2%TD amplitude

Table 4.3 Tube bundle specifications.

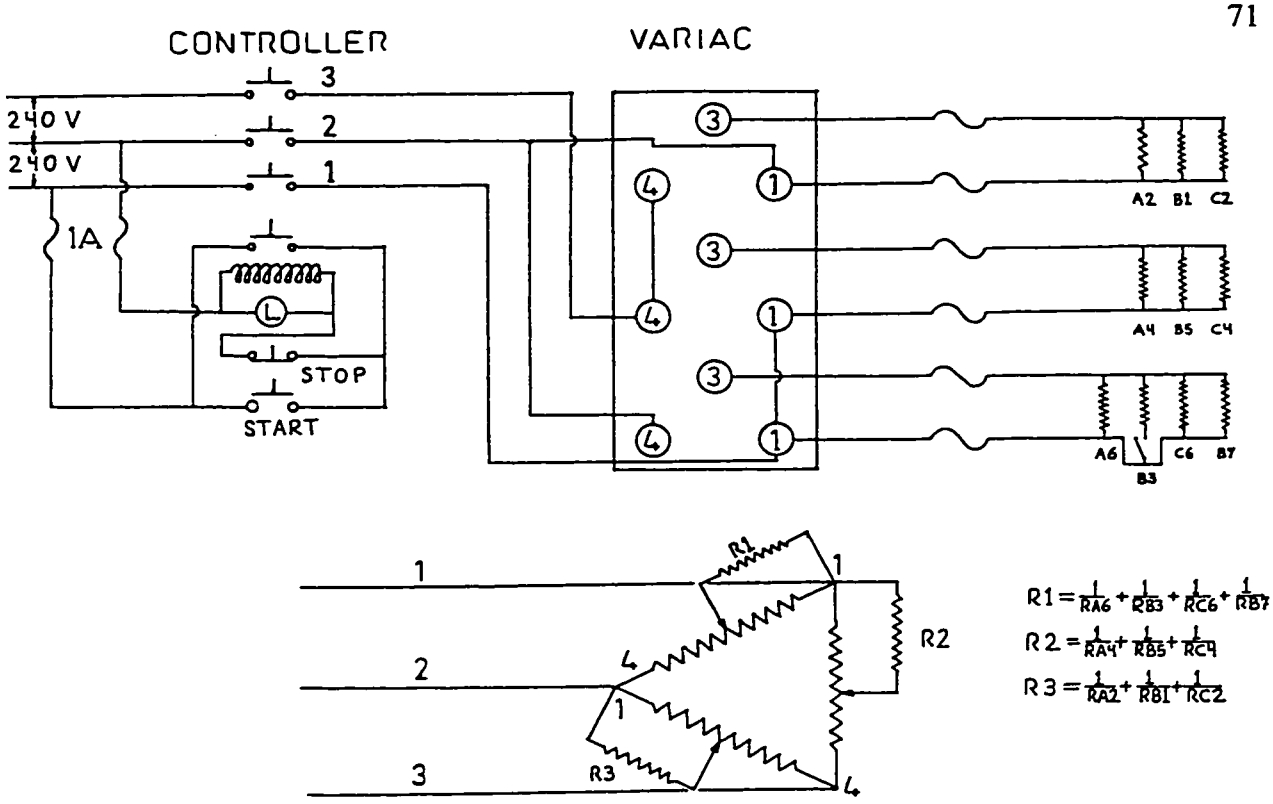

Figure 4.6 Power connection to cartridge heaters

4.2.5 Power Supply to the Bundle

Tube cartridge heaters were electrically connected in series in two groups of three and one group of four. Figure 4.6 depicts the electrical connections, the controller and the three phase Variac which supplied the power to the tubes. The Variac established a voltage range between 0 and 240 V. In order to perform some specific experiments, a switch was added to the system so that power to the monitored tube (B3) could be turned on or off without turning off the power to the rest of the bundle.

4.3 Data Measurement Techniques

Although experiments required the recording of several parameters such as temperatures and pressures, the most crucial measurements were tube vibration and void fraction, which are described in this section.

4.3.1 Tube Vibration Measurements

Due to the fact that the tubes used in this investigation were solid electric cartridge heaters, it was not possible to use the technique involving an optical fibre running through a hollow tube (Feenstra, 1993). Instead, a different optical technique had to be developed.. Figure 4.7 (a) shows a photograph of the apparatus. The system is comprised of a light source (2), four photo detectors (4), a nosepiece (5), a translating stage (6), and a plastic box containing the electronic circuit. The concept is described in Robinson et al. (1996).

The four phototransistors MRD200(4), were installed into the nosepiece (5) , where a light emitting diode (LED, MT4000-UR) was located at the centre. The nose piece was fixed to a tube (7), which was mounted in the XYZ translating stage. The Z stage moves the nosepiece in the direction parallel to the tube axis, and the X and Y stages move the nosepiece in orthogonal directions parallel to the surface of the mirror (perpendicular to the tube axis). A circular light beam is emitted from the LED source (2) situated in the centre of the photo sensing array. The light beam passes through the test section side window and

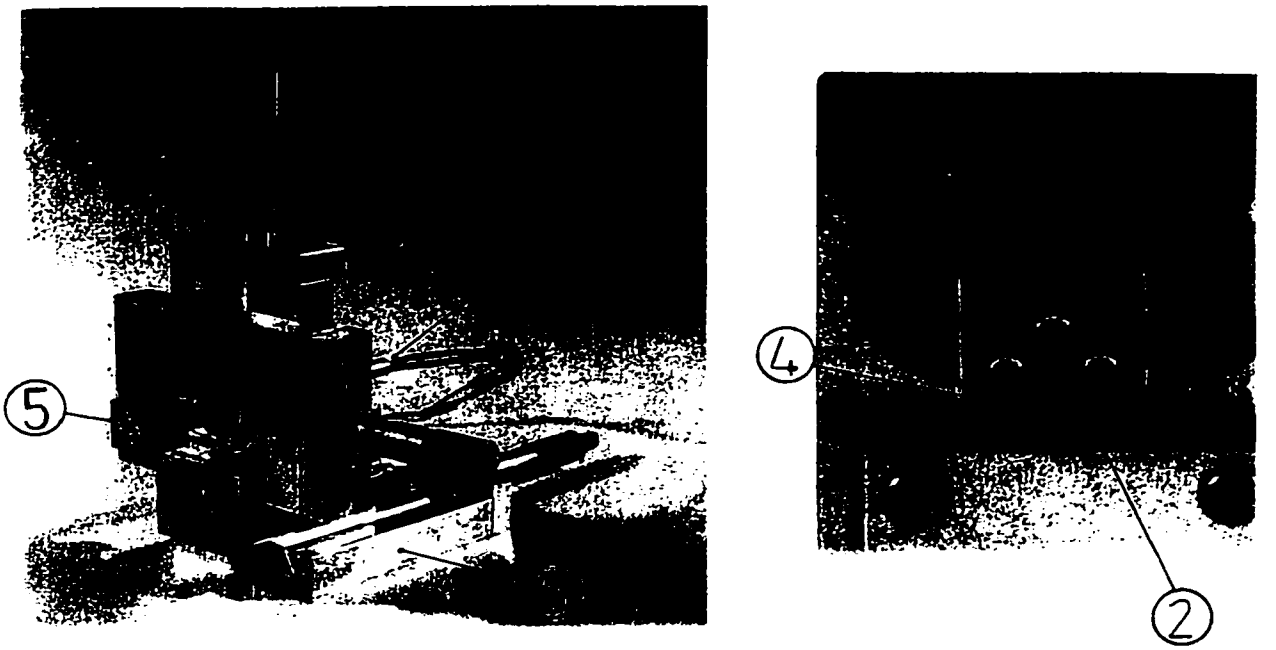

(a)

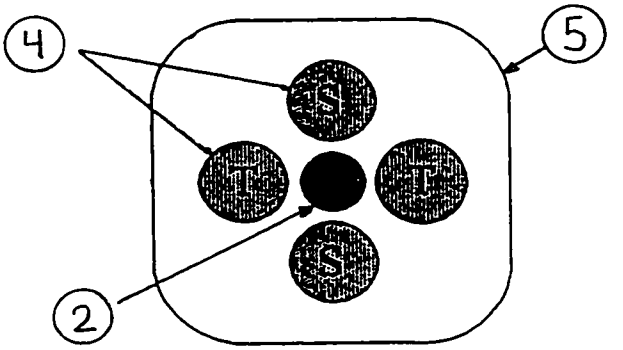

(b)

Figure 4.7 The vibrometer a) The XYZ translating stage and optical nosepiece
b) View of light source and photosensing array.

impinges on the mirror mounted at the tip of the tube. This light is then reflected back onto the photo sensors . The reflected light beam can be considered as concentric rings of uniform light intensity with the intensity decreasing radially from the centre. For a given direction, streamwise or transverse, the output voltage signal responds to the difference in total light power impinging on two opposing transducers. If the reflected light spot is exactly centred on the photo sensors, the total power impinging on each of the transducers is equal and hence the differential output voltage is zero. In this case, the concentric rings will be similar to the ones shown in figure 4.8 centred on the LED source. A small relative displacement of the light beam due to a deflection of the tube tip results in unequal light intensity falling onto the photo sensors. For two identical sensors with the same receiving area, this produces different output voltages from the photo sensors. Hence, a differential voltage signal is generated which is proportional to the tube tip displacement as depicted in figure 4.8.

Figure 4.9 depicts the electronic circuit of the system, comprised of the LED source (1), the four photosensors (2), the constant electrical resistors (3), the variable resistors (4), the amplifier (5) and the power supply (6). Values for the variables resistors shown in the circuit were: TR1=2496Ω, TR3=1005Ω, SW2= 2246Ω, SW4=1150Ω. Through adjustment of the variable resistors, it was possible to compensate for differences in photosensor sensitivity in the vibrometer, so that the voltage output from the vibrometer per unit of tube tip displacement was the same for both directions of tube motion.

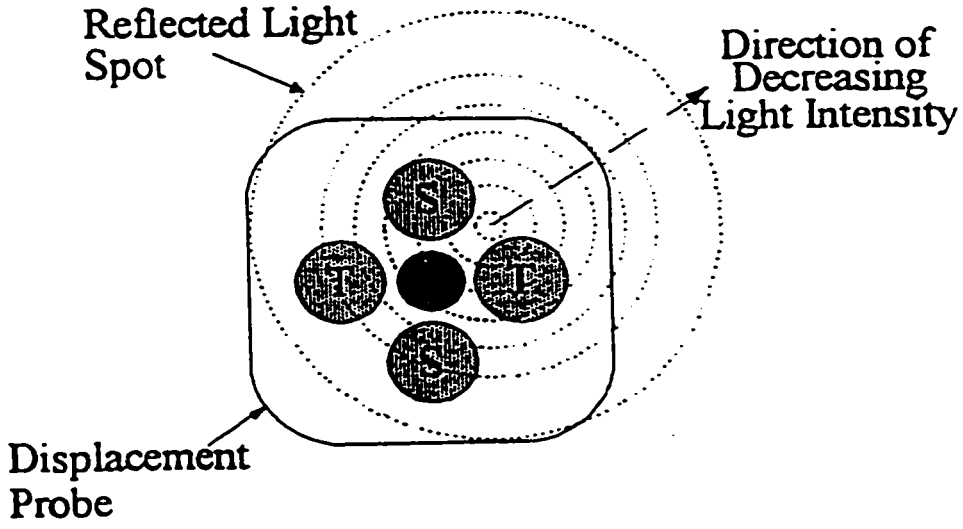

Figure 4.8 Relative motion of reflected light spot due to tube tip displacement

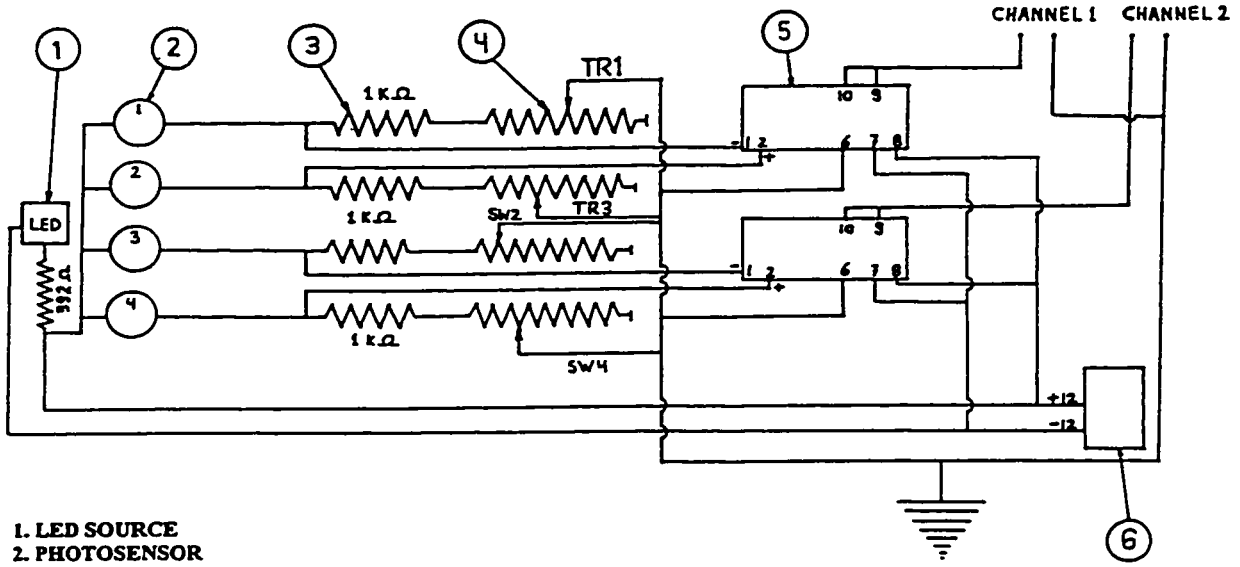

1. LED SOURCE
2. PHOTOSENSOR
3. CONSTANT RESISTOR
4. VARIABLE RESISTOR
5. SIGNAL AMPLIFIER
6. POWER SUPPLY

Figure 4.9 Optical vibrometer signal processing circuit

Figure 4.10 shows the calibration curves used for both the streamwise and transverse directions obtained with the system installed outside the test section. Whether the calibration was performed with the optical system installed in the test section or on the bench, the calibration procedure was the same. The graph shows that vibrometer voltage output in both directions is proportional to the relative motion between the nosepiece and the tube, up to a value of about 15% of tube diameter. The curves in figure 4.10 were obtained by first positioning the nosepiece at the centre of the tube, for which the output voltage was zero (0.000 ± 0.001 V) in both directions (X and Y). Then the nosepiece was displaced by known increments, along one axis (X or Y) with the other axis (Y or X) held fixed at the zero displacement position.

The dynamic response of the optical system was evaluated by placing a high precision accelerometer at the free-end of the cantilevered tube. Voltage signals from the accelerometer and the optical vibrometer were captured by the FFT analyser. Both signals gave the same tube vibration frequency (Robinson et al.1996) and the same frequency spectrum.

In calibrating the optical probe, it was assumed that during the dynamic displacement of the tube tip, the surface of the mirror remained perpendicular to the impinging light beam, whereas in reality as the tube was deflected, the plane of the mirror tilted relative to

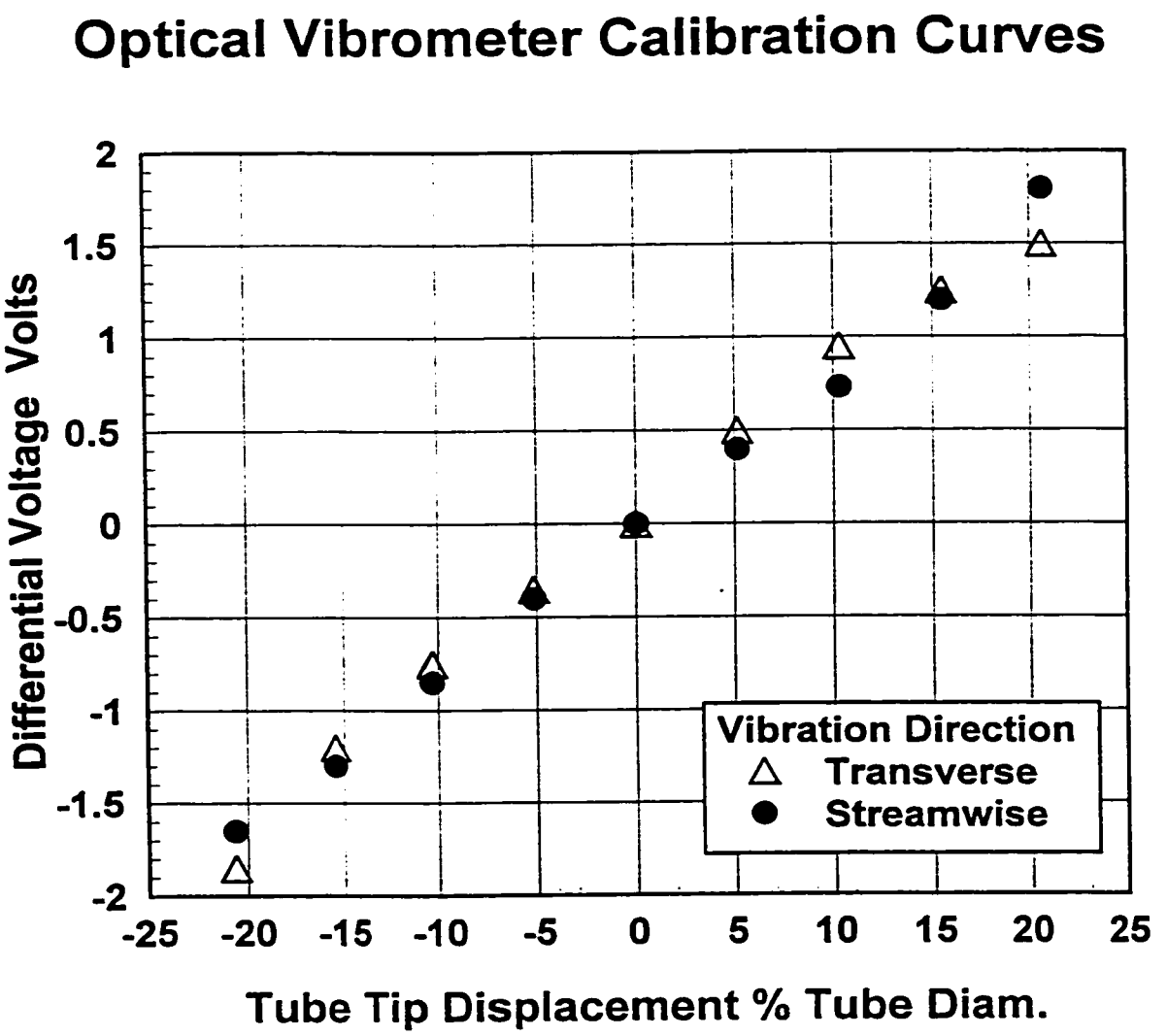

Figure 4.10 Optical vibrometer calibration curves

the stationary optics plane. Some preliminary measurements obtained by displacing the tube instead of the nosepiece indicated that when the distance between the nosepiece and the tube was less than or equal to 0.75 inch (aproximately the glass thickness), the maximum error was less than 6% of the full voltage scale. This error is similar in magnitude to that predicted by Judd et al.(1992).

The range of linearity between the voltage signal and tube displacement defines the maximum amplitudes that can be measured confidently with this technique. Currently, the linear range is approximately 15% of the tube diameter (D). Previous experimental studies (Feenstra, 1993) showed that RMS tube amplitude values rarely exceeded 10%D and that tube to tube clashing occurs at a tube vibration amplitude of 24%D.

The results of a computer program indicated that the size of the light spot impinging on the mirror had the same diameter as the mirror. Consequently, if the tube were to be displaced beyond 15% of its diameter , the light spot would fall partially outside the surface of the mirror. As a result, the amount of light that is reflected from the mirror onto the photo sensors would decrease, producing a decrease in the differential voltage output from the photo sensors. Although the use of a concave lens in front of the LED source produced a larger spot light, it reduced the light intensity impinging on the mirror surface. Since phototransistors respond to the total light power impinging on them rather than light

intensity, the signal produced using this technique was not increased. A more powerful LED source with a sharper angle of incidence would be the desired solution, but no LED with these characteristics was found to be commercially available. As a result, vibrations having amplitudes greater than 15%D cannot be detected with the precision desired. Fortunately, previous experimental studies (Feenstra, 1993) show that fluidelastic instability threshold is reached with a RMS tube amplitude of about 3%D or less.

Cross-Directional Sensitivity

When the optic vibrometer is being calibrated in one direction, the signal output of the opposite channel should ideally remain zero. To test the effect of the signal output in one direction on the signal output in the other direction, a simple test was performed. After centering the sensor array such that zero voltage was registering on both output channels, the stage was displaced to the full extent (15% of tube diameter) in one direction and reading of the voltage produced in the other direction was observed. Then this procedure was repeated in the other direction. It was found that the cross voltage variation did not exceed 2% of the full voltage signal in either direction.

The vibration signals generated by the vibrometer were captured by a data acquisition system, which consisted of a data acquisition board, DI-200 from Dataq Instruments,Ohio, a personal computer, a switch board and software packages for acquisition

and data post processing. The board had input and output I/O features for up to 16 single (8 differential) input channels with 12 bit resolution. Maximum frequency sampling was 83 kHz for one channel. Data obtained through the system was captured by WINDAQ/200 data acquisition package. Post processing of the data was performed using WINDAQ/EX software from the same company. Typical acquisition rates for the tube vibration signals were between 1000 and 1500 samples per second (Hz).

Fast Fourier Transformation of Vibration Data

In order to measure tube vibration in real time accurately and to perform experiments in two sessions run on different days, output (voltage) signals from the optical vibrometer were processed by a Fast Fourier Transformation Dynamic Analyser (FFT), which calculated the RMS amplitude and frequency spectrum in the frequency range from 0 to 100 Hz, in each vibration direction. The RMS amplitude was averaged over 75 samples (5 minutes). The data files generated by the FFT dynamic analyser were converted to ASCII files for data post processing. When performing an experiment run on different days, the power spectra from the FFT Analyser obtained in the first portion was used to reset the test loop in order to continue the experiment for the second portion.

4.3.2 Void Fraction Measurements

Gas-liquid two-phase flows are physically characterized by their void fraction value. Radiation absorption of a gamma beam is one of the most attractive methods of determining void fraction due to its non-intrusiveness and high reliability features . Gamma ray densitometry was used in this study to measure void fraction values of the two-phase Freon-11 flows passing through the test section at two different locations, upstream of the tube bundle and at the bundle location.

In previous investigations, such as those reported in Feenstra (1993), void fraction measurements were performed upstream of the tube bundle. In this study, void fraction values were needed at the monitored tube location. This was a consequence of the fact that void was being generated at the surface of the tubes. Since the void fraction at the monitored tube location in many experiments was a combination of the void generated upstream of the bundles (main heaters) and the void generated in the bundle (cartridge heaters located within the tubes), void fraction had to be known upstream and in the bundle (monitored tube) simultaneously , so that the contributions of each source could be quantified properly.

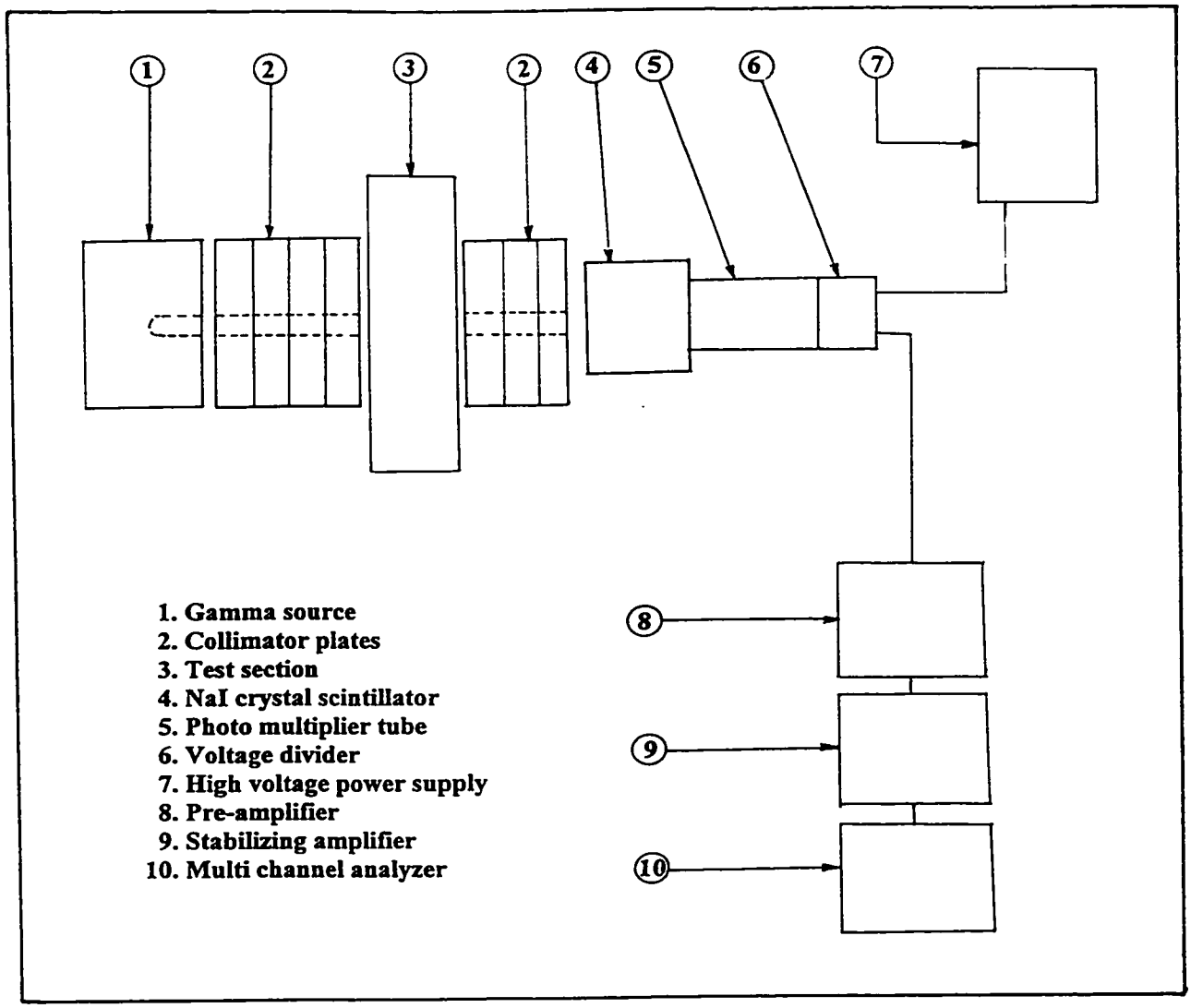

Figure 4.11 Schematic diagram of gamma densitometer setup.

Figure 4.11 shows a schematic of the gamma densitometry system as installed in the Freon-11 test section. The beam from the gamma source (1) goes through the open channel in the collimator plates (2) and then through the test section (3). At the other side of the test section, more collimator plates are located after the NaI crystal scintillator (4) which

transforms the gamma photons into electric charges is located. The photo multiplier tube (5) amplifies the electric signal from the scintillator. The voltage divider (6) classifies the electric charges according to their voltage and sends the signals to the pre amplifier (8) and the stabilizing amplifier (9). The signals then reach the multi channel analyser (10), followed by the PC acquisition system (not shown). The window of the gamma source was 0.5 inch high by 2.5 inches wide, centred at the monitored tube location.

Determination of void fraction values using the gamma absorption method is predicated on two basic conditions. The first is that a beam with intensity I_0 at the source (Ba 133), will be attenuated to a value of I after passing through a medium of thickness y and density ρ according to the following equation.

$$I = I_0 e^{-\eta \rho y} \qquad 4.1$$

where η is the absorption constant that characterizes the combination of the gamma source and the medium. The second is that two-phase density is defined by the Homogeneous Equilibrium Model (HEM) according to:

$$\rho = \phi \rho_G + (1 - \phi) \rho_L \qquad 4.2$$

where ρ is the density of the gas-liquid mixture, ρ_G is the density of the gas, ρ_L the density of the liquid and ϕ the HEM void fraction. When the first equation is applied to the test

section filled with Freon liquid, filled with Freon gas and filled with a combination of gas and liquid, the intensity of the beam at the opposite side of the gamma source in the test section is designated as I_L , I_G, I respectively. By combining the three resulting equations with equation 2, it can be shown that:

$$\alpha = \frac{Ln(I/I_L)}{Ln(I_G/I_L)} \qquad 4.3$$

The intensity I can be determined by the number of counts registered by the detector situated at the other side of the source. The counts are then turned into voltage and the voltage is measured using the data acquisition system. The use of gamma absorption has some restrictions which have been well described in Feenstra (1993). For further information on the subject, see Chan and Banerjee (1981).

An important question when determining void fraction is how the accuracy in the measurements affects the void fraction value. By taking the differential of α with respect to I, I_G , and I_L, an expression for the void fraction uncertainty $\epsilon(\alpha)$ can be obtained:

$$\epsilon(\alpha) = \frac{1}{\alpha\, Ln\frac{I_G}{I_L}} \sqrt{(\frac{\sigma_I}{I})^2 + \alpha^2(\frac{\sigma_{I_G}}{I_G})^2 + (\alpha-1)^2(\frac{\sigma_{I_L}}{I_L})^2} \qquad 4.4$$

where $\epsilon(\alpha)$ is the relative uncertainty in the void fraction value, I_G is the average counts or voltage for 100% void fraction, I_L is the average counts or voltage for 0% void fraction, σ_{Ii} is the standard deviation of I_i and I is the average counts or voltage determining the void fraction.

Table 4.4 shows typical values of $\epsilon(\alpha)$, for different values of α and two types of experiment, one with pure bundle boiling and one with pure upstream void generation. Voltage values were obtained by the data acquisition computer system for a time period of 300 seconds in each case.

Experiment	α	I_α	σ_I	$\epsilon(\alpha)$ %
Tube bundle void generation	α =19	4.34	0.013	9.6
	α =47	4.60	0.017	4.3
	α =67	4.82	0.014	2.6
upstream void generation	α =15	4.29	0.015	13.6
	α =30	4.44	0.025	9.5
	α =43	4.57	0.030	7.6
Exp. conditions: Gp=250 kg/m2s, I_{100} = 5.090 ± 0.015 V and I_0 = 4.120 ± 0.012V				

Table 4.4 Void fraction uncertainty for different void fraction values.

Calculation of void fraction using equation 4.3 does not take into account changes in the absorption of the gamma rays due to changes in density of the liquid Freon-11 as a

consequence of changes in temperature. When the calibration of the gamma densitometer was done for 0% void fraction and 100% void fraction, the fluid was at room temperature (22 °C). However, the liquid is less dense when the loop is running at its thermodynamic equilibrium condition. Since absorption of the gamma rays is sensitive to density changes, equation 4.3 had to be corrected to :

$$\alpha = \frac{Ln\left(\frac{\rho_{T_L}}{\rho_{T_0}}\right)^{1/2}(I/I_L)}{Ln(I_G/I_L)} \qquad 4.5$$

where the expression $(\rho_{TL} / \rho_{T0})^{1/2}$ was found empirically by calibration of the gamma densitometer at different liquid Freon temperatures with the tube bundle submerged in still fluid, ρ_{TL} is the fluid density at the test section temperature T, ρ_{T0} is the fluid density at room ambient temperature (22 °C).

Gamma Densitometer Transient Response

For no apparent reason, counts or voltage output of the gamma densitometer fluctuated after the equipment was turned on. Two experiments were performed in order to evaluate the gamma densitometer performance as a function of time. In the first, the gamma source was installed upstream of the bundle. The gamma densitometer was turned on and

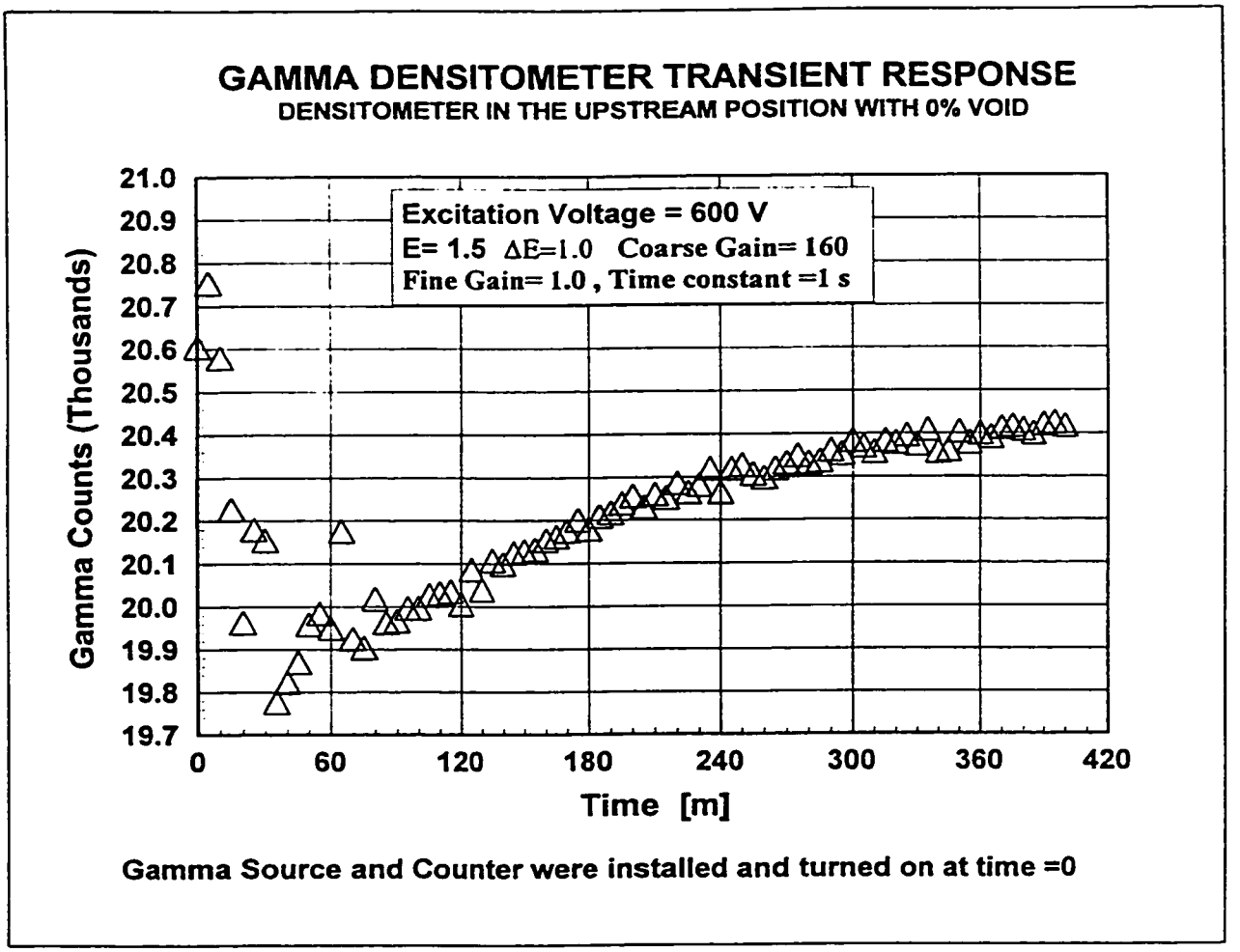

Figure 4.12 Transient response of gamma densitometer

the output (counts) was recorded every five minutes. Signals were recorded for a period of 400 minutes. Figure 4.12 shows the experimental results. On the vertical axis, the counts taken in 30 seconds divided by 100 are plotted against time in minutes on the horizontal axis. Although many attempts were made to unveil the source of this anomaly, no positive results were obtained. The graph in figure 4.12 shows an erratic response during the first 80 minutes with an asymptotic trend afterwards. The outcome of the experiment is that the gamma source and the densitometer had to be installed and turned on seven hours in advance of the commencement of any data measurements.

In the second experiment, the gamma source was installed at the tube bundle level. The results were identical to the ones described in the previous paragraph and shown in figure 4.12.

Gamma densitometer signals were sent to the PC data acquisition system at the rate of 100 samples per second.

4.4 Experimental Procedures

The general experimental procedure and flow loop operation have been described in previous investigations (Dam, 1991). For the sake of clarity, a brief description of the data acquisition procedures are described here.

After reaching the mass flux Gp and the initial void fraction α target values, the data acquisition software WINDAQ/200 and the FFT analyser were triggered simultaneously to take void fraction data and vibration amplitude measurements respectively for a period of five minutes. During this time, all six data temperatures from the recorder, the pressure reading in the main line and the secondary Freon line, the water cooling pressure reading, the pump speed, the power dissipated by the main heaters, the voltage reading at the Variac that supplied power to the tube bundle, the pressure reading upstream and down stream of the main pump, core temperature of the instrumented tubes and pressure of the test section were recorded. Figure 4.13 shows a schematic of the arrangement of the tube vibration amplitude and void fraction measuring equipment.

When the FFT analyser finished the acquisition of data, two FFT files (one for each vibration direction) were saved on a 3 ½ inch floppy disk installed in the analyser (each disk holds the data from only one experiment). The file from WINDAQ/200 containing the voltage readings from the gamma densitometer was saved on the computer hard disk and then accessed by the WINDAQ/EX software to obtain average void fraction and standard deviation values, which were written on the data sheet. After this, the power to the heaters (main or cartridge or both) were changed to different values to obtain a different void fraction or a different combination of upstream and bundle generated void fraction ratio.

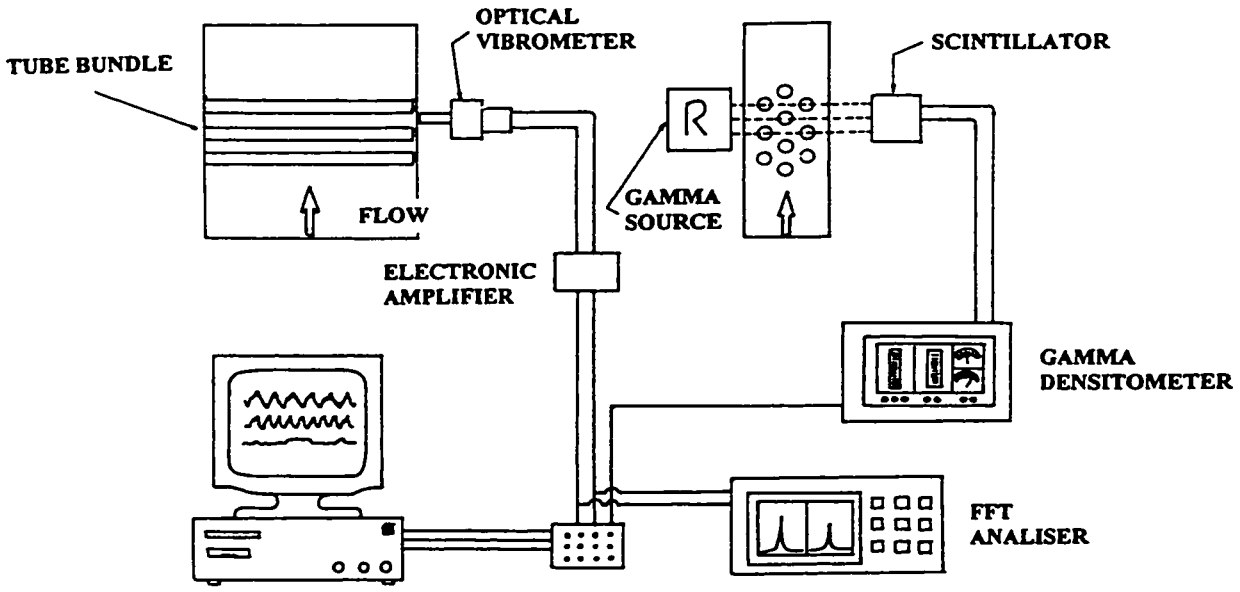

Figure 4.13 Data acquisition system for tube vibration and void fraction measurements

4.4.1 Upstream Void Generation Experiments

To be able to perform valid comparisons with experiments in which the void was generated in the tube bundle, gamma void fractions were measured in these experiments at the monitored tube location, instead of upstream of the bundle which is more customary. Void fractions values measured at these locations are different from each other due to the presence of the tube bundle, which produces a change in the slip ratio between the gas and liquid Freon phases. For more details see appendix C.

4.4.2 Bundle Void Fraction Generation Experiments

In these experiments, all the void was generated at the surface of the tubes in the tube bundle. In order to obtain a numerical value of the void at the monitored tube location, saturation conditions were established in the fluid by using the main heaters.

Another important issue in this case is the void fraction variation in the bundle in the flow direction, which changes from zero at the upstream edge of the bundle to the maximum value at the downstream edge of the bundle. The latter value is higher than the void fraction at the monitored tube location, due to the fact that the three tubes located downstream of the monitored tube contribute only partially to the generation of void that affects the monitored tube. The HEM void fraction at the monitored tube location was based on the full heat contribution of the six tubes located upstream of the monitored tube, the heat from the

monitored tube and the partial contribution of the three tubes located downstream of the monitored tube.

A special consideration had to be taken with respect to the cooling requirements at the fixed end of the tube bundle. As described earlier, a small fan installed at the exterior surface of the fixing plate was turned on at the beginning of the experiments and kept running during the entire duration. This technique permitted the tube fixing region to be kept close to the ambient temperature, in order to maintain the tube structural damping ratio within the acceptable range.

The core temperature of the tubes that were instrumented with thermocouples was monitored every time the power to the bundle was increased, especially when the power to the bundle went over 60% of maximum.

The void fraction intended in each trial was obtained by controlling the power to the bundle through adjustment of the voltage supplied to it. The time to reach steady state condition was longer than in the upstream case and a minimum of one hour was allowed for the loop to reach this condition, identified by the appearance of invariant readings of the temperature recorder (less than 0.5% variation in five minutes).

In order to obtain the desired void fraction value at the monitored tube, the power to the bundle was increased. This, however, would produced an overall increase in the pressure and temperature of the test loop, provided that the water cooling flow through the heat exchangers and the Freon secondary line flow were not changed. An increase in the fluid temperature would reduce the heat needed for the fluid to reach the saturation condition at the location of the main heaters. If the heat dissipated by the main heaters were to remain constant, a heat surplus would be produced, which would be spent in the generation of void. Therefore, to maintain the conditions of fluid saturation and zero void content upstream of the bundle the power to the main heaters had to be reduced.

Whenever the temperature of the cooling water permitted, the water cooling flow was increased to compensate for this effect, so that only small changes in temperature and pressure would occur in the test loop, which in turn drastically reduced the time needed to reach the steady state condition.

4.4.3 Combined Void Fraction Generation Experiments.

Experiments of this kind were more complex than the previous experiments, due to the difficulties in controlling the contribution of void fraction from upstream and from the bundle in the desired proportions. The difficulty was mainly due to the effect that each void contribution had on the other source. When these experiments were conducted, two types

of void fraction conditions were established. Initially, the power to the bundle was set at a constant value and the power in the main heaters was changed. After obtaining the initial conditions at the first trial, the power to the main heaters was increased in each subsequent trial. As a consequence, the void fraction generated from upstream was increased in each trial. Since flow was already saturated at the entrance of the bundle all power rejected in the bundle was converted into vapour generation and since the power dissipated by the tube bundle was constant, so was the void fraction generated in the bundle. However, since the void fraction produced upstream was increasing at each trial, the relative contribution of this void to the total void at the tube location was also increasing.

A more complex approach was to maintain the ratio of the void generated in the bundle with respect to the total void fraction at the monitored tube location constant. To achieve this condition, adjustments of the power at the main heaters and at the bundle had to be made at each trial. Since the power in the bundle affected the values of the void generated upstream, the process of achieving the void fraction ratio at each trial was a lengthy and cumbersome process guided by trial and error in which consecutives steps of finer adjustments in both powers were required.

Some experiments of this type were performed at a constant value of void fraction at the monitored tube location. This approach was used to compare the effect that each type

of void generation had on the tube vibration response. With this technique, an evaluation of the equivalence between the void fraction generated in the bundle and the void fraction generated upstream could be achieved.

4.4.4 Intermittent Boiling Experiments

The objective of the intermittent boiling experiments was to examine instantaneous amplitude tube response versus instantaneous void fraction values at the monitored tube location. To achieve this purpose, the flow loop was operated under the normal conditions for an upstream void fraction generation experiment, and once a specified set of conditions had been achieved, continuous readings of tube vibration in both directions and the gamma void fraction at the tube location were measured simultaneously by the data acquisition system. The power to the tube bundle was then turned on and off at intervals of one minute, until enough data had been collected. The data acquisition rate for the tube amplitude was 1000 Hz per channel and the void fraction was recorded at 100 Hz.

A period of one minute was selected as a good balance between the limitations imposed by the requirements of obtaining enough data during each cycle and avoiding changes in the upstream flow conditions due to the incapacity of the test rig to reject the extra heat generated in the tube bundle during the periods in which the heat was on.

Shorter periods involved a risk of accessing a tube response that was not representative of the steady state vibration condition.

For the reason given , the duration of this type of experiments was short, between 8 to 10 minutes, so that upstream conditions were not changed by a cumulative effect of several cycles. Due to the short duration of these experiments, instantaneous data of the flow loop operating conditions could not be obtained. However, some of the critical parameters, such as the temperature of the tube fixing region was measured at the end of each period, during which the power to the bundle had been on. In general it was found that this temperature did not vary by more than 1 °C when compared to the temperature level established during the periods when the power had been off.

In some cases, a small variation of the experiments was performed, in which the power to the monitored tube was off all the time, inclusive of when the power to the rest of the bundle was on. The intention of this experiment was to detect whether the generation of bubbles on the surface of the monitored tube had any effect on its vibrational response.

4.4.5. Experimental Data Processing

Tube Vibration Data

In all experiments, with the exception of the intermittent boiling experiments, data files from the dynamic analyser needed post processing for the final analysis. Each experimental trial produced two FFT files containing the vibration amplitude for the direction associated with it.

All of the files generated by the same experiment were permanently saved on one computer disk 3.5 inches for ease of processing and for preventing file mixup. FFT files were converted to ASCII files using the SDFTOASC.EXE command from DOS. A computer program written by Paul Feenstra, ASCTOQP.EXE converted the ASCII files into text files that were readable by Quattro Spreadsheet software. The program also converted the amplitude data into the proper units. For this purpose, an auxiliary data file called ASCTOQP.DAT was used to introduce data about the tube bundle design and particular experimental conditions. The data used in this file are listed below.

Data parameter	Value
Low frequency	0 Hz
High frequency	100 Hz
Number of lines from FFT screen	400
STRM Streamwise Conversion Constant V/inches	29.5

TRNS Transverse Conversion constant V/inches	33.2
Tube diameter	6.18 mm
Beginning of trial number	01
Ending trial number	14
Experiment Number	01
Letter to identify experiment type (U,B, M or S)	B

The program ASCTOQP generated two output files for each trial. These files were formatted to the specifications needed to be used by the 2D.EXE program from AECL in order to calculate damping ratio for the case of a frequency spectra containing two clear frequency peaks. Another output file, one for each experiment, contained all the amplitude data in both directions, in the format to be used by the QuattroPro spreadsheet software. Once the data was in the spreadsheet file, the RMS amplitude of vibration for each direction and each trial was calculated. Tube vibration amplitude data together with void fraction data described in the following section were used to produce the amplitude void fraction graphs which will be presented in Chapter 5.

Void Fraction Data

The void fraction values derived from gamma densitometry were obtained from the program WINDAQ/EX, by averaging the voltage signal for the period during which the data were collected (five minutes). The void fraction standard deviation was also calculated using

the same procedure. The average voltage value was then inserted into the spreadsheet containing all experimental data. Equations in the spreadsheet used the voltage values for 100% void and 0% void (full liquid) and temperature of the liquid Freon in the test section to calculate the gamma void fraction value as described in section 4.3.2 .

Due to the special type of data, intermittent boiling experiments had a different procedure for processing data than the one just described. Data files obtained from WINDAQ/200 containing the instantaneous tube amplitude in both directions, and the instantaneous gamma void fraction were used by WINDAQ/EX to calculate RMS amplitude values and RMS void fraction values at each period during which the power was on or off, which was usually in the range of one minute. The instantaneous amplitude and void fraction graphs are presented in section 5 of Chapter 5.

CHAPTER 5

EXPERIMENTAL RESULTS AND ANALYSIS

5.1 Introduction

The experimental results presented in this chapter are organized in four major categories, each presented in a separate section. These categories, which represent the technique by which the void fraction was generated in the test rig or the particular technique by which the void fraction was applied to the tube bundle are upstream void generation, bundle void generation, combined cases of these two and intermittent bundle void fraction generation. Table 5.1 shows the main features of each type of experiment.

At the end of section 5.4, experimental data from the first three types of void fraction generation have been plotted together in order to discern the common features and form some basic conclusions.

This chapter also presents the analysis of fluidelastic instability data in the form of reduced velocity-mass damping parameter diagrams (section 5.6), as well as an analysis that shows a reducing effect in force correlation length as the main explanation for the vibration amplitude reduction due to bundle boiling (section 5.7). Calculation of Boiling

Type of experiment	Void generation technique	General objectives
Upstream (U)	Upstream of tube bundle only. Continuous.	Generate benchmark data for comparison with results from other investigations and with the other types of experiments
Bundle boiling (B)	At the surface of the tubes only. Continuous.	Evaluate overall effect of boiling on the tube response due to Fluidelastic and Turbulence excitations
Combined (M)	Upstream of the tube bundle and at the surface of the tubes. Continuous generation.	Evaluate the effects of boiling on tube response under steam generator conditions.
Intermittent (I)	Combined type with intermittent void generation	Evaluate instantaneous effects of bundle boiling on tube response.

Table 5.1 Main features and objectives of each type of experiment.

numbers, as a method of comparing tube boiling in experimental tests and nuclear steam generators is presented in section 5.8. Finally, tube motion visualization data for bundle boiling, upstream void generation and a combined case are described in section 5.9.

5.2 Upstream Void Fraction Generation

The experiments described in this section were performed with the objective of testing the overall performance of the tube bundle and also establishing a bench mark

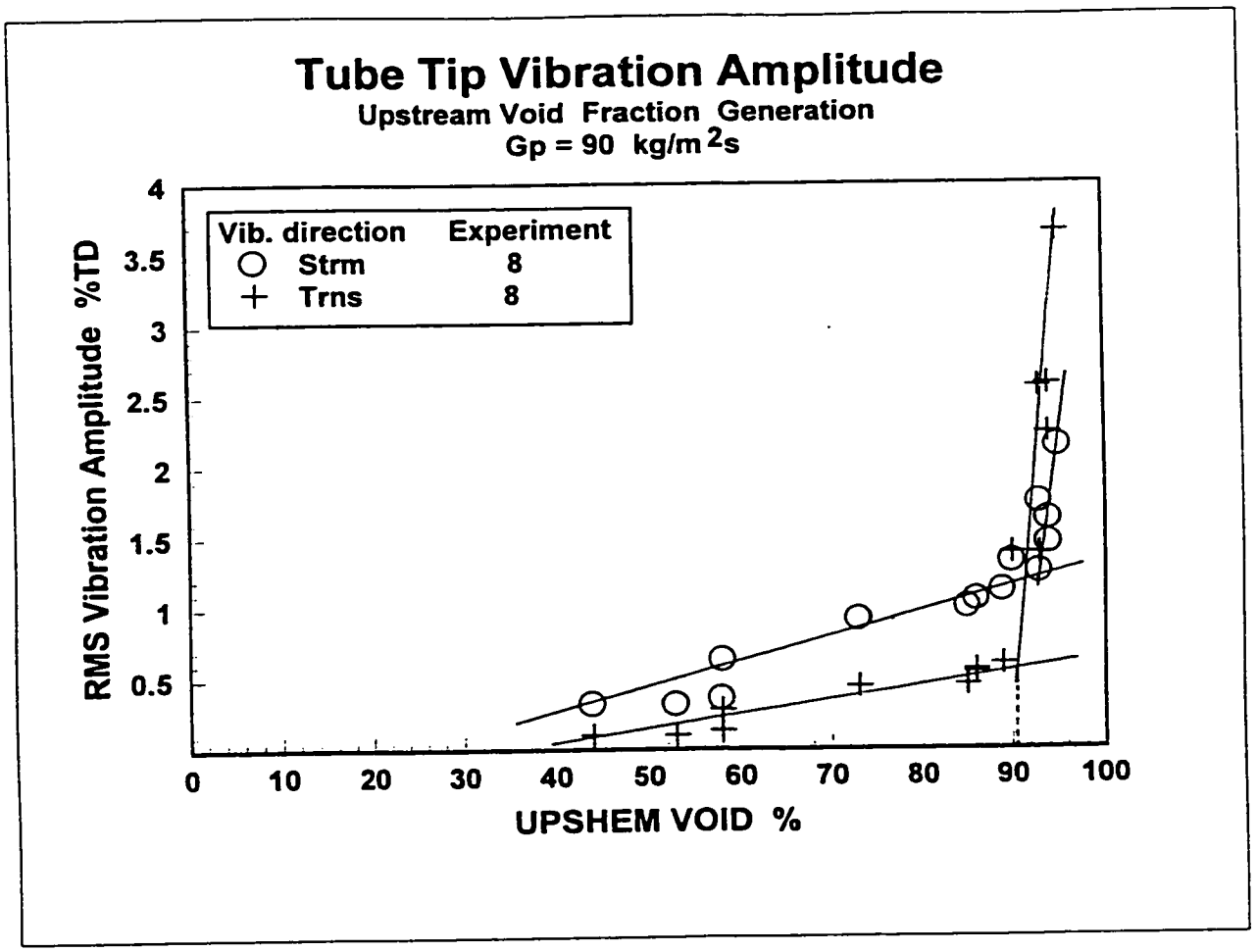

Figure 5.1 Tube vibration amplitude versus homogeneous void fraction associated with upstream void fraction generation and pitch mass flux Gp=90 kg/m^{2}s.

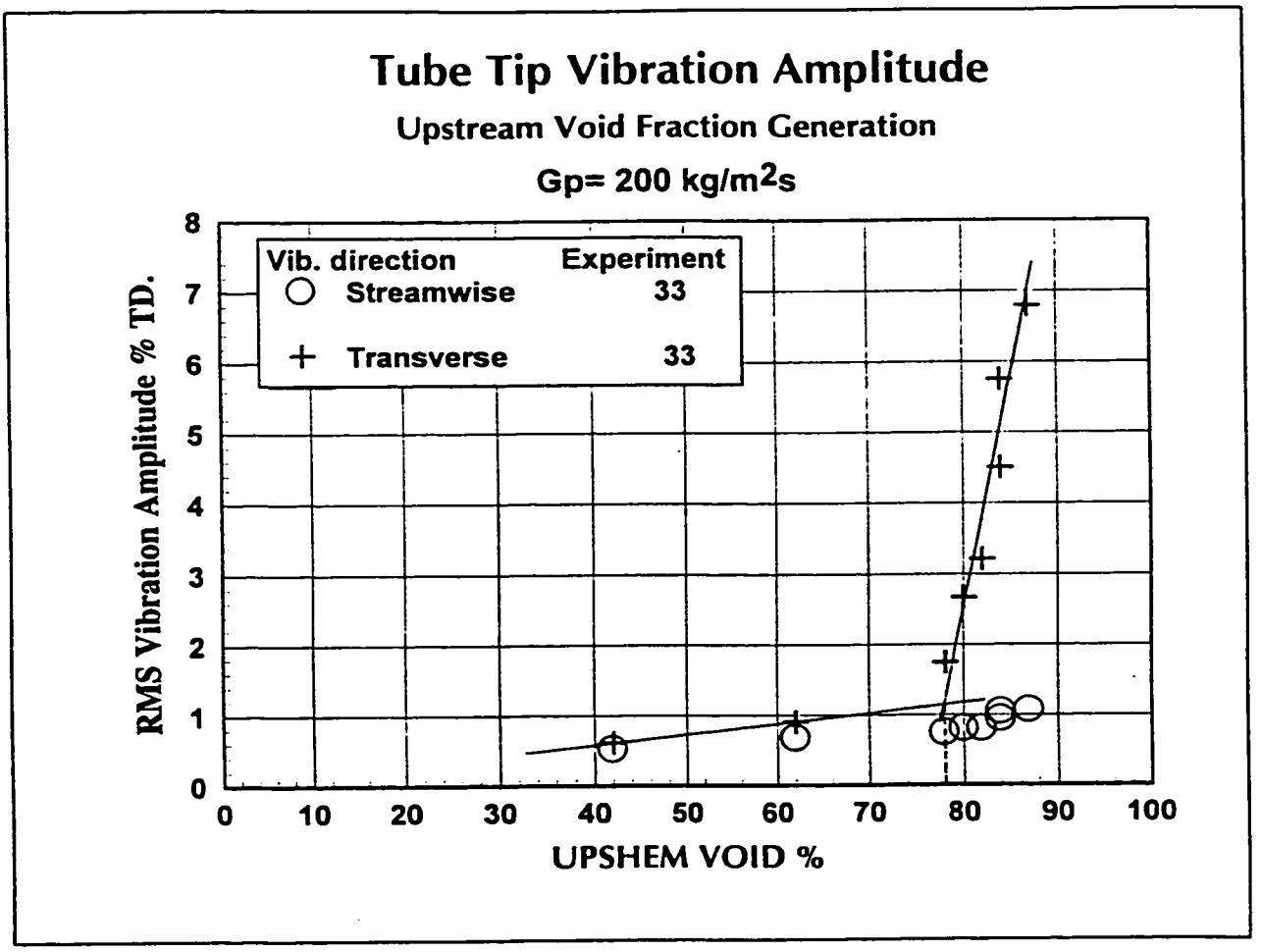

Figure 5.2 Tube vibration amplitude versus homogeneous void fraction associated with upstream void fraction generation and pitch mass flux Gp= 200 kg/m^{2}s.

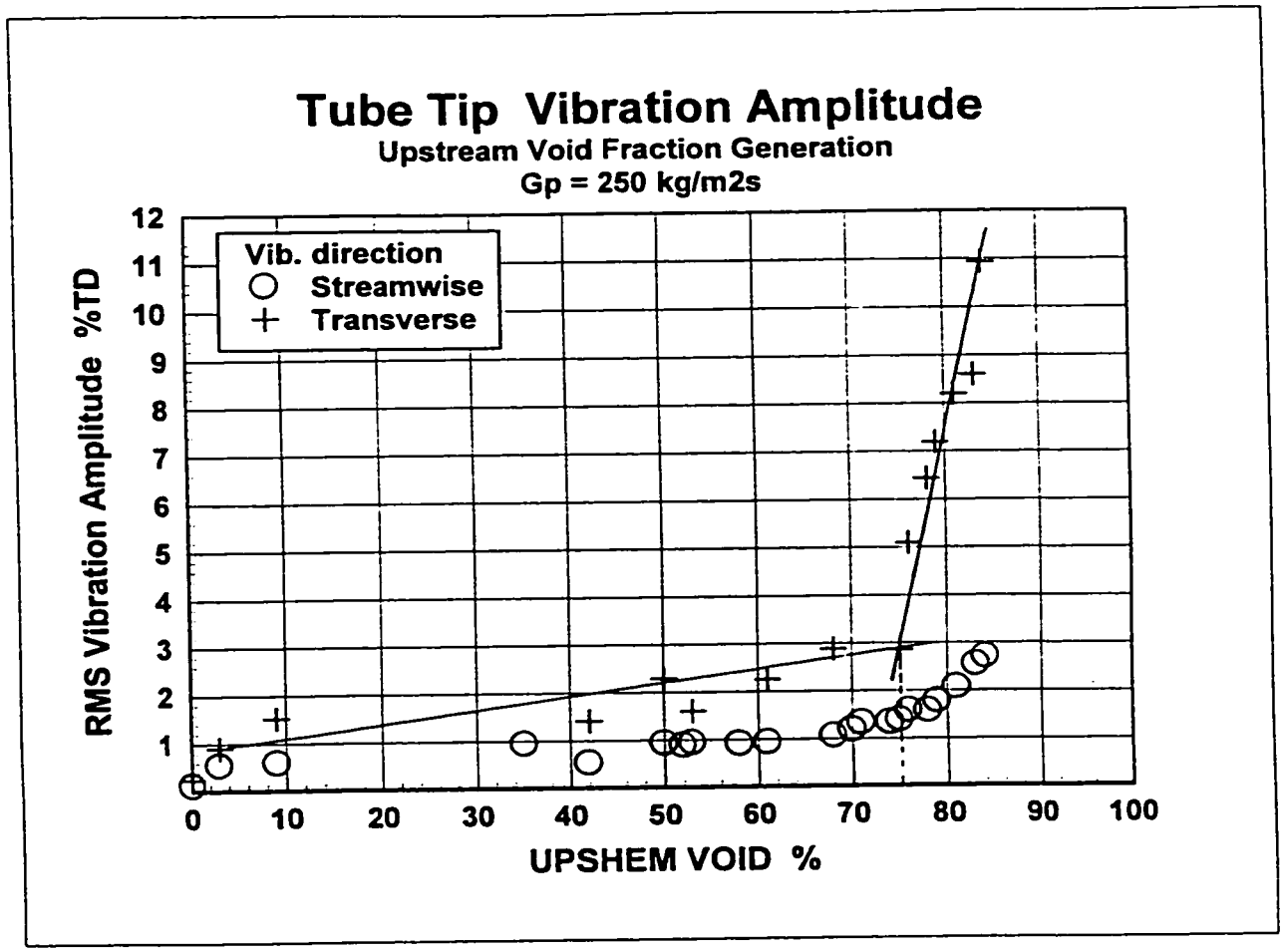

Figure 5.3 Tube vibration amplitude versus homogeneous void fraction associated with upstream void fraction generation and pitch mass flux Gp=250 kg/m ^{2}s

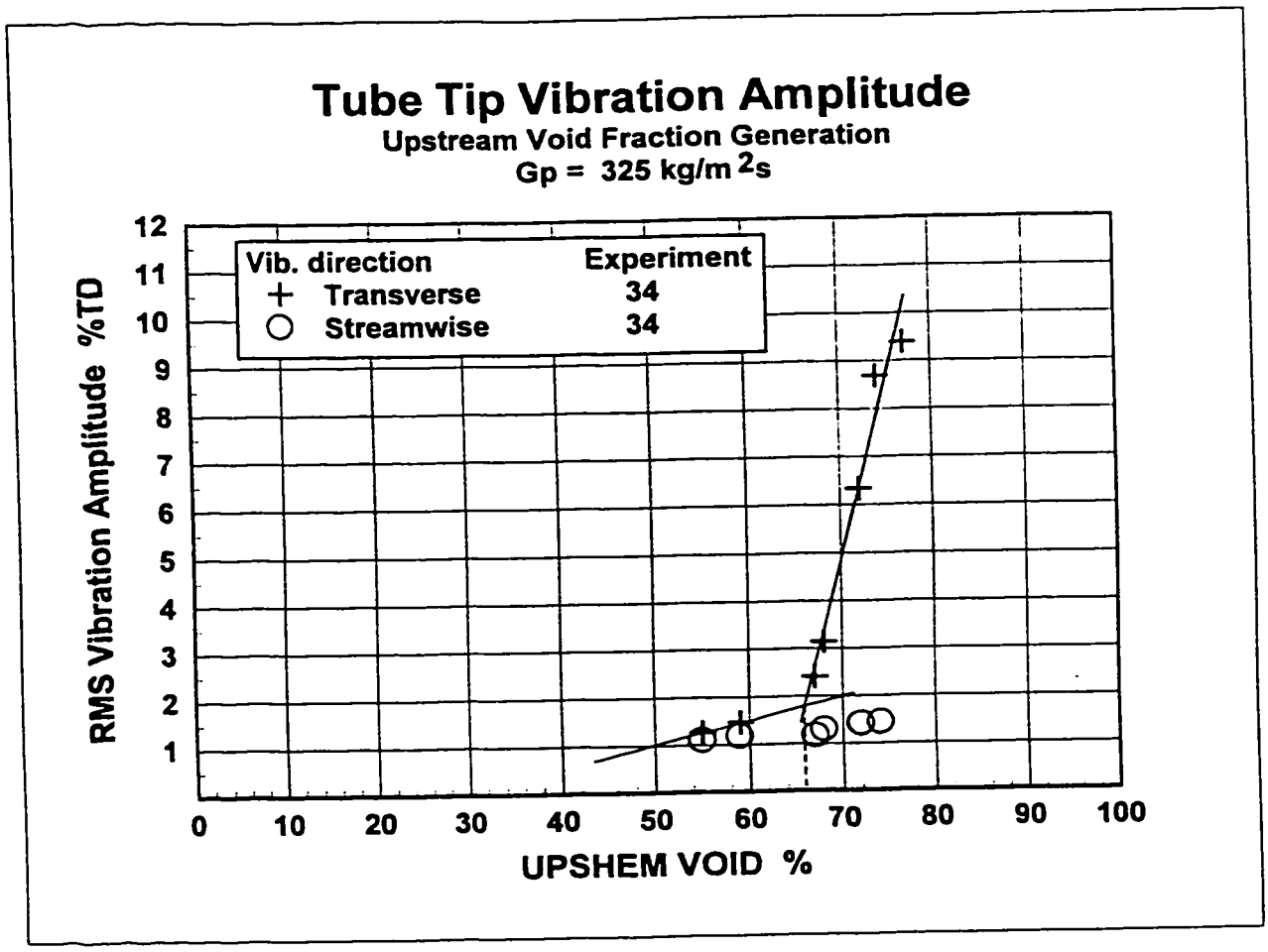

Figure 5.4 Tube vibration amplitude versus homogeneous void fraction for upstream void fraction generation and pitch mass flux Gp=325 kg/m^{2}s.

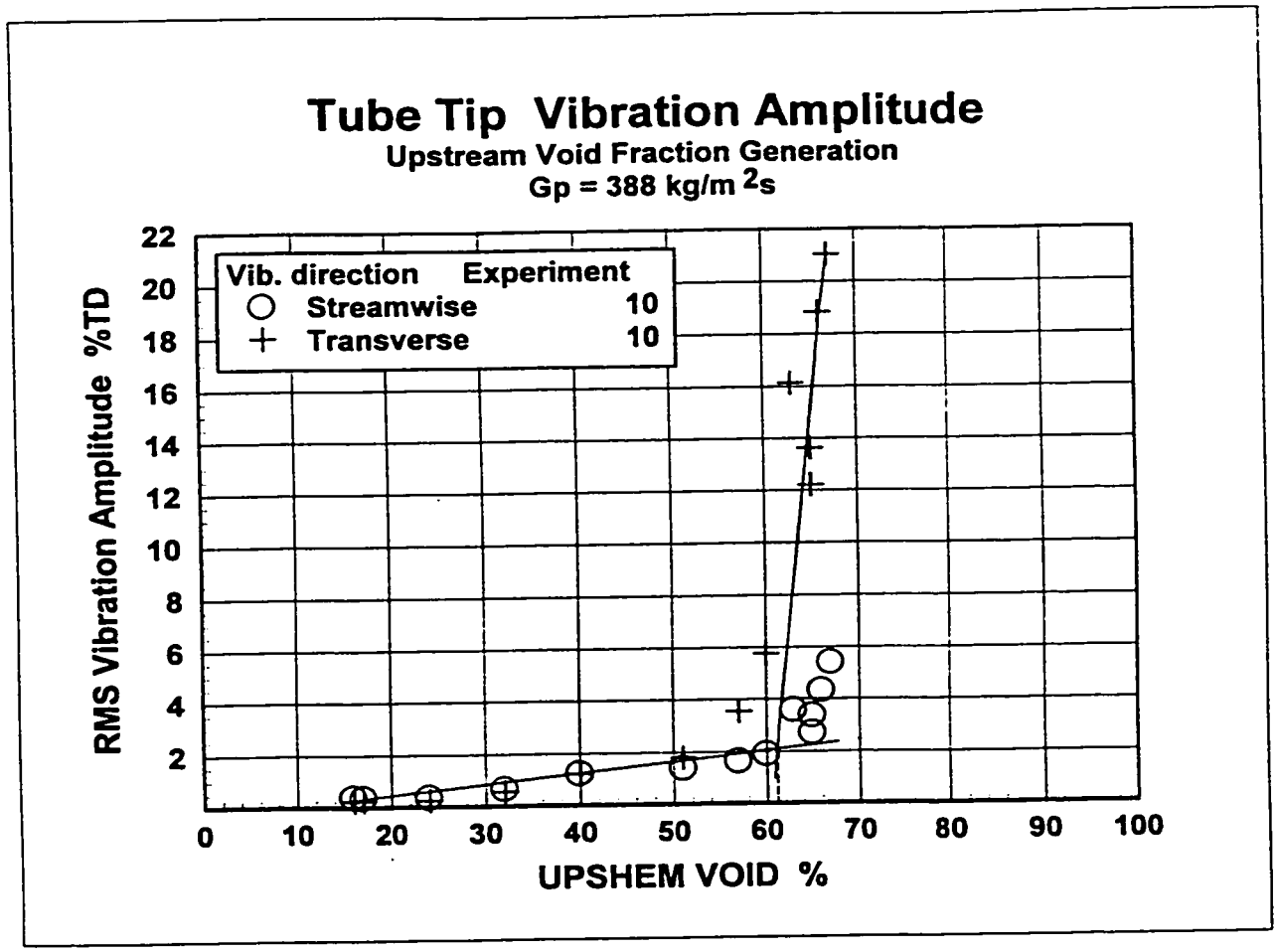

Figure 5.5 Tube vibration amplitude versus homogeneous void fraction associated with upstream void fraction generation and pitch mass flux Gp=388 kg/m^{2}s.

against which further experiments with bundle boiling could be compared. Since the bundle used in this study was different than tube bundles used in previous investigations (Feenstra, 1993), mainly due to the fact that hollow tubes had to be replaced by solid electric cartridge heaters, it was not known for certain that tube dynamics were going to be similar to those of a standard tube.

Figures 5.1, 5.2, 5.3, 5.4 and 5.5 show the Root Mean Square (RMS) amplitude of vibration in both the streamwise (drag) and the transverse (lift) directions of the tube tip versus void fraction for mass flows of 90, 200, 250, 325 and 388 kg/m^2s respectively. These mass flux values cover the range allowed by the test loop.The tube vibration amplitude has been normalized by tube diameter to give displacement as a percentage of tube diameter.

The graph presented in figure 5.1 shows a clear instability threshold in both directions. The Upstream Homogeneous Equilibrium Model void fraction (UPSHEM) at which instability occurs is about 90% in the transverse direction, which is normally the direction in which the tube first become unstable. The graphs presented in figures 5.2, 5.3 5.4 and 5.5 show that the void fractions at which the instability threshold occurs in the transverse direction are 78%, 75%, 66% and 61%, respectively.

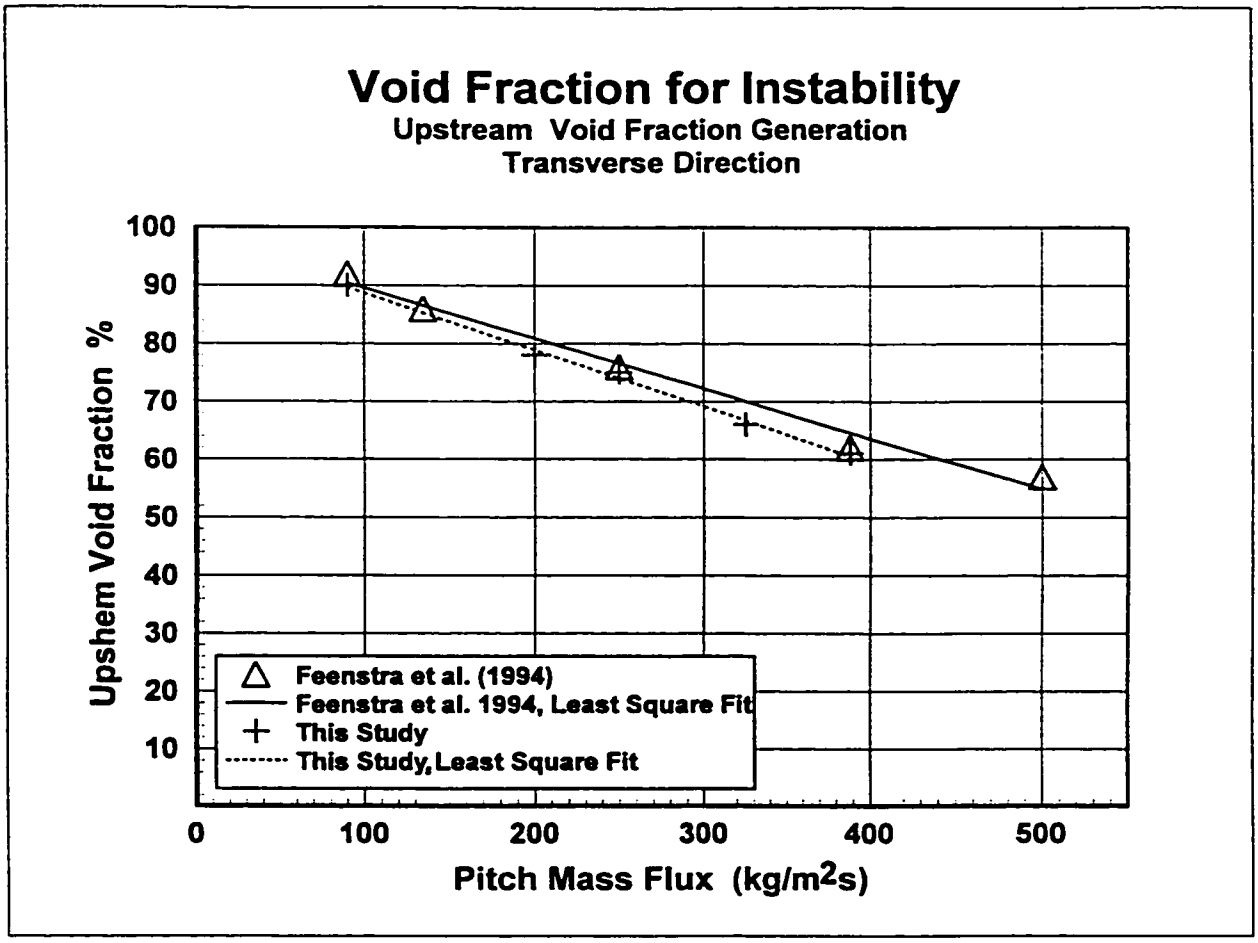

Figure 5.6 Void fraction at which instability occurred versus pitch mass flux associated with upstream void fraction generation. Instability defined by transverse direction vibration response.

The void fraction at which instability occurred in the transverse direction obtained from these five experiments are plotted against mass flux in figure 5.6. Data from Feenstra et al. (1995) have also been plotted in the same graph. It is clear from the graph that the data obtained in this study are similar to those obtained by Feenstra et al. (1995), since the data follow the same trend and dependence with respect to mass flux. Nevertheless, the data points obtained in this study appear to be slightly lower than their counterparts by two to four percent void fraction. This difference can perhaps be explained in terms of the method used to define the fluidelastic instability in the two studies. In both studies, the instability point was estimated by the intersection of the two straight lines defined by the data points in the pre-instability (low slope line) and post-instability (high slope line) regions. However, in Feenstra et al.(1995), the instability point was selected by taking the nearest data point to this intersection, located in the post-instability region, while in this study, the void fraction for the instability data plotted in figure 5.6 is the void fraction determined at the intersection, which does not necessarily correspond to any experimental data point. Uncertainty in the determination of the instability point has been calculated in this study at about ± 2% void fraction

Comparison between data from this study (cartridge heaters) and that from Feenstra et al. (hollow tubes) shows that the dynamic behaviour and instability of the tube bundles

do not differ from each another in any significant way . Thus , it has been established that any difference in dynamic behaviour observed in the presence of tube surface boiling ought to be attributable to the effects of surface boiling rather than other structural effects.

5.3 Bundle Void Fraction Generation

This section presents experiments in which one hundred per cent of the void fraction was generated in the tube bundle by means of the electric heaters contained inside the tubes. Upstream of the tube bundle, the flow was saturated liquid Freon-11. Therefore, most of the heat being generated within the tube heaters was used to produce vapour. This characteristic allowed for the generation of very high void fraction values within the bundle, in excess of 95%.

Determination of the void fraction values at the bundle was accomplished by direct measurements using gamma densitometry and by calculation of the void fraction using the Homogeneous Equilibrium Model (HEM). Since the void fraction had to be calculated at the position of the monitored tube, the heat contribution of each tube in the bundle was dependent on its relative position with respect to the monitored tube (B3). Figure 5.7 shows the tube designation in the tube bundle. Some of the void fraction generated in the bundle was generated downstream of the monitored tube, and consequently this void fraction did not contribute to the two phase flow that was affecting the monitored tube response. Only

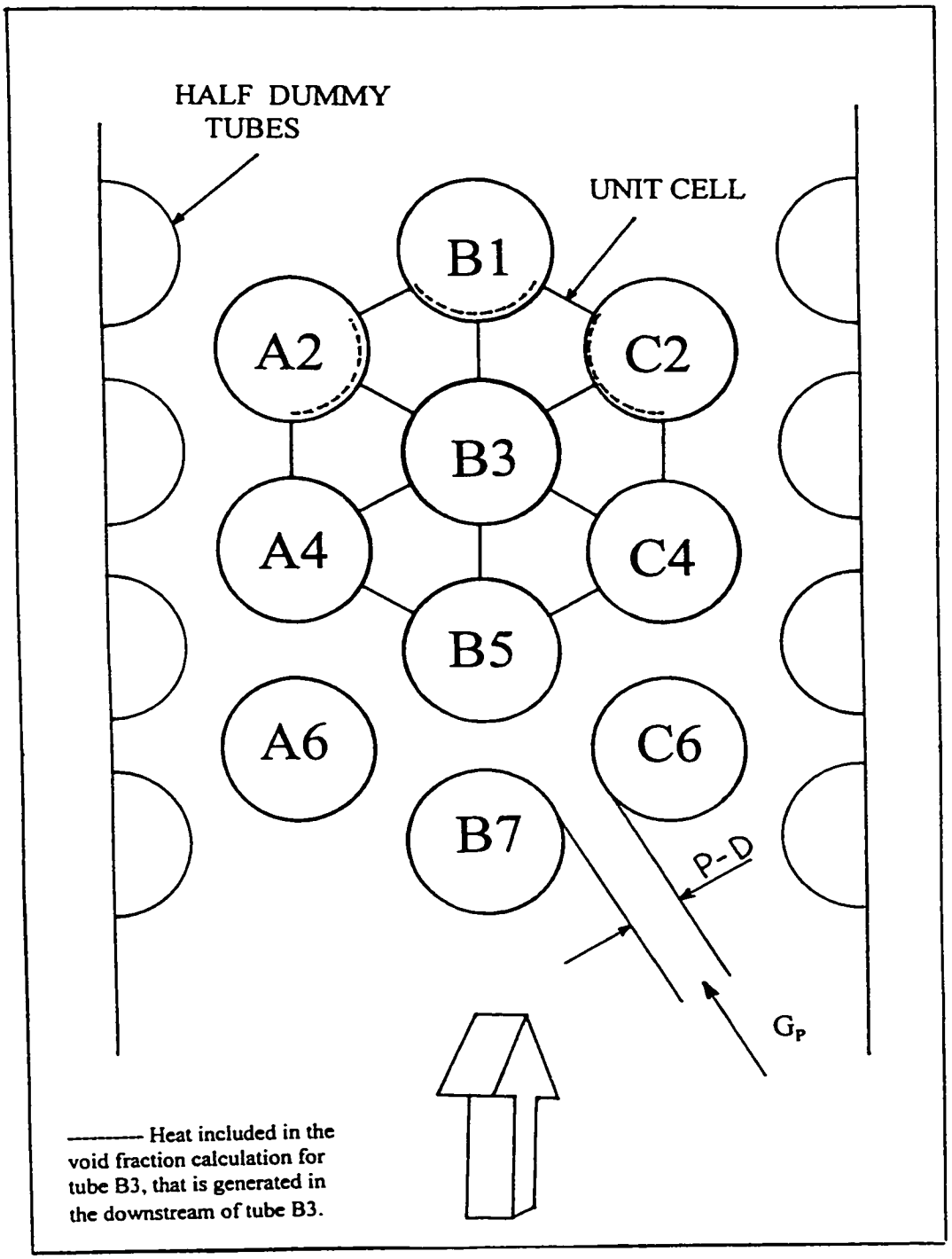

Figure 5.7 Tube designation in the tube bundle. View from the free end. B3 is the monitored tube.

a third of the heat rejected into the flow by the three tubes immediately downstream of the tube B3 (C2,B1 and A2) was included in the calculation of the total void fraction generated up to the monitored tube location. The one third proportion was established by the assumption that the vapour generated by these tubes that could affect the monitored tube was proportional to the view angle (120°) between these tubes and the monitored tube, as shown in figure 5.7. This means that an equivalent of only eight tubes, including the monitored tube, were contributing to the generation of void fraction which defined the two-phase flow affecting the dynamics of the monitored tube. The void fraction calculated using the method described was designated as Bundle Originated HEM (BOHEM) void.

The void fraction values obtained by gamma densitometry corresponded to those at the monitored tube location, since the gamma source was installed at the monitored tube level. Void values obtained by this technique were designated as total gamma void fraction (TOTGAM) void.

To be compatible with the previous investigations in which void fraction was only generated upstream of the bundle, TOTGAM values were converted when necessary to an equivalent upstream void fraction value using the conversion graph in Appendix C (figure C1). The conversion graph between UPSHEM and TOTGAM was obtained by collecting UPSHEM void fraction data from all the upstream void generated experiments in this investigation and plotting them against the corresponding gamma value TOTGAM

measured at the monitored tube location. Void fraction data were separated in three groups, one for each value of mass flux Gp relevant to this study, ie. 100 kg/m²s, 250 kg/m²s and 450 kg/m²s. Consequently, the graph contains three conversion curves, one for each mass flux value.

For experiments in which the entire void fraction present was generated in the tube bundle, or those experiments in which a combination of upstream and bundle void fraction generation was present, the gamma void fraction value TOTGAM could be converted using the conversion graph into an "equivalent" UPSHEM void fraction value. This procedure allowed direct comparison of results obtained from the three types of void fraction generation experiments. To simplify the void fraction designations, the converted value of TOTGAM was also named UPSHEM.

Figure 5.8 presents a graph of tube vibration amplitude in transverse (Trns) and streamwise (Strm) directions for two experiments performed using a mass flux of 250 kg/m²s. The data show a clear instability in the transverse (lift) direction at about 94% UPSHEM void. Although the data in the drag direction is not as clear, it also shows the onset of instability at about the same void fraction value. This void fraction value is considerably higher that the 75% value needed for instability under upstream void fraction generation for the same mass flux. This difference suggests that, in general, the void generated in the bundle is not equivalent to the void generated upstream.

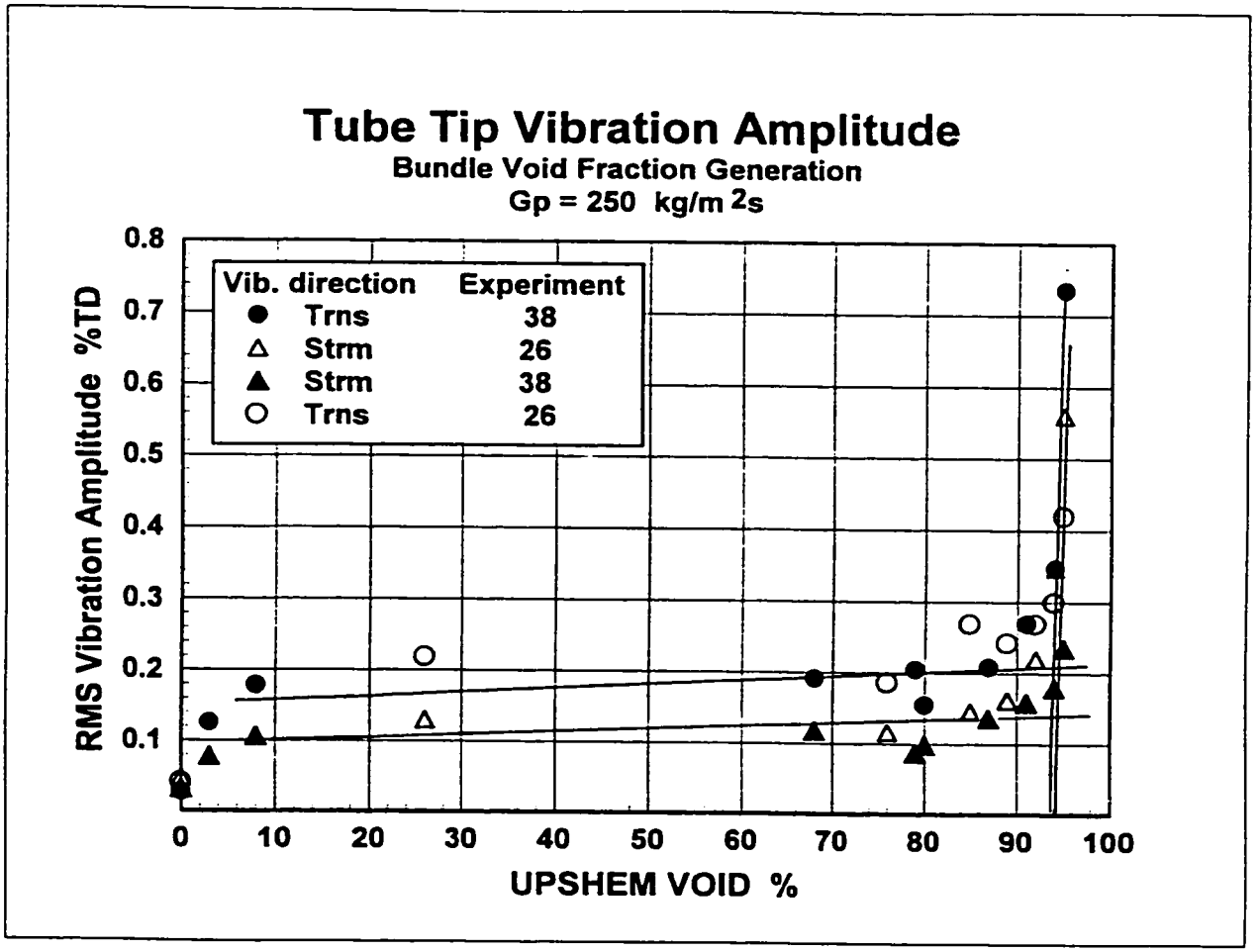

Figure 5.8 Tube vibration amplitude versus homogeneous void fraction at the monitored tube location associated with bundle void fraction generation and pitch mass flux Gp=250 kg/m 2s.

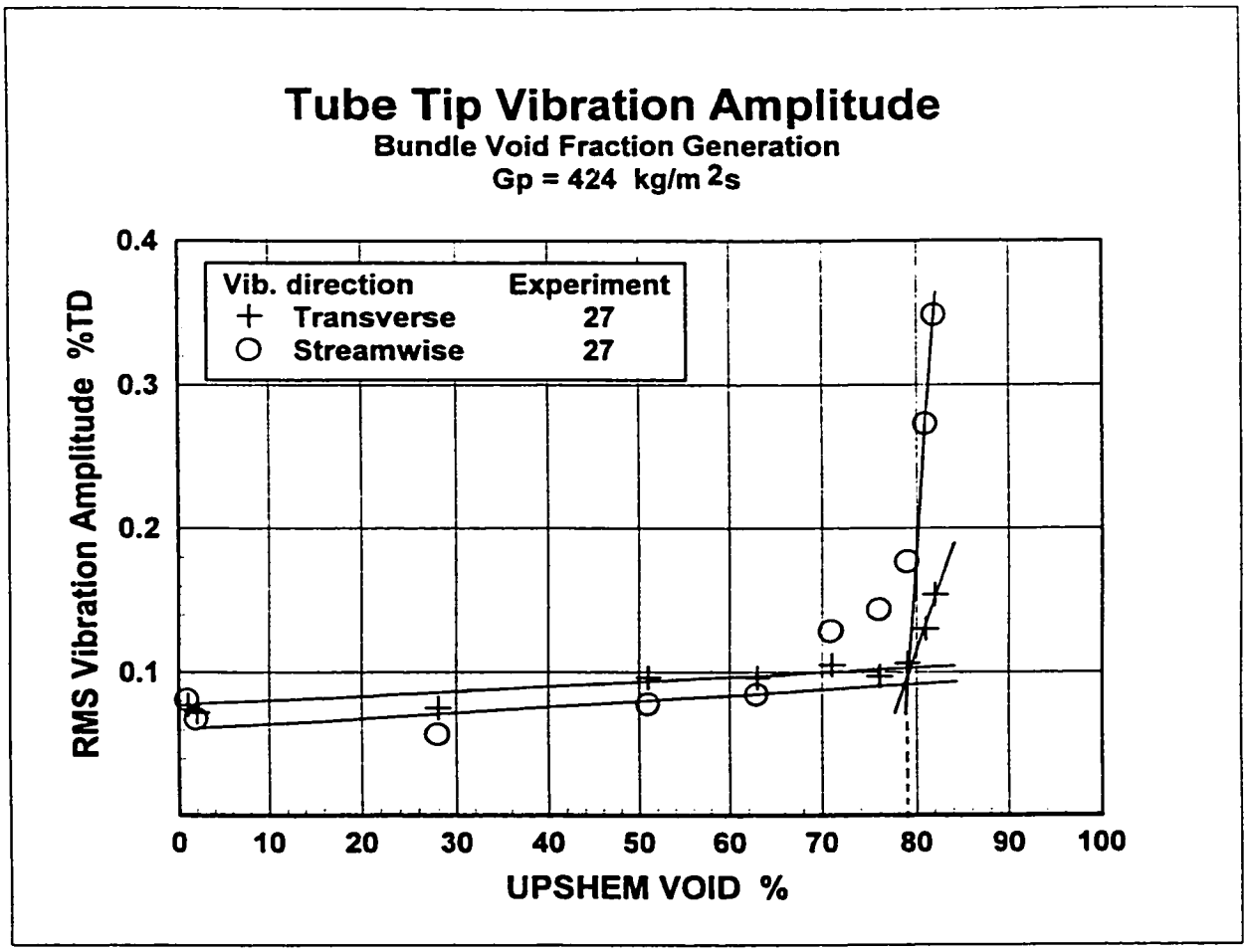

Figure 5.9 Tube vibration amplitude versus homogeneous void fraction at the monitored tube location associated with bundle void fraction generation and pitch mass flux Gp=424 kg/m 2s.

In the same graph, it can be seen that the RMS vibration amplitudes in both directions are extremely low, mostly in the range of 0.1-0.3% of tube diameter (TD) with a maximum of 0.74% for the transverse direction. The normal amplitude for the same conditions under upstream void generation is about 3% to a maximum of 11% TD as seen in figure 5.3. Unfortunately, no data points were taken at higher void fraction values due to limitations imposed by the power capabilities of the tube bundle.

Figure 5.9 presents a graph with data from a similar experiment for a mass flux of 424 kg/m^2s. The data again show a clear instability in the streamwise direction with an indication of instability in the transverse direction. The void fraction for the instability in both directions is about 79%. The amplitude of vibration is very low, similar to that of the previous experiments with the pure bundle boiling condition, in the range of 0.1% with a maximum about 0.35%TD.

Although these instabilities differ in void fraction values and amplitude of vibration from those associated with upstream void fraction generation, it will be shown later that the instability seems to be driven by the same mechanism. A comparison among amplitude data obtained from all three types of experiments, upstream void fraction generation, bundle void fraction generation and combined void fraction generation reveals the presence of a smooth transition between them.

5.4 Combined Cases of Void Fraction Generation

Experiments performed with void fraction generated purely upstream or purely in the bundle are extreme cases of the situation that is encountered in steam generators. The two-phase mixture flowing around a tube in the tube bundle at the U-bend region of the steam generator is exposed to a combination of vapour that has been generated upstream of the tube and vapour that is being generated at its own surface and at the surface of the neighbouring tubes .

It is clear that the upstream-generated void fraction experiments performed in this study confirm the findings obtained by other investigations (Feenstra el al. 1995). It is also clear that bundle generated void experiments show results that differ quantitatively from those found in the upstream generated void fraction cases.

The rest of the experiments described in this chapter are combined upstream/bundle generated void fraction cases . These experiments are more interesting from a practical point of view, since as was explained, they are closer to the real situation in a steam generator. They also have the potential to uncover the connection between the two previously described cases, giving information about the mechanism of fluidelastic instability.

The graph presented in figure 5.10 shows the amplitude of tube vibration for both streamwise and transverse directions versus void fraction for a mass flux of 100 kg/m^{2}s. Upstream Homogeneous equivalent Void Fraction (UPSHEM) has been used to plot the data. UPSHEM is calculated based on heat contributions from the upstream heaters, which produce the upstream generated void fraction plus the heat rejected by the heaters inside the tubes in the tube bundle. The instability in both directions can be seen to occur at about 92% void fraction. It is interesting to observe that the onset of instability occurred at the same void fraction values for both directions, which is unusual in upstream generated void fraction cases of instability, where the tube reaches instability in the transverse direction at a much lower void fraction than that for instability in the streamwise direction. It can be hypothesized that vapour generation within the bundle somehow alters the two-phase flow field around the tube in such a manner that the tube vibration behaviour becomes the same in both directions.

The vibration amplitude is found to be in the range of 0.05 to 0.45%TD, very similar to the cases of pure bundle void fraction generation as described in section 5.3. In this experiment the upstream void generation changed from 59% to 0%, while void fraction generated in the bundle increased from 0% to 94%. This technique allowed a gradual increase in the proportion of void generated in the bundle with respect to the total void present at the tube location. The results indicate that under a predominance of void

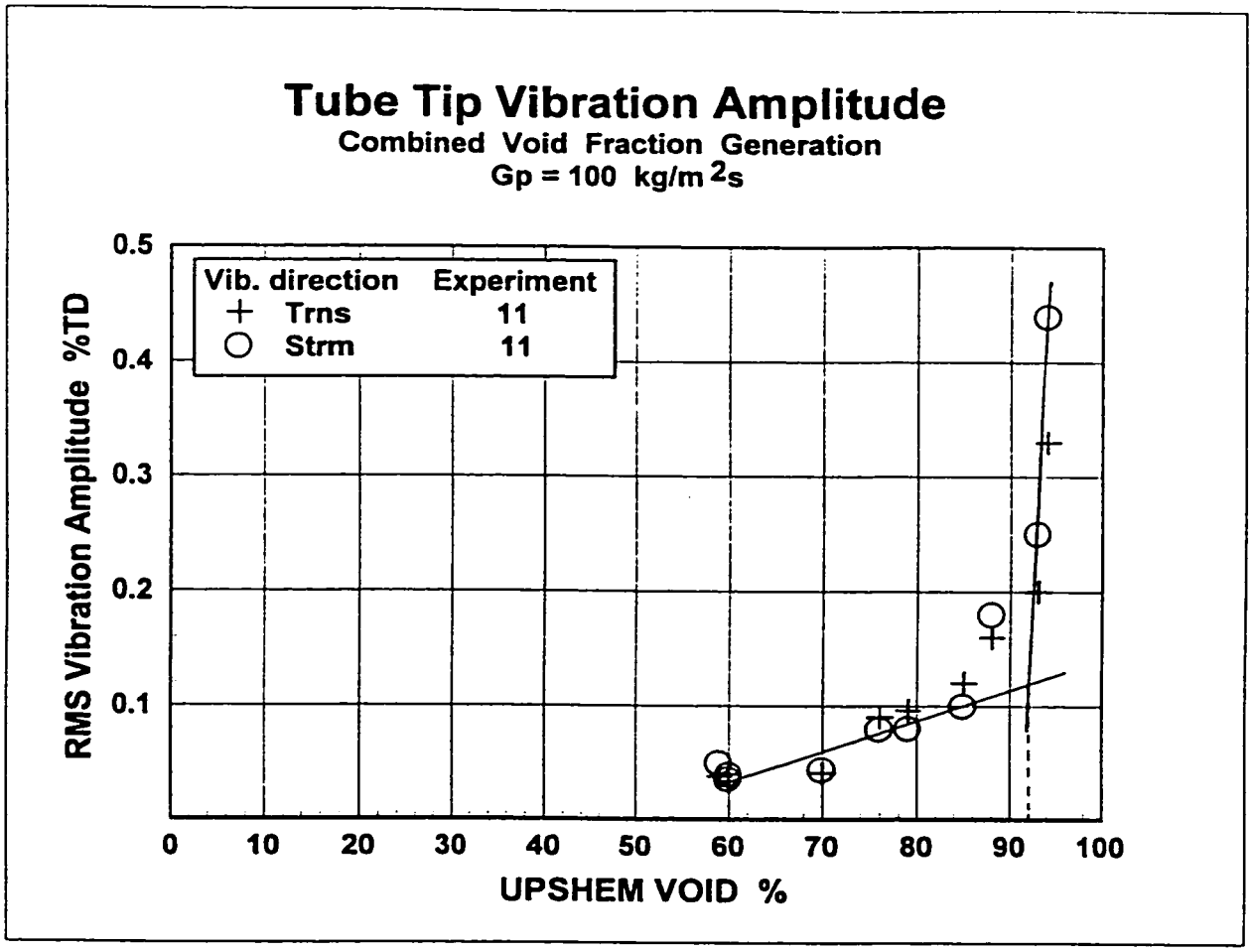

Figure 5.10 Tube vibration amplitude versus homogeneous void fraction at the monitored tube location associated with combined void fraction generation and pitch mass flux Gp=100 kg/m 2s.

generated in the bundle, tube behaviour is similar to the case of bundle only generated void, even for the case in which some void fraction is being generated upstream.

One of the disadvantages of the experiment described above is that the combination of void fraction generated upstream and in the bundle did not remain constant during the experiment. Although this allowed confirmation that fluidelastic instability occurred under a mixed void generation, it did not answer the question of equivalency between the upstream void and the bundle generated void as was suggested in the discussion of the graph presented in figure 5.8.

In figure 5.11, data from two experiments is shown in which the HEM total void fraction, TOTHEM was maintained constant during the entire experiment. The amplitude of vibration in both directions has been plotted against the void fraction generated in the bundle based on BOHEM. The mass flux is 100 kg/m^2s. BOHEM is calculated as the difference between TOTHEM and UPSHEM. In experiment 11B, TOTHEM was maintained at 91% with a standard deviation of 3%. The data in experiment 11B show that for both directions, the amplitude decreased from about 0.95% to 0.2% (transverse) and from 0.78% to 0.25% (streamwise) when void fraction produced in the bundle changed from 10% to 86%.

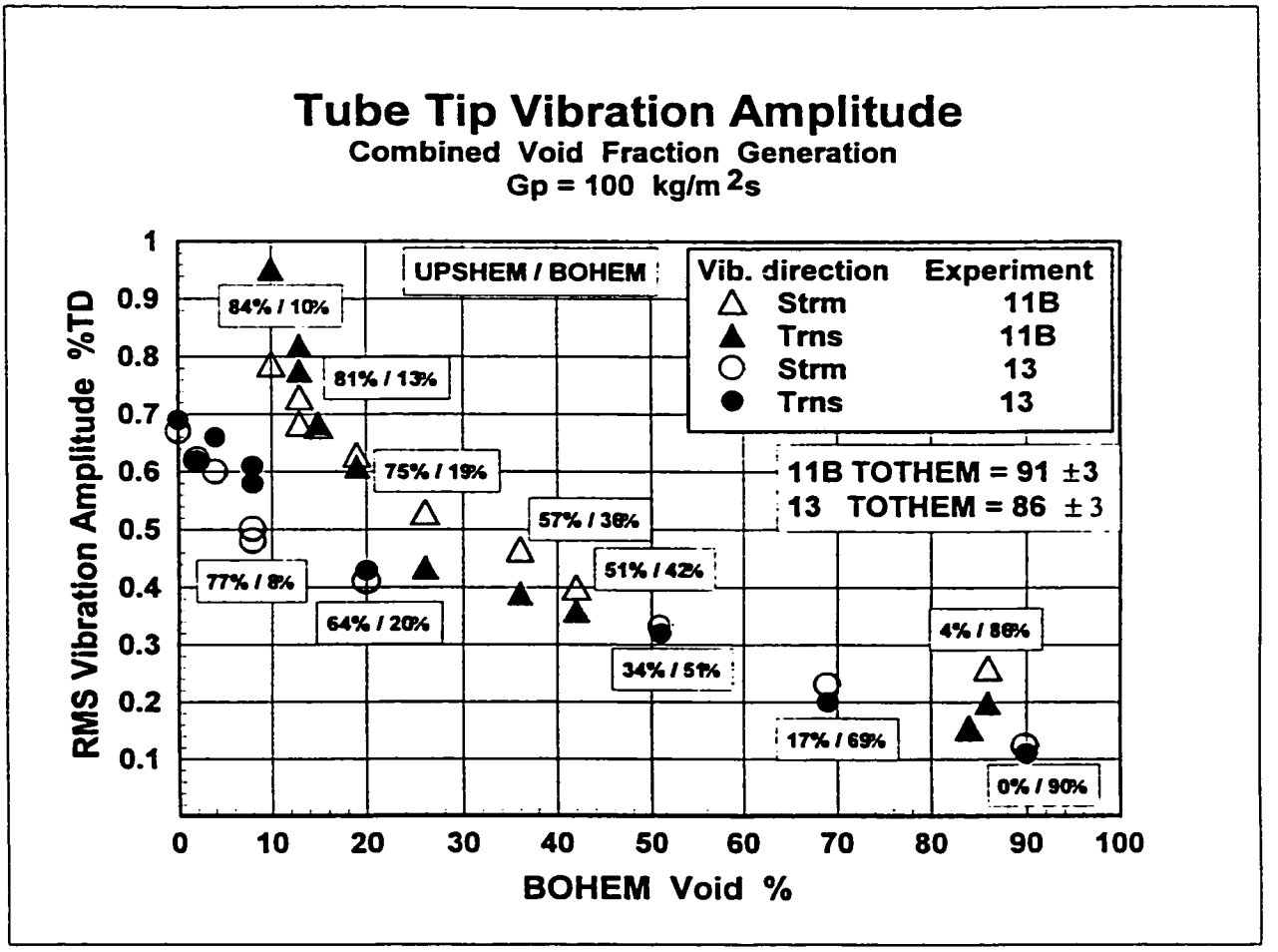

Figure 5.11 Tube vibration amplitude versus homogeneous void produced within the bundle under constant total void fraction (TOTHEM) at the tube location. Pitch mass flux Gp=100 kg/m 2s.

In experiment 13, TOTHEM was maintained at 86% ± 2%. The data show that the vibration amplitude for transverse and streamwise directions decreased monotonically from about 0.7% TD to 0.11%TD when BOHEM changed from 0% to 90%. When comparing the data from both experiments, it is clear that for BOHEM void values lower than 40%, the vibration amplitude for experiment 11B is larger than the vibration amplitude for experiment 13. This difference is expected since the value of void fraction TOTHEM in experiment 11B is 91% compared to only 86% for experiment 13. Since both have a BOHEM value of 10% and the difference between TOTHEM and BOHEM must be generated upstream, it is obvious that the upstream void fraction value is larger for experiment 13 than for 11B, which translates into a higher vibration amplitude. After 40% BOHEM void, both amplitudes seem to fall according to the same decreasing trend until the end of the void scale. This is an indication that as more vapour is being generated in the bundle, the more this bundle boiling affects the tube behaviour up to a point after which it takes control and the upstream void fraction is no longer of importance.

In order to maintain a constant value of TOTHEM at the tube location and at the same time increase the void fraction produced in the bundle (BOHEM), the void fraction contribution from upstream (UPSHEM) had to be reduced in each trial. The continuous reduction in amplitude as BOHEM increased in both experiments confirmed again, as suggested in section 5.3, that for the purpose of tube dynamic response, the void fraction

produced in the bundle is not equivalent to the void fraction produced upstream of the tube bundle. If both void fractions had been equivalent, a constant vibration amplitude would have been seen in the graph, indicated by data points following a horizontal line rather than a descendent curve.

One of the normal challenges of the type of experiments described in this study is the proper and reliable evaluation of the void fraction. Although homogeneous equilibrium model calculations provide a reasonably good evaluation of void fraction, they are often affected by two main sources of error. The first is the uncertainty in the thermodynamic conditions of the flow, in particular the temperature of the flow, in as much as void fraction values are extremely sensitive to changes in flow temperature. The second is the effect of slip which is the ratio of the gas velocity to the liquid velocity in the mixture. HEM equations are based on the assumption that the slip ratio is always unity and hence both phases travel at the same velocity.

In previous investigations, (i.e. Feenstra et al. 1995), gamma densitometry was used to evaluate void fraction values upstream of the tube bundle, in order to compare these values with values determined using HEM at the same location. This meant that although a slip value different than unity was expected at the location of the void evaluation, the difference between the gamma densitometer determined void values and the upstream void

values would follow a clear trend as the void fraction changed in the range 0% to 100%. The trend has been confirmed experimentally. The correlation was possible due to the fact that no void fraction was being generated within the bundle and hence no evaluation was needed for the potential changes in slip value of the two-phase flow due to its passage through the bundle.

In this study, as void is often generated in the bundle as well as upstream of the bundle simultaneously, both contributions had to be taken into account in the calculation of the total HEM void (TOTHEM) at the monitored tube location. The calculation of void fraction by this method introduced a new potential source of error, the possibility that void fraction contributions from the two sources were distinguished by different slip values. This new effect had the potential to prevent the existence of a unique correlation between the TOTHEM and TOTGAM voids. In this new situation, it would not be clear which void fraction would better represent the two-phase flow mixture for the purpose of characterizing the tube vibration response. In order to better minimize this potential source of error, it was important that void fraction values be obtained using the gamma densitometry technique at the tube location (TOTGAM void value). It was also important that constant void fraction experiments be performed twice, the first time wherein the controlling parameter was TOTHEM and the second time wherein the controlling parameter was the void fraction TOTGAM.

Experiments 12A and 12C were performed with two objectives in mind; first to confirm that reduction of vibration amplitude detected in experiments 11B and 13 under bundle void generation (G = 100 kg/m^{2}s) were also obtainable for a higher mass flux and second, to investigate whether or not the slip phenomena occurring within the bundle might play a significant role in the tube vibration behaviour and in particular in the reduction of vibration amplitude due to the presence of void generated within the tube bundle.

The graph in figure 5.12 contains vibration amplitude data in transverse and streamwise directions for both experiments. The mass flux Gp was equal to 250 kg/m^{2}s. The data points identified by a filled circle and an open circle represent transverse and streamwise vibrations in experiment 12A, respectively. In this experiment, the gamma void fraction value TOTGAM was maintained at 41%±1%, which is equivalent to an upstream void fraction UPSHEM of 72%. In experiment 12C, a value of TOTHEM equal to 77% was maintained constant during the entire experiment. The void fraction generated in the bundle was increased from 0% to 76% in experiment 12C and from 0% to 77% in experiment 12A. For this void fraction variation, it can be clearly seen in the graph that the vibration amplitude in the transverse direction decreased for both experiments from near 3%TD to a low of 0.25%TD. For the same void fraction variation, the streamwise vibration amplitude decreased from about 0.85%TD to 0.2%TD. In the streamwise vibration direction, the coincidence of the data from both experiments is remarkably good considering that the experiments were run at different times and the fact that the void fraction controlling parameter was different in each case.

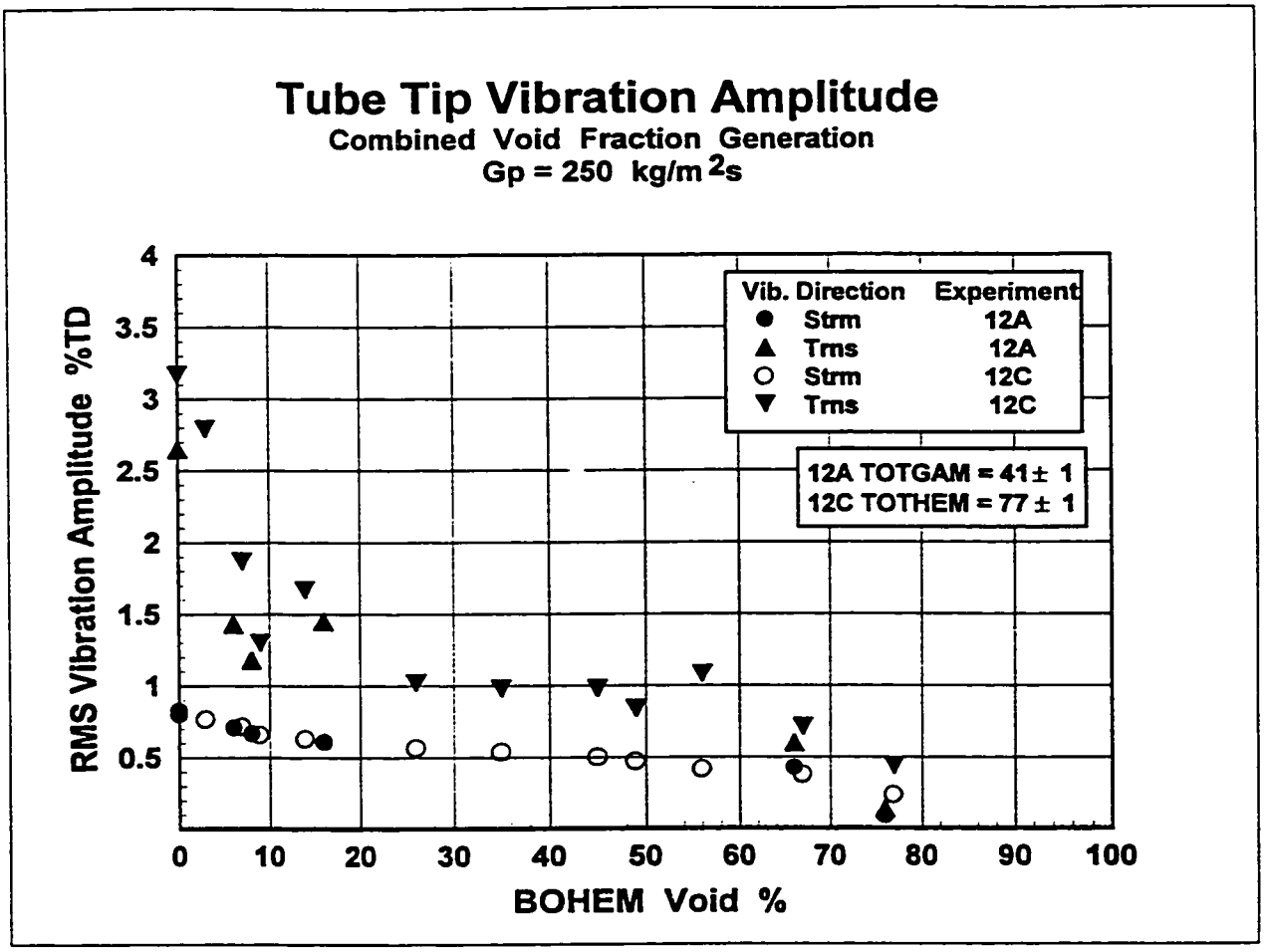

Figure 5.12 Tube vibration amplitude versus homogeneous void produced within the bundle under constant total void fraction (TOTGAM and TOTHEM) at the tube location. Pitch mass flux Gp=250 kg/m 2s.

The data from these experiments confirmed the overall reduction in vibration amplitude found in experiments 11B and 13, for a mass flux of 250 kg/m²s. Moreover, it was also confirmed that for experiments run at constant void fraction values at the monitored tube location, whether the total gamma void fraction (TOTGAM) was used or the total HEM void fraction (TOTHEM) was used to control the experiment, the results showed no difference in the tube vibration behaviour. This conclusion suggests that although slip phenomena may exist in the two-phase flow upstream or within the bundle, its influence on the overall effect of bundle boiling on the tube vibration response is not detectable.

Nevertheless, TOTGAM and TOTHEM void values, along with UPSHEM, were evaluated throughout the remaining experiments in this research investigation as a method of confirmation and also as a potential backup in case one of the void fraction measuring methods failed during an experiment.

Constant Void Fraction Ratio Experiments

Experiments up to now have been conducted under three different types of conditions, pure upstream void generation, pure bundle void generation and combined cases of void generation conducted under constant void fraction conditions.

Important information has been obtained by means of these experiments, in particular the one is relevant to the fluidelastic instability phenomenon under pure bundle void generation and the reduction in vibration amplitude in the presence of bundle void fraction generation. Nevertheless, the relationship between these three cases must be rationalized such that the case of classical fluidelastic instability under upstream void fraction generation can be included as part of a more comprehensive phenomena, which will include instability in pure bundle boiling and combined cases of void fraction generation as well.

A unifying parameter among cases of upstream, bundle and combined void generation is the Void Fraction Ratio (VFR). VFR is defined as the ratio of the void fraction produced in the bundle (BOHEM) up to the tube location, divided by the total void fraction at the tube location (TOTHEM, or TOTGAM converted to equivalent UPSHEM void). A value of VFR=0 means that no vapour is being produced in the tube bundle (BOHEM=0) and hence it represents a typical two-phase flow experiment with vapour being generated upstream of the tube bundle. A value of VFR=1 means that all of the vapour is generated in the bundle and therefore no vapour is produced upstream (BOHEM=TOTHEM, UPSHEM=0). In these circumstances, the upstream edge of the bundle is exposed to saturated liquid Freon-11 only. A value of VFR=0.35 implies that 35% of the vapour at the tube location has been generated in the bundle, while the other 65% has been generated upstream.

Experiments performed with VFR=0 and VFR=1 have already been described in previous sections, along with experiments in which VFR was not the controlling parameter. In this section, an experiment where VFR was kept constant (within the limitations of the test loop) is presented.

The graph in figure 5.13 shows experimental data for a mass flux of Gp=250 kg/m^{2}s VFR was maintained constant at 0.38 ± 0.14. The amplitude of vibration in transverse and streamwise directions has been plotted against TOTHEM void. The graph shows instability in the transverse direction at about 82% void. In the streamwise direction, the onset of instability occurs at about the same void fraction as the transverse case. Scatter in the data is probably due to fluctuations in the VFR value. The test loop, which was designed for constant mass flux experiments, was never intended for this type of experiment, where the ratio of two void fractions is to be maintained constant. Although the average VFR value during the experiment was 0.38, at the fluidelastic instability threshold VFR had a value of 0.35.

The amplitude of vibration changed from 0.5%TD to a maximum value of 2.55%TD in transverse direction and to 1.3% in streamwise direction. It can be seen that these values are in between those values representing VFR=0 (upper bound from graph 5.3) and VFR=1 (lower bound, from graph 5.8), which suggests that this fluidelastic instability phenomenon is the same phenomenon as that observed in the previous experiments.

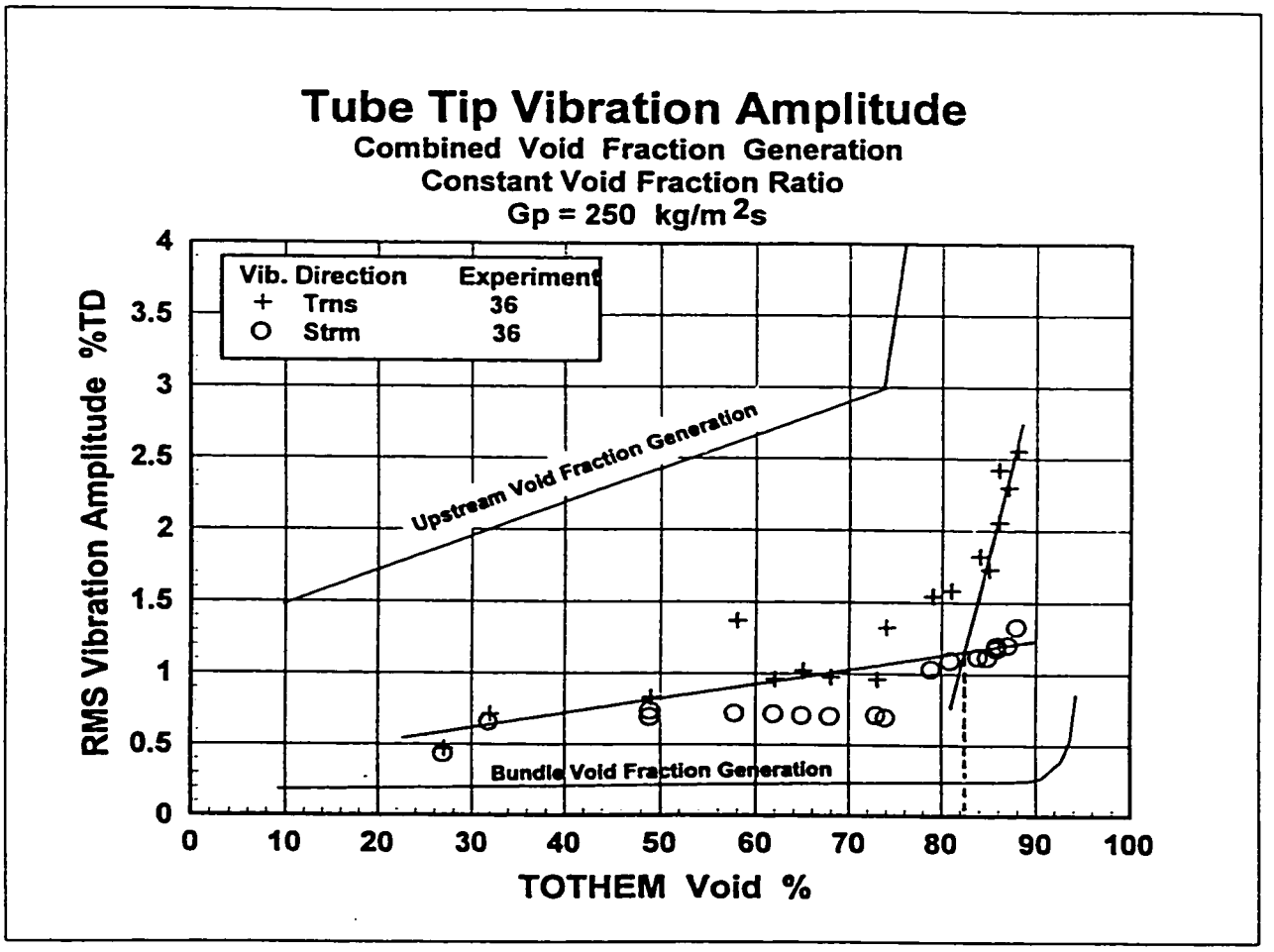

Figure 5.13 Tube vibration amplitude in transverse and streamwise direction versus total homogeneous void (TOTHEM) at the tube location for a constant void fraction ratio experiment (VFR=0.38). Pitch mass flux Gp=250 kg/m 2s.

Fluidelastic Instability for Different VFR

Figure 5.14 shows a graph which represents data from three experiments, 37 with a VFR=0.0, 36 with a VFR=0.38 and 38 with a VFR=1.0. The data represents the vibration amplitude in the transverse direction plotted against the HEM void at the monitored tube location. In experiments 36 and 38, void fraction was obtained by converting TOTGAM into an UPSHEM equivalent void by using the conversion graph presented in Appendix C, section C1. This procedure allows for direct comparison of the data obtained with different void generation techniques.

The graph shows that the tube vibration response in all experiments follows the same trend. The amplitude of vibration increases gradually with increasing TOTHEM up to a certain value after which a more rapid increase in amplitude is observed, which indicates the onset of fluidelastic instability. A smooth transition from one curve to another is seen as the VFR changes from 0 to 1. This confirms the hypothesis that the different cases of void fraction generation are similar and that fluidelastic instability is governed by the same mechanism in all of them.

When comparing the three curves in Figure.5.14, it is evident that the amplitude of vibration diminishes with an increase in bundle generated void (BOHEM). For the same value of TOTHEM, the amplitude is highest for the upstream void generation case, where

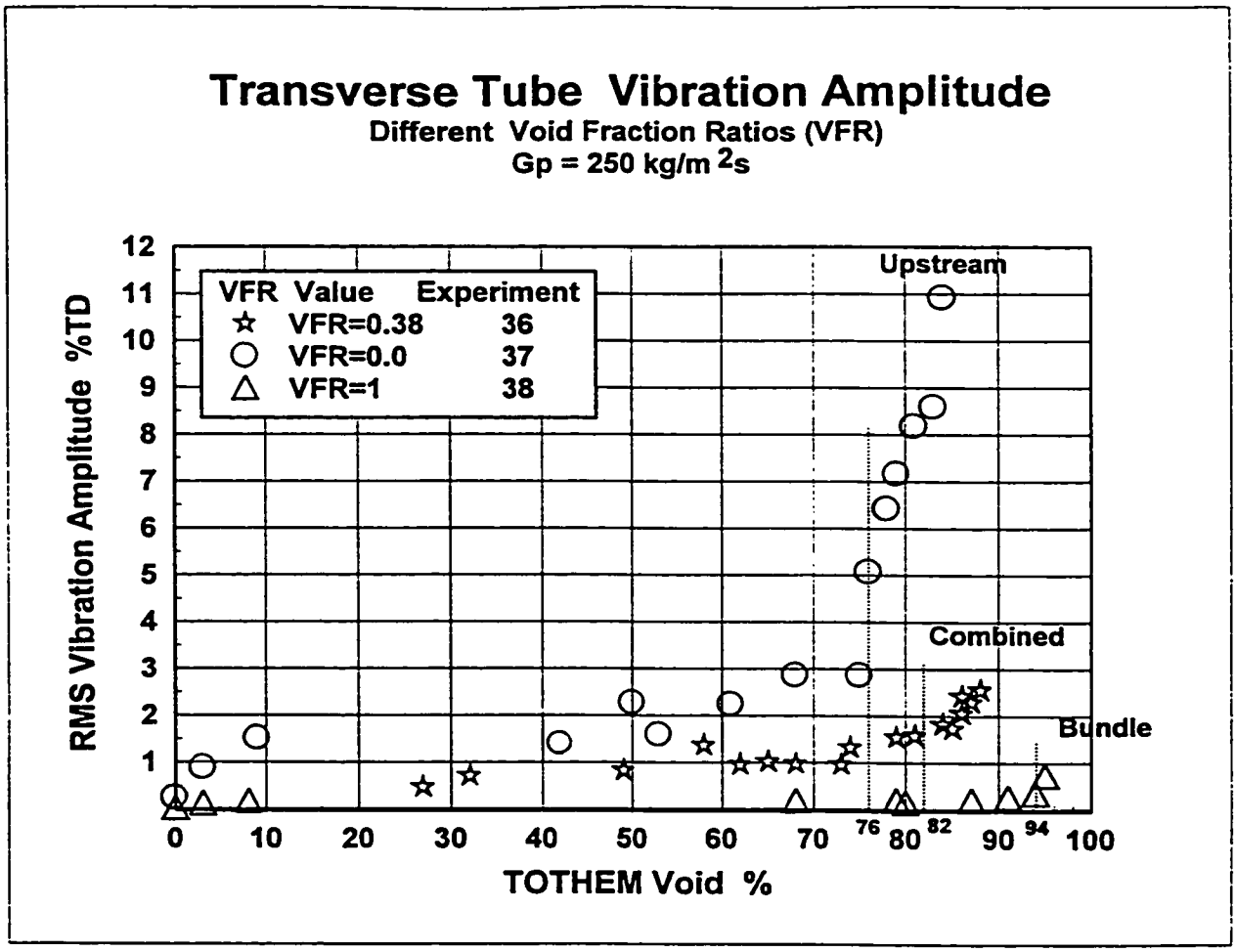

Figure 5.14 Transverse tube vibration amplitude versus total homogeneous model void (TOTHEM) at the tube location for different void fraction ratios. Pitch mass flux Gp= 250 kg/m 2s.

no void was generated in the bundle (VFR=0), then it decreases for the void fraction ratio of VFR= 0.38 and finally, the amplitude reduces to values lower than 0.7% when the void was generated in the bundle only (VFR= 1.0). Void fraction values for fluidelastic instability threshold are similarly affected. As the void fraction generated in the bundle increases from VFR= 0 to VFR= 0.38 and then to VFR= 1.0, the critical void fraction changed from 76% to 82% and to 94% respectively.

Figure 5.15 shows the vibration amplitude response in the streamwise direction for the same experiments. The trend in the streamwise data is similar to the trend in the transverse data. The main difference is that amplitude of vibration for void fractions between 30% and 65% does not differ significantly for the upstream and combined boiling cases, while in the transverse direction, the difference in amplitude for the same void range is considerable. It is also clear from figures 5.14 and 5.15, that bundle boiling has a much greater effect of reducing transverse tube vibration than streamwise tube vibration.

In figure 5.16, the void fraction values at which instability occurred is presented for different methods of void fraction generation as a function of mass flux. The data from Feenstra et al. 1994, obtained with upstream void fraction generation has also been plotted as a reference. From the graph it can be observed that the data for upstream void fraction generation from this study, indicated by open circles, falls slightly lower than that from the

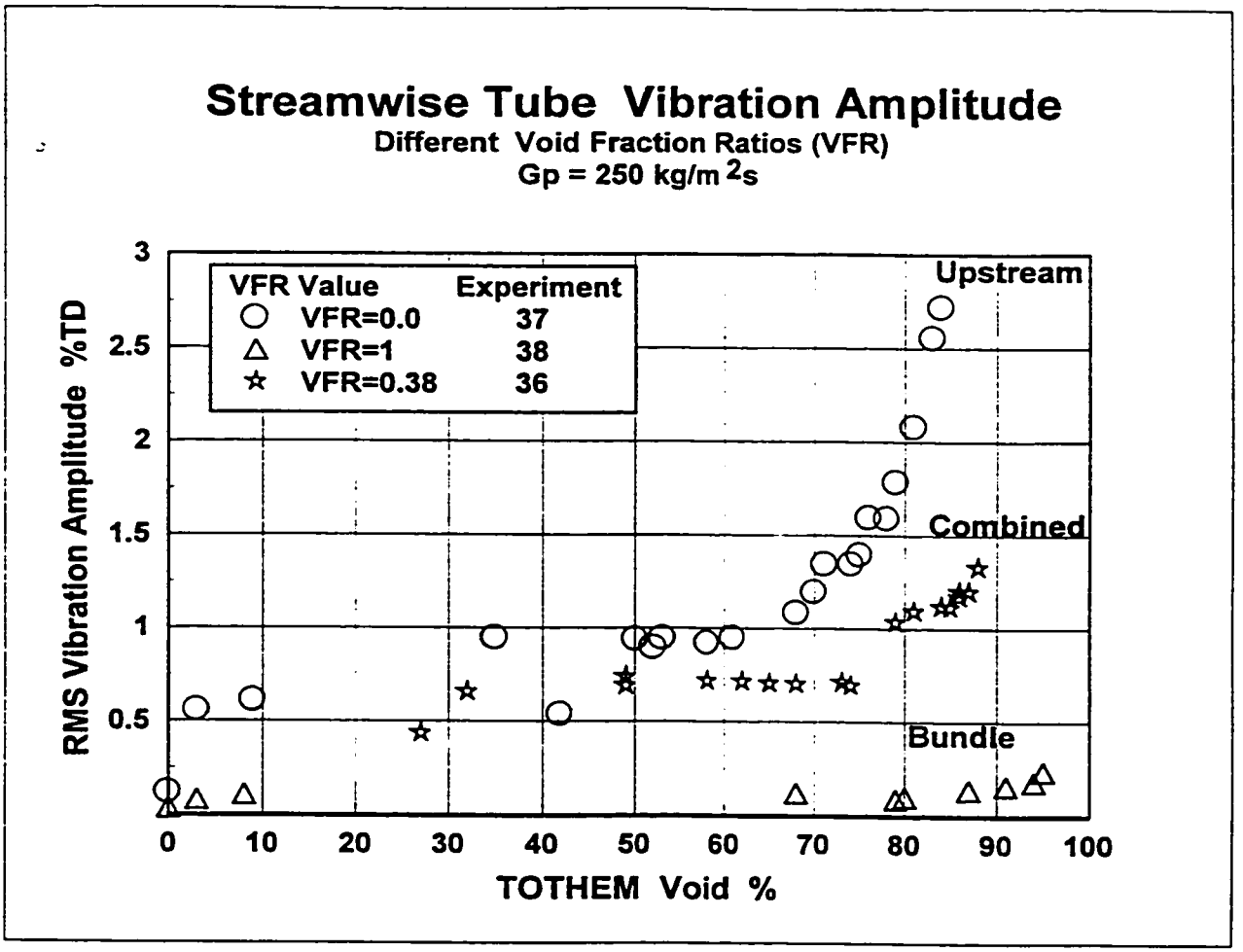

Figure 5.15 Streamwise tube vibration amplitude versus total homogeneous model void (TOTHEM) at the tube location for different void fraction ratios. Pitch mass flux Gp= 250 kg/m 2s.

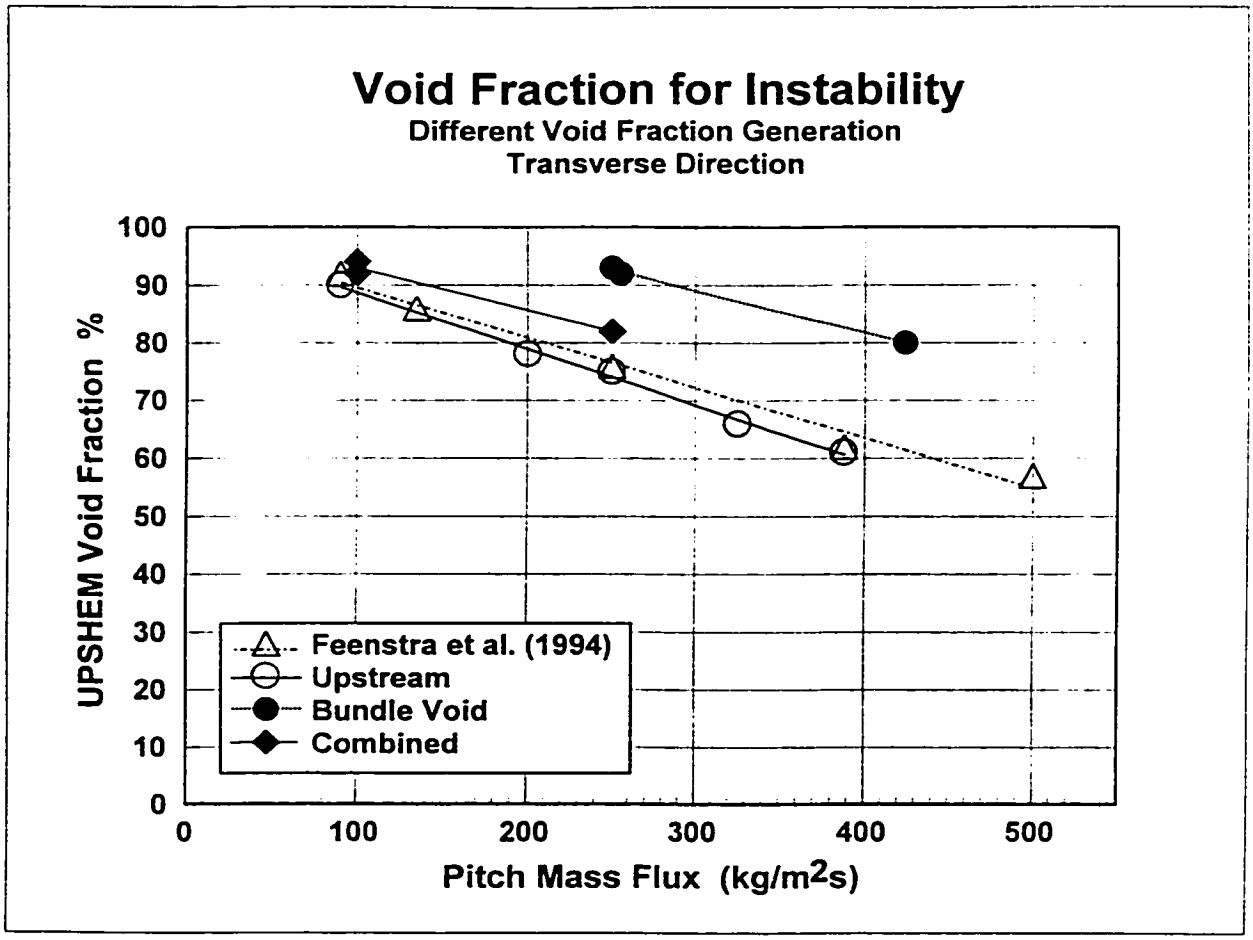

Figure 5.16 Void fraction at which instability occurred versus pitch mass flux for different methods of void fraction generation. Instability defined by transverse direction vibration response.

investigation of Feenstra et al. represented by the open triangles. The difference, not larger than 4%, can be accounted for by the method of obtaining the void fraction at which instability occurred in each case, which as explained earlier in section 5.2, was different. Other factors such as a slight difference in pitch ratio could also contribute to this difference, although it must be said that this difference is scarcely larger than the void fraction experimental uncertainty. The data for pure bundle boiling (filled circles), however, falls clearly above data for upstream cases for both studies, with not less than 16% difference over the closest one. The data for the combined cases, represented by diamonds, falls as expected, between the two previous cases, although, the difference with the upstream cases (8%) is rather smaller than in the case of pure bundle boiling.

5.5 Intermittent Boiling Experiments

In previous experiments, the data was taken under steady state conditions, and hence no changes in flow conditions were present in a particular trial. This is the correct approach when tube response data has to be collected over long periods of times and averages are to be used in the analysis. Although this approach is useful for generating experimental data in a format that can be used for design purposes in industry, it can easily hide relationships between some important parameters such as the instantaneous thermodynamic conditions of the flow and the tube response. In this section, a number of experiments are described in which the tube vibration amplitude and void fraction at the monitored tube location

were recorded continuously by a data acquisition system, using the optical sensor and gamma densitometry technique, respectively. Each experiment consisted of turning the power on and off a number of times at regular intervals, typically 60 seconds duration, for each set of conditions. Each set of two intervals , one with the power on and one with the power off, is referred to as a cycle.

An important consideration in performing these experiments was to check that initial conditions were the same at the beginning of each new cycle. In this manner, each cycle could be considered to be the repetition of the same experiment and the tube response observed in each of them could be used to compile a more representative and reproducible tube average response for those conditions.

5.5.1 Intermittent Boiling in Full Bundle

In figure 5.17, the instantaneous transverse tube vibration amplitude and void fraction observed in experiment 32 are plotted against time. Four full cycles in which the heat was turned off and on in the full bundle (ten tubes) were observed in this experiment. Every time the heat was turned on, with the exception of the initial transient period, boiling occurred at the surface of the tubes. Table 5.2 shows the length of time the heat was on and off in each period, the average vibration amplitude and void fraction for that particular period. The conditions were mass flux Gp= 255 kg/m^{2}s, the void fraction coming from

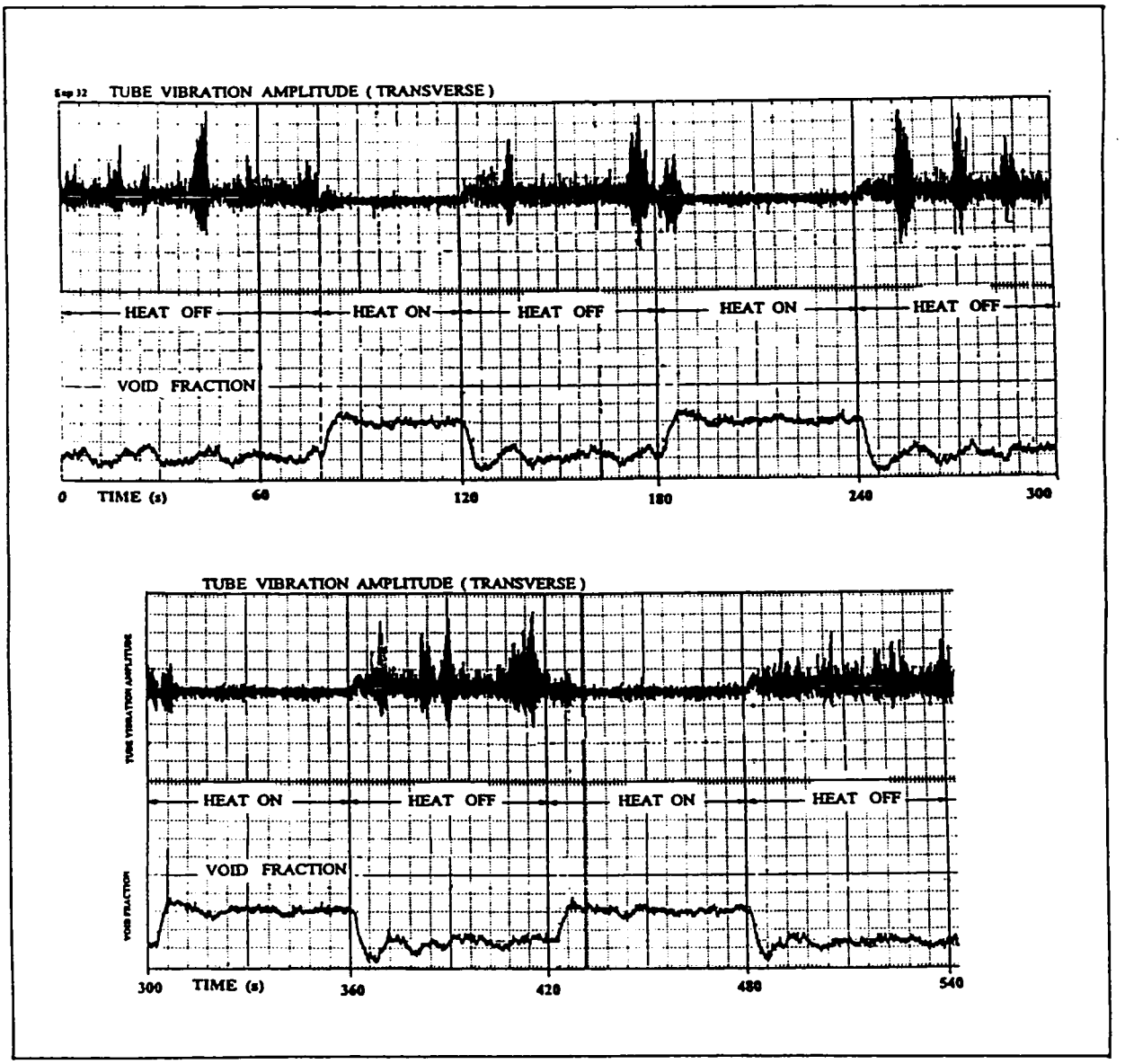

Figure 5.17 Instantaneous tube vibration amplitude and void fraction for intermittent boiling in the full tube bundle

upstream was 75% HEM (UPSHEM) and 44% based on gamma densitometry measurements (TOTGAM, equivalent to 76% UPSHEM).

Time -period seconds	Transverse Amplitude % Tube diam.	Void Fraction TOTGAM %	Heating condition in the bundle
0-78	2.50	0.44	OFF
81-120	0.69	0.55	ON
123-180	2.97	0.44	OFF
185-240	1.43	0.55	ON
243-303	3.52	0.44	OFF
306-360	0.99	0.56	ON
363-423	3.60	0.44	OFF
426-480	0.87	0.56	ON
483-544	2.39	0.44	OFF
Averages Off	**3.00**	**0.44**	
Std Dev Off	**0.56**	**0.00**	
Averages On	**1.00**	**0.56**	
Std Dev On	**0.32**	**0.006**	

Table 5.2 Amplitude and void fraction averages for intermittent boiling in the full bundle.Table corresponds to figure 5.15, with 21% increase in TOTGAM void fraction when the heat is on.

The void fraction values indicated in the table are the average void fractions for each period. A transient response time of about 3 s at the beginning and end of each period was disregarded in these calculations. In the table, the average of the averages of all periods with the same condition (heat on or off) is presented. The standard deviation of this average is also calculated. Numbers show that amplitude of vibration decreased substantially from an average of 3% to 1% tube diameter each time that void fraction was produced in the

bundle at the surfaces of the tubes. Void fraction in the bundle changed from 75% when heat was off to 86%, when the heat was on (TOTGAM=55%).

As stated, in previous steady state experiments in which a similar reduction in vibration amplitude was observed for cases of combined void fraction generation, this reduction effect is in opposition to the classical case of upstream void generation. In this case, an increase of void fraction in the bundle, while the mass flux is kept constant produces an increase in the vibration amplitude.

The vibration bursts observed in Fig. 5.17 are due to the coupling effect between the fluid forces and the tube motion. The initial condition corresponds to relatively small amplitude tube vibration, typically less than 1% of the tube diameter, in which the fluid force fluctuations come into phase with the tube motion (off the centre position) in the same direction as the tube velocity (Pettigrew et al. 1989). This synchronizing phenomenon produces an increase in tube vibration amplitude during each cycle. However, when the tube vibration amplitude reaches a certain level, these synchronizing conditions can no longer be maintained and the coupling effect disappears. Then the tube vibration amplitude returns to the original condition until the process repeats itself again. These coupling effects are strongly nonlinear and the vibration "bursts" appear to be random in amplitude and time. As the flow condition gets closer to the instability threshold, the duration of these vibration

bursts increases (see section 5.9). This is a typical example of nonlinear, amplitude limited self-excited vibration. It is thought that when the heat is on, the bubbles generated in a unit cell may disturb the synchronization of the fluid forces and tube motion.

5.5.2 Monitored Tube Unheated.

The heating condition in the experiment described in the previous sub-section did not permit the question of the effect of boiling at the surface of the monitored tube on the tube vibration response to be tested. Figure 5.18, 5.19, and 5.20 show the tube response when intermittent heating was applied to all tubes in the bundle except for the monitored one,which had no heating. The flow conditions at the upstream edge of the bundle were Gp=252 kg/m^{2}s and UPSHEM = 79%.

As in the previous case, Table 5.3 presents the time periods in which the heat was on and off , the averages for the tube amplitude in both directions and the average void fraction for each period. The table also shows the average and standard deviation of the amplitude and void fraction for those periods with the same heat condition (on or off). As was done in the previous experiment, a time lag between the time the application of power

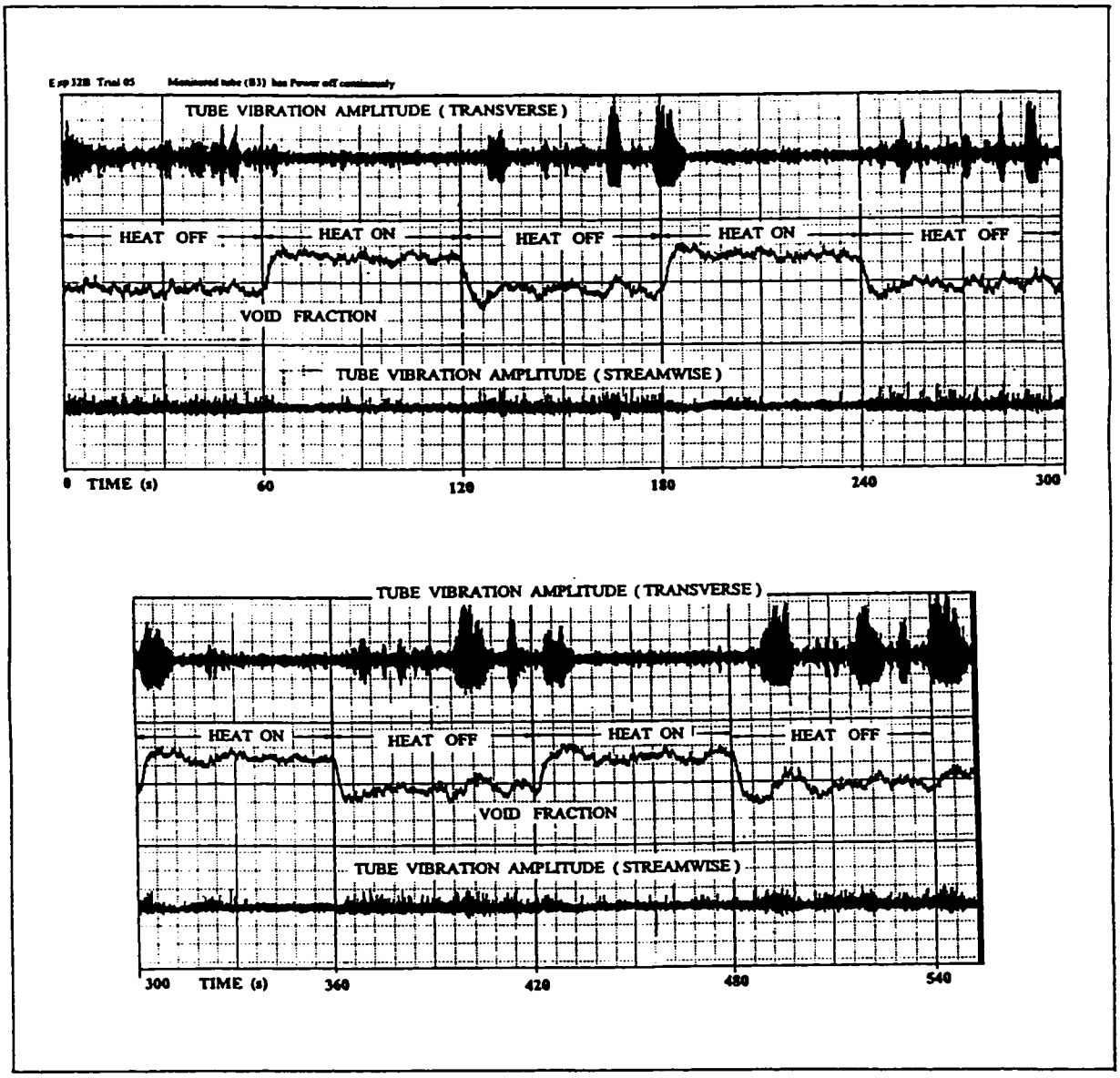

Figure 5.18 Instantaneous tube vibration amplitude and void fraction for intermittent boiling in the tube bundle. Monitored tube unheated

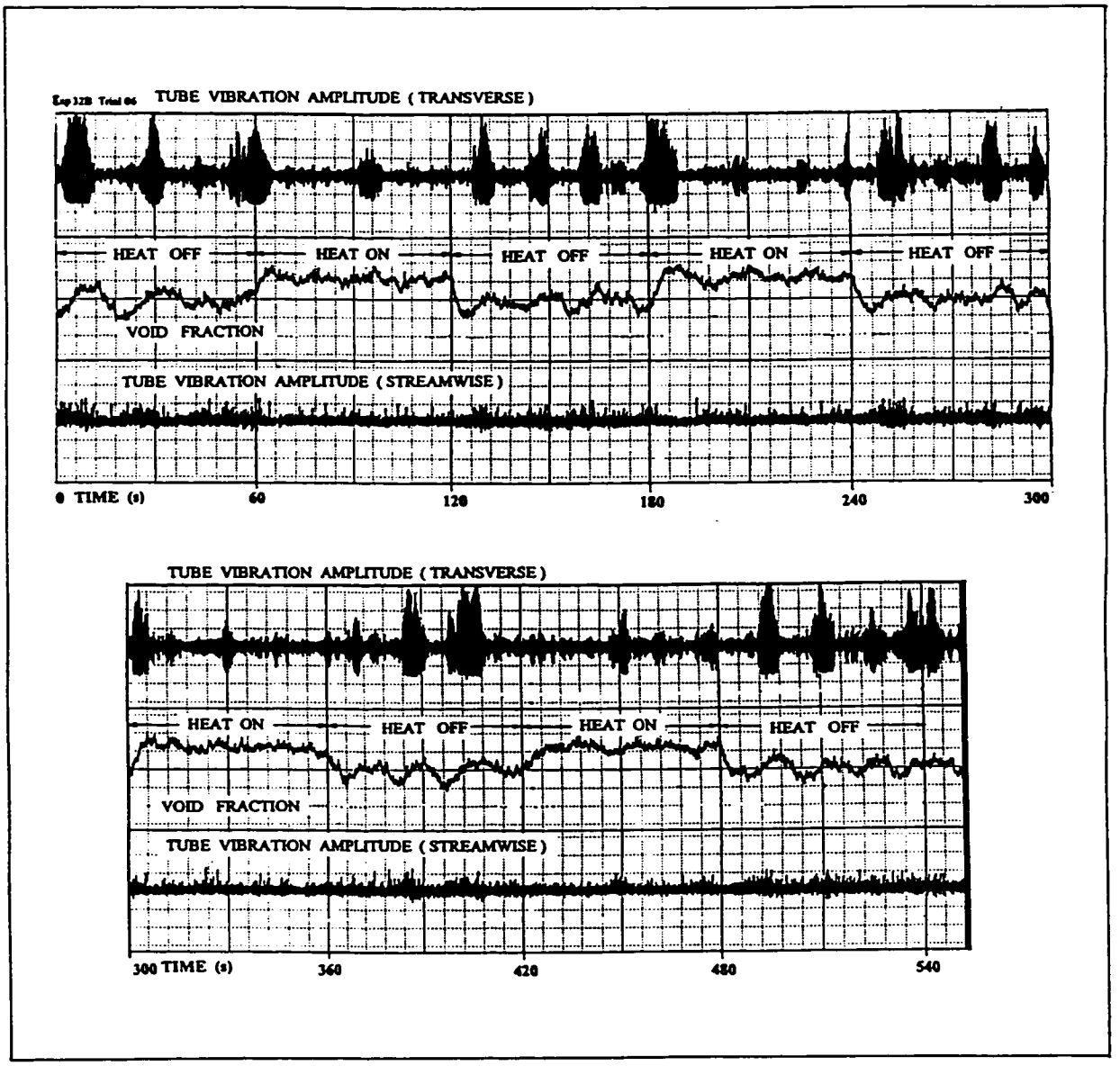

Figure 5.19 Instantaneous tube vibration amplitude and void fraction for intermittent boiling in the tube bundle. Monitored tube unheated .

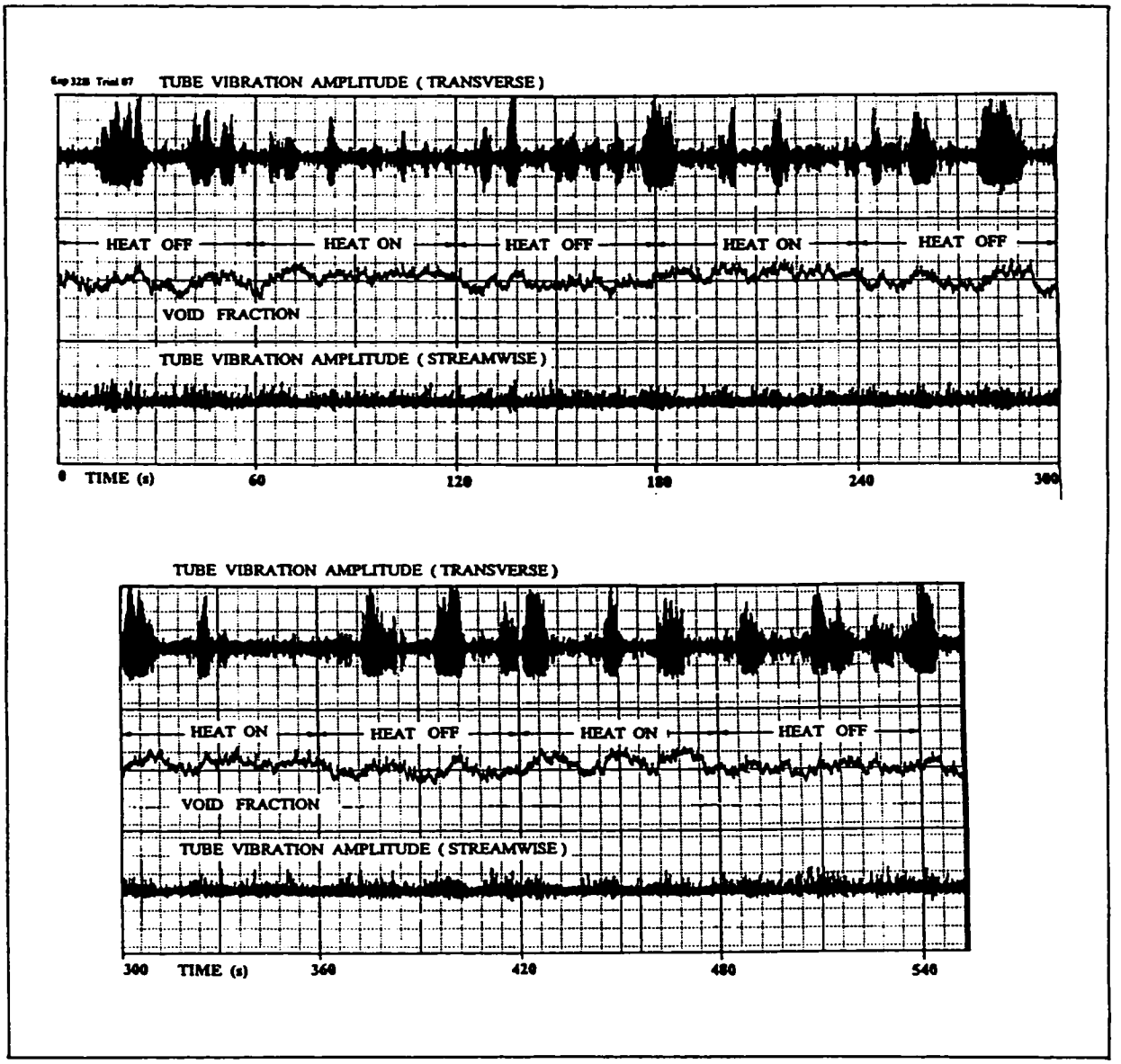

Figure 5.20 Instantaneous tube vibration amplitude and void fraction for intermittent boiling in the tube bundle. Monitored tube unheated

a)

Time -period seconds	Transverse Amplitude % tube Diam.	Streamwise Amplitude % tube Diam.	Void Fraction Totgam %	Heat Condition in the bundle
0-66	3.4	1.4	0.38	OFF
66-126	1.3	0.9	0.57	ON
126-186	5.1	1.4	0.37	OFF
186-246	1.4	0.9	0.58	ON
246-306	4.5	1.4	0.39	OFF
306-366	2.7	1.0	0.58	ON
366-426	4.9	1.5	0.38	OFF
426-486	2.6	1.0	0.58	ON
486-546	6.7	1.6	0.39	OFF
Avg. Power Off	**4.9**	**1.44**	**0.38**	
Std. Dev. Off	**1.2**	**0.08**	**0.01**	
Avg Power On	**2.0**	**0.94**	**0.57**	
Std. Dev. On	**0.7**	**0.04**	**0.005**	

b)

Time -period seconds	Transverse Amplitude % tube Diam.	Streamwise Amplitude % tube Diam.	Void Fraction Totgam %	Heat Condition in the bundle
0-66	6.7	1.5	0.38	OFF
66-126	2.4	1.1	0.51	ON
126-186	6.5	1.4	0.37	OFF
186-246	3.3	1.1	0.52	ON
246-306	6.0	1.6	0.38	OFF
306-366	2.8	1.1	0.52	ON
366-426	6.3	1.5	0.38	OFF
426-486	3.0	1.2	0.51	ON
486-546	6.7	1.5	0.39	OFF
Avg. Power Off	**6.4**	**1.5**	**0.38**	
Std. Dev. Off	**0.3**	**0.0**	**0.01**	
Avg Power On	**2.9**	**1.2**	**0.51**	
Std. Dev. On	**0.4**	**0.0**	**0.01**	

c) Time -period seconds	Transverse Amplitude % tube Diam.	Streamwise Amplitude % tube Diam.	Void Fraction Totgam %	Heat Condition in the bundle
0-66	5.9	1.5	0.38	OFF
66-126	3.1	1.3	0.42	ON
126-186	5.6	1.5	0.37	OFF
186-246	4.2	1.3	0.43	ON
246-306	6.6	1.5	0.39	OFF
306-366	4.1	1.3	0.43	ON
366-426	6.7	1.5	0.38	OFF
426-486	5.2	1.3	0.44	ON
486-546	6.2	1.6	0.39	OFF
Avg. Power Off	**6.2**	**1.5**	**0.38**	
Std. Dev. Off	**0.5**	**0.0**	**0.01**	
Avg Power On	**4.1**	**1.3**	**0.43**	
Std. Dev. On	**0.8**	**0.0**	**0.01**	

Table 5.3 Amplitude and void fraction averages for intermittent boiling in the bundle except the monitored tube, which is not heated. Table correspond to (a) figure 5.18, (b) figure 5.19 and (c) figure 5.20.

begun and the starting time of the averaging period was identified. In this particular set of experiments, the time lag was 6 seconds. This rule does not apply to the void fraction averaging, where the time lag was applied only at the beginning of the period. When power was applied between the 60th and 120th second, void was calculated for the time between the 66th and the 120th second, while average amplitude was computed from the 66th to the 126th second. The difference in time lag used in these experiments differs from the 3 seconds used in the previous experiment. The explanation is that the monitored tube needs a longer time to be affected the bubbles produced by the other tubes when there is no bubble generation on its surface.

The graph in figure 5.18 shows the instantaneous tube vibration in both transverse and streamwise directions along with void fraction for 66% of full electric power in the bundle. The effect of boiling on the monitored tube vibration was similar to that observed in Fig 5.17. The average vibration amplitude in the transverse direction decreased from 4.9%TD when heat was off to 2%TD when heat was on. For the streamwise direction, the reduction was from 1.44%TD to 0.95%TD for same the conditions. This is suggestive that the reduction in tube vibration due to boiling in the bundle is not a consequence of a tube surface phenomenon, but rather a local effect caused by the void generated on the surrounding tubes. This latter experiment also indicates that the reduction in tube vibration amplitude can not be attributed to changes in the structural damping ratio of the tube due to changes in internal temperature when heat is being generated by electrical resistance heating.

The graphs in figure 5.19 and 5.20 show data similar to that shown in figure 5.18. In these cases, electric power to the bundle was reduced to 40% and 21% respectively. It is observed that as the heat dissipated in the bundle decreases, the reducing effect in the tube vibration amplitude decreases as well.

5.5.3 Intermittent Boiling on the Monitored Tube

The last set of experiments of this type consisted of applying intermittent power to the monitored tube when the heat to the rest of the bundle was on continuously. This experiment was repeated for three levels of bundle heating. Table 5.4 shows the average amplitude and void fraction for each period and each level of bundle power. It also shows the averages and standard deviation for those periods correponding to the same power condition (on or off). Figures 5.21, 5.22 and 5.23 show the amplitude of vibration for the streamwise and transverse directions and the void fraction versus time, for 20.9%, 40.2% and 65.7% bundle electric power level respectively. Clear differences in vibration amplitude for on and off heat conditions cannot be observed on the graphs or in the average values for each period as seen in table 5.3. However, the standard deviation of the transverse amplitude is reduced significantly when the power is on to the monitored tube, especially for the lower void fraction tests.

The data from the seven trials performed in these experiments were analysed and plotted to investigate the possibility of a relationship among them. In figure 5.24, the reduction in amplitude in the transverse direction as a percentage of the amplitude corresponding to the heat off condition has been plotted against the increase in void fraction as a percentage of the void in the heat off condition. Although the data are quite scattered it seems reasonable to conclude that an increase in void fraction generated by bundle

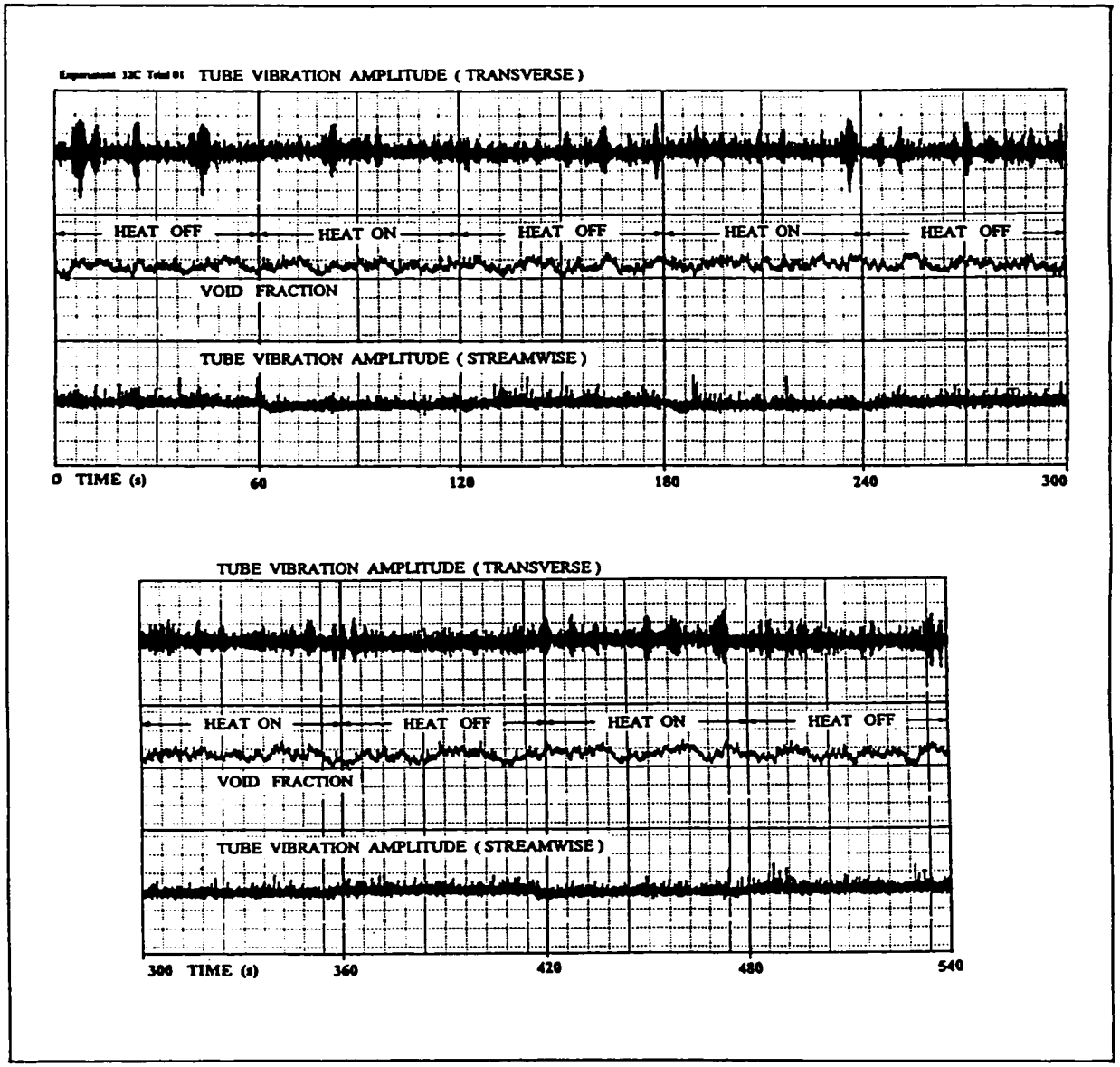

Figure 5.21 Instantaneous tube vibration amplitude and void fraction for intermittent boiling on the monitored tube (2% increase in void fraction). Rest of bundle with continuous power.

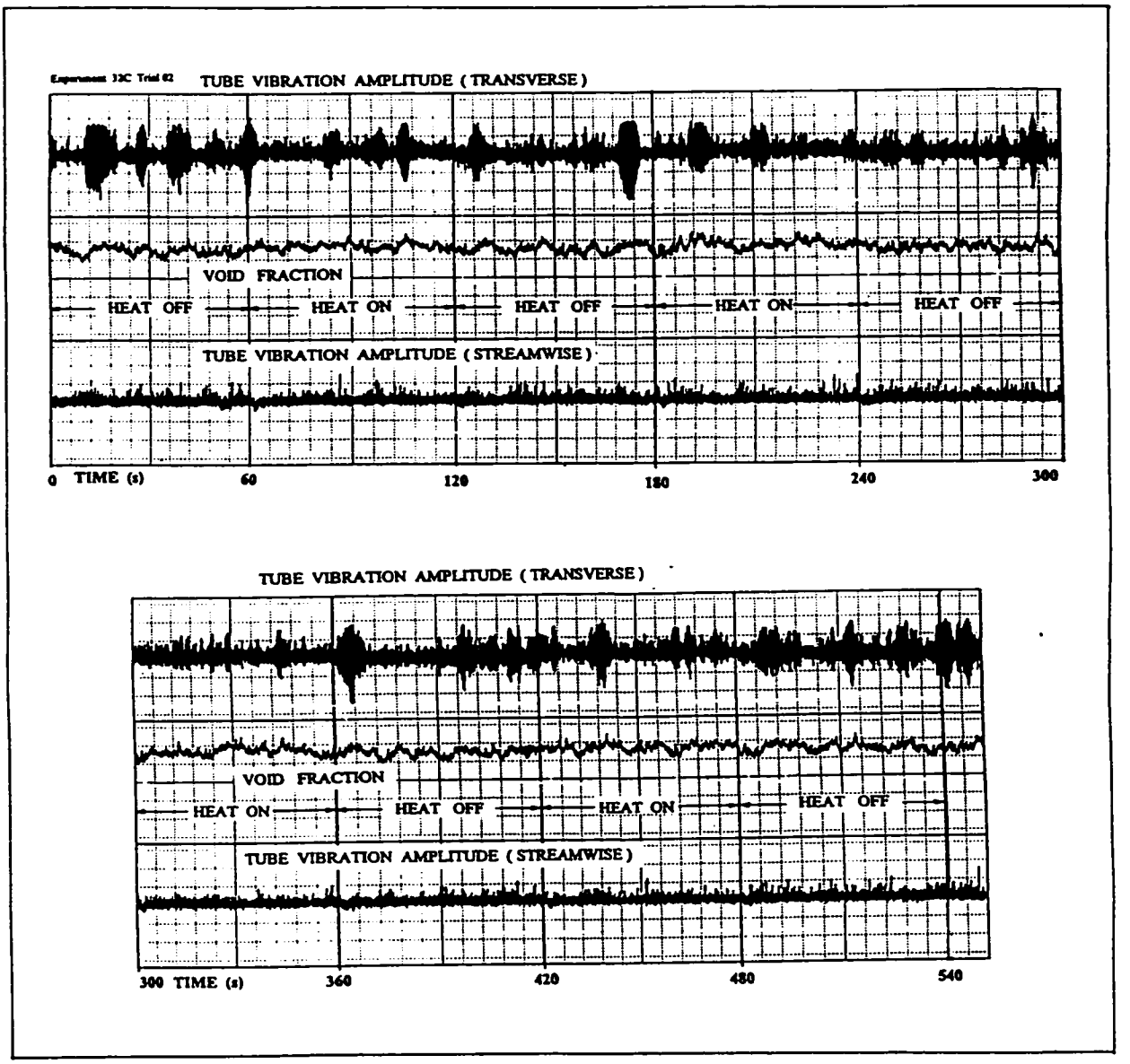

Figure 5.22 Instantaneous tube vibration amplitude and void fraction for intermittent boiling on the monitored tube (3.2 % increase in void fraction). Rest of bundle with continuous power.

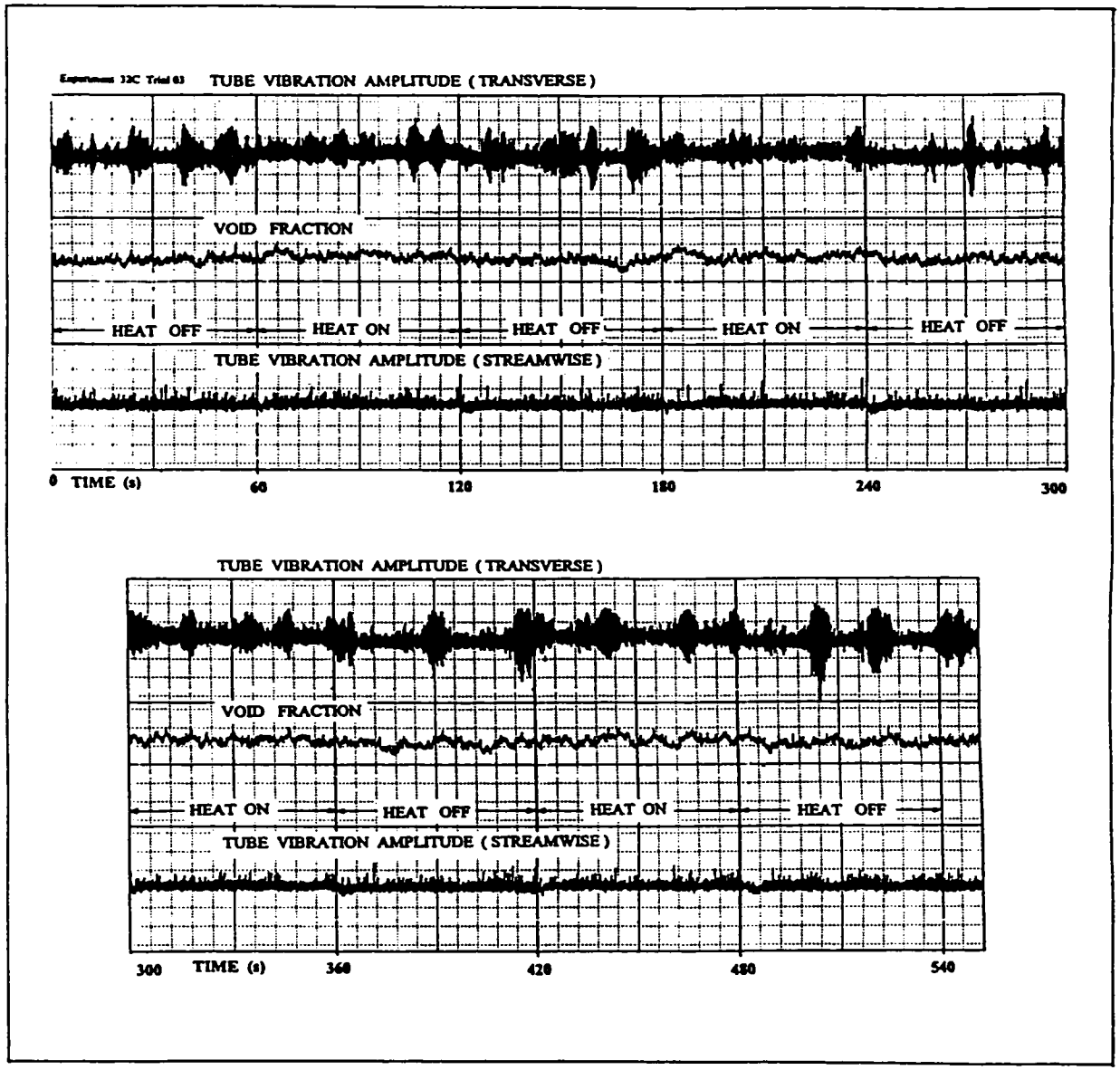

Figure 5.23 Instantaneous tube vibration amplitude and void fraction for intermittent boiling in the monitored tube (3.5 % increase in void fraction). Rest of bundle with continuous power.

(a)

Time -period seconds	Transverse Amplitude % tube Diam.	Streamwise Amplitude % tube Diam.	Void Fraction TOTGAM %	Heating Condition in the Tube
0-60	3.8	1.3	0.46	OFF
63-120	2.6	1.2	0.46	ON
123-180	2.7	1.3	0.46	OFF
183-240	3.1	1.3	0.47	ON
243-300	2.8	1.3	0.46	OFF
303-360	2.5	1.2	0.47	ON
363-420	2.4	1.2	0.45	OFF
423-480	3.0	1.3	0.47	ON
483-540	2.5	1.3	0.46	OFF
Avg. Power Off	**2.8**	**1.27**	**0.459**	
Std. Dev. Off	**0.6**	**0.02**	**0.004**	
Avg Power On	**2.8**	**1.24**	**0.469**	
Std. Dev. On	**0.3**	**0.04**	**0.005**	

(b)

Time -period seconds	Transverse Amplitude % tube Diam.	Streamwise Amplitude % tube Diam.	Void Fraction TOTGAM %	Heating Condition in the Tube
63-120	3.2	1.1	0.57	ON
123-180	4.6	1.2	0.55	OFF
183-240	3.6	1.2	0.57	ON
243-300	3.4	1.2	0.55	OFF
303-360	2.9	1.1	0.57	ON
363-420	4.5	1.2	0.55	OFF
423-480	3.8	1.1	0.57	ON
483-540	4.5	1.2	0.55	OFF
Avg. Power Off	**3.4**	**0.98**	**0.44**	
Std. Dev. Off	**2.0**	**0.55**	**0.25**	
Avg Power On	**3.4**	**1.12**	**0.57**	
Std. Dev. On	**0.4**	**0.03**	**0.00**	

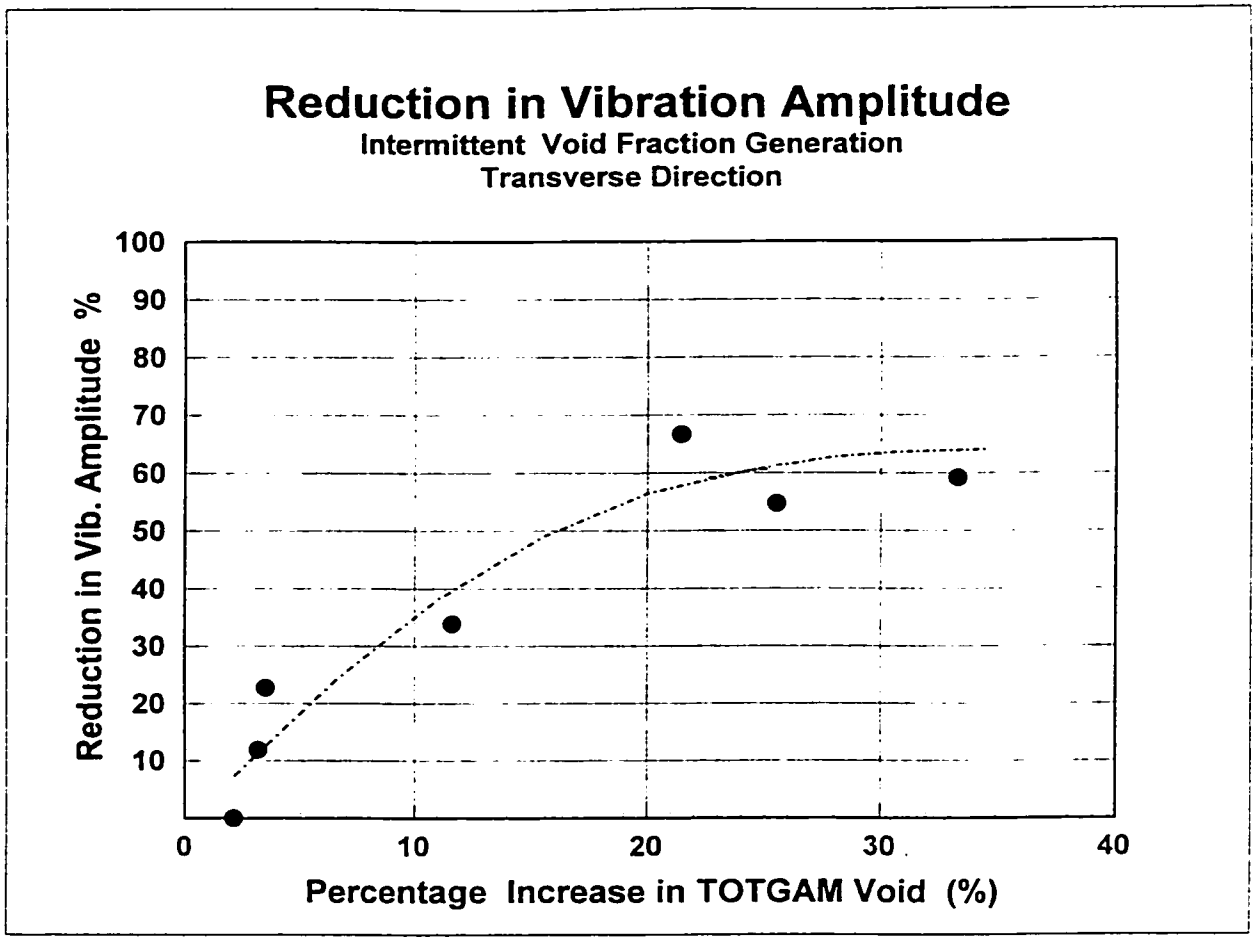

Figure 5.24 Percentage reduction in transverse tube vibration amplitude versus percentage increase in void fraction due to bundle boiling in the intermittent heating experiments. Pitch mass flux Gp = 250 kg/m^{2}s.

c)				
Time -period	Transverse	Streamwise	Void Fraction	Heating
seconds	Amplitude	Amplitude	TOTGAM	Condition
	% tube Diam.	% tube Diam.	%	in the Tube
0-60	4.1	1.2	0.60	OFF
63-120	3.8	1.1	0.63	ON
123-180	4.5	1.2	0.60	OFF
183-240	3.1	1.1	0.63	ON
243-300	3.3	1.1	0.61	OFF
303-360	3.8	1.1	0.62	ON
363-420	4.3	1.2	0.61	OFF
423-480	4.1	1.1	0.63	ON
483-540	4.5	1.3	0.61	OFF
Avg. Power Off	**4.2**	**1.19**	**0.61**	
Std. Dev. Off	**0.5**	**0.05**	**0.01**	
Avg Power On	**3.7**	**1.09**	**0.63**	
Std. Dev. On	**0.4**	**0.01**	**0.00**	

Table 5.4 Amplitude and void fraction averages for intermittent boiling in the monitored tube. Heat is on continuously to the rest of the bundle.Table correspond to (a) figure 5.19, (b) figure 5.20 and (c) figure 5.21.

boiling does produce a reduction in the vibration amplitude and that the larger the increase in void generated, the larger is the reduction in amplitude.

5.6 Fluidelastic Instability Diagram

Fluidelastic instability data for upstream (VFR= 0), combined (0<VFR< 1.0) and pure bundle boiling (VFR = 1.0) void generation were plotted on a reduced velocity/mass-damping parameter diagram along with the data of some other researchers. The experiments are identified by a number and a letter, the number corresponding to the pitch mass flux Gp, and the letter corresponding to the type of void fraction generation, U

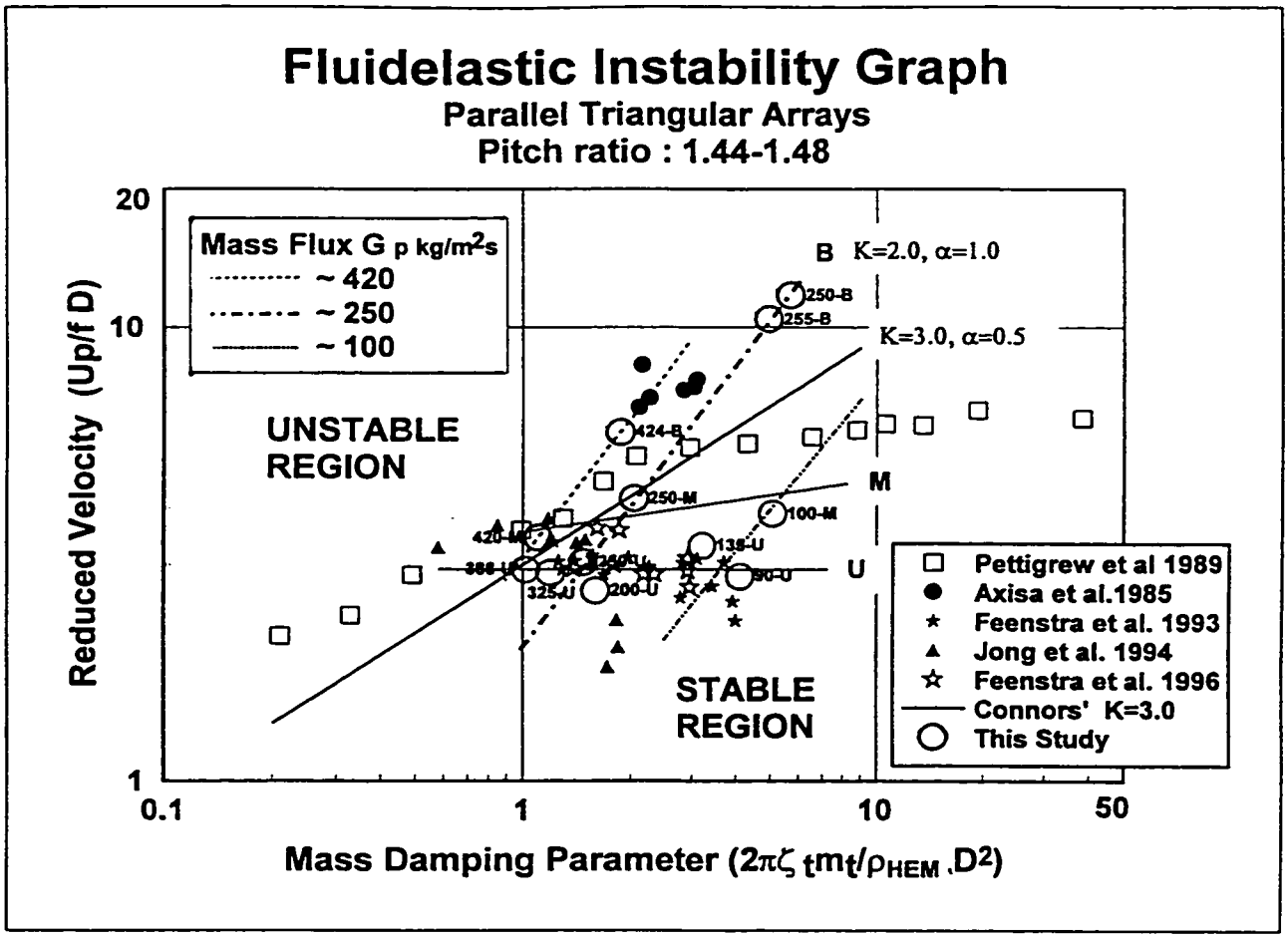

Figure 5.25 Instability data obtained in this study and relevant data from other investigations.

DATA TABLE

Fluidelastic Instability Data

Exp. data Label	Mass Flux (Pitch) Gp Kg/m2s	HEM Void Upshem %	Gas density Kg/m3	Liquid density Kg/m3	HEM Density Kg/m3	Pitch Velocity Up m/s	Reduced Velocity	Tube Frequency Hz	Total Damping	Total mass per unit length kg/m	Mass Damping Parameter
90-U	90	0.90	8.06	1455.20	152.8	0.59	2.83	33.80	0.024	0.159	4.135
135-U	135	0.87	8.14	1454.40	196.2	0.69	3.31	33.80	0.024	0.159	3.220
250-U	250	0.75	8.73	1448.80	368.7	0.68	3.03	36.30	0.024	0.138	1.485
388-U	388	0.61	9.80	1439.00	567.2	0.68	2.92	38.00	0.028	0.126	1.028
200-U	200	0.77	8.26	1453.00	340.6	0.59	2.63	36.30	0.024	0.138	1.608
325-U	325	0.67	8.68	1449.20	484.1	0.67	2.87	38.00	0.028	0.126	1.204
250-B	250	0.94	9.71	1439.90	95.5	2.62	11.70	36.30	0.024	0.138	5.733
424-B	424	0.79	10.80	1430.50	308.9	1.37	5.86	38.00	0.028	0.126	1.887
100-M	100	0.92	8.26	1453.20	123.9	0.81	3.88	33.80	0.024	0.159	5.100
250-M	250	0.82	10.14	1436.00	266.8	0.94	4.19	36.30	0.024	0.138	2.053
255-B	255	0.93	10.13	1436.00	109.9	2.32	10.37	36.30	0.024	0.138	4.981
420-M	420	0.64	10.33	1434.60	523.1	0.80	3.43	38.00	0.028	0.126	1.115

for upstream, B for bundle and M for combined cases of these two. Figure 5.25 shows the plot and presents the tabulated data for the data points obtained in this study, which have been represented by circles and labelled according to the experiment designation. Since conclusive values of two-phase flow damping ratios were not determined in this study, the corresponding data from Feenstra et al. (1996) were used in the calculation of the mass-damping parameter.

It is interesting to observe that the results of the 250-B, 255-B and 424-B experiments, all of which correspond to pure bundle boiling are located in the upper part of the graph, near the steam-water data obtained by Axisa et al.(1985). These data points are found in the unstable region defined by the dotted line which is based upon Connors' equation using K=3.0.

The results of experiments 388-U, 325-U, 250-U, 200-U, 135-U and 90-U, which correspond to classical upstream void fraction generation fall in the same region as those of Feenstra et al.(1996) and Pettigrew et al. (1994). Moreover, the data points with the same mass flux as Feenstra's data fell in the same region of the graph. These data points define a trend which can be represented by an almost horizontal line, where the highest mass flux (Gp=388 kg/m²s) is located at the left end and the lowest at the right end (Gp=90 kg/m²s). This trend is also seen in the higher mass-damping parameter range of Pettigrew et al.(1989) data.

The results of experiments 420-M, 250-M and 100-M were determined by experiments in which both sources were contributing to the total void fraction at the monitored tube location. In 420-M, VFR= 0.14 indicating that at the instability threshold, 14% of void was being generated in the bundle. In 250-M, VFR= 0.35 and in 100-M , VFR=0.90. These data points are above the data collected with upstream void generation and below the data for bundle void generation. These data points also follow a similar trend as the upstream ones, following a horizontal line that seems to be parallel and above the one for the upstream case. The relative location of these data in the diagram indicates that cases of combined void fraction generation are members of a family which is defined by combinations of pure bundle and upstream void generation cases.

In experiments 250-U, 250-M, 250-B and 255-B (mass flux about 250 kg/m²s) the only distinguishing difference is the value of the void fraction ratio VFR, the percentage of void generated in the bundle with respect to the total void at the tube location. As VFR increases from 0% in experiment 250-U to 0.35 in experiment 250-M and to 1.0 in experiments 250-B and 255-B, the data points at which instability occurred moved upwards and to the right. The data also follow a straight line which crosses the line defined by Connors' relationship, but with an inclination $\alpha = 1.0$ and a coefficient $K = 2.0$. This trend clearly indicates that the flow velocity at which instability occurs increases substantially as the bundle generated void increases. It would seem that bundle boiling suppresses the phenomenon that causes the instability data points to fall into the stable region to the right side of the Connors' line.

Experiments 388-U, 420-M and 424-B were conducted at a similar mass flux, the only difference being the void fraction ratio, VFR, which was 0.0 in experiment 388-U, 0.14 in experiment 420-M and 1.00 in experiment 424-B. The location of the data points on the graph suggests a similar trend as for the previous case of mass flux Gp= 250 kg/m^{2}s. Here again, it is observed that as bundle boiling increases, the velocity for instability increases so that the data points move in the same direction upwards and to the right as in the previous case.

5.7 Effect of Correlation Length on Tube Vibration Response.

Based on experimental data presented in this investigation, it has been conclusively demonstrated that tube vibration amplitude decreases substantially under the presence of tube surface boiling, other factors such as pitch mass flux (Gp) and void fraction at the monitored tube location (UPSHEM) being constant. From the graph in figure 5.14, one vibration amplitude data point corresponding to 50% UPSHEM void fraction for each of the three cases: pure upstream, combined, and bundle void fraction generation have been extracted and presented in table 5.5. Analysis shows that a factor of 1.72 exists between the transverse amplitudes of upstream and combined cases, as presented in the same table Similarly, a factor of 7.8 exists between amplitudes of upstream and bundle cases and a factor of 4.5 exists between the combined and bundle cases.

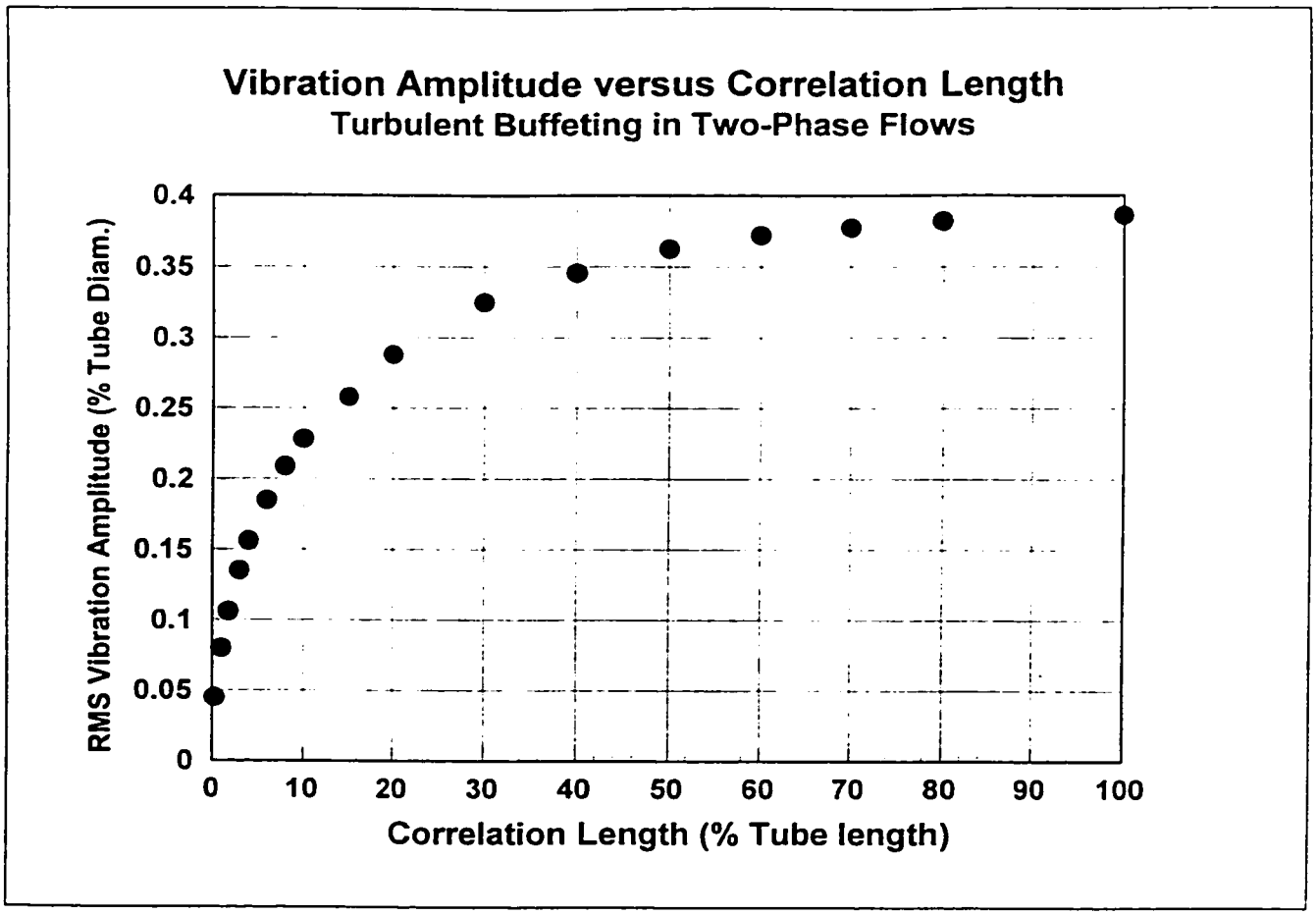

Figure 5.26 Tube vibration response due to turbulent buffeting versus correlation length in the forcing function. Model used Axisa et al. 1990

One possible explanation for this effect is the reduction of correlation length in the turbulent buffeting forces affecting the tube. Using the approach developed by Axisa et al. (1990), calculations of the tube response due to turbulent buffeting forces in two-phase flows were performed (see Appendix D) and presented in table 5.5. A cantilevered tube in a parallel triangular array with a pitch to diameter ratio of 1.48 was assumed in the calculations. The void fraction used was 50% HEM, which corresponds to a value where the tube response is only due to turbulence excitation. The mass flux was taken to be Gp=250 kg/m^{2}s. The total damping ratio used (3.5%) was taken from Pettigrew et al. 1989. The dimensionless power spectral density used was obtained from Taylor et al. (1989). Figure 5.26 shows the RMS vibration amplitude predicted as percentage of the tube diameter versus the correlation length as percentage of the tube length of the turbulent forces. Using a force correlation length based on the estimated bubble size diameter, a correlation length value of 6% (20 mm) of the tube length for the upstream case, 1.8% (6 mm) for the combined case and 0.3% (1 mm) for the bundle case, were selected. The bubble size diameter estimation was based on flow vizualization through the test section window.

The amplitude ratio between the upstream case and the combined case is represented by the expression Au/Ac. Similar notation was used for the other two ratios. From the table it is clear that considering the complexity of the subject, the theoretically based amplitude ratios are similar to the ones for the experimental case. It is interesting to notice that

	Experimental			Theoretical		
	Upstream	Combined	Bundle	Upstream	Combined	Bundle
Ampl.%TD	1.63	0.95	0.21	0.185	0.106	0.045
Corr.Length	----------	----------	---------	6%	1.8%	0.3%
Bubble Size	20	6	1	20	6	1
	Au/Ac	Au/Ab	Ac/Ab	Au/Ac	Au/Ab	Ac/Ab
Ampl.Ratio	1.72	7.76	4.52	1.74	4.1	2.3

Table 5.5 Experimental and theoretical amplitude ratios for turbulent buffeting response

vibration amplitude predicted by the mathematical model is in average nearly 7.5 (±2) times lower that the experimental values in all the three cases. Furthermore, a bubble size of 0.3 mm instead of 1 mm for the bundle case, produces an average of 8.4 (±0.6). This finding suggests that the reduction in vibration due to the presence of boiling in the bundle is indeed due to a change in correlation length, although a suitable model and experimental data to determine correlation length values of the forcing function as well as bubble size in two-phase flows is not presently available.

5.8 Boiling Numbers in Nuclear Steam Generators

In the previous section, it was concluded that bundle boiling changes the values of reduced velocity at which fluidelastic instability occurs . The higher the percentage of void generated in the bundle, the higher the reduced velocity value. Bundle boiling is present in the U-bend region of nuclear steam generators and so a numerical comparison between

these experimental results and their corresponding values under steam generator operating conditions is appropriate. A boiling number Bo may be defined according to:

$$Bo = \left(\frac{\pi\, q''}{Gp\ \lambda}\right) / \left(\frac{P}{D}-1\right) \qquad 5.1$$

where q''= heat flux at the tube surface in kW/m², λ = heat of vaporization of the fluid in kJ/kg, P/D = pitch to diameter ratio and Gp = pitch mass flux in kg/m²s.

The boiling number is the ratio of the total power rejected from the tube per tube unit length to the total power needed to vaporize all the flow contained in a cross section of dimension P-D (tube gap) and a unit length parallel to the tube axis (see figure 5.7). The Bo value in the U-bend region of a typical nuclear steam generator, such as the Wolsung 2 station (Pettigrew 1996), assuming Gp=1000 kg/m²s, and water-steam at 4.5 MPa and 450K is $5.8\cdot10^{-4}$. The Bo values for experiments 420-M, 250-M and 100-M at the instability threshold are $13.2\cdot10^{-4}$, $8.7\cdot10^{-3}$, and $1.0\cdot10^{-1}$ respectively.

Since boiling numbers in the nuclear steam generators are lower than the ones used in these experiments, the void fraction ratio encountered in them should also be lower. Hence, the effects of boiling observed in these experiments are expected to be greater than those in real steam generators. Nevertheless, it is clear from Figure 5.25 that the main effect of bundle boiling is to move the tube instability threshold to a higher reduced

velocity. Therefore, the effect of boiling in a nuclear steam generator tube bundle would be to reduce vibration levels and increase the reduced velocity for instability. The results obtained under upstream void generation (no bundle boiling) are therefore conservative estimates of vibration amplitudes and instability thresholds in actual steam generators.

Instability data points obtained in the presence of bundle boiling do not experience the trend of moving to the right and down as those of Feenstra et al. (1996) or those of Pettigrew et al. (1994) or moving to the right and slightly up as those of Pettigrew et al.(1989) when the mass flux decreases. Instead, they tend to follow a straight line with a slope close to one and K=2.0 which differs from the line defined by Connors' equation using K=3.0, which has a slope of 0.5. As discussed above, this may be explained by the effects of bundle boiling on the correlation length of fluid forces applied to the tubes and also due to a stabilization of the bubbly flow regime.

5.9 Tube Motion Visualization

Tube motion visualization experiments were performed with two main objectives in mind. First, the objective was to visually confirm the tube vibration reduction due to bundle boiling found through the other experiments. Second, the objective was to obtain a physical image of the tube motion during the transition from the pre-instability to the post-instability condition.

Two experiments, 23 and 24 performed with a mass flux Gp = 250 kg/m^{2}s, involved video recording with a high speed camera at 250 frames per second. In experiment 23, the tube was subjected to bundle void fraction generation only. Five trials with UPSHEM void fractions values of 72, 82, 90, 92 and 94 were recorded. After careful examination of the video film, tube vibration amplitude in both directions was found to be negligible in all cases. Using a transparent grid located on the external side of the window, the tube motion was compared to a reference length. This technique allowed an approximate value of the tube vibration peak amplitude to be obtained. The results indicated that peak amplitude never exceeded 1% of tube diameter. This value is very small considering that tube instability for this mass flux is about 78% void fraction and that the corresponding transverse amplitude in the upstream void generation case is about 6 %TD. However, these results are in complete agreement with other experiments in this study, in which the maximum RMS vibration amplitude for identical flow conditions was recorded at 0.74% of tube diameter (see figure. 5.8) .

Experiment 24 was performed at the same flow conditions as experiment 23 except that void fraction was produced upstream of the bundle in five of the six trials. By examining the video film, it was found that large tube vibration amplitudes were present from the first trial to the last. It was also found that tube vibration was characterized by large peak amplitude pulsations, in excess of 20% tube diameter, which changed in time length and period as the void fraction increased. Table 5.6 presents the tabulated data of void

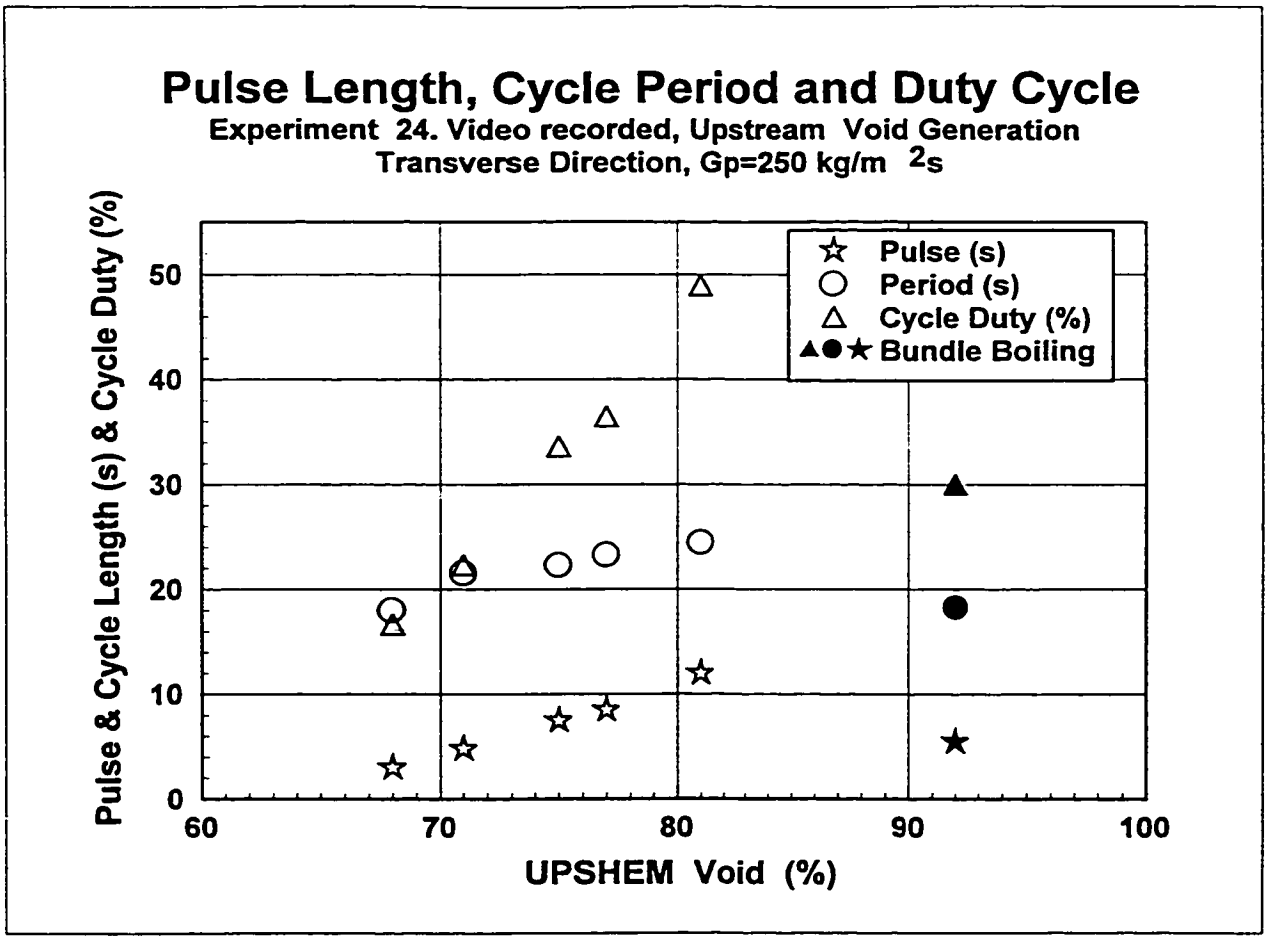

Fig.5.27 Pulse length, cycle period and cycle duty versus upstream generated void fraction. Gp=250 kg/m ^{2}s. Filled symbol with the addition of bundle boiling.

fraction and a schematic of the vibration amplitude pulse. Average pulse length, pulse period and the ratio between the pulse duration to the pulse period (cycle duty) are also presented. It is interesting to notice the drastic reduction in pulse length and period at the sixth trial when tube boiling was added to the upstream two-phase flow. Figure 5.27 shows the pulse length, the cycle period and cycle duty, versus the UPSHEM void.

It is clear from the graph that pulse length, and cycle duty are linearly proportional to void fraction. Pulse period also increases with void fraction but the rate of increase reduces as the void increases. The implication of these results on the tube vibration are that tube instability is not only obtained by a constant increase in tube amplitude but rather by a constant increase in the time that the tube is vibrating at large amplitude. By examining the video, it can be observed that when the tube is vibrating at large amplitude it corresponds to the time when the tube motion is synchronized with the motion of the rest of the tubes in the bundle. A reasonable hypothesis is that a coupling effect exists between tube motion in the bundle and the fluid flow.

These experiments confirm the reduction in tube vibration due to bundle boiling visually. They also shed some light on the transition of tube vibration from pre-instability to post-instability as the void fraction increases. The effect of tube boiling on tube vibration is to diminish the time that the tube is vibrating in synchronized motion with the rest of the

Trial #	UPSHEM Void %	Amplitude Pulse Schematics	Pulse Length (s)	Pulse Period (s)	Cycle Duty %
1	68	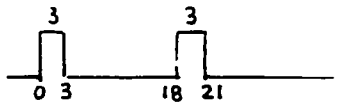	3	18	16
2	71	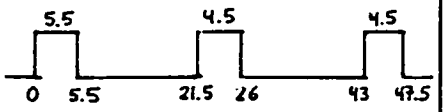	4.8	21.5	22
3	75	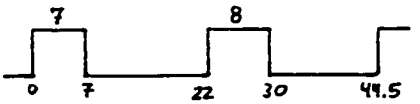	7.5	22.3	33
4	77	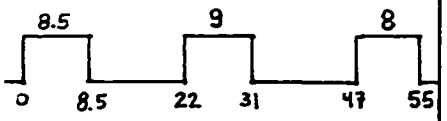	8.5	23.3	36
5	81	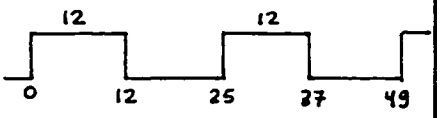	12	24.5	48
6	92	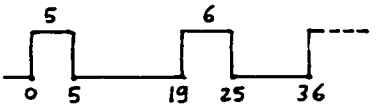	5.5	18.3	30

Table 5.6 Experimental data of tube amplitude pulsations in experiment 24.

tubes in the bundle. Synchronized motion is always accompanied by large vibration amplitude. The tube visualization in pure bundle boiling does not indicate large synchronized tube motion.

CHAPTER 6

CONCLUSIONS AND RECOMMENDATIONS

Conclusions derived from the information and knowledge obtained in this experimental investigation are summarized in the first part of this chapter. The second part of the chapter presents the recommendations to be considered in planning future investigations on this particular subject.

6.1 Conclusions

Nuclear steam generators have suffered the effect of flow induced vibrations for many years, in particular the U-bend region of the generator tube bundle, when exposed to a two-phase flow consisting of steam and water at high pressure and temperature. Tubes located in this region of the tube bundle have experienced high amplitude vibrations leading to tube failures and plant shut downs. Turbulent buffeting and fluidelastic instability have been identified as the main causes for these vibrations. Previous investigations have focused their objectives on gaining knowledge of subjects such as flow regime (Pettigrew et al.1989), two-phase flow damping ratio, (Feenstra et al.1996) and the importance of single or two components on tube vibration response (Taylor et al.1987). One phenomenon that has not been studied is the effect of tube surface boiling on the tube response. Vapour

generated on tube bundles in nuclear steam generators has the potential to affect the flow regime, void fraction distribution, turbulence levels and tube-flow interaction. All of these phenomena have the potential to change the tube vibration response .

A tube bundle consisting of 10 tubes, which were electric cartridge heaters was built and tested in a two-phase Freon-11 flow loop. The 10 tubes were arranged in a parallel triangular configuration with pitch to diameter ratio of 1.48. Tubes were installed in a cantilevered condition and had a natural frequency in air of 39 Hz. The tube bundle was exposed to two-phase flows consisting of different combinations of void from two sources. Void was generated upstream of the bundle and void was generated at the surface of the tubes. The pitch mass flux values were in the range of 100 to 430 kg/m²s. Tube tip vibration response in both directions, streamwise and transverse to the flow were measured with an optical sensor connected to a FFT analyser. Void fraction was measured by a gamma densitometry technique and void fraction values were also calculated by the HEM equation.

The most important effects of void fraction generated at the tube surface on the tube vibration response are the following:

1) The RMS tube vibration amplitude in the transverse direction was observed to be reduced by a factor of 8 when void fraction was generated upstream of the tube bundle, with respect

to the vibration amplitude observed when void was generated on the tube surface only (tube bundle void generation, or tube bundle boiling). The RMS vibration amplitude was reduced by about 2 for the case of upstream generated void case with respect to the combined upstream and bundle boiling case. Although this comparison was made for a mass flux of 250 kg/m^{2}s, similar reductions were observed at higher (424 kg/m^{2}s) and lower values of mass flux (100 kg/m^{2}s).

2) The effects on tube vibration response of void fraction generated in the tube bundle was found to be different from void fraction generated upstream of the tube bundle. Tube vibration amplitude decreased every time that void generated upstream of the bundle was replaced by an equivalent amount of void generated in the bundle.

3) The effect of tube vibration reduction when the void was generated in the tube bundle was not due to the generation of void on the monitored tube. Almost the same reduction was found when the void fraction was generated within the unit cell, which is defined as the volume encompassed by the neighbouring tubes around the monitored tube. As a consequence, it is clear that the effect of bubble generation at the surface of the vibrating tube is not the cause of the difference in tube vibration response.

4) Reduction of the tube vibration amplitude due to tube bundle void generation can be explained in terms of a reduction in the correlation length of the turbulent buffeting forces. Theoretical calculations of tube vibration response due to turbulent buffeting excitation under experimental conditions similar to the ones involved in this study and using correlation length values based on estimated bubble size predicted a reduction in tube vibration amplitude similar to the reductions found experimentaly.

5) The two-phase flow regime under tube bundle void fraction generation was observed to be bubbly and homogeneous over the full range of void fraction values, much different than the churn type of flow found in the upstream void fraction generation cases. Observations of bubble size under tube bundle void generation indicated that bubbles are much smaller than those accompanying the upstream void generation case.

6) The void fraction for the fluidelastic instability threshold under the presence of tube bundle void fraction generation was found to be higher (94% HEM) than that commonly found for the upstream void fraction generation case (76% HEM). A value of 82% HEM was required to reach the fluidelastic instability threshold in the cases of combined void fraction generation when the pitch mass flux was 250 kg/m^2s. These results clearly indicate that fluidelastic instability is possible under the three cases described above, and hence the upstream void generation cases studied in many of the previous investigations are only part of a spectrum of such cases.

7) The effect of tube bundle void fraction generation on tube vibration amplitude was more pronounced in the transverse direction that in the streamwise direction. In previous investigations, it has generally been found the transverse direction is the first to become unstable. The streamwise direction does not show a tendency to become unstable in some cases. It is postulated that the presence of vapour generated on the tube bundle changes the void fraction distribution around the tubes in such a manner that the tube motion in both streamwise and transverse directions become similar.

8) Void fraction measurements obtained by a gamma densitometry technique upstream of the tube bundle and at the tube bundle (monitored tube location) for the case of upstream void fraction generation (Gp=250 kg/m^{2}s) showed that void fraction values for the upstream location were higher than the ones measured at the bundle location by 4% to 10% void. The difference of 4% was for low void fraction values and increased to 10% as the void fraction increased. This indicated that vapour/liquid velocity ratio (slip ratio) values increased when the two-phase flow went through the tube bundle, which means that the gas phase increases velocity as it goes through the tube bundle. Nevertheless, as it was observed in some experiments, this higher slip value is not strong enough as to affect the conclusions obtained in this investigation.

9) Damping ratio measurements performed under the tube bundle void fraction generation condition showed similar values and the same dependence on void fraction as previously published values (Pettigrew et al. 1989). This indicates that tube bundle boiling does not change the "two-phase flow damping ratio" significantly.

10) The data show that fluidelastic instability for tube bundle void generation was found at higher reduced velocity values than that associated with the upstream case for the same value of pitch mass flux. This tendency is opposed to that reported by other investigators (Feenstra et al. 1996, Pettigrew et al. 1994), in which a decrease of reduced velocity for instability versus an increase in mass damping parameter was found. Data from this study in which tube bundle boiling was applied and data from a previous investigation (Axisa et al. 1985) in which steam-water was used, did not show this downward tendency in the diagram. There are two possible explanations for this difference. The first one is based on the level of turbulent buffeting forces to which the tube bundle is exposed. Increased values of turbulence may lower the void fraction needed for instability and hence produce a reduction in the reduced velocity value required for instability to occur. The second one is based on the flow regime to which the tube bundle is exposed. In this study, it was clear that flow regime for tube bundle boiling was at all times bubbly and homogeneous. The upstream void fraction generation cases in this study and in previous investigations showed a clear tendency to churn flow. A change in flow regime from bubbly to churn flow will produce

the same effect as an increase in tubulence buffeting levels, and hence it seems difficult with the present knowledge to distinguish between the two.

11) A comparison between the degree of tube bundle boiling in CANDU nuclear steam generators and that encountered in this investigation was performed by means of a dimensionless boiling number. It was found that in proportion to the total void fraction present, tube bundle boiling at the U-bend region of steam generators is lower than that attained in this investigation. Consequently, the reduction effect on tube vibration under bundle boiling condition found in this investigation will not be as pronounced in the steam generators. This leads to the conclusion that disregarding the effect of tube bundle boiling in the design of the vibration response of the tubes in the steam generators will predict instability thresholds that are lower that the real ones. However, as explained above, the presence of strong turbulence buffeting forces or a flow regime different than bubbly flow will substantially reduce the void fraction and hence the reduced velocity required for instability to occur. Since, turbulence forces seem to be related to flow regime, it is essential to have a clear knowledge of the flow regime at the U-bend region of the nuclear steam generator in order to accurately predict the fluidelastic instability threshold of the tubes.

6.2 Recommendations

When planning further work on this subject, the following recommendations should be considered.

Flow regime identification within the tube bundle continues to be the most crucial issue in understanding the tube vibration response. Visualization of the flow regime will probably allow for the understanding of the difference in tube response in the streamwise and transverse directions, which is undoubtedly related to the void fraction distribution around the tube. However, it will be preferable to quantify the flow regime using an appropriate measurement technique.

An investigation to understand the effect of turbulence level on the tube fluidelastic instability threshold under the presence of tube bundle boiling is suggested. Since tube bundle boiling will likely produce bubbly flow in the bundle, regardless of the void fraction value, this investigation will be able to elucidate the question of whether the flow regime or the reduction in the turbulence level in the bundle is the mechanism responsible for the increase in the reduced velocity value needed for instability.

The two-phase flow damping ratio of a single flexible tube in a rigid array under tube bundle boiling should be studied. Data obtained for this parameter in previous

investigations present substantial scatter, which reduces its suitability for design purposes Under tube bundle boiling, the flow regime will be mainly bubbly and the damping ratio data would be independent of potential recirculation flows or flow turbulence levels. It is expected that the two-phase damping ratio data taken in these conditions will be more reproducible and will probably present less scatter that previous data obtained under upstream void fraction generation conditions.

BIBLIOGRAPHY

Blevins R.D., 1990, Flow-Induced Vibration, Van Nostrand Reinhold, New York.

Connors H.J. Jr., 1970, "Fluidelastic Vibration of Tube Arrays Excited by Cross Flow." Flow-Induced Vibration in Heat Exchangers, D.D. Reiff (ed.) ASME, New York, 1979.

REFERENCES

Andjelic, M., K. Popp, 1988, "Stability Effects in a Normal Triangular Cylinder Array", *International Symposium on Flow-Induced Vibration and Noise.*, Vol 3. pp 57-76. Winter Annual Meeting of ASME. Chicago, Illinois.

Axisa, F., B. Villard, R.J. Gibert, G. Hetsroni, P. Sundheimer, 1984, "Vibration of Tube Bundles Subjected to Air-Water and Steam-Water Cross-Flow. Preliminary Results on Fluidelastic Instability", *Proceedings of ASME. Symposium on Flow-Induced Vibration, Vol.2 New Orleans*, pp 269-284.

Axisa F., Boheas M.A., Villard B., 1985, " Vibration of Tube Bundles Subjected to Steam Water Cross Flow: A Comparative Study of Square and Triangular Arrays", *Paper B1/2 in the 8th International Conference on Structural Mechanics in Reactor Technology*, Brussels, Aug.

Axisa F., Antunes J., Villard B., 1990, "Random Excitation of Heat Exchanger Tubes by Cross-Flows", *Journal of Fluids and Structures*, Vol. 4, pp. 321-341.

Bates, J.M. and Stewart, C.W., 1979, "Experimental Study of Single-and Two-Phase Flows Fields Around PWR Steam Generator Tube Support Plates" *EPRI NP-1142. Research Project 1121*, Palo Alto, California.

Carlucci, L.N., J.D. Brown, 1983, "Experimental Studies of Damping and Hydrodynamic Mass of a Cylinder in Confined Two-Phase Flow", *Journal of Vibration, Acoustics, Stress and Reliability in Design,* Vol 105, pp 83-89.

Carlucci L.N. , 1980, " Damping and Hydrodynamic Mass of a Cylinder in Simulated Two-Phase Flow", *Journal of Mechanical Design*, Vol. 102, pp. 597-602.

Catton, I., J. Marn, 1993, "Some Models for the Prediction of Fluid Elastic Instability", *Nuclear Engineering and Design*, Vol 139, pp 105-119.

Chan A.M.C., Banerjee S., 1981, "Design Aspects of Gamma Densitometer for Void Fraction Measurements in Small Scale Two Phase Flows", *Nuclear Instruments and Methods*, Vol. 190, pp. 135-148.

Chen, S.S., 1988, "Some Issues Concerning Fluidelastic Instability of a Group of Circular Cylinders in Crossflow", *International Symposium on Flow-Induced Vibration and Noise,* Vol 3. pp 1-24. Winter Annual Meeting of ASME. Chicago,Illinois.

Chen, S.S., J.A. Jendrzejczyk, 1987, "Characteristics of Fluidelastic Instability of Tube Rows in Cross Flow", *International Conference on Flow Induced Vibrations*. Bowness-on-Windermere, England, May, pp. 77-84, Paper B3.

Chen S.S., 1984, "Guidelines for the Instability Flow Velocity of Tube Arrays in Crossflow", *Journal of Sound and Vibration*, Vol. 93(3), pp. 439-455.

Chen S.S., Jendrzejczyk J.A., 1981, "Experiments on Fluid Elastic Instability in Tube Banks Subjected to Liquid Cross Flow", *Journal of Sound and Vibration*, Vol. 78(3), pp. 355-381.

Chen S.S., 1983, "Instability Mechanisms and Stability Criteria of a Group of Circular Cylinders Subjected to Cross-Flow, Part I:Theory; Part II: Numerical Results and Discussions", ASME *Journal of Vibration, Acoustics, Stress and Reliability in Design*. Vol. 105, pp. 51-58 and 235-260

Dam R., 1991, "Two Phase Flow-Induced Vibrations for Tube Banks in Cross Flow: Creating an Experimental Facility", Master's Thesis, McMaster University.

DUPONT CO., Freon-11 Saturation Properties Tables, Willmington, Delaware, Dupont Publication.

Eisinger, F.L., M.S.M. Rao, D.A. Steininger, K.H. Haslinger, 1995, "Numerical Simulation of Cross-Flow-Induced Fluid Elastic Vibration of Tubes Arrays and Comparison with Experimental Results", *Journal of Pressure Vessel Technology*, Vol 117, pp. 31-39.

Feenstra, P.A., D.S. Weaver, R.L. Judd, 1996, "Instability Analysis of Parallel Triangular Tube Arrays Subjected to Two-Phase Cross Flow", *Canadian Society of Mechanical Engineers, Annual Conference,* May 1996, McMaster University, Hamilton, Ontario, Canada.

Feenstra, P.A., Judd, R.L., Weaver, D.S., 1995, "Fluidelastic Instability in a Tube Array Subjected to Two-Phase R-11 Cross-Flow," *Journal of Fluids and Structures*, Vol. 9, pp. 747-771.

Feenstra, P.A. , 1993, "Two-Phase Flow Induced Vibration in Heat Exchangers Tube Arrays: An Experimental Investigation", M.Eng. Thesis, McMaster University, Hamilton, Ontario, Canada.

Feenstra, P.A., D.S. Weaver , R.L. Judd, 1996, "Damping and Fluidelastic Instability of a Tube Array in Two Phase R-11 Cross-Flow", *American Society of Mechanical Engineering, Pressure Vessel and Piping Conference Flow Induced Vibration Symposium*, Montreal Canada.

Gay, N., P. Decembre, J. Launay, 1988, "Comparison of Air-Water to Water-Freon Two-Phase Cross Flow Effects on the Vibratory Behaviour of a Tube Bundle", *International Symposium on Flow-Induced Vibration and Noise*. Vol 3. pp. 139-158. Winter Annual Meeting of ASME. Chicago,Illinois.

Gidi A., D.S. Weaver, R.L. Judd, 1997, "Two-Phase Flow Induced Vibrations of Tube Bundles with Tube Surface Boiling", *Fourth International Symposium on FluidStructure Interactions, Aeroelasticity and Flod Induced Vibrations and Noise, ASME International Mechanical Engineering Congress and Exposition*, Dallas, Texas.

Goyder, H.G.D., 1988, "Fluidelastic Instability and Buffeting of Heat Exchanger Tube Bundles Due to Single and Two-Phase Flows", *International Symposium on Flow-Induced Vibration and Noise.*, Vol 2. pp. 151-168. Winter Annual Meeting of ASME. Chicago, Illinois.

Granger, S., 1991, "A Global Model for Flow-Induced Vibration of Tube Bundles in Cross-Flow", *Journal of Pressure Vessel Technology*, Vol 113, pp. 446.

Grant, I.D.R., D. Chisholm, 1979, "Two-Phase Flow on the Shell-Side of a Segmentally Baffled Shell-and-Tube Heat Exchanger", *ASME, Journal of Heat Transfer*, Vol 101, pp. 38-42.

Grant I.D.R., Murray I., 1974, "Pressure Drop on the Shell Side of a Segmentally Baffled Shell-and-Tube Heat Exchanger with Horizontal Two Phase Flow", *NEL Report No. 560, National Engineering Laboratory*, East Kilbride, Glasgow.

Grant I.D.R., Murray I., 1972, "Pressure Drop on the Shell Side of a Segmentally Baffled Shell-and-Tube Heat Exchanger with Vertical Two Phase Flow", *NEL Report No. 500, National Engineering Laboratory*, East Kilbride, Glasgow.

Grover, L.K., D.S. Weaver, 1978, "Cross-Flow Induced Vibrations in a Tube Bank", *Journal of Sound and Vibration*, Vol 59, pp. 263-276.

Hartlen R.T., 1974, "Wind Tunnel Determination of Fluidelastic Vibration Thresholds for Typical Heat Exchanger Tube Patterns", *Ontario Hydro Report No. 74-309-K*, Toronto, Canada.

Heilker W.J., Vincent R.Q., 1981, "Vibration in Nuclear Heat Exchangers Due to Liquid and Two Phase Flow", *ASME Journal of Engineering for Power*, Vol. 103, pp. 358-365.

Kaplunov, S., N. Makhutov, 1992, "Dynamics of Fluid Elastic Vibrations of Tube Bundles in Heat Exchangers". *Heat Transfer Research*, Vol 24, N°5, pp. 641-662.

Lever, J.H., G. Rzentkowski, 1988, "Determination of Fluidelastic Stability Threshold in the Presence of Turbulence: A Theoretical Study", *International Symposium on Flow-Induced Vibration and Noise.*,Vol 2. pp. 131-150. Winter Annual Meeting of ASME. Chicago, Illinois.

Lever, J.H., D.S. Weaver, 1982, "A Theoretical Model for Fluid-Elastic Instability in Heat Exchanger Tube Bundles", *Journal of Pressure Vessel Technology*, Vol 104, pp. 147-158.

Lever, J.H., G. Rzentkowski, 1988, "An Investigation Into the Post-Stable Behaviour of a Tube Array in Cross-Flow", *International Symposium on Flow-Induced Vibration and Noise.*, Vol 3 pp. 95-110. Winter Annual Meeting of ASME. Chicago, Illinois.

Lian, H.Y., G. Noghrehkar,P. Middleton, A.M.C. Chan, M. Kawaji, 1994, "Investigation of Two-Phase Cross Flow Parameters in Vibrational Behaviour of Tubes in an In-line Tube Bundle", *Proceedings of 12th Symposium on Engineering Applications of Mechanics*. June, McGill University, Montreal, Canada, pp. 399-408.

Lian H.Y., Chan A.M.C., Kawaji M., 1992, "Effects of Void Fraction on Vibration of Tubes in Tube Bundles under Two-Phase Cross-Flow", *International Symposium on Flow Induced Vibration and Noise*, Vol. 1, pp. 109-118.

McAdams, Second Printing 1942 , "Heat Transmission", McGraw Hill Series in Chemical Engineering, McGraw Hill Book Company.

Minakami, K., K. Ohtomi, 1987, "Flow Direction and Fluid Density Effects on the Fluid Elastic Vibrations of a Triangular Array of Tubes". *International Conference on Flow Induced Vibrations*. Bowness-on-Windermere, England, May, pp. 65-75, Paper B2.

Nakamura, T. K. Fujita, K Kawanishi, N. Yamaguchi, A. Tsuge, 1992, "Study on the Vibrational Characteristics of a Tube Array Caused by Two-Phase Flow-Part 1: Random Vibration", *Journal of Pressure Vessel Technology*, Vol 114, pp. 472-478.

Nakamura, T. K. Fujita, K. Kawanishi, N. Yamaguchi, A. Tsuge, 1992, "Study on the Vibrational Characteristics of a Tube Array Caused by Two-Phase Flow-Part 2: Fluidelastic Vibration", *Journal of Pressure Vessel Technology*, Vol 114, pp. 479-485.

Nakamura, T., K. Fujita, A. Tsuge, 1993, "Two-Phase Cross-Flow-Induced Vibration of Tubes Arrays", *Japanese Society of Mechanical Engineering, International Journal Series B*, Vol 36, N3, pp. 429-438.

Nakamura T., Fujita K., Kawanishi K., Yamaguchi N., Tsuge A., 1991, "Study on the Vibrational Characteristics of a Tube Array Caused by Two-Phase Flow, Part 1 - Random Vibration", *ASME Publication PVP* Vol. 206, pp. 19-24.

Nakamura T., K. Fujita, K. K Shiraki, H. Kanazawa, K Sakata, 1982, "An Experimental Study on Exciting Force by Two-Phase Cross-Flow", *Proceedings of Pressure Vessel and Piping Conference, ASME,* Vol. 63, p.19.

Nakamura T., Fujita K., Kawanishi K., Saito I., 1986 (b), "A Study on the Flow-Induced Vibration of a Tube Array by a Two-Phase Flow. 2nd Report: Large Amplitude Vibration by Steam-Water Flow", *Transactions of JSME*, Vol. 52, No. 473.

Nakamura T., Fujita K. , 1988, "Large Amplitude Vibration of a Tube Bundle by Two Phase Flow", *Journal of Wind Engineering*, No. 37, Oct., pp. 599-608.

Nakamura T., Fujita K., Kawanishi K., Yamaguchi N., Tsuge A., 1991, "Study on the Vibrational Characteristics of a Tube Array Caused by Two Phase Flow, Part 2 - Fluidelastic Vibration", *ASME Publication PVP* Vol. 206, pp. 25-30.

Paidoussis, M.P., 1981, "Fluidelastic Vibration of Cylinder Arrays in Axial and Cross Flow: State of the Art", *Journal of Sound and Vibration*, Vol 76(3), pp. 329-360.

Paidoussis, M.P., S.J. Price, D. Mavriplis, 1985, "A Semipotential Flow Theory for the Dynamics of Cylinder Arrays in Cross Flow", *Journal of Fluids Engineering*, Vol 107, pp. 500-506.

Paidoussis M.P., Price S.J., Nakamura T., Mark B., And W. Njuki Mureithi, 1989, "Flow-Induced Vibrations and Instabilities in a Rotated-Square Cylinder Array in Cross-Flow", *Journal of Fluids and Structures*, Vol. 3, pp. 229-254.

Papp L. , S.S. Chen, 1994, "Turbulence-Induced Vibration of Tube Arrays in Two-Phase Flows", *Journal of Pressure Vessel Technology*, ASME, Vol. 116, August, pp. 312-316.

Pettigrew, M.J., J.H. Tromp, C.E. Taylor, B.S. Kim, 1989, "Vibration of Tube Bundles in Two-Phase Cross-Flow: Part 2- Fluid-Elastic Instability", *Journal of Pressure Vessel Technology*, Vol 111, pp. 478-487.

Pettigrew, M.J., C.E. Taylor, B.S. Kim, 1989, "Vibration of Tube Bundles in Two-Phase Cross-Flow: Part 1- Hydrodynamics Mass and Damping ", *Journal of Pressure Vessel Technology*, Vol 111, pp. 466-477.

Pettigrew, M.J., J.H. Tromp, J. Mastorakos, 1989, "Vibration of Tube Bundles Subjected to Two-Phase Cross-Flow", *Journal of Pressure Vessel Technology*, Vol 107, pp. 335-343.

Pettigrew, M.J., Y. Silvestre, A.O. Campagna, 1978, "Vibration Analysis of Heat Exchanger and Steam Generator Designs", *Nuclear Engineering and Design*, Vol 48, pp. 97-115.

Pettigrew, M.J., C.E. Taylor, 1991, "Fluidelastic Instability of Heat Exchanger Tube Bundles: Review and Design Recommendations", *Journal of Pressure Vessel Technology*, Vol 113, pp. 242.

Pettigrew M.J., G.D. Knowles, 1992, "Some Aspects of Heat Exchanger Tube Damping in Two-Phase Mixtures", *International Symposium on Flow Induced Vibration and Noise*, Vol. 1, pp. 141-160.

Pettigrew M.J., D.J. Gorman, 1978, "Vibration of Heat Exchanger Tube Bundles in Liquid and Two-Phase Cross-Flow", *Proceedings B.E.N.S.International Conference on Vibration in Nuclear Plant*, Keswick U.K., Paper 2.3.

Pettigrew M.J. and C.E. Taylor, 1994, "Two-Phase Flow-Induced Vibration: An Overview", *Journal of Pressure Vessel Technology*, Vol. 116, pp. 233-253.

Pettigrew M.J., C.E. Taylor, A. Yasou, 1994, "Vibration Damping of Heat Exchanger Tube Bundles in Two-Phase Flow", *Welding Research Council Bulletin*, No. 389, New York, Feb., pp. 1-41.

Pettigrew M.J., A.O. Campagna, 1980, "Heat Exchanger Tube Vibration: Comparison Between Operating Experiences and Vibration Analysis", Naudascher E., Rockwell D. (eds.) *Proceedings IUTAM-IAHR Symposium on Practical Experiences with Flow Induced Vibrations*, Springer-Verlag, Berlin.

Pettigrew, M.J., C.E. Taylor, J.H. Jong, I.G. Currie, 1994, "Fluidelastic Instability of a Tube Bundle in Two-Phase Freon-22 Cross-Flow", *Proceedings of the 12th Symposium on Engineering Applications of Mechanics*, Montreal, Canada, pp. 425-434.

Pettigrew M.J., D.J. Gorman, 1973, "Experimental Studies on Flow-Induced Vibration to Support Steam Generator Design, Part III: Vibration of Small Tube Bundles in Liquid and Two Phase Cross Flow", *Atomic Energy of Canada Ltd.*, Report AECL-5804.

Pettigrew M.J., 1996, AECL, Heat Flux Map in a CANDU Steam Generator.

Price, S.J., M.P. Paidoussis, 1987, "The Flow-Induced Response of a Single Flexible Cylinder in an In-Line Array of Rigid Cylinders", *International Conference on Flow Induced Vibrations*. Bowness-on-Windermere, England, May, pp. 51-63. Paper B1.

Price, S.J., M.P. Paidoussis, N. Giannias, 1988, "A Generalized Constrained-Mode Analysis for Cylinder Arrays in Cross-Flow", *International Symposium on Flow-Induced Vibration and Noise,* Vol 1. pp. 25-55. Winter Annual Meeting of ASME. Chicago, Illinois.

Price S.J., Paidoussis M.P., Macdonald R., Mark B., 1989, "The Flow-Induced Vibration of a Single Flexible Cylinder in a Rotated Square Array of Rigid Cylinders with Pitch over Diameter Ratio of 2.12", *Journal of Fluids and Structures*, Vol. 1, pp. 359-378.

Remy R.M., 1982, "Flow Induced Vibration of Tube Bundles in Two Phase Cross Flow", Paper 1.9, *Proceedings of the 3rd International Conference of Vibrations in Nuclear Plants*, Keswick UK, Vol. 1, pp. 135-160.

Robinson A., A. Gidi, R.L. Judd, M. Bardeleben, 1996, "Development of an Optical Device for Measuring Tube Vibrations in Tube Bundles". *Proc. CSME Annual Conference*, May1996, McMaster University, Hamilton, Ontario, Canada, pp. 49-54.

Saito T., T. Miwa, T. Onozawa, T. Iwase, K. Tomomatsu, N. Nakamori, Y. Watanabe, T. Nakamura., "Verification Tests of Flow Induced Vibration in U-Bend Regions of Steam Generator Tube Bundles", *Mitsubichi Heavy Industries, Internal Document*, 1993-1994, 9 pag.

Scott P., 1986, A Flow Visualization Study on Tube Arrays in Water Flows, Master Thesis, McMaster University.

Southworth P.J., M.M. Zdravkovich, 1975, "Effect of Grid Turbulence on the Fluidelastic Vibrations of In-Line Tube Banks in Cross Flow", *Journal of Sound and Vibration*, Vol. 39, pp. 461-469.

Symolon P.D., *1990,* "Scaling of Two-Phase Flow Regimes in a Rod Bundle with Freon", Knolls Atomic Power Laboratory, KAPL-4718. N.York. July.

Taitel Y., D. Bornea, A.E. Dukler, 1980, "Modelling Flow Pattern Transitions for Steady Upward Gas-Liquid Flow in Vertical Tubes". *AIChE Journal*, Vol. 26, pp. 345-354.

Taylor, C.E., M.J., Pettigrew, F. Axisa, B. Villard, 1988, "Experimental Determination of Single and Two-Phase Cross-Flow-Induced Forces on Tube Rows". *Journal of Pressure Vessel Technology*, Vol 110, pp. 22-28.

Taylor, C.E., I.G. Currie, M.J. Pettigrew, B.S. Kim, 1989, "Vibration of Tube Bundles in Two-Phase Cross-Flow: Part 3-Turbulence- Induced Excitation" , *Journal of Pressure Vessel Technology*, Vol 111, pp. 488-500.

Teh, C.E., H.G.D. Goyder, 1988, "Data for the Fluidelastic Instability of Heat Exchanger Tube Bundles", *International Symposium on Flow-Induced Vibration and Noise*, Vol 3. pp. 77-94. Winter Annual Meeting of ASME. Chicago, Illinois.

Ulbrich R., D. Mewes, 1994, "Vertical, Upward Gas-Liquid Two-Phase Flow Across a Tube Bundle", *International Journal of Multiphase Flow*, Vol. 20, No. 2, pp. 249-272.

Weaver, D.S., D. Koroyannakis, 1983, " Flow-Induced Vibrations of Heat Exchanger U-Tubes: A Simulation to Study the Effects of Asymmetric Stiffness", *Journal of Vibration, Acoustics, Stress and Reliability in Design*, Vol 105, pp. 67-75.

Weaver, D.S, M. El-Kashlan, 1981, "On the Number of Tube Rows Required to Study Cross-Flow Induced Vibrations in Tube Banks", *Journal of Sound and Vibration*, Vol 75(2), pp. 265-273.

Weaver, D.S, J.A. Fitzpatrick, 1988, "A Review of Cross-Flow-Induced Vibrations in Heat Exchanger Tube Arrays", *Journal of Fluids and Structures.*, Vol 2, pp. 73-93.

Weaver D.S., L.K. Grover, 1978, "Cross-Flow Induced Vibrations in a Tube Bank: Turbulent Buffeting and Fluidelastic Instability", *Journal of Sound and Vibration*, Vol. 59, pp. 277-294.

Weaver, D.S, 1992, private conversation.

Whalley, P.B., 1987, "Boiling Condensation and Gas-Liquid Flow", The Oxford Engineering Science Series, Oxford University Press.

Yamaguchi, N., K. Sakata, A.Tsuge, T. Nakamura, I. Saito, 1993, "Study on Two-Phase Flow Behaviour and Turbulent Excitation Mechanism in a U-Bend Tube Bundle in Steam Generators Based on Air-Water Two-Phase Flow Model Tests", *Japanese Society of Mechanical Engineering, International Journal Series B*, Vol 36, N 3, pp. 439-448.

Yetisir, M., D.S. Weaver, 1993, "An Unsteady Theory for Fluidelastic Instability in an Array of Flexible Tubes in Cross-Flow. Part I: Theory", *Journal of Fluids and Structures*, Vol 7, pp. 751-766.

Yeung, H.C., D.S. Weaver, 1983, "The Effect of Approach Flow Direction on the Flow-Induced Vibrations of a Triangular Tube Array", *Journal of Vibration, Acoustics, Stress and Reliability in Design*, Vol 105, pp. 76-82.

Appendix A

TEMPERATURE EFFECTS ON TUBE STRUCTURAL DAMPING RATIO

Introduction:

The tube structural damping ratio is one of the components of the total damping ratio associated with the tube vibration in two-phase flow. The total damping ratio determines the tube vibration amplitude by allowing the tube to dissipate the vibration energy absorbed from the flow. As has been mentioned, the tubes in this investigation were comprised of tubular cartridge heaters which dissipated heat to produce some of the void fraction necessary in the experiment. This heat dissipation would undoubtedly increase the tube temperature above the flow temperature. There was concern that the tube structural damping ratio would change due to changes in the tube temperature and that it would affect the tube response. Two temperatures were considered important for this investigation, the internal temperature of the cartridge heater and the temperature of the tube fixing point, both of which were functions of the power dissipated in the tube cartridge heaters. A summary of what was found in this investigation is presented in this appendix.

Objectives

To measure the tube structural damping ratio in air as a function of the internal temperature of the cartridge heater and the temperature of the tube fixing point. In the case of tubes with thermocouples (WT), the temperature was measured with a thermocouple located on the centre line of the cartridge at its midspan position. For the case of tubes without thermocouples (NT), the temperature was measured by installing a thermocouple at the tube fixing point, in the vicinity of the ferrule position.

Equipment

Two tubular heaters, one of type WT and one of type NT were fixed to the same brass plate using nylon ferrules. Fixing conditions were clamped-free, identical to those in the setup for two-phase flow tube bundle experiments.

Instrumentation and Data Acquisition

The optical vibration measuring system described previously, was used to obtain the tube amplitude. Tube vibration frequency was measured by means of the FFT Analyzer. A surface measuring thermocouple was used to obtain the temperature at the surface of the tube at three different locations, the midspan, and both the inside and outside surfaces of the fixing plate. A clamping system was in place to prevent the tube whose vibration was not being measured from interfering with the measurements.

The Test Procedure

Each test consisted of manually disturbing the tube in the vertical direction and obtaining the instantaneous amplitude response of the tube by capturing the signal coming from the optical vibration measuring system with the Windaq Data Acquisition System. Ten tests were performed for each tube and each temperature, since there were two tubes involved and seven temperatures investigated, one hundred and forty tests were performed in total.

In response to different combinations of these parameters, the core tube temperature changed from 22°C to 145°C. The tube fixing point temperature changed from 22°C to 54°C. Amplitude of vibration ranged from 1% to 10% of the tube diameter at the free end. The amplitude signal sampling rate was 1000 data points per second.

Data Processing

Each test generated a data file containing the instantaneous tube amplitude response versus time. Data files from Windaq DI-200 were analyzed with the Windaq Analysis package, time decay signals were observed and saved in the format that the computer program (LOGDEC2) uses for damping ratio calculations. A typical tube amplitude response is presented in Figure A.1.

There were about three thousand amplitude data points in each data file, which represented one hundred and twenty vibration cycles. Using LOGDEC2, twelve damping ratio averages of nine cycles each were obtained. In the ten tests performed for each tube and each temperature, a total of one hundred an twenty damping ratio averages were obtained.

Results and Analysis.

Each set of ten tests corresponding to one tube and one temperature was transferred to a data spreadsheet to be plotted in a single graph. Graph A.2 shows the average values of the damping ratio versus tube vibration amplitude for a NT tube at a tube core temperature of 21 °C. The Least Square Method (LSM) correlation line obtained from the data values is also plotted.

In graph A.3, the average values of the damping ratio versus tube vibration amplitude for tube type WT at a tube core temperature of 94° C are shown. The LSM correlation line obtained from the data values is also plotted.

In both graphs, it can be seen that damping ratio is a function of tube vibration amplitude. The scatter in the data is normal for this type of measurement, which is dependent on the excitation mechanism involved in disturbing the tube.

For the rest of the temperatures, both tubes showed similar data trends with respect to amplitude, and the data scatter was similar as well. In all cases, the damping ratio values increased with tube core temperature.

In graph A.4, the LSM correlations for all temperatures for the NT tube are shown. Graph A.5 shows corresponding data for a WT tube. In both graphs, each line represents the correlation for a specific tube core midspan temperature. It is clear that damping ratio increases with both amplitude and core temperature. The damping ratios for the WT tube were higher than these of the NT tube. For a core temperature of 22°C, the damping ratio range for the WT tube was 0.4 to 0.7, while for the NT tube one was 0.22 to 0.6.

A better comparison can be observed in graphs A.6 and A.7 in which the amplitude has been restricted to 2% tube diameter (TD). Graph A.6 shows damping ratio plotted as a function of the tube core temperature, while graph A.7 shows the same data plotted as a function of the tube fixing point temperature. The graphs show that damping ratio increases with both temperatures in a linear fashion. In both graphs, data for the WT tube corresponding to 140°C at the tube core and 55°C at the tube fixing point show values much higher than the trend defined by the values corresponding to lower temperatures. Considering that these extreme temperatures were never achieved during the experiments, they will not be considered for comparison purposes and practical conclusions.

In both graphs, the damping ratios for the WT tube are higher than those for the NT tube by 0.1 to 0.2%. Since, it is desirable from an experimental point of view to have the monitoring tube with a damping ratio as low as possible, a NT type tube was used as the monitored tube. Nevertheless, since measurements of the tube core temperatures were necessary, type WT tubes were used in the most downstream and most upstream tubes in the central column of the bundle.

Graph A.8 shows the same damping ratio data plotted as a function of the tube fixing point temperature for the NT tube. Each line represents the correlation for a different tube vibration amplitude.

Graph A.9 shows the temperature profiles of both types of cartridge heaters plotted as a function of the heat flux at the tube surface. The data include the tube core midspan temperatures, the tube surface midspan temperature and the tube fixing point temperatures. The general trend is that the temperature increases with an increase in heat flux. The graph shows similar temperature values for both tubes and also negligible temperature difference between core and surface midspan values.

Conclusions.

The following conclusions were drawn:

a) Tube structural damping ratio has been found to be dependent on tube vibration amplitude. The experimental results show that as the amplitude increases, the damping does as well, following a linear correlation within an amplitude range of 1 to 10% TD.

b) The tube damping ratio is also a function of both tube temperatures, the tube core midspan and the tube fixing point temperature. However, the dependency of damping ratio on the tube fixing point was stronger than that on the tube core midspan temperature. For the purpose of this investigation, the temperature at the tube fixing point was regarded as the controlling parameter in determining the values of damping ratio that might interfere with the normal operating conditions of an experiment.

c) The tube with a thermocouple (WT) showed damping ratio values that were higher than those of the NT tube for the same temperature and vibration amplitude. It also showed larger increases in damping ratio with respect to tube temperature than the NT tube. This observation suggests that the monitored tube should not be the WT type.

d) The maximum temperature tested at the tube fixing point during the damping tests was 54°C. The highest temperature measured in the tube fixing region during boiling experiments was 46°C. The maximum tube amplitude measured in tube bundle boiling experiments never excedeed 4% TD. Therefore, tube damping ratio during boiling experiments is not expected to exceed the value of 0.6 % as determined from graph A.8.

This means that the temperature effects of the tube fixing point will not affect significantly the tube response during boiling experiments as to modify the conclusions obtained from these experiments.

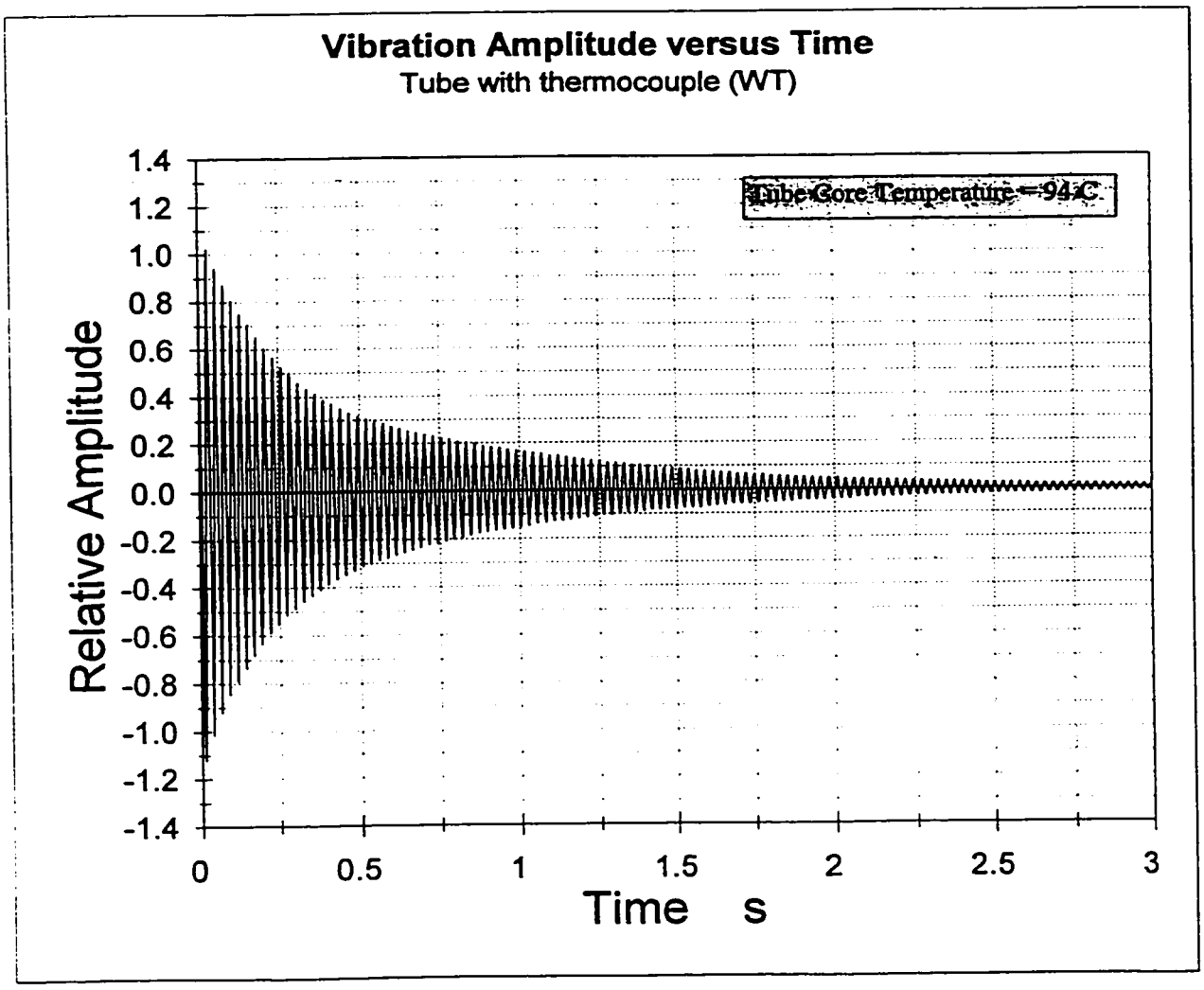

Figure A.1 Instantaneous Tube Amplitude Versus Time

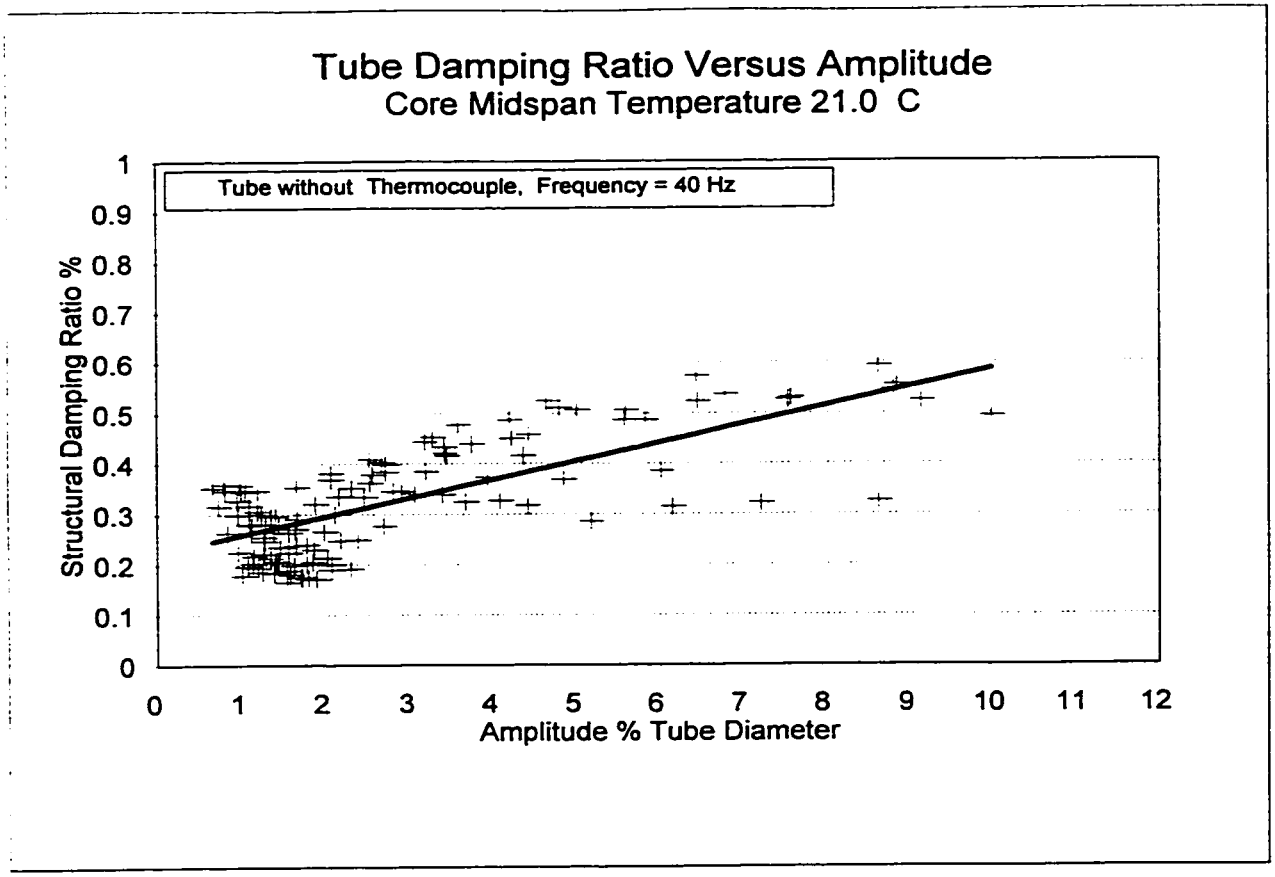

A.2 Tube damping Ratio Versus Amplitude for a NT tube.

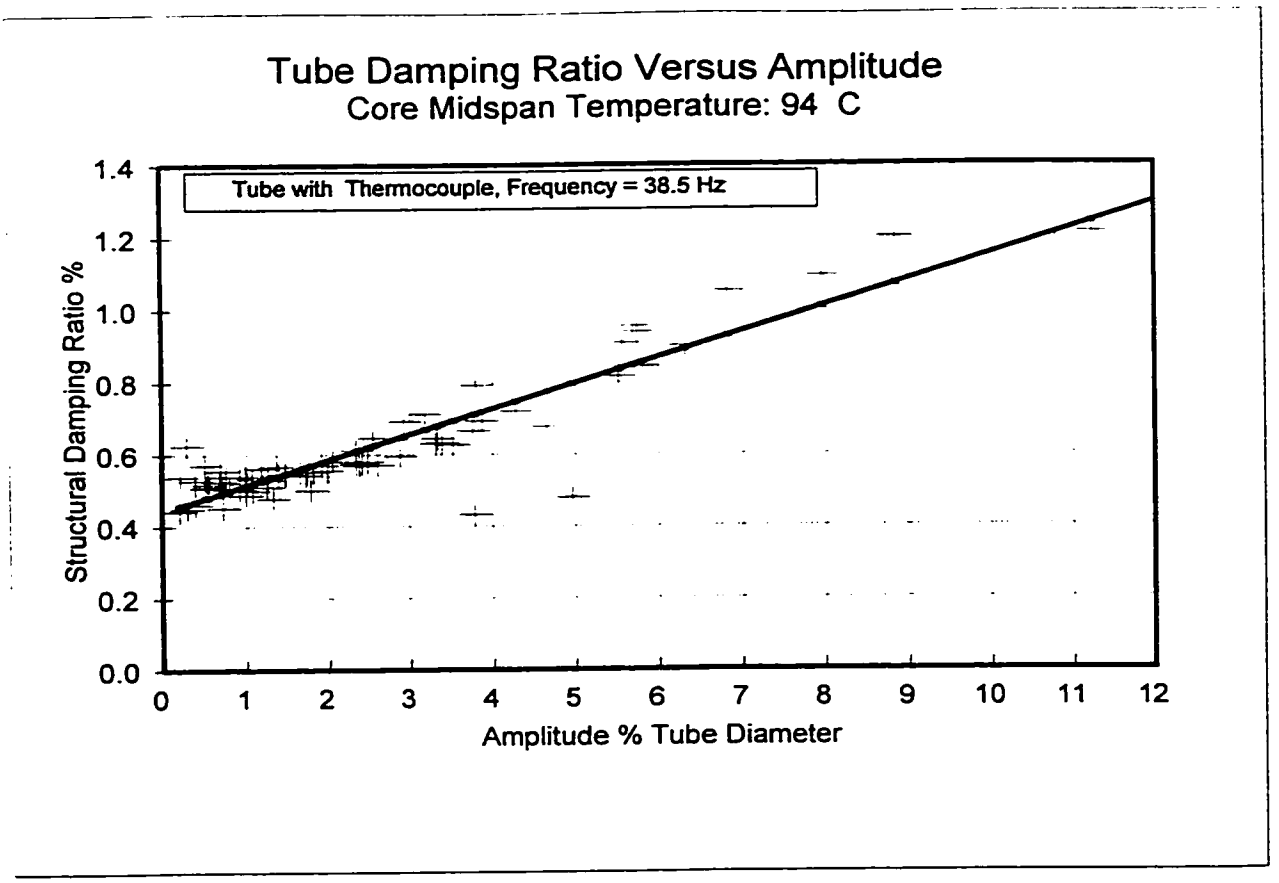

Figure A.3 Tube Structural Damping Ratio Versus Tube Amplitude.

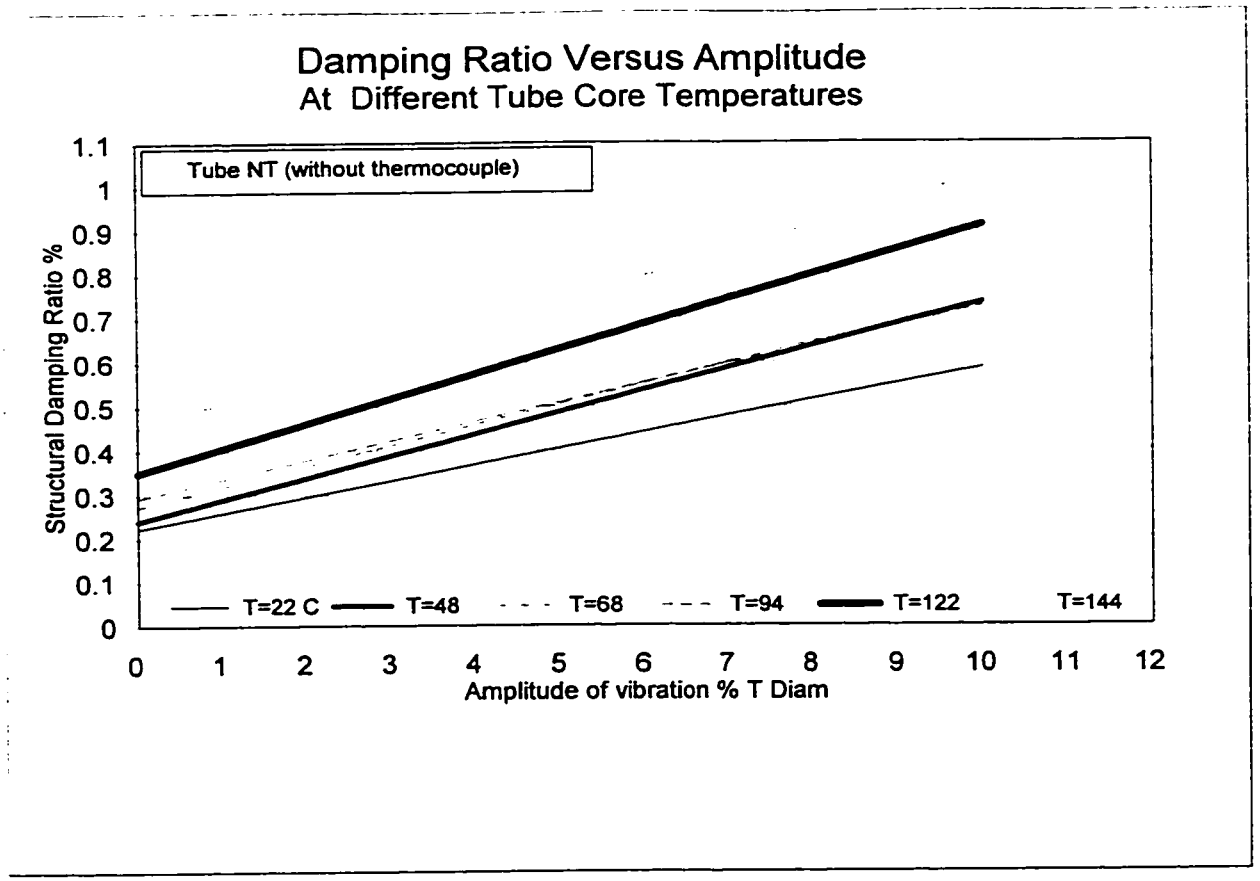

Figure A.4 Damping ratio vs. amplitude for different tube core temperature

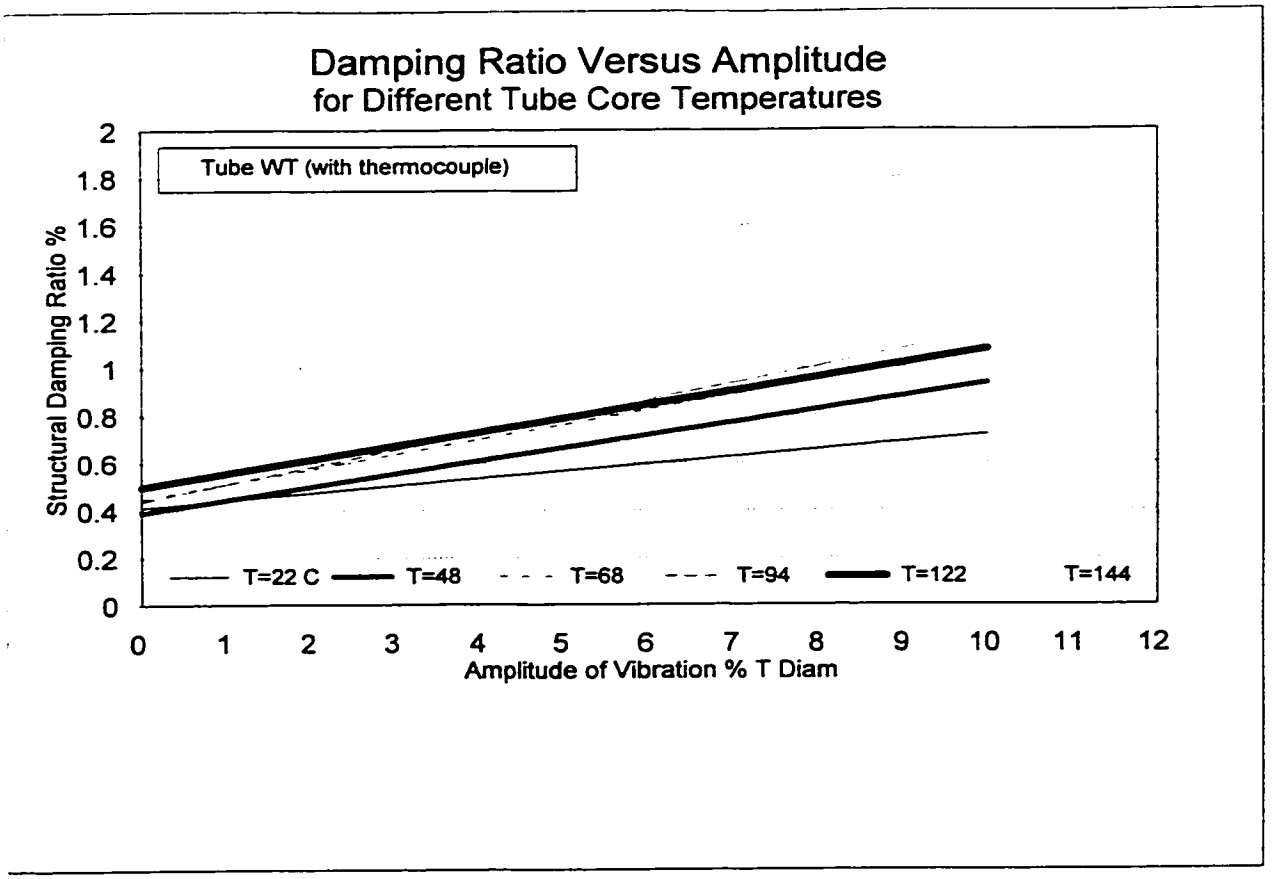

Figure A.5 Damping ratio vs.amplitude for different tube core temperatures

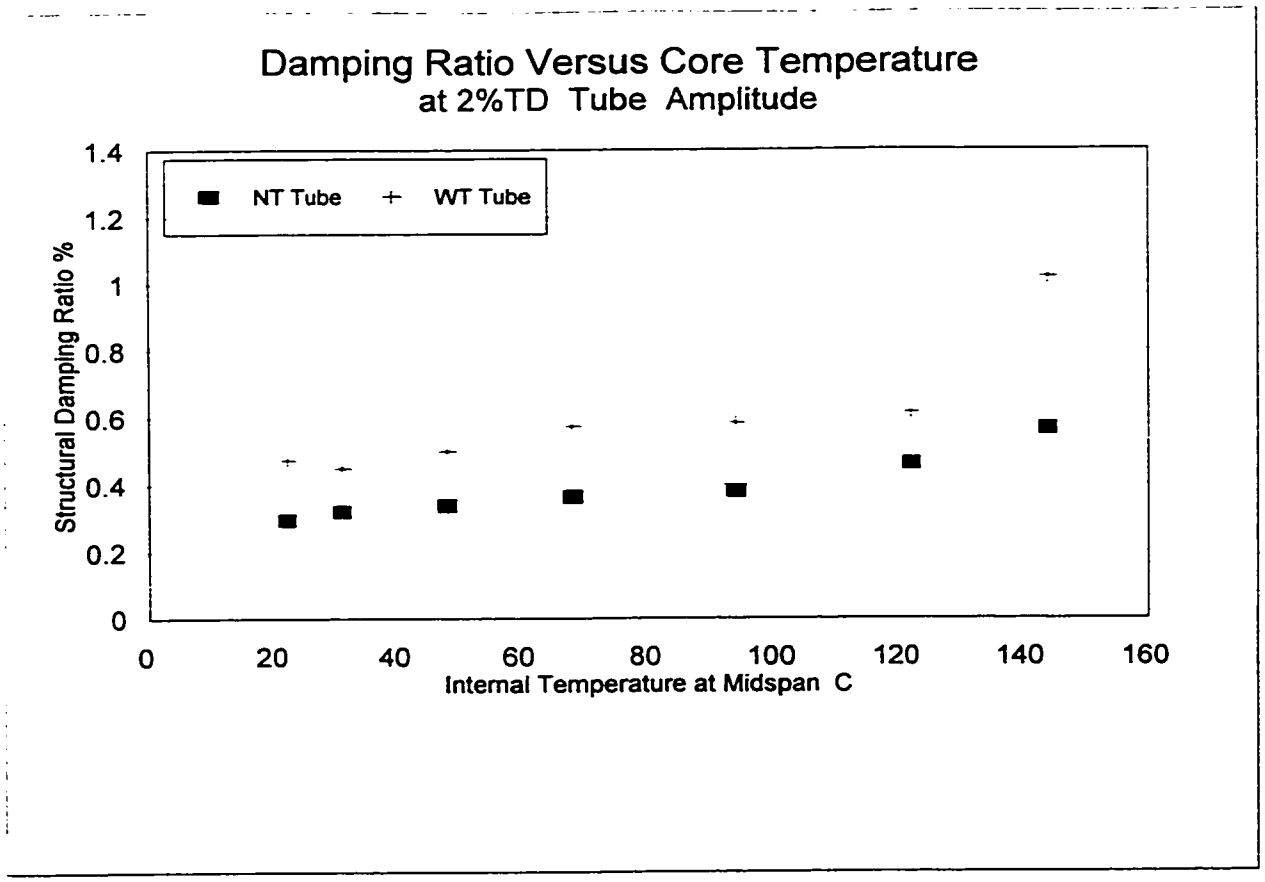

Figure A.6 Damping ratio vs. tube internal core temperature

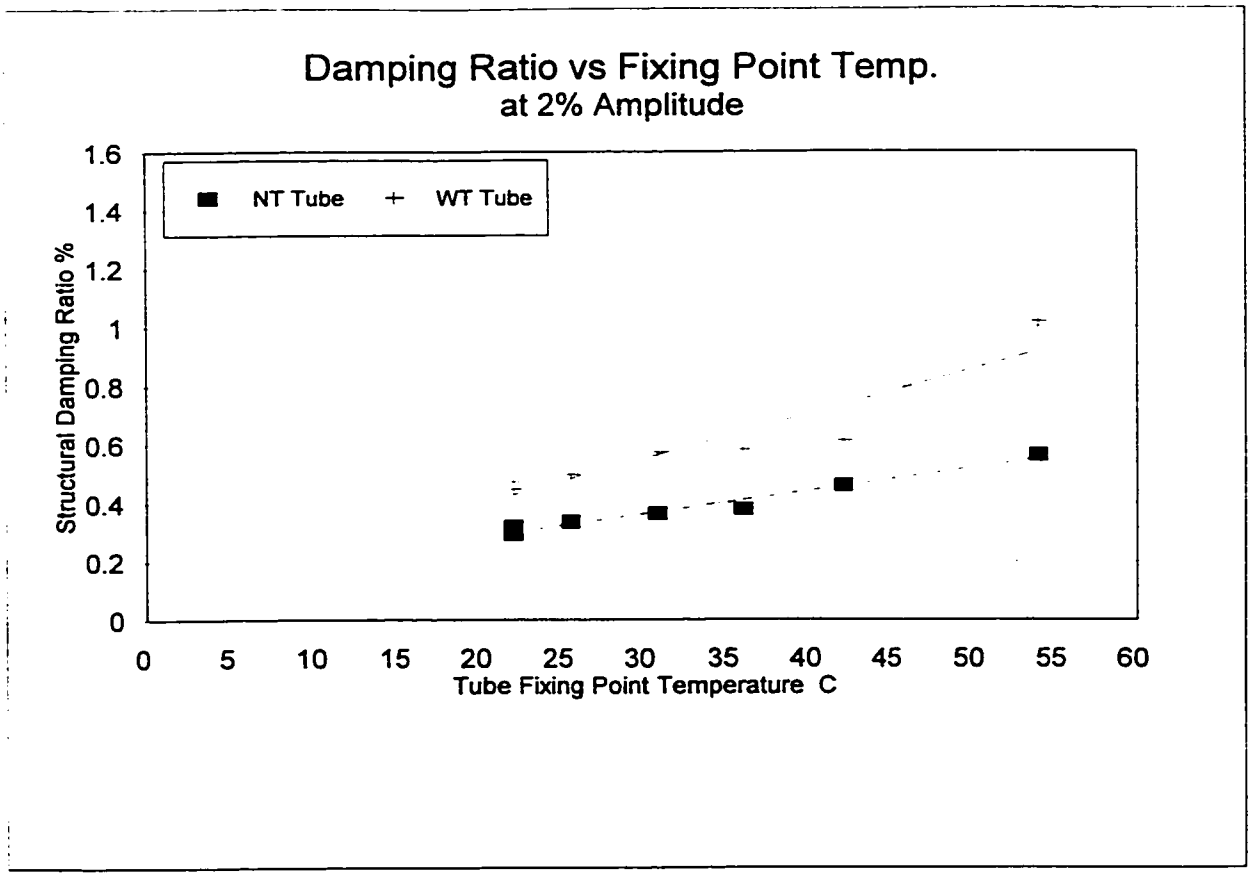

Figure A.7 Damping ratio vs.tube fixing temperature

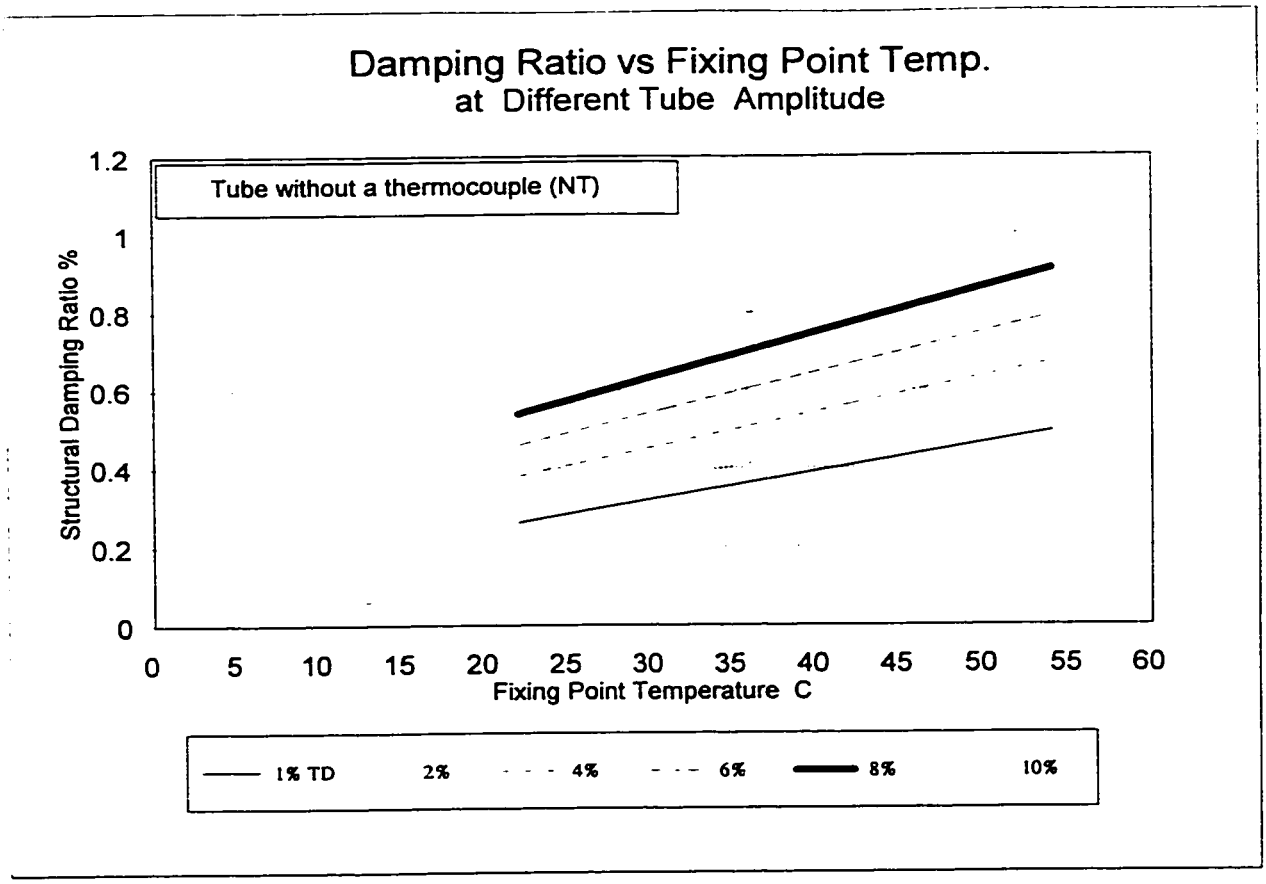

Figure A.8 Damping ratio vs.tube fixing temp. at different tube amplitude

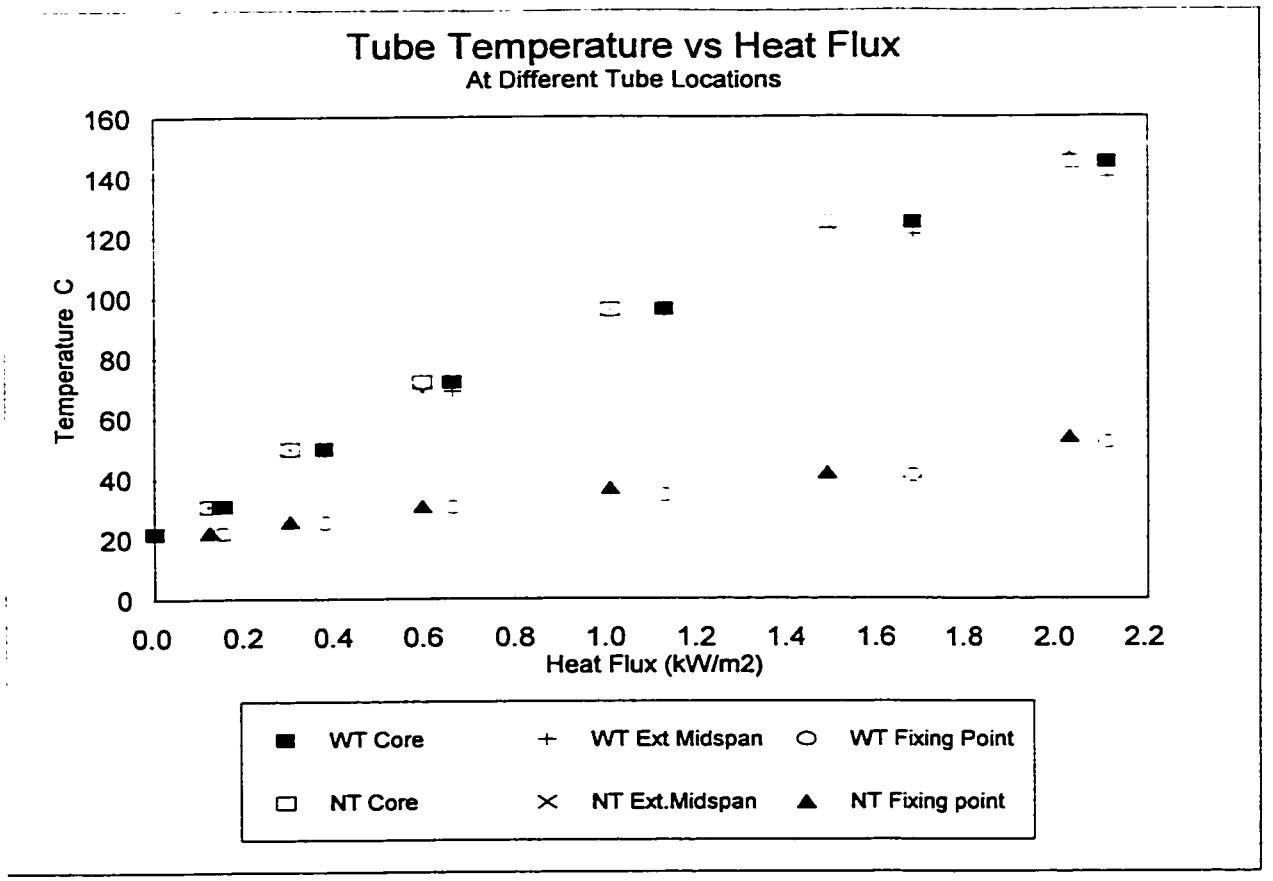

Figure A.9 Tube temperature vs heat flux at the tube surface

Appendix B

EXPERIMENTAL DATA SHEETS

In each experiment, the mass flow rate was adjusted to attain a specific value. Experiments consisted of several trials, in which a specific void fraction value or a combination of void fraction generated upstream and void fraction generated at the tube bundle surface had to be obtained. In order to verify that mass flux and void fraction had been obtained, several parameters of the test rig and physical properties of the fluid had be continuously measured. The values obtained were used to calculate other parameters and properties, such as system pressure, density and enthalpy of the fluid, which were ultimately used to verify the void fraction and mass flux.

In the following pages, the experimental data measurements of some of the important experiments are presented. On each page, the experiment number, date and gamma densitometer values (counts or voltage) for 100% liquid and 100% gas (100% void) are recorded in the first two lines. The following 15 lines after the trial number present the data that was obtained by direct measurements. The remaining lines are filled with data calculated from the measured data. An explanation of each parameter is presented on the following page.

Experimental Data for Two-Phase Freon-11 Flow Loop Operation

Experiment 36			Gamma Densitometer Calibration			
Jan 17th 1997			Voltage at Bundle		Excitation Voltage	600 Volts
		100% Liquid	3.96	Volts	rho_L =	1483.0 kg/m3
Atm. Pressure (MPa)	0.1030	100% Gas	4.95	Volts	File:	Jan17EXP.Wb2

Trial #	Trial number
Q1 (in) U tube	Pressure from U-tube (Hg) at the Freon-11 main line, used to calculate flow through the line
Q2 (in)	Pressure from digital manometer at the Freon-11 secondary (cooling) line, used to calculate flow rate
Q2 (in) U tube	Pressure from U-tube (Hg) manometer at the Freon-11 secondary (cooling) line, used to calculate flow rate
T1 (mV)	Temperature of Freon-11 downstream of tube bundle
T2 (mV)	Temperature of Freon-11 downstream of main heaters
T3 (mv)	Temperature of tube fixing plate
T5 (mV)	Temperature of Freon-11 upstream of main heaters
Power (kW)	Power delivered at the main heaters, used to calculate HEM void fraction
N (rpm)	Speed of the main pump, used to obtain the Freon flow rate through test section
Gamma Volt	Counts or voltage from the gamma densitometer, used to obtain void fraction
P1 (psi)	Pressure at the test section, used to calculate Freon density.
T4 (mV)	Temperature of the outlet water of the heat exchanger
T6 (mV)	Temperature of the inlet water of the heat exchanger
Qw (inHg)	Pressure of the flow in the water cooling line, used to obtain water flow.
Powerstat %	Fraction of the full voltage delivered to the tubular cartridge heaters
CALCULATED DATA	
Q (L/s)	Previous data converted to proper units
Q1 (L/s)	
Q2 (L/s)	
T1 (C)	
T2 (C)	
T3 (C)	
T5 (C)	
Volt (Bundle) V	
Physical Properties Freon-11	
rhoL1 (kg/m3)	Liquid density at the main heaters
rhoG1 (kg/m3)	Gas density at the main heaters
rhoL2 (kg/m3)	Liquid density upstream of the test section
rhoG2 (Kg/m3)	Gas density upstream of the test section
rhoL5 (kg/m3)	Liquid density downstream of the test section
hf1 (kJ/kg)	Enthalpy at the main heaters
hfg2 (kJ/kg)	Phase change enthalpy
hf2 (kJ/kg)	Enthalpy upstream of the test section
hf5 (kJ/Kg)	Enthalpy downstream of the test section
Void fraction upstreams calculations based on HEM	
dhu (kJ/kg)	Energy added to the fluid at the main heaters
xu heaters	Quality of the mixture downstream of the main heaters
UPSHEM Void	Void fraction calculated upstream of the test section
Void fraction @ bundle calculations	
dh@ (kJ/kg)	Energy added to the fluid at the cartridge heaters
Power kW	Power delivered to the fluid by the cartridge heaters
x tub heater	Quality of the mixture after the tube bundle
BOHEM Tube	HEM void added to the fluid by the cartridge heaters
Heat flux kW/m²	Heat flux at the surface of the cartridge heaters
Boiling Number	Boiling number
Overall Calculations	
delth (kJ/kg)	Energy added to the fluid by both heat sources
x	Quality of the fluid after the tube bundle, due to contributions of both heat sources
Void total	HEM void fraction at the monitored tube considering contributions of both heat sources
Gp (kg/m2s)	Pitch mass flux at the monitored tube
rhoH (kg/m3)	HEM mixture density at the monitored tube location
HEM Vp (m/s)	Pitch velocity at the tube location
bund/total ratio	Ratio between HEM void generated in the tube bundle to the total HEM void at the tube location
Separated Flow	
Corr. Factor	Correction factor for the gamma 100% liquid calibration value due to temperature change of the Freon
Rad Void Volts	Actual void fraction at the monitored tube location
Slip	Calculated ratio of the gas velocity to the liquid velocity at the tube location
Ug (m/s)	Average gas velocity at the tube location
Ul (m/s)	Average liquid velocity at the tube location
rho (kg/m3)	Density of the mixture based on the actual void fraction

Experimental Data for Two-Phase Freon-11 Flow Loop Operation
Experiment 36
Jan 17th 1997

Gamma Densitometer Calibration
Voltage at Bundle
100% Liquid 3.96 Volts
100% Gas 4.95 Volts

Excitation Voltage 600 Volts
rho_L = 1483.0 kg/m3
File: Jan17EXP.Wb2

Atm. Pressure (MPa) 0.1030
file: gama33XX.wdq

Trial #	1	2	3	4	5	6	7	8	9
Q1 (in) U tube	0.62	0.60	0.60	0.60	0.60	0.60	0.60	0.60	0.60
Q2 (in)	0.00	0.00	0.00	0.00	0.00	0.00	0.00	0.00	0.00
Q2 (in) U tube	1.80	2.00	2.00	2.00	2.05	2.00	2.00	2.00	2.00
T1 (mV)	1.87	1.88	1.90	1.90	1.93	1.95	1.99	2.01	2.06
T2 (mV)	1.91	1.94	1.95	1.98	2.00	2.01	2.05	2.09	2.13
T3 (mv)	1.66	1.67	1.67	1.68	1.73	1.73	1.75	1.79	1.83
T5 (mV)	1.60	1.61	1.64	1.66	1.71	1.73	1.78	1.83	1.90
Power (kW)	4.00	4.12	4.30	4.25	3.87	4.00	3.90	3.70	3.60
N (rpm)	582	579	581	580	579	581	581	580	580
Gamma Volt	4.00	4.07	4.10	4.08	4.21	4.22	4.28	4.33	4.38
P1 (psi)	5.20	5.30	5.40	5.50	5.80	6.00	6.40	6.70	7.20
T4 (mV)	0.82	0.83	0.84	0.86	0.90	0.90	0.92	0.96	0.99
T6 (mV)	0.27	0.26	0.26	0.27	0.27	0.28	0.27	0.27	0.29
Qw (inHg)	0.45	0.45	0.45	0.45	0.45	0.45	0.45	0.45	0.45
Powerstat %	24	24	24	30	40	41	46.0	52.0	58.0
CALCULATED DATA									
Q (L/s)	0.944	0.938	0.942	0.940	0.938	0.942	0.942	0.940	0.940
Q1 (L/s)	0.571	0.545	0.549	0.547	0.541	0.549	0.549	0.547	0.547
Q2 (L/s)	0.372	0.392	0.392	0.392	0.397	0.392	0.392	0.392	0.392
T1 (C)	31.1	31.3	31.6	31.6	32.1	32.5	33.1	33.4	34.3
T2 (C)	31.8	32.3	32.5	32.9	33.3	33.4	34.1	34.8	35.4
T3 (C)	27.7	27.9	27.9	28.0	28.8	28.8	29.2	29.8	30.5
T5 (C)	26.7	26.9	27.4	27.7	28.5	28.8	29.7	30.5	31.6
Volt (Bundle) V	57.3	57.3	57.3	70.7	93.7	95.3	106.5	120.0	133.4
Physical Properties Freon-11									
rhoL1 (kg/m3)	1461.5	1461.1	1460.3	1460.3	1459.1	1458.4	1456.8	1456.0	1454.0
rhoG1 (kg/m3)	7.4255	7.4638	7.5408	7.5408	7.6576	7.7362	7.8952	7.9756	8.1793
rhoL2 (kg/m3)	1459.9	1458.8	1458.4	1457.2	1456.4	1456.0	1454.4	1452.8	1451.2
rhoG2 (Kg/m3)	7.5796	7.6968	7.7362	7.8552	7.9353	7.9756	8.1383	8.3034	8.4710
rhoL5 (kg/m3)	1472.1	1471.7	1470.5	1469.7	1467.8	1467.0	1465.1	1463.1	1460.3
hf1 (kJ/kg)	227.67	227.82	228.11	228.11	228.56	228.86	229.45	229.75	230.49
hfg2 (kJ/kg)	178.75	178.55	178.49	178.29	178.16	178.10	177.84	177.58	177.31
hf2 (kJ/kg)	228.26	228.71	228.86	229.30	229.60	229.75	230.34	230.94	231.54
hf5 (kJ/Kg)	223.68	223.83	224.27	224.56	225.30	225.60	226.34	227.08	228.11
Void fraction upstreams calculations based on HEM									
dhu (kJ/kg)	4.6334	5.0001	5.1860	5.1465	4.7492	4.8339	4.7188	4.4975	4.3825
xu heaters	0.0003	0.0007	0.0034	0.0023	0.0025	0.0038	0.0040	0.0036	0.0054
UPSHEM Void	0.05	0.11	0.39	0.30	0.32	0.41	0.42	0.38	0.48
Void fraction @ bundle calculations									
dh@ (kJ/kg)	0.38517	0.40344	0.40102	0.61292	1.09143	1.11195	1.39052	1.77376	2.19616
Power kW	0.33	0.33	0.33	0.51	0.89	0.92	1.15	1.46	1.81
x tub heater	0.00215	0.00226	0.00225	0.00344	0.00613	0.00624	0.00782	0.00999	0.01239
BOHEM Tube	0.3	0.3	0.3	0.4	0.5	0.5	0.6	0.6	0.7
Heat flux kW/m²	5.6	5.6	5.6	8.6	15.1	15.6	19.5	24.8	30.6
Boiling Number	1.21E-07	1.26E-07	1.26E-07	1.92E-07	3.42E-07	3.49E-07	4.37E-07	5.58E-07	6.91E-07
Overall Calculations									
delth (kJ/kg)	4.9224	5.3009	5.4853	5.6149	5.6039	5.7052	5.8140	5.9006	6.1257
x	0.0019	0.0024	0.0050	0.0049	0.0073	0.0087	0.0102	0.0115	0.0152
Void total	0.27	0.32	0.49	0.49	0.58	0.62	0.65	0.68	0.73
Gp (kg/m2s)	262	250	252	251	248	251	251	250	250
rhoH (kg/m3)	1384.2	1292.8	887.2	1013.6	986.3	848.9	840.8	884.2	743.6
HEM Vp (m/s)	0.203	0.208	0.305	0.266	0.269	0.318	0.321	0.304	0.361
bund/total ratio	0.81	0.64	0.22	0.39	0.46	0.34	0.36	0.43	0.34
Separated Flow									
Corr. Factor	0.993	0.993	0.992	0.992	0.992	0.992	0.991	0.991	0.990
Rad Void Volts	0.01	0.09	0.12	0.10	0.24	0.25	0.31	0.36	0.41
Slip	29.38	4.55	6.91	8.31	4.34	4.88	4.11	3.62	3.85
Ug (m/s)	5.33	0.85	1.35	1.58	0.96	1.11	1.02	0.96	1.10
Ul (m/s)	0.18	0.19	0.20	0.19	0.22	0.23	0.25	0.27	0.29
rho (kg/m3)	1442.0	1328.9	1282.6	1313.3	1111.6	1097.7	1008.6	934.1	863.3

Continued from previous page

10	11	12	13	14	15	16	17	18
0.60	0.60	0.60	0.60	0.60	0.60	0.60	0.60	0.60
0.00	0.00	0.00	0.00	0.00	0.00	0.00	0.00	0.00
2.00	2.05	2.00	1.95	1.95	1.95	1.95	1.95	2.00
2.10	2.22	2.37	2.41	2.43	2.50	2.61	2.63	2.72
2.18	2.29	2.44	2.47	2.50	2.56	2.67	2.68	2.78
1.86	1.93	2.03	2.05	2.06	2.11	2.17	2.19	2.25
1.95	2.09	2.24	2.28	2.31	2.38	2.50	2.51	2.62
3.50	3.50	3.50	3.65	3.65	3.75	4.05	4.05	4.25
580	578	580	580	581	582	581	581	581
4.39	4.45	4.50	4.53	4.54	4.57	4.54	4.51	4.56
7.60	9.00	11.00	11.40	11.60	12.50	14.00	14.40	15.70
1.02	1.08	1.07	1.09	1.05	1.08	1.14	1.15	1.19
0.30	0.30	0.30	0.31	0.30	0.31	0.31	0.32	0.31
0.45	0.47	0.60	0.70	0.80	0.80	0.80	0.80	0.80
62.0	70.0	81.0	83	86	89	92	92	95
0.940	0.936	0.940	0.940	0.942	0.944	0.942	0.942	0.942
0.547	0.539	0.547	0.552	0.554	0.556	0.554	0.554	0.549
0.392	0.397	0.392	0.388	0.388	0.388	0.388	0.388	0.392
34.9	36.9	39.4	40.0	40.4	41.5	43.3	43.7	45.2
36.2	38.1	40.5	41.0	41.5	42.5	44.3	44.5	46.2
31.0	32.1	33.8	34.1	34.3	35.1	36.1	36.4	37.4
32.5	34.8	37.2	37.9	38.4	39.5	41.5	41.7	43.5
142.3	161.0	184.8	189.3	196.0	202.7	209.5	209.5	226.0
1452.4	1447.6	1441.5	1439.9	1439.1	1436.2	1431.7	1430.9	1427.2
8.3451	8.8571	9.5285	9.7134	9.8068	10.1386	10.6755	10.7751	11.2313
1449.2	1444.8	1438.7	1437.5	1436.2	1433.8	1429.3	1428.8	1424.7
8.6840	9.1661	9.8537	9.9955	10.1386	10.4291	10.9763	11.0270	11.5425
1458.4	1452.8	1446.8	1445.2	1444.0	1441.1	1436.2	1435.8	1431.3
231.09	232.88	235.13	235.74	236.04	237.09	238.75	239.06	240.42
176.99	176.26	175.26	175.06	174.85	174.45	173.70	173.63	172.95
232.29	233.93	236.19	236.64	237.09	238.00	239.66	239.81	241.33
228.86	230.94	233.18	233.78	234.23	235.29	237.09	237.24	238.91
4.2665	4.3496	4.2992	4.4478	4.4366	4.5512	4.9480	4.9495	5.2564
0.0047	0.0077	0.0074	0.0091	0.0090	0.0105	0.0137	0.0137	0.0164
0.44	0.55	0.52	0.57	0.56	0.59	0.64	0.64	0.67
2.50236	3.26683	4.25409	5.66858	6.06163	6.47415	6.96264	6.96462	8.20350
2.06	2.64	3.47	4.66	5.00	5.35	5.71	5.71	6.65
0.01414	0.01853	0.02427	0.03238	0.03467	0.03711	0.04008	0.04011	0.04743
0.7	0.7	0.8	0.8	0.8	0.8	0.8	0.8	0.9
34.8	44.6	58.8	78.9	84.6	90.5	96.7	96.7	112.5
7.89E-07	1.03E-06	1.35E-06	1.81E-06	1.93E-06	2.07E-06	2.23E-06	2.24E-06	2.64E-06
6.2550	6.9510	7.6904	8.9708	9.2740	9.7190	10.5061	10.5091	11.8071
0.0160	0.0225	0.0267	0.0349	0.0367	0.0402	0.0457	0.0457	0.0542
0.74	0.79	0.81	0.84	0.85	0.86	0.87	0.86	0.88
249	245	248	250	250	251	249	249	246
798.5	643.0	683.0	615.8	621.7	578.7	507.4	510.1	466.0
0.335	0.409	0.389	0.435	0.432	0.465	0.527	0.524	0.567
0.40	0.30	0.35	0.33	0.34	0.31	0.26	0.26	0.24
0.990	0.988	0.986	0.985	0.985	0.984	0.983	0.982	0.981
0.42	0.47	0.51	0.54	0.55	0.57	0.53	0.50	0.55
3.81	4.11	3.86	4.50	4.50	4.33	5.45	6.14	5.88
1.10	1.28	1.32	1.63	1.66	1.69	1.94	2.05	2.12
0.29	0.31	0.34	0.36	0.37	0.39	0.36	0.33	0.36
851.0	772.0	711.0	671.5	658.8	622.1	672.3	716.1	652.7

Experimental Data for Two-Phase Freon-11 Flow Loop Operation
Experiment 12C Gamma Densitometer Calibration
Jan 14th 1997 Voltage at bundle Excitation Voltage 600 Volts
100% Liq 3.99 Volts rho_L = 1483.0 kg/m3
Atm. Pressure (MPa) 0.1030 100% Ga 4.99 Volts File: Jan14EXP.Wb2

Trial #	1	2	3	4	5	6	7	8	9	10	11	12
Q1 (in) U tube	0.62	0.62	0.62	0.62	0.62	0.62	0.62	0.62	0.62	0.62	0.62	0.62
Q2 (in)	0.00	0.00	0.00	0.00	0.00	0.00	0.00	0.00	0.00	0.00	0.00	0.00
Q2 (in) U tube	1.95	1.95	1.95	1.95	1.95	1.95	1.95	1.95	1.95	1.95	1.95	1.95
T1 (mV)	2.22	2.24	2.27	2.29	2.30	2.29	2.30	2.30	2.35	2.33	2.35	2.37
T2 (mV)	2.27	2.32	2.33	2.34	2.36	2.36	2.37	2.39	2.42	2.41	2.43	2.45
T3 (mV)	2.14	1.90	1.93	1.97	1.99	1.99	2.04	2.04	2.08	2.09	2.09	2.13
T5 (mV)	2.08	2.12	2.13	2.15	2.17	2.15	2.16	2.17	2.21	2.21	2.22	2.25
Power (kW)	5.35	4.95	4.65	4.30	3.95	3.60	3.30	3.20	3.00	2.75	2.50	2.25
N (rpm)	582	575	581	581	580	582	583	583	583	583	582	582
Gamma Volt	4.36	4.32	4.27	4.30	4.59	4.43	4.43	4.45	4.45	4.50	4.49	4.43
P1 (psi)	8.70	9.00	9.40	9.60	9.80	9.75	9.75	9.80	10.40	10.30	10.50	10.60
T4 (mV)	1.19	1.16	1.18	1.15	1.17	1.15	1.10	1.10	1.12	1.05	1.05	1.08
T6 (mV)	0.37	0.31	0.31	0.30	0.30	0.29	0.28	0.28	0.28	0.28	0.28	0.28
Qw (inHg)	0.25	0.20	0.25	0.30	0.30	0.40	0.50	0.50	0.50	0.70	0.70	0.70
Powerstat %		30	40	50	58	67	74.0	76.0	79.0	83.0	87.0	89.0
CALCULATED DATA												
Q (L/s)	0.944	0.931	0.942	0.942	0.940	0.944	0.945	0.945	0.945	0.945	0.944	0.944
Q1 (L/s)	0.556	0.543	0.554	0.554	0.552	0.556	0.558	0.558	0.558	0.558	0.556	0.556
Q2 (L/s)	0.388	0.388	0.388	0.388	0.388	0.388	0.388	0.388	0.388	0.388	0.388	0.388
T1 (C)	36.9	37.2	37.7	38.1	38.2	38.1	38.2	38.2	39.0	38.7	39.0	39.4
T2 (C)	37.7	38.6	38.7	38.9	39.2	39.2	39.4	39.7	40.2	40.0	40.4	40.7
T3 (C)	35.6	31.6	32.1	32.8	33.1	33.1	33.9	33.9	34.6	34.8	34.8	35.4
T5 (C)	34.6	35.3	35.4	35.7	36.1	35.7	35.9	36.1	36.7	36.7	36.9	37.4
Volt (Bundle) V		70.7	93.7	115.5	133.4	153.5	169.2	173.7	180.4	189.3	198.3	202.7
Physical Properties Freon-11												
rhoL1 (kg/m3)	1447.6	1446.8	1445.6	1444.8	1444.4	1444.8	1444.4	1444.4	1442.3	1443.1	1442.3	1441.5
rhoG1 (kg/m3)	8.8571	8.9446	9.0770	9.1661	9.2108	9.1661	9.2108	9.2108	9.4370	9.3460	9.4370	9.5285
rhoL2 (kg/m3)	1445.6	1443.5	1443.1	1442.7	1441.9	1441.9	1441.5	1440.7	1439.5	1439.9	1439.1	1438.3
rhoG2 (Kg/m3)	9.0770	9.3008	9.3460	9.3914	9.4826	9.4826	9.5285	9.6206	9.7600	9.7134	9.8068	9.9008
rhoL5 (kg/m3)	1453.2	1451.6	1451.2	1450.4	1449.6	1450.4	1450.0	1449.6	1448.0	1448.0	1447.6	1446.4
hf1 (kJ/kg)	232.88	233.18	233.63	233.93	234.08	233.93	234.08	234.08	234.83	234.53	234.83	235.13
hfg2 (kJ/kg)	176.39	176.06	175.99	175.93	175.79	175.79	175.73	175.59	175.39	175.46	175.32	175.19
hf2 (kJ/kg)	233.63	234.38	234.53	234.68	234.98	234.98	235.13	235.44	235.89	235.74	236.04	236.34
hf5 (kJ/Kg)	230.79	231.39	231.54	231.84	232.14	231.84	231.99	232.14	232.73	232.73	232.88	233.33
Void fraction upstreams calculations based on HEM												
dhu (kJ/kg)	6.4396	6.1087	5.6244	5.2033	4.7985	4.3429	3.9688	3.8501	3.6130	3.3115	3.0218	2.7215
xu heaters	0.0204	0.0177	0.0149	0.0134	0.0111	0.0068	0.0047	0.0031	0.0026	0.0018	-0.0007	-0.0016
UPSHEM Void	0.77	0.74	0.70	0.68	0.63	0.51	0.42	0.32	0.28	0.21	-0.12	-0.31
Void fraction @ bundle calculations												
dh@ (kJ/kg)	0.00000	0.62557	1.07696	1.63728	2.19266	2.88218	3.49120	3.68039	3.97419	4.37599	4.81938	5.03983
Power kW	0.00	0.51	0.89	1.36	1.81	2.40	2.91	3.07	3.31	3.64	4.00	4.18
x tub heater	0.00000	0.00355	0.00612	0.00931	0.01247	0.01640	0.01987	0.02096	0.02266	0.02494	0.02749	0.02877
BOHEM Tube	0.0	0.4	0.5	0.6	0.7	0.7	0.8	0.8	0.8	0.8	0.8	0.8
Heat flux kW/m²	0.0	8.6	15.1	23.0	30.6	40.5	49.3	51.9	56.0	61.7	67.7	70.7
Boiling Number	0.0E+00	2.0E-07	3.4E-07	5.2E-07	7.0E-07	9.1E-07	1.1E-06	1.2E-06	1.3E-06	1.4E-06	1.5E-06	1.6E-06
Overall Calculations												
delth (kJ/kg)	6.4228	6.5922	6.4704	6.4994	6.5400	6.6359	6.7502	6.7827	6.7818	6.8030	6.8684	6.7458
x	0.0203	0.0204	0.0197	0.0208	0.0210	0.0198	0.0205	0.0198	0.0207	0.0217	0.0212	0.0214
Void total	0.77	0.77	0.76	0.77	0.77	0.76	0.77	0.76	0.76	0.77	0.77	0.77
Gp (kg/m2s)	253	246	251	251	250	252	253	253	253	253	252	251
rhoH (kg/m3)	335.6	376.4	429.7	466.3	529.3	699.5	836.0	970.1	1031.1	1135.6	1627.5	1904.9
HEM Vp (m/s)	0.808	0.703	0.628	0.578	0.508	0.387	0.325	0.280	0.263	0.239	0.166	0.142
Separated Flow												
Corr. Factor	0.988	0.988	0.987	0.987	0.987	0.987	0.987	0.987	0.986	0.986	0.986	0.986
Rad Void Volts	0.34	0.30	0.25	0.28	0.57	0.41	0.41	0.43	0.43	0.48	0.47	0.40
Slip	6.34	7.55	9.53	8.54	2.49	4.44	4.58	4.04	4.20	3.60	3.64	4.67
Ug (m/s)	1.65	1.81	2.16	2.01	0.98	1.29	1.33	1.22	1.26	1.18	1.17	1.34
Ul (m/s)	0.26	0.24	0.23	0.24	0.39	0.29	0.29	0.30	0.30	0.33	0.32	0.29
rho (kg/m3)	953.6	1013.2	1090.3	1046.9	629.2	855.6	856.2	827.0	830.8	757.8	773.4	860.7

Experimental Data for Two-Phase Freon-11 Flow Loop Operation

Experiment 12A				Gamma Densitometer Calibration			
January 6th 1997				Voltage at bundle	Excitation	Voltage	600 Volts
			100% Liquid	4.15		rho_L =	1483.0 kg/m3
Atm. Pressure (MPa)	0.1029		100% Gas	5.16		File:	Jan6EXP.Wb2

Trial #	1	2	3	4	5	6	7
Q1 (in) U tube	0.60	0.60	0.60	0.60	0.60	0.60	0.60
Q2 (in)	0.00	0.00	0.00	0.00	0.00	0.00	0.00
Q2 (in) U tube	2.00	2.00	2.00	2.00	2.00	2.00	1.95
T1 (mV)	2.22	2.25	2.27	2.26	2.25	2.20	2.17
T2 (mV)	2.28	2.31	2.31	2.31	2.31	2.26	2.21
T3 (mV)	2.15	2.19	2.28	1.99	1.99	1.97	1.97
T5 (mV)	2.06	2.10	2.09	2.10	2.09	2.01	1.98
Power (kW)	5.30	5.35	4.85	4.45	4.05	3.05	2.50
N (rpm)	576	577	580	579	581	583	581
Gamma Volt	4.54	4.58	4.60	4.59	4.60	4.58	4.59
P1 (psi)	9.00	9.50	9.70	9.60	9.60	9.00	8.60
T4 (mV)	1.19	1.20	1.15	1.15	1.15	1.13	1.11
T6 (mV)	0.37	0.35	0.34	0.34	0.35	0.35	0.34
Qw (inHg)	0.30	0.30	0.35	0.40	0.40	0.40	0.40
Powerstat %			40	50.0	55.0	60.0	65.0
CALCULATED DATA							
Q (L/s)	0.932	0.934	0.940	0.938	0.942	0.945	0.942
Q1 (L/s)	0.540	0.542	0.547	0.545	0.549	0.553	0.554
Q2 (L/s)	0.392	0.392	0.392	0.392	0.392	0.392	0.388
T1 (C)	36.9	37.4	37.7	37.6	37.4	36.6	36.1
T2 (C)	37.9	38.4	38.4	38.4	38.4	37.6	36.7
T3 (C)	35.7	36.4	37.9	33.1	33.1	32.8	32.8
T5 (C)	34.3	34.9	34.8	34.9	34.8	33.4	32.9
Volt (Bundle) V			93.7	115.5	126.7	138.0	149.0
Physical Properties Freon-11							
rhoL1 (kg/m3)	1447.6	1446.4	1445.6	1446.0	1446.4	1448.4	1449.6
rhoG1 (kg/m3)	8.8571	8.9886	9.0770	9.0327	8.9886	8.7702	8.6411
rhoL2 (kg/m3)	1445.2	1444.0	1444.0	1444.0	1444.0	1446.0	1448.0
rhoG2 (Kg/m3)	9.1215	9.2558	9.2558	9.2558	9.2558	9.0327	8.8136
rhoL5 (kg/m3)	1454.0	1452.4	1452.8	1452.4	1452.8	1456.0	1457.2
hf1 (kJ/kg)	232.88	233.33	233.63	233.48	233.33	232.58	232.14
hfg2 (kJ/kg)	176.32	176.13	176.13	176.13	176.13	176.46	176.79
hf2 (kJ/kg)	233.78	234.23	234.23	234.23	234.23	233.48	232.73
hf5 (kJ/Kg)	230.49	231.09	230.94	231.09	230.94	229.75	229.30
Void fraction upstreams calculations based on HEM							
dhu (kJ/kg)	6.5688	6.6144	5.9343	5.4642	4.9386	3.6876	3.0126
xu heaters	0.0186	0.0197	0.0150	0.0132	0.0093	-0.0003	-0.0024
UPSHEM Void	0.75	0.76	0.70	0.68	0.60	-0.04	-0.64
Void fraction @ bundle calculations							
dh@ (kJ/kg)	0.00000	0.00000	1.08913	1.66097	1.98464	2.33348	2.71211
Power kW	0.00	0.00	0.89	1.36	1.63	1.94	2.26
x tub heater	0.00000	0.00000	0.00618	0.00943	0.01127	0.01322	0.01534
BOHEM Tube	0.0	0.0	0.5	0.6	0.6	0.7	0.7
Heat flux kW/m²	0.0	0.0	15.1	23.0	27.6	32.8	38.2
Boiling Number	0.00E+00	0.00E+00	3.45E-07	5.26E-07	6.29E-07	7.39E-07	8.56E-07
Overall Calculations							
delth (kJ/kg)	6.5488	6.5952	6.7875	6.7771	6.5113	5.5417	5.1728
x	0.0185	0.0196	0.0198	0.0206	0.0183	0.0102	0.0098
Void total	0.75	0.76	0.76	0.77	0.75	0.63	0.63
Gp (kg/m2s)	245	246	249	248	249	251	252
rhoH (kg/m3)	360.0	348.4	428.4	466.9	579.7	1514.2	2397.4
HEM Vp (m/s)	0.731	0.758	0.622	0.569	0.462	0.178	0.113
Separated Flow							
Corr. Factor	0.988	0.988	0.987	0.987	0.988	0.988	0.989
Rad Void Volts	0.36	0.40	0.41	0.40	0.42	0.40	0.41
Slip	5.38	4.77	4.47	4.84	4.09	2.50	2.35
Ug (m/s)	1.39	1.32	1.29	1.36	1.19	0.72	0.69
Ul (m/s)	0.26	0.28	0.29	0.28	0.29	0.29	0.29
rho (kg/m3)	932.7	877.0	850.1	863.5	848.3	873.5	857.5

Experimental Data for Two-Phase Freon-11 Flow

Experiment 13

April 3rd 1996

Gamma Densitometer Calibration Counts

100% Liq. 12514

100% Gas 15367

rho_L = 1483.0 kg/m3

File: Exp13exp.wb2

Excitation 600 Volts

Trial #	1	2	3	4	5	6	7	8	9
Q1 (in)	0.10	0.10	0.10	0.10	0.10	0.10	0.10	0.10	0.10
Q2 (in)	3.60	3.48	3.41	3.44	3.49	3.50	3.44	3.34	3.51
T1 (mV)	2.00	2.01	2.01	2.03	2.01	2.01	2.01	2.03	2.03
T2 (mV)	2.06	2.06	2.07	2.07	2.05	2.03	1.98	1.94	1.81
T5 (mV)	1.45	1.47	1.50	1.52	1.50	1.50	1.50	1.56	1.59
Power (kW)	4.90	4.65	4.45	4.05	3.90	3.25	2.60	1.86	1.00
N (rpm)	427	427	428	430	427	427	426	427	429
SCA Count	13402	13409	13716	13826	13780	13953	14144	14354	14486
P1 (psi)	6.50	6.50	6.50	6.50	6.50	6.50	6.50	6.50	6.50
T4 (mV)	0.55	0.55	0.55	0.55	0.55	0.55	0.55	0.55	0.55
T6 (mV)	0.25	0.25	0.25	0.25	0.25	0.25	0.25	0.25	0.25
Qw (inHg)	2.00	2.00	2.00	2.00	2.00	2.00	2.00	2.00	2.00
Powerstat %	0	20	30	40	40	50	60	70	80
CALCULATED DATA									
Q (L/s)	0.642	0.642	0.644	0.648	0.642	0.642	0.640	0.642	0.646
Q1 (L/s)	0.219	0.226	0.232	0.234	0.226	0.225	0.227	0.235	0.228
Q2 (L/s)	0.423	0.416	0.412	0.414	0.417	0.417	0.414	0.408	0.418
T1 (C)	33.3	33.4	33.4	33.8	33.4	33.4	33.4	33.8	33.8
T2 (C)	34.3	34.3	34.4	34.4	34.1	33.8	32.9	32.3	30.2
T5 (C)	24.3	24.6	25.1	25.4	25.1	25.1	25.1	26.1	26.6
Physical Properties Freon-11									
rhoL1 (kg/m3)	1456.4	1456.0	1456.0	1455.2	1456.0	1456.0	1456.0	1455.2	1455.2
rhoG1 (kg/m3	7.94	7.98	7.98	8.06	7.98	7.98	7.98	8.06	8.06
rhoL2 (kg/m3)	1454.0	1454.0	1453.6	1453.6	1454.4	1455.2	1457.2	1458.8	1463.9
rhoG2 (Kg/m3	8.18	8.18	8.22	8.22	8.14	8.06	7.86	7.70	7.20
rhoL5 (kg/m3)	1477.9	1477.1	1475.9	1475.2	1475.9	1475.9	1475.9	1473.6	1472.5
hf1 (kJ/kg)	229.60	229.75	229.75	230.05	229.75	229.75	229.75	230.05	230.05
hfg2 (kJ/kg)	177.77	177.77	177.71	177.71	177.84	177.97	178.29	178.55	179.39
hf2 (kJ/kg)	230.49	230.49	230.64	230.64	230.34	230.05	229.30	228.71	226.78
hf5 (kJ/Kg)	221.48	221.77	222.21	222.50	222.21	222.21	222.21	223.09	223.53
Void fraction upstreams calculations based on HEM									
dhu (kJ/kg)	14.80	13.61	12.69	11.46	11.45	9.56	7.59	5.25	2.90
xu heaters	0.03	0.03	0.02	0.02	0.02	0.01	0.00	-0.00	-0.00
Upshem	0.86	0.83	0.81	0.77	0.77	0.64	0.34	-0.65	-0.65
Void fraction @ bundle calculations									
dh@ (kJ/kg)	-0.01	0.76	1.59	2.73	2.84	4.37	6.17	8.06	10.77
Power kW	-0.00	0.26	0.56	0.97	0.97	1.49	2.13	2.87	3.73
x tub heater	-0.000	0.004	0.009	0.015	0.016	0.025	0.035	0.045	0.060
HEM V Tube	-0.01	0.43	0.62	0.73	0.74	0.82	0.87	0.90	0.93
Tothem-Upshem	-0.00	0.01	0.04	0.08	0.08	0.20	0.51	1.52	1.56
Overall Calculations	at monitoring tube using quality from power at both sources								
delth (kJ/kg)	14.68	14.11	13.87	13.57	13.63	12.99	12.47	11.67	11.50
x	0.03	0.03	0.03	0.03	0.03	0.03	0.03	0.03	0.05
Void total	0.85	0.85	0.85	0.85	0.85	0.84	0.85	0.87	0.91
Gp (kg/m2s)	102	105	108	109	105	104	105	109	106
rhoH (kg/m3)	209.8	243.1	272.0	333.6	332.2	527.4	969.5	2321.5	2237.6
HEM Vp (m/s)	0.479	0.427	0.392	0.322	0.312	0.196	0.107	0.046	0.047
Separated Flow									
Corr. Factor	0.991	0.991	0.991	0.991	0.991	0.991	0.991	0.991	0.991
RAD Void	0.29	0.29	0.40	0.44	0.42	0.49	0.55	0.62	0.67
Slip	15.14	12.53	6.68	0.00	4.70	1.90	0.41	-0.23	-0.18
Ug (m/s)	1.44	1.24	0.81	0.57	0.58	0.26	0.07	-0.05	-0.04
Ul (m/s)	0.10	0.10	0.12	0.13	0.12	0.14	0.16	0.20	0.22
rho (kg/m3)	1036.8	1033.8	874.2	1.0	841.3	753.4	657.5	555.3	490.8

Data Sheet for Two-Phase Flow-Induced Vibration
Experiment 11B
March 19th 1996

Gamma Densitometer Calibration
Counts Shield 2 1/8" lead plates Excitatior 600 Volts
100% Liq. 7177 7177.00 rho_L = 1483.0 kg/m3
100% Gas 10744 File: mar25exp.wq2

Trial #	1	2	3	4	5	6	7	8	9	10	11
Q1 (in)	0.19	0.19	0.19	0.19	0.19	0.19	0.19	0.19	0.19	0.19	0.19
Q2 (in)	3.40	3.40	3.57	3.44	3.44	3.44	3.60	3.57	3.20	3.40	3.00
T1 (mV)	1.96	2.05	2.15	2.17	2.19	2.21	2.24	2.25	2.31	2.39	2.03
T2 (mV)	1.88	2.03	2.21	2.24	2.27	2.29	2.33	2.33	2.39	2.47	2.10
T5 (mV)	1.60	1.75	1.99	2.01	2.05	2.10	2.12	2.14	2.21	2.29	1.60
Power (kW)	1.40	1.40	1.40	1.60	1.80	2.00	2.25	2.45	2.65	3.15	5.25
N (rpm)	422	422	422	422	422	422	420	420	424	429	432
SCA Count	7319	7426	7871	7982	8224	8339	8532	8623	8539	8849	8794
P1 (psi)	6.20	7.00	8.30	8.40	8.70	9.00	9.40	9.50	10.30	11.40	12.00
T4 (mV)	0.62	0.69	0.69	0.75	0.75	0.82	0.80	0.80	0.80	0.80	0.59
T6 (mV)	0.21	0.25	0.25	0.20	0.20	0.23	0.23	0.23	0.23	0.23	0.17
Qw (inHg)	1.20	1.20	1.20	1.20	1.20	1.20	1.20	1.20	1.20	1.20	1.20
Powerstat %	70	80	90	90	90	90	90	90	90	90	0
CALCULATED DATA											
Q (L/s)	0.633	0.633	0.633	0.633	0.633	0.633	0.629	0.629	0.637	0.646	0.651
Q1 (L/s)	0.222	0.222	0.212	0.219	0.219	0.219	0.206	0.208	0.238	0.235	0.265
Q2 (L/s)	0.411	0.411	0.421	0.414	0.414	0.414	0.423	0.421	0.399	0.411	0.386
T1 (C)	32.6	34.1	35.7	36.1	36.4	36.7	37.2	37.4	38.4	39.7	33.8
T2 (C)	31.3	33.8	36.7	37.2	37.7	38.1	38.7	38.7	39.7	41.0	34.9
T5 (C)	26.7	29.2	33.1	33.4	34.1	34.9	35.3	35.6	36.7	38.1	26.7
Physical Properties Freon-11											
rhoL1 (kg/m3)	1458.0	1454.4	1450.4	1449.6	1448.8	1448.0	1446.8	1446.4	1444.0	1440.7	1455.2
rhoG1 (kg/m3	7.78	8.14	8.56	8.64	8.73	8.81	8.94	8.99	9.26	9.62	8.06
rhoL2 (kg/m3)	1461.1	1455.2	1448.0	1446.8	1445.6	1444.8	1443.1	1443.1	1440.7	1437.5	1452.4
rhoG2 (Kg/m3	7.46	8.06	8.81	8.94	9.08	9.17	9.35	9.35	9.62	10.00	8.35
rhoL5 (kg/m3)	1472.1	1466.2	1456.8	1456.0	1454.4	1452.4	1451.6	1450.8	1448.0	1444.8	1472.1
hf1 (kJ/kg)	229.01	230.34	231.84	232.14	232.44	232.73	233.18	233.33	234.23	235.44	230.05
hfg2 (kJ/kg)	178.94	177.97	176.79	176.59	176.39	176.26	175.99	175.99	175.59	175.06	177.51
hf2 (kJ/kg)	227.82	230.05	232.73	233.18	233.63	233.93	234.53	234.53	235.44	236.64	231.09
hf5 (kJ/Kg)	223.68	225.89	229.45	229.75	230.34	231.09	231.39	231.69	232.73	233.93	223.68
Void fraction upstreams calculations based on HEM											
dhu (kJ/kg)	4.17	4.19	4.42	4.87	5.49	6.10	7.31	7.89	7.49	9.04	13.14
xu heaters	0.00	0.00	0.01	0.01	0.01	0.02	0.02	0.03	0.03	0.04	0.03
Upshem	0.04	0.04	0.51	0.57	0.67	0.75	0.79	0.82	0.81	0.84	0.85
Void fraction @ bundle calculations											
dh@ (kJ/kg)	8.53	11.11	14.76	14.25	14.27	14.28	15.20	15.08	13.22	13.43	-0.01
Power kW	2.87	3.73	4.69	4.69	4.69	4.69	4.69	4.69	4.69	4.69	-0.00
x tub heater	0.048	0.062	0.084	0.081	0.081	0.081	0.086	0.086	0.075	0.077	-0.000
HEM V Tube	0.91	0.92	0.94	0.93	0.93	0.93	0.94	0.94	0.92	0.92	-0.01
Tothem-Upshem	0.85	0.87	0.41	0.36	0.26	0.19	0.15	0.12	0.13	0.10	-0.00
Overall Calculations at monitoring tube using quality from power at both sources											
delth (kJ/kg)	10.98	13.07	16.21	16.26	16.88	17.51	19.45	19.94	18.05	19.76	13.05
x	0.04	0.05	0.07	0.07	0.08	0.08	0.09	0.10	0.09	0.10	0.03
Void total	0.89	0.90	0.93	0.93	0.93	0.93	0.94	0.94	0.93	0.94	0.85
Gp (kg/m2s)	103	102	97	100	100	100	94	95	108	107	123
rhoH (kg/m3)	1404.4	1403.5	697.0	614.7	473.9	360.2	301.1	258.9	276.4	225.8	214.0
HEM Vp (m/s)	0.073	0.072	0.139	0.163	0.211	0.278	0.312	0.366	0.391	0.472	0.568
Separated Flow											
Corr. Factor	0.992	0.990	0.989	0.989	0.988	0.988	0.988	0.988	0.987	0.986	0.991
RAD Void	0.03	0.06	0.20	0.24	0.31	0.34	0.40	0.42	0.40	0.48	0.48
Slip	1.36	0.57	4.34	0.00	4.70	5.95	5.93	6.46	6.62	6.01	6.53
Ug (m/s)	0.10	0.04	0.36	0.40	0.46	0.61	0.63	0.71	0.80	0.83	1.02
Ul (m/s)	0.07	0.07	0.08	0.09	0.10	0.10	0.11	0.11	0.12	0.14	0.16
rho (kg/m3)	1418.1	1367.1	1160.3	0.4	1004.4	955.3	874.5	837.0	873.5	749.2	760.4

Experimental Data for Two-Phase Freon-11 Flow

Experiment 11				Gamma Densitometer Calibration						
March 18th 1996				Counts		Shield	2 1/8" plates		Excitation	600 V
		100% Liquid		7138		7138	rho_L =	1483.0	kg/m3	
		100% Gas		10685.6				File:	march18dat.wq2	
Code	s	b	b	b	b	b	b	b	b	m
Trial #	1	2	3	4	5	6	7	8	9	10
Q1 (in)	0.22	0.22	0.22	0.22	0.22	0.19	0.19	0.19	0.19	0.19
Q2 (in)	3.3	3.3	3.4	3.4	3.4	3.5	3.5	3.5	3.8	3.53
T1 (mV)	1.45	1.47	1.53	1.57	1.7	1.87	1.93	1.98	2.06	2.2
T2 (mV)	1.45	1.46	1.49	1.53	1.61	1.72	1.79	1.90	2.08	2.29
T5 (mV)	1.05	1.06	1.09	1.14	1.24	1.35	1.46	1.59	1.81	2.07
Power (kW)	2.40	2.40	2.30	2.20	2.20	2.15	1.80	1.40	1.20	1.30
N (rpm)	422	422	421	421	421	421	420	422	420	421
SCA Count	7253		7256		7294		7332		7426	7907
P1 (psi)	3.90	3.80	4.00	4.30	4.60	5.10	5.80	6.40	7.00	8.70
T4 (mV)	0.49	0.47	0.47	0.47	0.47	0.55	0.58	0.6	0.6	0.74
T6 (mV)	0.26	0.24	0.23	0.23	0.23	0.23	0.23	0.19	0.19	0.17
Qw (inHg)	1.2	1.2	1.2	1.2	1.2	1.2	1.2	1.2	1.2	1.2
Powerstat %	0	10	20	30	40	50	60	70	80	90
CALCULATED DATA										
Q (L/s)	0.633	0.633	0.631	0.631	0.631	0.631	0.629	0.633	0.629	0.631
Q1 (L/s)	0.228	0.228	0.220	0.220	0.220	0.214	0.212	0.216	0.195	0.212
Q2 (L/s)	0.405	0.405	0.411	0.411	0.411	0.417	0.417	0.417	0.435	0.419
T1 (C)	24.3	24.6	25.6	26.2	28.4	31.1	32.1	32.9	34.3	36.6
T2 (C)	24.3	24.4	24.9	25.6	26.9	28.7	29.8	31.6	34.6	38.1
T5 (C)	17.8	17.9	18.4	19.2	20.8	22.6	24.4	26.6	30.2	34.4
Volt (Bundle) V	0.0	26.0	48.4	70.7	93.1	115.5	137.9	160.2	182.6	205.0
Physical Properties Freon-11										
rhoL1 (kg/m3)	1477.9	1477.1	1474.8	1473.2	1468.2	1461.5	1459.1	1457.2	1454.0	1448.4
rhoG1 (kg/m3)	5.95	6.02	6.21	6.35	6.80	7.43	7.66	7.86	8.18	8.77
rhoL2 (kg/m3)	1477.9	1477.5	1476.3	1474.8	1471.7	1467.4	1464.7	1460.3	1453.2	1444.8
rhoG2 (Kg/m3)	5.95	5.99	6.08	6.21	6.48	6.87	7.12	7.54	8.26	9.17
rhoL5 (kg/m3)	1493.1	1492.7	1491.6	1489.7	1485.9	1481.7	1477.5	1472.5	1463.9	1453.6
hf1 (kJ/kg)	221.48	221.77	222.65	223.24	225.15	227.67	228.56	229.30	230.49	232.58
hfg2 (kJ/kg)	181.67	181.61	181.42	181.17	180.67	179.97	179.52	178.81	177.64	176.26
hf2 (kJ/kg)	221.48	221.62	222.06	222.65	223.83	225.45	226.48	228.11	230.79	233.93
hf5 (kJ/Kg)	215.65	215.79	216.23	216.95	218.41	220.01	221.62	223.53	226.78	230.64
Void fraction upstreams calculations based on HEM										
dhu (kJ/kg)	6.88	6.88	6.83	6.54	6.56	6.61	5.59	4.29	4.10	4.10
xu heaters	0.0057486	0.00575	0.00549	0.00466	0.0063	0.00651	0.00408	-0.0016	0.00049	0.00459
HEM Void	0.59	0.59	0.57	0.53	0.59	0.58	0.46	-0.46	0.08	0.42
Void fraction @ bundle calculations										
dh@ (kJ/kg)	0.00	0.20	0.71	1.52	2.64	4.20	6.04	8.04	11.62	13.50
Power kW	0.00	0.07	0.24	0.51	0.88	1.36	1.93	2.61	3.39	4.27
x tub heater	0.000	0.000	0.001	0.005	0.007	0.011	0.022	0.038	0.067	0.084
HEM V Tube	0.00	0.06	0.14	0.55	0.63	0.70	0.82	0.89	0.93	0.94
Common calculations at test section										
Void total	0.59	0.60	0.60	0.70	0.76	0.79	0.85	0.88	0.93	0.94
Gp (kg/m2s)	106	106	102	102	102	99	98	99	89	96
rhoH (kg/m3)	610.4	613.9	642.1	0.2	623.4	642.4	822.8	2081.4	1338.1	825.8
HEM Vp (m/s)	0.186	0.185	0.170	0.513	0.175	0.164	0.127	0.051	0.071	0.125
Separated Flow										
Corr. Factor	0.998	0.998	0.997	0.012	0.995	0.993	0.992	0.991	0.990	0.988
RAD Void	0.04	N/A	0.03	N/A	0.04	N/A	0.05	N/A	0.07	0.22
Slip	39.20	N/A	37.48	N/A	31.93	N/A	16.06	N/A	1.10	2.64
Ug (m/s)	0.00	0.00	0.00	N/A	0.00	N/A	0.00	N/A	0.00	0.00
Ul (m/s)	0.07	0.07	0.07	N/A	0.07	N/A	0.07	N/A	0.07	0.09
rho (kg/m3)	1425.9	1477.1	1425.2	N/A	1408.1	N/A	1391.8	N/A	1347.6	1125.4

Experimental Data for Two-Phase Freon-11 Flow

Experiment 27 Gamma Densitometer Calibration

August 13th 1996 bundl bundle Excitation voltage SCA 600 Volts

11830 11830 100% Liq. rho_L = 1483.0 kg/m3

Atm. Pressure (MPa) 0.1019 14533 14533 100% Gas Name of file: AUG13EXP.WQ2

Trial #	1	2	3	4	5	6	7	8	9	10	11
Q1 (in) U tube	2	2	2	2.00	2.00	2.00	2.00	2.00	2.00	2.00	2
Q2 (in)											
Q2 (in) U tube	2.4	2.45	2.45	2.45	2.45	2.45	2.45	2.45	2.50	2.50	2.5
T1 (mV)	2.36	2.34	2.36	2.37	2.39	2.45	2.51	2.55	2.57	2.65	2.79
T2 (mV)	2.37	2.4	2.43	2.43	2.47	2.53	2.59	2.65	2.63	2.71	2.87
T5 (mV)	2.14	2.17	2.2	2.21	2.23	2.29	2.37	2.43	2.43	2.51	2.65
Power (kW)	4.4	4.2	4.15	4.15	4.15	4.05	4.05	3.95	3.75	3.70	3.85
N (rpm)	*812*	*811*	*811*	*812*	*812*	*812*	*808*	*808*	*817*	*818*	*818*
SCA Count	12021	12317	12545	12814	12983	13144	13326	13450	13535	13609	13692
P1 (psi)	10	10.2	10.5	10.80	11.00	12.00	12.60	13.40	13.5	14.5	16.5
T4 (mV)	1.64	1.57	1.56	1.51	1.47	1.46	1.47	1.44	1.42	1.4	1.44
T6 (mV)	1.18	1.17	1.19	1.19	1.19	1.19	1.19	1.18	1.18	1.17	1.17
Qw (inHg)	0.6	0.8	1	1.80	2.45	3.00	3.70	4.40	5.45	6.8	7.6
Powerstat %	0	30	37	45	52	60	67	75	82	90	98
CALCULATED DATA											
Q (L/s)	1.371	1.369	1.369	1.371	1.371	1.371	1.364	1.364	1.381	1.382	1.382
Q1 (L/s)	0.941	0.935	0.935	0.937	0.937	0.937	0.930	0.930	0.942	0.944	0.944
Q2 (L/s)	0.430	0.434	0.434	0.434	0.434	0.434	0.434	0.434	0.439	0.439	0.439
T1 (C)	39.2	38.9	39.2	39.4	39.7	40.7	41.7	42.4	42.7	44.0	46.3
T2 (C)	39.4	39.9	40.4	40.4	41.0	42.0	43.0	44.0	43.7	45.0	47.7
T5 (C)	35.6	36.1	36.6	36.7	37.1	38.1	39.4	40.4	40.4	41.7	44.0
Physical Properties Freon-11											
rhoL1 (kg/m3)	1441.9	1442.7	1441.9	1441.5	1440.7	1438.3	1435.8	1434.2	1433.4	1430.1	1424.3
rhoG1 (kg/m3)	9.4826	9.3914	9.4826	9.5285	9.6206	9.9008	10.1866	10.3803	10.4781	10.8754	11.5950
rhoL2 (kg/m3)	1441.5	1440.3	1439.1	1439.1	1437.5	1435.0	1432.5	1430.1	1430.9	1427.6	1421.0
rhoG2 (Kg/m3)	9.5285	9.6669	9.8068	9.8068	9.9955	10.2832	10.5765	10.8754	10.7751	11.1800	12.0200
rhoL5 (kg/m3)	1450.8	1449.6	1448.4	1448.0	1447.2	1444.8	1441.5	1439.1	1439.1	1435.8	1430.1
hf1 (kJ/kg)	234.984	234.684	234.984	235.135	235.435	236.339	237.243	237.847	238.150	239.360	241.485
hfg2 (kJ/kg)	175.726	175.525	175.324	175.324	175.056	174.652	174.245	173.838	173.974	173.428	172.328
hf2 (kJ/kg)	235.135	235.586	236.037	236.037	236.640	237.545	238.452	239.360	239.057	240.270	242.703
hf5 (kJ/Kg)	231.688	232.136	232.585	232.735	233.034	233.933	235.135	236.037	236.037	237.243	239.360
Void fraction upstreams calculations based on HEM											
dhu (kJ/kg)	3.1349	3.0152	2.9818	2.9763	2.9788	2.9119	2.9410	2.8733	2.6914	2.6563	2.7760
xu heaters	-0.0018	-0.0025	-0.0027	-0.0019	-0.0036	-0.0040	-0.0022	-0.0026	-0.0019	-0.0021	-0.0033
UPSHEM Void	-0.37	-0.58	-0.65	-0.38	-1.06	-1.26	-0.41	-0.51	-0.33	-0.37	-0.63
Void fraction @ bundle calculations											
dh@ (kJ/kg)	-0.00155	0.40253	0.60034	0.8723	1.15353	1.52464	1.9089	2.38248	2.79922	3.35987	3.98658
Power kW	-0.00218	0.56251	0.83824	1.22005	1.6125	2.12772	2.63689	3.28551	3.91141	4.69343	5.5466
x tub heater	-0.0000	0.0023	0.0034	0.0050	0.0066	0.0087	0.0110	0.0137	0.0161	0.0194	0.0231
BOHEM Tube	-0.00	0.26	0.34	0.42	0.49	0.55	0.60	0.65	0.68	0.72	0.74
Heat flux W/in2	-0.02	6.14	9.15	13.32	17.60	23.23	28.79	35.87	42.70	51.23	60.55
Overall Calculations											
delth (kJ/kg)	3.1237	3.3275	3.4525	3.6650	3.8916	4.1218	4.4590	4.7703	4.9231	5.3366	5.9564
x	-0.0018	-0.0007	-0.0000	0.0021	0.0016	0.0029	0.0066	0.0083	0.0109	0.0133	0.0152
Void total	-0.39	-0.12	-0.00	0.24	0.20	0.30	0.48	0.54	0.60	0.64	0.65
Gp (kg/m2s)	427	424	423	424	424	423	419	418	424	424	422
rhoH (kg/m3)	1443.8	1068.7	950.4	824.8	727.6	636.6	566.8	498.0	450.0	405.3	373.0
HEM Vp (m/s)	0.317	0.425	0.478	0.552	0.625	0.713	0.793	0.902	1.011	1.122	1.214
Separated Flow											
Corr. Factor	0.986	0.986	0.986	0.986	0.986	0.985	0.984	0.983	0.983	0.982	0.980
RAD Void	0.01	0.13	0.22	0.32	0.38	0.44	0.50	0.54	0.57	0.59	0.61
Slip	-0.14	2.31	1.82	1.56	1.55	1.58	1.50	1.54	1.63	1.74	1.77
Ug (m/s)	-0.0411	0.7779	0.6811	0.6736	0.7316	0.8206	0.8673	0.9713	1.1072	1.2391	1.3258
Ul (m/s)	0.2989	0.3369	0.3742	0.4307	0.4734	0.5192	0.5783	0.6300	0.6802	0.7141	0.7475
rho (kg/m3)	1427.8	1255.5	1129.0	982.6	892.7	811.8	721.4	660.4	619.2	588.4	558.4

Experimental Data for Two-Phase Freon-11 Flow

Experiment 26				Gamma Densitometer Calibration						
July 22nd 1996				Counts		Excitation Voltage		SCA	600 Volts	
			100% Liq	12206			rho_L =	1483.0	kg/m3	
Atm. Pressure (MPa)		0.1017	100% Ga	15001			Name of file:		Feb11EXP.Wb2	
Trial #	1	2	3	4	5	6	7	8	9	10
Q1 (in) U tube	0.65	0.65	0.65	0.65	0.65	0.65	0.65	0.65	0.65	0.60
Q2 (in)	1.0									
Q2 (in) U tube	0.95	0.95	0.95	0.95	0.90	0.90	0.90	0.90	0.90	0.90
T1 (mV)	1.78	1.79	1.93	1.98	2.02	2.10	2.17	2.29	2.38	2.52
T2 (mV)	1.82	1.93	2.00	2.08	2.12	2.21	2.29	2.41	2.50	2.65
T3 (mv)	0.00	0.00	0.00	0.00	0.00	0.00	0.00	0.00	0.00	0.00
T5 (mV)	1.51	1.64	1.71	1.78	1.85	1.93	2.03	2.16	2.26	2.41
Power (kW)	2.95	2.90	2.90	2.90	2.65	2.55	2.45	2.35	2.30	2.15
N (rpm)	520	521	520	520	522	520	520	519	519	516
Gamma Volt	12246	12363	12669	13055	13477	13770	13920	14055	14140	14206
P1 (psi)	5.00	5.60	6.00	6.50	7.00	8.00	8.60	10.40	11.50	13.10
T4 (mV)	0.87	0.87	0.88	0.89	0.90	0.91	0.93	0.96	0.96	0.95
T6 (mV)	0.73	0.69	0.69	0.67	0.69	0.69	0.69	0.69	0.69	0.71
Qw (inHg)	1.50	1.50	1.50	1.50	1.50	1.60	1.60	1.80	2.00	3.40
Powerstat %		30	37	45	52	60	67	75	82	90
CALCULATED DATA										
Q (L/s)	0.828	0.830	0.828	0.828	0.832	0.828	0.828	0.826	0.826	0.821
Q1 (L/s)	0.558	0.560	0.558	0.558	0.569	0.565	0.565	0.563	0.563	0.557
Q2 (L/s)	0.270	0.270	0.270	0.270	0.263	0.263	0.263	0.263	0.263	0.263
T1 (C)	29.7	29.8	32.1	32.9	33.6	34.9	36.1	38.1	39.5	41.9
T2 (C)	30.3	32.1	33.3	34.6	35.3	36.7	38.1	40.0	41.5	44.0
T3 (C)	0.8	0.8	0.8	0.8	0.8	0.8	0.8	0.8	0.8	0.8
T5 (C)	25.2	27.4	28.5	29.7	30.8	32.1	33.8	35.9	37.6	40.0
Volt (Bundle) V	0.0	70.7	86.4	104.3	120.0	137.9	153.5	171.4	187.1	205.0
Physical Properties Freon-11										
rhoL1 (kg/m3)	1465.1	1464.7	1459.1	1457.2	1455.6	1452.4	1449.6	1444.8	1441.1	1435.4
rhoG1 (kg/m3)	7.0877	7.1246	7.6576	7.8552	8.0160	8.3451	8.6411	9.1661	9.5745	10.2348
rhoL2 (kg/m3)	1463.5	1459.1	1456.4	1453.2	1451.6	1448.0	1444.8	1439.9	1436.2	1430.1
rhoG2 (Kg/m3)	7.2363	7.6576	7.9353	8.2619	8.4289	8.8136	9.1661	9.7134	10.1386	10.8754
rhoL5 (kg/m3)	1475.6	1470.5	1467.8	1465.1	1462.3	1459.1	1455.2	1450.0	1446.0	1439.9
hf1 (kJ/kg)	226.34	226.48	228.56	229.30	229.90	231.09	232.14	233.93	235.29	237.39
hfg2 (kJ/kg)	179.33	178.62	178.16	177.64	177.38	176.79	176.26	175.46	174.85	173.84
hf2 (kJ/kg)	226.93	228.56	229.60	230.79	231.39	232.73	233.93	235.74	237.09	239.36
hf5 (kJ/Kg)	222.36	224.27	225.30	226.34	227.37	228.56	230.05	231.99	233.48	235.74
Void fraction upstreams calculations based on HEM										
dhu (kJ/kg)	3.4914	3.4318	3.4497	3.4567	3.1026	3.0121	2.9012	2.8017	2.7494	2.6069
xu heaters	-0.0060	-0.0048	-0.0048	-0.0056	-0.0052	-0.0066	-0.0056	-0.0054	-0.0049	-0.0059
UPSHEM Void	5.75	-10.30	-6.71	-61.14	-7.53	14.60	-7.07	-3.92	-2.26	-3.25
Void fraction @ bundle calculations										
dh@ (kJ/kg)	0.00000	0.59963	0.89927	1.31299	1.70680	2.27397	2.82775	3.54995	4.24008	5.16294
Power kW	0.00	0.51	0.76	1.11	1.46	1.93	2.40	2.99	3.56	4.27
x tub heater	0.00000	0.00336	0.00505	0.00739	0.00962	0.01286	0.01604	0.02023	0.02425	0.02970
BOHEM Tube	0.0	0.4	0.5	0.6	0.6	0.7	0.7	0.8	0.8	0.8
Heat flux kW/m²	0.0	8.6	12.8	18.7	24.8	32.7	40.6	50.6	60.2	72.3
Boiling Number	0.0E+00	1.9E-07	2.8E-07	4.1E-07	5.4E-07	7.2E-07	9.0E-07	1.1E-06	1.4E-06	1.7E-06
Overall Calculations										
delth (kJ/kg)	3.4771	3.8982	4.1557	4.4931	4.4567	4.8198	5.1530	5.6319	6.1322	6.7283
x	-0.0061	-0.0022	-0.0008	0.0002	0.0025	0.0036	0.0072	0.0107	0.0144	0.0179
Void total	4.95	-0.82	-0.18	0.04	0.31	0.39	0.55	0.63	0.69	0.72
Gp (kg/m2s)	257	257	255	255	260	257	257	255	254	251
rhoH (kg/m3)	-6143.4	87843.9	15064.4	-38453.3	20903.8	-10513.6	21318.2	9394.1	5440.4	7746.0
HEM Vp (m/s)	-0.045	0.003	0.018	-0.007	0.013	-0.026	0.013	0.029	0.050	0.035
bund/total ratio	-0.16	-11.57	-36.24	1639.89	25.19	-36.52	13.89	7.21	4.28	5.53
Separated Flow										
Corr. Factor	0.994	0.994	0.992	0.991	0.991	0.990	0.989	0.987	0.986	0.984
Rad Void Volts	-0.01	0.03	0.14	0.28	0.44	0.53	0.58	0.62	0.64	0.66
Slip	91.02	-12.70	-0.89	0.09	0.56	0.52	0.82	0.98	1.15	1.25
Ug (m/s)	15.84	-2.31	-0.18	0.02	0.18	0.20	0.35	0.45	0.56	0.63
Ul (m/s)	0.17	0.18	0.20	0.24	0.32	0.38	0.42	0.46	0.49	0.50
rho (kg/m3)	1483.4	1413.0	1251.8	1043.5	823.6	679.2	609.2	552.1	518.0	497.9

Experimental Data for Two-Phase Freon-11 Flow
Experiment 38
Feb 11th 1997

Gamma Densitometer Calibration
Voltage — Excitation Voltage — SCA — 600 Volts
100% Liqu 4.12 — rho_L = 1483.0 kg/m3
Atm. Pressure (MPa) 0.1022 *100% Gas* 5.09 — Name of file: Feb11EXP.Wb2

Trial #	1	2	3	4	5	6	7	8	9	10
Q1 (in) U tube	0.63	0.62	0.60	0.60	0.60	0.62	0.60	0.60	0.60	0.60
Q2 (in)	0.00	0.52			0.00	0.00	0.00	0.00	0.00	0.00
Q2 (in) U tube	2.05	2.10	2.10	2.05	2.05	2.05	2.05	2.06	2.05	2.08
T1 (mV)	2.11	2.20	2.27	2.28	2.19	2.25	2.32	2.35	2.33	2.41
T2 (mV)	2.10	2.23	2.33	2.31	2.20	2.29	2.37	2.41	2.38	2.47
T3 (mv)	2.03	1.92	1.99	2.00	1.97	2.03	2.11	2.15	2.15	2.21
T5 (mV)	1.86	1.99	2.09	2.07	1.97	2.07	2.15	2.19	2.17	2.27
Power (kW)	3.00	2.70	2.70	2.60	2.55	2.45	2.40	2.35	2.35	2.20
N (rpm)	587	587	587	586	588	582	586	586	587	585
Gamma Volt	4.16	4.34	4.41	4.52	4.60	4.62	4.69	4.75	4.78	4.82
P1 (psi)	7.75	8.60	9.50	9.60	5.80	9.40	10.20	10.60	10.40	11.40
T4 (mV)	1.03	1.08	1.08	1.09	1.08	1.09	1.10	1.09	0.92	0.83
T6 (mV)	0.33	0.27	0.28	0.26	0.26	0.25	0.23	0.24	0.23	0.24
Qw (inHg)	0.10	0.20	0.15	0.20	0.30	0.30	0.40	0.50	0.90	1.50
Powerstat %		40	46	52	60	68	75.0	82.0	90.0	99.0
CALCULATED DATA										
Q (L/s)	0.953	0.953	0.953	0.951	0.955	0.944	0.951	0.951	0.953	0.949
Q1 (L/s)	0.555	0.551	0.551	0.554	0.557	0.546	0.554	0.553	0.555	0.549
Q2 (L/s)	0.397	0.402	0.402	0.397	0.397	0.397	0.397	0.398	0.397	0.400
T1 (C)	35.1	36.6	37.7	37.8	36.4	37.4	38.6	39.0	38.7	40.0
T2 (C)	34.9	37.1	38.7	38.4	36.6	38.1	39.4	40.0	39.5	41.0
T3 (C)	33.8	32.0	33.1	33.3	32.8	33.8	35.1	35.7	35.7	36.7
T5 (C)	31.0	33.1	34.8	34.4	32.8	34.4	35.7	36.4	36.1	37.7
Volt (Bundle) V	0.0	93.1	106.5	120.0	137.9	155.8	171.4	187.1	205.0	225.1
Physical Properties Freon-11										
rhoL1 (kg/m3)	1452.0	1448.4	1445.6	1445.4	1448.8	1446.4	1443.5	1442.3	1443.1	1439.9
rhoG1 (kg/m3)	8.3869	8.7702	9.0770	9.0992	8.7270	8.9886	9.3008	9.4370	9.3460	9.7134
rhoL2 (kg/m3)	1452.4	1447.2	1443.1	1444.0	1448.4	1444.8	1441.5	1439.9	1441.1	1437.5
rhoG2 (Kg/m3)	8.3451	8.9008	9.3460	9.2558	8.7702	9.1661	9.5285	9.7134	9.5745	9.9955
rhoL5 (kg/m3)	1461.9	1456.8	1452.8	1453.6	1457.6	1453.6	1450.4	1448.8	1449.6	1445.6
hf1 (kJ/kg)	231.24	232.58	233.63	233.71	232.44	233.33	234.38	234.83	234.53	235.74
hfg2 (kJ/kg)	177.51	176.66	175.99	176.13	176.85	176.26	175.73	175.46	175.66	175.06
hf2 (kJ/kg)	231.09	233.03	234.53	234.23	232.58	233.93	235.13	235.74	235.29	236.64
hf5 (kJ/Kg)	227.52	229.45	230.94	230.64	229.15	230.64	231.84	232.44	232.14	233.63
Void fraction upstreams calculations based on HEM										
dhu (kJ/kg)	3.5951	3.2755	3.2846	3.1443	3.0544	3.0024	2.9081	2.8556	2.8391	2.6971
xu heaters	0.0001	-0.0017	-0.0017	-0.0025	-0.0021	-0.0016	-0.0022	-0.0025	-0.0018	-0.0018
UPSHEM Void	0.02	-0.39	-0.37	-0.65	-0.54	-0.35	-0.50	-0.60	-0.36	-0.34
Void fraction @ bundle calculations										
dh@ (kJ/kg)	0.00000	1.06581	1.39917	1.76362	2.30741	3.01395	3.60949	4.31154	5.14690	6.30020
Power kW	0.00	0.88	1.15	1.46	1.93	2.47	2.99	3.56	4.27	5.15
x tub heater	0.00000	0.00603	0.00795	0.01001	0.01305	0.01710	0.02054	0.02457	0.02930	0.03599
BOHEM Tube	0.0	0.5	0.6	0.6	0.7	0.7	0.8	0.8	0.8	0.8
Heat flux kW/m²	0.0	14.9	19.5	24.8	32.7	41.7	50.6	60.2	72.3	87.2
Boiling Number	0.00E+00	3.37E-07	4.44E-07	5.59E-07	7.28E-07	9.54E-07	1.15E-06	1.37E-06	1.63E-06	2.01E-06
Overall Calculations										
delth (kJ/kg)	3.5834	4.1174	4.3930	4.5448	4.8907	5.4044	5.7868	6.2961	6.9483	7.7297
x	0.0001	0.0030	0.0045	0.0054	0.0083	0.0120	0.0142	0.0171	0.0216	0.0270
Void total	0.01	0.33	0.42	0.46	0.58	0.66	0.69	0.73	0.77	0.80
Gp (kg/m2s)	254	251	250	251	254	248	251	250	252	248
rhoH (kg/m3)	1417.1	2026.3	1998.6	2407.9	2233.2	1957.6	2192.9	2347.0	1978.3	1946.9
HEM Vp (m/s)	0.192	0.133	0.134	0.112	0.122	0.136	0.123	0.114	0.137	0.137
bund/total ratio	-0.84	2.18	1.88	2.40	1.93	1.52	1.73	1.83	1.47	1.42
Separated Flow										
Corr. Factor	0.989	0.988	0.987	0.987	0.988	0.988	0.987	0.986	0.986	0.985
Rad Void Volts	-0.00	0.19	0.26	0.38	0.47	0.48	0.55	0.61	0.64	0.67
Slip	-3.15	2.10	2.00	1.40	1.57	2.05	1.78	1.66	1.89	1.94
Ug (m/s)	-0.55	0.45	0.47	0.39	0.51	0.67	0.68	0.72	0.89	1.00
Ul (m/s)	0.17	0.21	0.23	0.28	0.33	0.33	0.38	0.43	0.47	0.51
rho (kg/m3)	1458.6	1173.6	1068.5	902.4	777.5	751.9	655.2	571.4	527.3	477.5

Data Sheet for Two-Phase Flow-Induced Vibration
Experiment 10 Gamma Densitometer Calibration
March 12 1996 Trials 9-14 1-8

	Counts 100% Liq.			7173	7082		7082 rho_L =	1454.0 kg/m3	Trials 1-8					
	Counts 100% gas			10738	10573		7173 rho_L =	1483 kg/m3	Trials 9-14					
Trial #	1	2	3	4	5	6	7	8	9	10	11	12	13	14
Q1 (in)	1.6	1.59	1.63	1.65	1.65	1.65	1.65	1.65	1.61	1.61	1.61	1.61	1.61	1.61
Q2 (in)	1.54	1.58	1.6	1.64	1.67	1.67	1.67	1.67	1.41	1.41	1.41	1.41	1.41	1.41
T1 (mV)	2.06	2.08	2.15	2.18	2.24	2.29	2.33	2.39	2.25	2.29	2.35	2.37	2.38	2.4
T2 (mV)	2.06	2.09	2.17	2.21	2.31	2.36	2.41	2.45	2.32	2.36	2.41	2.43	2.45	2.47
T5 (mV)	1.81	1.83	1.9	1.93	2.03	2.09	2.15	2.22	2.06	2.12	2.18	2.21	2.23	2.25
Power (kW)	5.00	5.15	5.50	5.90	6.20	6.55	6.90	7.20	6.50	6.85	6.95	7.00	7.15	7.35
N (rpm)	692	692	692	694	694	694	698	698	692	692	692	692	692	692
SCA Count	7298	7313	7396	7635	8125	8384	8527	8696	8470	8638	8726	8775	8781	8843
P1 (psi)	8.00	8.00	8.50	8.60	9.30	9.80	10.40	11.00	9.60	10.00	10.60	11.00	11.20	11.50
T4 (mV)	0.55	0.58	0.56	0.55	0.58	0.58	0.61	0.62	0.59	0.59	0.59	0.6	0.6	0.6
T6 (mV)	0.15	0.15	0.15	0.15	0.18	0.18	0.18	0.18	0.18	0.18	0.16	0.16	0.16	0.16
Qw (inHg)	1	1	1	1.4	1.4	1.4	1.4	1.4	1.4	1.4	1.4	1.4	1.4	1.4
Powerstat %	0	0	0	0	0	0	0	0	0	0	0	0	0	0
CALCULATED DATA														
Q (L/s)	1.124	1.124	1.124	1.128	1.128	1.128	1.135	1.135	1.124	1.124	1.124	1.124	1.124	1.124
Q1 (L/s)	0.848	0.844	0.842	0.843	0.840	0.840	0.847	0.847	0.860	0.860	0.860	0.860	0.860	0.860
Q2 (L/s)	0.277	0.280	0.282	0.286	0.288	0.288	0.288	0.288	0.265	0.265	0.265	0.265	0.265	0.265
T1 (C)	34.3	34.6	35.7	36.2	37.2	38.1	38.7	39.7	37.4	38.1	39.0	39.4	39.5	39.9
T2 (C)	34.3	34.8	36.1	36.7	38.4	39.2	40.0	40.7	38.6	39.2	40.0	40.4	40.7	41.0
T5 (C)	30.2	30.5	31.6	32.1	33.8	34.8	35.7	36.9	34.3	35.3	36.2	36.7	37.1	37.4
Physical Properties Freon-11														
rhoL1 (kg/m3)	1454.0	1453.2	1450.4	1449.2	1446.8	1444.8	1443.1	1440.7	1446.4	1444.8	1442.3	1441.5	1441.1	1440.3
rhoG1 (kg/m3	8.18	8.26	8.56	8.68	8.94	9.17	9.35	9.62	8.99	9.17	9.44	9.53	9.57	9.67
rhoL2 (kg/m3)	1454.0	1452.8	1449.6	1448.0	1444.0	1441.9	1439.9	1438.3	1443.5	1441.9	1439.9	1439.1	1438.3	1437.5
rhoG2 (Kg/m3	8.18	8.30	8.64	8.81	9.26	9.48	9.71	9.90	9.30	9.48	9.71	9.81	9.90	10.00
rhoL5 (kg/m3)	1463.9	1463.1	1460.3	1459.1	1455.2	1452.8	1450.4	1447.6	1454.0	1451.6	1449.2	1448.0	1447.2	1446.4
hf1 (kJ/kg)	230.49	230.79	231.84	232.29	233.18	233.93	234.53	235.44	233.33	233.93	234.83	235.13	235.29	235.59
hfg2 (kJ/kg)	177.77	177.58	177.05	176.79	176.13	175.79	175.46	175.19	176.06	175.79	175.46	175.32	175.19	175.06
hf2 (kJ/kg)	230.49	230.94	232.14	232.73	234.23	234.98	235.74	236.34	234.38	234.98	235.74	236.04	236.34	236.64
hf5 (kJ/Kg)	226.78	227.08	228.11	228.56	230.05	230.94	231.84	232.88	230.49	231.39	232.29	232.73	233.03	233.33
Void fraction upstreams calculations based on HEM														
dhu (kJ/kg)	3.92	4.06	4.35	4.67	4.94	5.23	5.47	5.71	5.06	5.34	5.43	5.47	5.59	5.75
xu heaters	0.00117	0.0011	0.0019	0.0028	0.0043	0.0067	0.0089	0.0129	0.0067	0.0099	0.0113	0.0124	0.0131	0.014
HEM Void	0.17	0.16	0.24	0.32	0.40	0.51	0.57	0.65	0.51	0.60	0.63	0.65	0.66	0.67
Void fraction @ bundle calculations														
dh@ (kJ/kg)	-1.71	-1.72	-1.73	-1.73	-1.74	-1.74	-1.73	-1.73	-1.70	-1.70	-3.30	-3.30	-3.31	-3.31
Power kW	-2.18	-2.18	-2.18	-2.18	-2.18	-2.18	-2.18	-2.18	-2.18	-2.18	-4.22	-4.22	-4.22	-4.22
x tub heater	-0.010	-0.009	-0.008	-0.007	-0.004	-0.004	-0.003	-0.005	-0.004	-0.004	-0.014	-0.014	-0.013	-0.013
HEM V Tube	2.44	2.87	3.91	6.51	-1.55	-1.47	-0.79	-2.15	-1.33	-1.27	2.00	2.02	2.19	2.21
Common calculations at test section														
Void total	2.1214	2.4557	3.3692	5.5222	-0.84	-0.666	-0.064	-1.0691	-0.552	-0.415	2.2279	2.2615	2.4059	2.4373
Gp (kg/m2s)	388	386	384	384	381	381	384	383	390	390	389	389	389	389
rhoH (kg/m3)	1205.0	1220.0	1102.9	987.5	857.4	703.2	608.7	493.7	700.3	565.1	531.9	504.2	488.1	469.6
HEM Vp (m/s)	0.345	0.339	0.373	0.417	0.477	0.581	0.677	0.833	0.598	0.740	0.785	0.828	0.855	0.888
Separated Flow														
Corr. Factor	1.000	1.000	1.001	1.002	1.002	1.003	1.004	1.005	0.988	0.987	0.986	0.986	0.986	0.986
RAD Void	0.07	0.08	0.11	0.19	0.35	0.43	0.47	0.52	0.38	0.43	0.45	0.46	0.47	0.48
Slip	2.57	2.19	2.54	2.00	1.31	1.44	1.58	1.82	1.75	2.11	2.12	2.18	2.28	2.26
Ug (m/s)	0.74	0.63	0.76	0.65	0.53	0.66	0.78	0.99	0.76	0.99	1.03	1.09	1.14	1.16
Ul (m/s)	0.29	0.29	0.30	0.33	0.40	0.46	0.50	0.54	0.43	0.47	0.49	0.50	0.50	0.51
rho (kg/m3)	1345.6	1336.6	1290.4	1174.1	948.1	833.7	771.8	699.7	898.8	830.0	795.7	776.4	774.3	749.9

Experimental Data for Two-Phase Freon-11 Flow

Experiment 17				Gamma Densitometer Calibration					
Jun 10th 1996		Counts	at bundle				Excitation	Voltage =	600 Volts
Probe Axial Pos.	0.622 in		100% Liq.	12593			rho_L =	1483.0	kg/m3
Atm. Pressure (MPa)		0.1019	100% gas	15500		Name of file:		Exp17exp.wb2	
Trial #	1	2	3	4	5	6	7	8	9
Q1 (in) U tube	0.65	0.65	0.65	0.65	0.65	0.65	0.65	0.65	0.65
Q2 (in)	1.5	1.4	1.39	1.39	1.4	1.45	1.5	1.5	1.5
Q2 (in) U tube	1	1	1	1	1	1	1	1	1
T1 (mV)	1.8	1.83	1.87	2.01	2.03	2.07	2.13	2.18	2.25
T2 (mV)	2.01	2.03	2.05	2.09	2.11	2.15	2.19	2.25	2.31
T5 (mV)	1.73	1.75	1.8	1.87	1.92	1.97	2.01	2.08	2.15
Power (kW)	3.85	4	4.2	4.6	4.85	5.15	5.45	5.8	6.25
N (rpm)	*518*	*518*	*518*	*517*	*518*	*517*	*518*	*517*	*517*
SCA Count	13535	13639	13698	13929	13992	13955	14010	14145	14193
P1 (psi)	5.4	5.5	6	6.7	7.1	6.5	8.2	9	10
T4 (mV)	0.89	0.92	0.92	0.95	0.96	0.97	0.97	0.97	0.97
T6 (mV)	0.61	0.63	0.63	0.64	0.63	0.63	0.63	0.63	0.63
Qw (inHg)	1.5	1.5	1.5	1.5	1.5	1.5	1.5	1.5	1.5
Powerstat %	0	0	0	0	0	0	0	0	0
CALCULATED DATA									
Q (L/s)	0.824	0.824	0.824	0.823	0.824	0.823	0.824	0.823	0.823
Q1 (L/s)	0.547	0.547	0.547	0.545	0.547	0.545	0.547	0.545	0.545
Q2 (L/s)	0.278	0.278	0.278	0.278	0.278	0.278	0.278	0.278	0.278
T1 (C)	30.0	30.5	31.1	33.4	33.8	34.4	35.4	36.2	37.4
T2 (C)	33.4	33.8	34.1	34.8	35.1	35.7	36.4	37.4	38.4
T5 (C)	28.8	29.2	30.0	31.1	32.0	32.8	33.4	34.6	35.7
Physical Properties Freon-11									
rhoL1 (kg/m3)	1464.3	1463.1	1461.5	1456.0	1455.2	1453.6	1451.2	1449.2	1446.4
rhoG1 (kg/m3)	7.1617	7.2738	7.4255	7.9756	8.0566	8.2205	8.4710	8.6840	8.9886
rhoL2 (kg/m3)	1456.0	1455.2	1454.4	1452.8	1452.0	1450.4	1448.8	1446.4	1444.0
rhoG2 (Kg/m3)	7.9756	8.0566	8.1383	8.3034	8.3869	8.5557	8.7270	8.9886	9.2558
rhoL5 (kg/m3)	1467.0	1466.2	1464.3	1461.5	1459.5	1457.6	1456.0	1453.2	1450.4
hf1 (kJ/kg)	226.632	227.076	227.669	229.749	230.047	230.643	231.538	232.286	233.334
hfg2 (kJ/kg)	178.099	177.969	177.839	177.577	177.446	177.184	176.920	176.524	176.126
hf2 (kJ/kg)	229.749	230.047	230.345	230.941	231.240	231.837	232.435	233.334	234.233
hf5 (kJ/Kg)	225.597	225.893	226.632	227.669	228.411	229.154	229.749	230.792	231.837
Void fraction upstreams calculations based on HEM									
dhu (kJ/kg)	4.6716	4.8562	5.1039	5.6174	5.9082	6.3028	6.6545	7.1188	7.6850
xu heaters	0.0029	0.0039	0.0078	0.0132	0.0174	0.0204	0.0224	0.0259	0.0300
UPSHEM Void	0.35	0.42	0.58	0.70	0.75	0.78	0.79	0.81	0.83
Void fraction @ bundle calculations									
dh@ (kJ/kg)	-0.0026306	-0.00263196	-0.00263548	-0.00265	-0.00264	-0.00266	-0.00265	-0.00266	-0.00267
Power kW	-0.0021761	-0.0021761	-0.0021761	-0.00218	-0.00218	-0.00218	-0.00218	-0.00218	-0.00218
x tub heater	-0.0000	-0.0000	-0.0000	-0.0000	-0.0000	-0.0000	-0.0000	-0.0000	-0.0000
BOHEM Tube	-0.00	-0.00	-0.00	-0.00	-0.00	-0.00	-0.00	-0.00	-0.00
Heat flux W/in2	-0.02	-0.02	-0.02	-0.02	-0.02	-0.02	-0.02	-0.02	-0.02
Overall Calculations									
delth (kJ/kg)	4.6519	4.8358	5.0845	5.5985	5.8908	6.2851	6.6360	7.1000	7.6658
x	0.0028	0.0038	0.0077	0.0131	0.0173	0.0203	0.0223	0.0258	0.0299
Void total	0.37	0.44	0.60	0.71	0.76	0.79	0.80	0.82	0.83
Gp (kg/m2s)	250	250	250	249	250	249	249	248	248
rhoH (kg/m3)	918.9	817.7	577.3	428.5	353.4	316.6	301.1	273.4	249.3
HEM Vp (m/s)	0.294	0.330	0.467	0.624	0.759	0.843	0.888	0.974	1.065
Separated Flow									
Corr. Factor	0.994	0.993	0.993	0.991	0.991	0.990	0.989	0.989	0.988
RAD Void	0.32	0.35	0.37	0.44	0.46	0.45	0.46	0.50	0.52
Slip	1.11	1.28	2.37	2.94	3.55	4.37	4.43	4.20	4.52
Ug (m/s)	0.2783	0.3383	0.6411	0.8906	1.1132	1.3239	1.3824	1.4133	1.5517
Ul (m/s)	0.2510	0.2643	0.2709	0.3028	0.3140	0.3033	0.3121	0.3367	0.3434
rho (kg/m3)	997.4	946.3	919.5	815.5	785.6	807.0	784.6	721.9	704.1

Experimental Data for Two-Phase Freon-11 Flow
Experiment 8 Gamma Densitometer Calibration
March 5th 1996 Shield SCA 2 1/8" thick lead plates Excitation Voltage = 600 Volts
Counts for 100% liquid 7137.9 7145 rho_L = 1473.6 kg/m3
Counts for 100% gas 10658

Trial #	1	2	3	4	5	6	7	8	9	10	11	12
Q1 (in)	0.22	0.22	0.22	0.22	0.22	0.22	0.22	0	0	0	0	0
Q2 (in)	3.75	3.77	3.78	3.7	3.8	3.86	3.86	4.03	4.1	4.12	4.19	3.86
T1 (mV)	1.56	1.57	1.59	1.67	1.77	1.9	1.98	1.97	2.01	2.03	2.05	1.98
T2 (mV)	1.58	1.60	1.64	1.69	1.83	1.96	2.05	2.03	2.06	2.07	2.11	2.05
T5 (mV)	1.05	1.05	1.07	1.09	1.17	1.32	1.42	1.43	1.54	1.57	1.65	1.42
Power (kW)	2.50	2.65	2.80	3.00	3.50	4.25	4.80	4.65	5.50	5.90	6.30	4.80
N (rpm)	419	419	419	419	418	419	419	419	420	420	420	419
SCA Counts	7295	7348	7368	7466	7719	8130	8353	9015	9252	9397	9582	8353
P1 (psi)	4.50	4.50	4.50	4.50	5.00	5.60	6.40	6.00	6.50	6.60	7.00	6.40
T4 (mV)	0.49	0.48	0.45	0.46	0.47	0.56	0.6	0.6	0.64	0.63	0.69	0.6
T6 (mV)	0.25	0.22	0.19	0.18	0.16	0.21	0.2	0.21	0.21	0.21	0.21	0.2
Qw (inHg)	1	1	1	1	1	1	1	1	1	1	1	1
Powerstat %	0	0	0	0	0	0	0	0	0	0	0	0
CALCULATED DATA												
Q (L/s)	0.628	0.628	0.628	0.628	0.626	0.628	0.628	0.628	0.629	0.629	0.629	0.628
Q1 (L/s)	0.196	0.195	0.194	0.199	0.191	0.189	0.189	0.180	0.178	0.177	0.173	0.189
Q2 (L/s)	0.432	0.433	0.434	0.429	0.435	0.438	0.438	0.448	0.452	0.453	0.456	0.438
T1 (C)	26.1	26.2	26.6	27.9	29.5	31.6	32.9	32.8	33.4	33.8	34.1	32.9
T2 (C)	26.4	26.7	27.4	28.2	30.5	32.6	34.1	33.8	34.3	34.4	35.1	34.1
T5 (C)	17.8	17.8	18.1	18.4	19.7	22.1	23.8	23.9	25.7	26.2	27.5	23.8
Physical Properties Freon-11												
rhoL1 (kg/m3)	1473.6	1473.2	1472.5	1469.4	1465.4	1460.3	1457.2	1457.6	1456.0	1455.2	1454.4	1457.2
rhoG1 (kg/m3)	6.31	6.35	6.41	6.69	7.05	7.54	7.86	7.82	7.98	8.06	8.14	7.86
rhoL2 (kg/m3)	1472.8	1472.1	1470.5	1468.6	1463.1	1458.0	1454.4	1455.2	1454.0	1453.6	1452.0	1454.4
rhoG2 (Kg/m3	6.38	6.45	6.59	6.76	7.27	7.78	8.14	8.06	8.18	8.22	8.39	8.14
rhoL5 (kg/m3)	1493.1	1493.1	1492.3	1491.6	1488.5	1482.8	1479.0	1478.6	1474.4	1473.2	1470.1	1479.0
hf1 (kJ/kg)	223.09	223.24	223.53	224.71	226.19	228.11	229.30	229.15	229.75	230.05	230.34	229.30
hfg2 (kJ/kg)	180.86	180.73	180.48	180.16	179.26	178.42	177.84	177.97	177.77	177.71	177.45	177.84
hf2 (kJ/kg)	223.39	223.68	224.27	225.01	227.08	229.01	230.34	230.05	230.49	230.64	231.24	230.34
hf5 (kJ/Kg)	215.65	215.65	215.94	216.23	217.39	219.57	221.04	221.18	222.80	223.24	224.42	221.04
Void fraction upstreams calculations based on HEM												
dhu (kJ/kg)	8.35	8.91	9.45	9.90	12.04	14.80	16.76	17.09	20.49	22.12	24.19	16.76
xu heaters	0.003395	0.0048	0.0062	0.0062	0.0131	0.0301	0.0419	0.0462	0.0719	0.0828	0.0979	0.0419
HEM Void	0.44	0.53	0.58	0.58	0.73	0.85	0.89	0.90	0.93	0.94	0.95	0.89
Void fraction @ bundle calculations												
dh@ (kJ/kg)	-7.32	-7.37	-7.39	-7.23	-7.55	-7.64	-7.65	-8.06	-8.16	-8.21	-16.28	-14.83
Power kW	-2.18	-2.18	-2.18	-2.18	-2.18	-2.18	-2.18	-2.18	-2.18	-2.18	-4.22	-4.22
x tub heater	-0.039	-0.038	-0.037	-0.039	-0.037	-0.038	-0.037	-0.040	-0.042	-0.043	-0.087	-0.078
HEM V Tube	1.13	1.13	1.14	1.14	1.16	1.17	1.18	1.17	1.16	1.16	1.08	1.08
Common calculations at test section												
Void total	1.345024	1.4341	1.4967	1.489	1.6569	1.7905	1.8345	1.8311	1.8632	1.8688	1.8119	1.754
Gp (kg/m2s)	91	90	90	92	88	87	87	82	81	81	79	87
rhoH (kg/m3)	823.7	695.0	610.1	623.6	394.5	214.9	167.0	152.2	103.5	91.6	79.1	167.0
HEM Vp (m/s)	0.118	0.139	0.158	0.158	0.239	0.434	0.557	0.580	0.843	0.946	1.071	0.557
Separated Flow												
Corr. Factor	1.000	1.000	1.001	1.003	1.006	1.009	1.011	1.011	1.012	1.013	1.013	1.011
RAD Void	0.05	0.07	0.08	0.12	0.21	0.34	0.41	0.59	0.66	0.70	0.74	0.41
Slip	13.84	14.35	16.21	10.20	10.64	11.68	11.73	6.19	7.38	7.14	6.71	11.73
Ug (m/s)	0.90	0.94	1.07	0.72	0.79	1.02	1.13	0.82	1.12	1.19	1.28	1.13
Ul (m/s)	0.06	0.07	0.07	0.07	0.07	0.09	0.10	0.13	0.15	0.17	0.19	0.10
rho (kg/m3)	1393.9	1366.2	1353.8	1296.0	1164.6	967.0	864.8	597.2	504.1	448.8	379.9	864.8

Appendix C

Void Fraction Conversion

In this investigation, three types of experiments were performed under the condition of thermodynamic equilibrium. Upstream generated void fraction experiments, tube bundle void generated experiments , and experiments in which a combination of these two cases was used. Previous investigations, where only upstream void fraction generation was used had the flexibility to measure void fraction at a different location than the tube bundle. In this study, however, void fraction measurements of the void contribution of each source were necessary. This requirement necesitated measurements of void fraction at the monitored tube location to be obtained. For comparison purposes, it was desirable to be able to convert these void fraction values to equivalent values of upstream void generation. This procedure allowed for a direct comparison of experiments performed under upstream void fraction generation with experiments in which total or partial void was generated at the surface of the tubes.

Figure C1, presents a graph of void fraction values measured at the monitored tube location using the gamma densitometry technique (TOTGAM) and void fraction calculated using the HEM relationship for identical flow conditions (UPSHEM). In all these experiments void was generated upstream of the tube bundle only. Data are presented for three different values of the pitch mass flux.

For experiments in which void was generated in the bundle and upstream of the bundle, it was necessary to evaluate the void contribution of each source. For this purpose, TOTGAM void fraction measurements were converted to UPSHEM void fraction values using the curves in graph C1. These UPSHEM values represent the total void fraction present at the monitored tube location.

If void were being generated in the bundle only, then these UPSHEM void values were the "equivalent of the upstream generated void fraction value" and then they could be used to compare experiments with upstream only generated void. If the experiment had void contributed from both sources, then the HEM calculated void fraction for the upstream portion was deducted from these UPSHEM values to obtain the bundle generated void equivalent to the upstream generation void fraction.

These measurements were made with the tube free to vibrate, which prevented the experiments from being run for higher values of void fraction. This is due to the fact that the tubes became unstable and vibration levels in the tubes reached the maximum permissible levels.

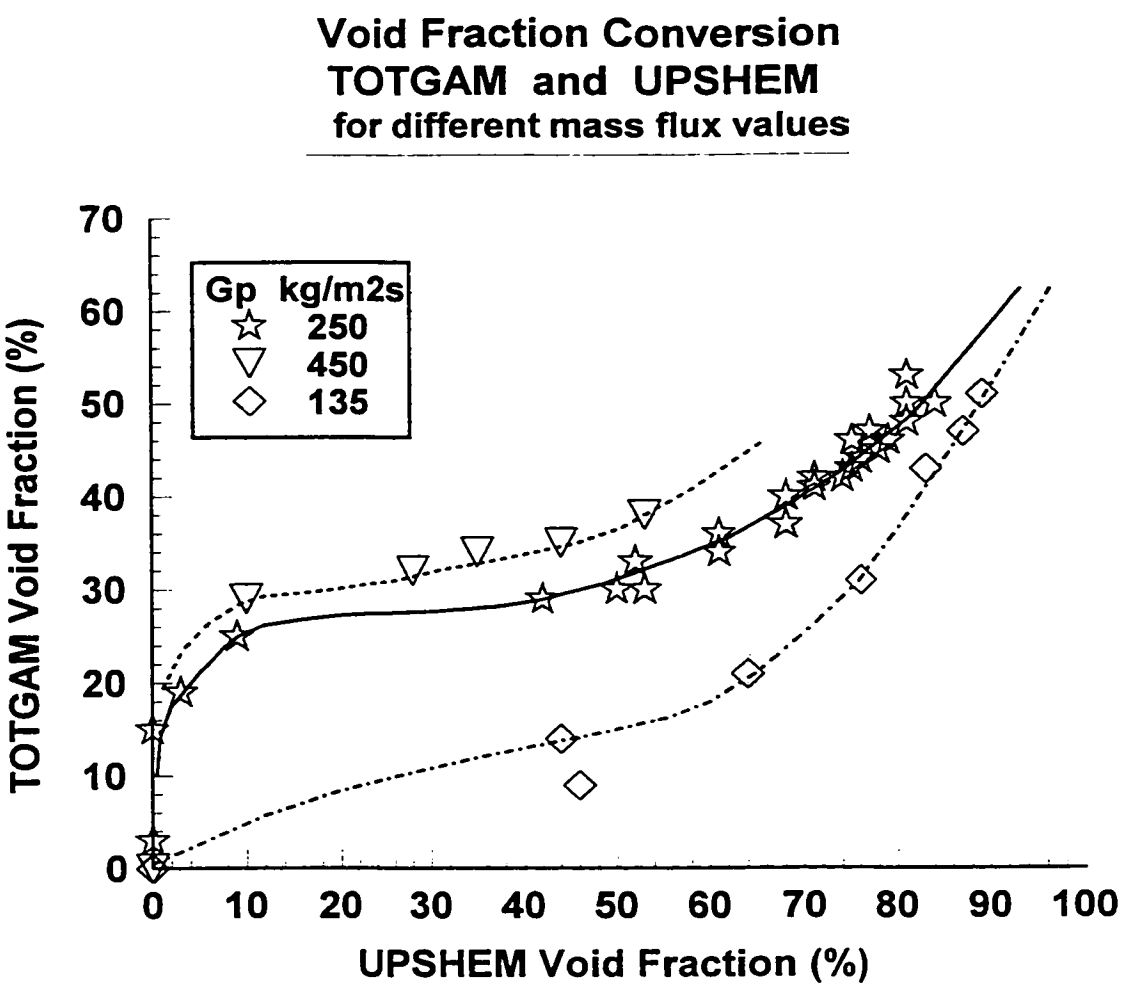

Figure C1. Void fraction conversion between TOTGAM and UPSHEM at the monitored tube location.

Appendix D

Tube Vibration Response due to Turbulent Buffeting

Based on experimental data presented in this investigation, it has been conclusively demonstrated that tube vibration amplitude decreases substantially under the presence of tube surface boiling, other factors such as pitch mass flux (Gp) and void fraction at the monitored tube location (UPSHEM) being constant. In order to give an explanation to this effect, tube turbulent buffeting vibration response in two-phase flow was calculated using the approach developed by Axisa et al. (1990). A cantilevered tube in a parallel triangular array with a pitch to diameter ratio of 1.48 was assumed in the calculations. The void fraction used was 50% HEM, which corresponds to a value where the tube response is only due to turbulence excitation. The mass flux was taken to be Gp=250 kg/m^2s. The total damping ratio used (3.5%) was taken from Pettigrew et al. 1989. The dimensionless power spectral density used was obtained from Taylor et al. (1989).

Using a force correlation length based on the estimated bubble size diameter, a correlation length value of 6% (20 mm) of the tube length for the upstream case, 1.8% (6 mm) for the combined case and 0.3% (1 mm) for the bundle case, were selected. The bubble size diameter estimation was based on flow vizualization through the test section window.

Equations and values for all parameters that were used in the calculations, and also the numerical results are presented in the next pages of this appendix.

Determination of Tube Response due to Turbulence Buffeting **Feb 22/99**

$D := .00618 \cdot m \quad L_t := 0.325 \cdot m \quad T := 40 \quad \phi := .5 \quad G_p := 250 \cdot \frac{kg}{m^2 \cdot s} \quad m_t := 0.121 \cdot \frac{kg}{m}$

$P := \left[\left[\left(\frac{3}{4}\right)^{0.5} \cdot 0.00917\right]\right] \cdot m \quad f_L := 29.25 \cdot Hz \quad f_a := 39.75 \cdot Hz \quad f := 36.0 \cdot Hz$

$m_L := m_t \cdot \left(\frac{f_a}{f_L}\right)^2 \quad m_L = 0.223 \cdot \frac{kg}{m}$ **added mass per unit lenth of tube in liquid flow**

$m_{TP} := m_t \cdot \left(\frac{f_a}{f}\right)^2 \quad m_{TP} = 0.148 \cdot \frac{kg}{m}$ **mass per unit length of tube in two-phase flow**

The fluid properties of R-11 can be determined from the temperature, T, using the following polynomial expressions.

$\mu_L := (563.5 - 6.228 \cdot T + .0262 \cdot T^2) \cdot 10^{-6} \cdot Pa \cdot s \quad \rho_L := (1533.1 - 2.1962 \cdot T - .003287 \cdot T^2) \cdot \frac{kg}{m^3}$

$\mu_G := (10.16 + 0.0353 \cdot T) \cdot 10^{-6} \cdot Pa \cdot s$

$\rho_G := (2.8291 + .062313 \cdot T + .0027383 \cdot T^2) \cdot \frac{kg}{m^3}$

$h_f := (199.92 + .87863 \cdot T + .0003982 \cdot T^2) \cdot \frac{kJ}{kg}$

$h_{fg} := (190.5 + .34876 \cdot T + .00070376 \cdot T^2) \cdot \frac{kJ}{kg}$

$\mu_L = 3.563 \cdot 10^{-4} \cdot Pa \cdot s \quad \mu_G = 1.157 \cdot 10^{-5} \cdot Pa \cdot s$

$\rho_L = 1.44 \cdot 10^3 \cdot kg \cdot m^{-3} \quad \rho_G = 9.703 \cdot kg \cdot m^{-3}$

$h_f = 235.702 \cdot \frac{kJ}{kg} \quad h_{fg} = 205.576 \cdot \frac{kJ}{kg}$

$\rho := \phi \cdot \rho_G + (1 - \phi) \cdot \rho_L \quad \rho = 724.848 \cdot kg \cdot m^{-3} \quad V_p := \frac{G_p}{\rho} \quad V_p = 0.345 \cdot \frac{m}{s}$

$\nu_L := \frac{\mu_L}{\rho_L} \quad \nu_G := \frac{\mu_G}{\rho_G} \quad \nu_L = 2.474 \cdot 10^{-7} \cdot \frac{m^2}{s} \quad \nu_G = 1.193 \cdot 10^{-6} \cdot \frac{m^2}{s}$

The two-phase viscosity is given by McAdam (1942).

$\nu_{TP} := \frac{\nu_L}{\left[1 + \phi \cdot \left(\frac{\nu_L}{\nu_G} - 1\right)\right]} \quad \nu_{TP} = 4.098 \cdot 10^{-7} \cdot \frac{m^2}{s}$ **two-phase viscosity**

$\left(\frac{\rho \cdot D^2}{m_{TP}}\right) = 0.188$ **inverse mass ratio** $\quad \frac{2 \cdot \nu_{TP}}{\pi \cdot f \cdot D^2} = 1.898 \cdot 10^{-4}$ **Stokes No.**

The damping of the structure is assumed to consist of a structural component and a viscous component. The viscous component is obtained from Pettigrew et al. (1994).

$$D\_D_e = \left[\left(0.96 + 0.50\cdot\frac{P}{D}\right)\cdot\frac{P}{D}\right]^{-1} \qquad D\_D_e = 0.486 \qquad \textbf{confinement term}$$

$$CONF = \frac{1 + (D\_D_e)^3}{\left[1 - (D\_D_e)^2\right]^2} \qquad CONF = 1.908 \qquad \textbf{confinement factor}$$

$$\zeta_v = \frac{\pi}{\sqrt{8}}\cdot\left(\frac{\rho\cdot D^2}{m_{TP}}\right)\cdot\left(\frac{2\cdot v_{TP}}{\pi\cdot f\cdot D^2}\right)^{.5}\cdot CONF \qquad \zeta_v = 0.005 \qquad \textbf{viscous component}$$

The two-phase damping coefficient can be determined from developing correlations but here it will be given. Damping in air is also given but is generally small.

$\zeta_{TP} = .025$ $\zeta_a = 0.005$

The overall damping in two-phase R-11 cross flow is,

$$\zeta = \zeta_a + \zeta_v + \zeta_{TP} \qquad \zeta = 0.035 \qquad \textbf{overall damping ratio in two-phase R-11}$$

The mode shape for the first mode of a fixed-free tube (cantilevered) is estimated by,

$$\sigma(z) = 1 - \cos\left(\frac{\pi\cdot z}{2}\right) \qquad \sigma(0) = 0 \quad \textbf{fixed end has zero displacement}$$

$\sigma(1) = 1$ **free end has maximum displacement**

As a first aproximation, let us calculate the approximate joint acceptance.

$\lambda_{cu} = 0.06$ $\lambda_{cc} = 0.018$ $\lambda_{cb} = 0.003$ **axial correlation length of fluid forces**

$a_n = 0.5$ $J_a = \sqrt{a_n\cdot\lambda_{cc}}$ $J_a = 0.095$ **approx. joint acceptance (error, see note below)**

However, the previous calculation is valid only if the correlation length is less than about 1% of the tube length. Hence the actual correlation length is given as follows.

Joint acceptance of a cantilevered tube to the uniform fluid forcing, assuming full axial correlation.

$$J_{cu} = \sqrt{\int_0^1 \int_0^1 \sigma(z_1)\cdot\sigma(z_2)\cdot\exp\left[\frac{-|z_1 - z_2|}{(\lambda_{cu})}\right] dz_1\, dz_2} \qquad J_{cu} = 0.154$$

$$J_{cc} = \sqrt{\int_0^1 \int_0^1 \sigma(z_1)\cdot\sigma(z_2)\cdot\exp\left[\frac{-|z_1 - z_2|}{(\lambda_{cc})}\right] dz_1\, dz_2} \qquad J_{cc} = 0.089$$

$$J_{cb} = \sqrt{\int_0^1 \int_0^1 \sigma(z_1)\cdot\sigma(z_2)\cdot\exp\left[\frac{-|z_1 - z_2|}{(\lambda_{cb})}\right] dz_1\, dz_2} \qquad J_{cb} = 0.037$$

Generalized mass of tube per unit length.

$$m_g = (m_t + m_L)\cdot\int_0^1 \sigma(z)^2\, dz \qquad \int_0^1 \sigma(z)^2\, dz = 0.227 \qquad m_g = 0.078\cdot kg\cdot m^{-1}$$

If a tube is in an array of tubes with a pitch ratio, P/D = 1.48 and subjected to a homogeneous, axially correlated turbulent cross-flow with a given equivalent pitch velocity, its r.m.s. midspan displacement will be as follows.

$$Re = V_p\cdot\frac{D}{\nu_{TP}} \qquad \frac{f\cdot D}{V_p} = 0.645 \qquad \text{dimensionless frequency}$$

Dimensionless Power Spectral density (Taylor et. al 1989).

$$\Phi_T = \frac{450}{Re\cdot\frac{\phi}{1-\phi}} \qquad Re = 5.201\cdot 10^3 \qquad \Phi_T = 0.087$$

The free-end tube response for homogeneous turbulence and full axial correlation is,

$$Y_{rms} = \left(\frac{1}{2}\cdot\rho\cdot V_p^{\,2}\cdot D\right)\cdot\left(\frac{f\cdot D}{V_p}\right)^{0.5}\cdot\left[\frac{J_{cu}^{\,2}\cdot(\Phi_T)\cdot\sigma(1)^2}{64\cdot\pi^3\cdot\zeta\cdot(m_g)^2\cdot f^4}\right]^{0.5} \qquad Y_{rms} = 1.143\cdot10^{-5}\ \cdot m$$

$$Ampl = \frac{Y_{rms}}{D}\cdot 100 \qquad Ampl = 0.185 \qquad \textbf{\%Dia amplitude}$$

$$Y_{rms} = \left(\frac{1}{2}\cdot\rho\cdot V_p^{\,2}\cdot D\right)\cdot\left(\frac{f\cdot D}{V_p}\right)^{0.5}\cdot\left[\frac{J_{cc}^{\,2}\cdot(\Phi_T)\cdot\sigma(1)^2}{64\cdot\pi^3\cdot\zeta\cdot(m_g)^2\cdot f^4}\right]^{0.5} \qquad Y_{rms} = 6.573\cdot10^{-6}\ \cdot m$$

$$Ampl = \frac{Y_{rms}}{D}\cdot 100 \qquad Ampl = 0.106 \qquad \textbf{\%Dia amplitude}$$

$$Y_{rms} = \left(\frac{1}{2}\cdot\rho\cdot V_p^{\,2}\cdot D\right)\cdot\left(\frac{f\cdot D}{V_p}\right)^{0.5}\cdot\left[\frac{J_{cb}^{\,2}\cdot(\Phi_T)\cdot\sigma(1)^2}{64\cdot\pi^3\cdot\zeta\cdot(m_g)^2\cdot f^4}\right]^{0.5} \qquad Y_{rms} = 2.774\cdot10^{-6}\ \cdot m$$

$$Ampl = \frac{Y_{rms}}{D}\cdot 100 \qquad Ampl = 0.045 \qquad \textbf{\%Dia amplitude}$$

APPENDIX E

TUBE BUNDLE DESIGN BASED ON HEAT PIPES

E1. Experimental testing.

At the onset of this investigation, electric cartridge heaters, which were intended to be used as the tubes in the tube bundle were not commercially available. The alternative to this option was based on the use of heat pipes. For this purpose, a heat pipe from Noren Products Inc, California, was acquired and tested at one of the laboratories in the department of Mechanical Engineering at McMaster University. Results from these tests are presented in figure E.1. The graph shows the heat transport capacity of the heat pipe as a function of the temperature difference between the evaporator and the condenser. The data represented by triangles are the results for the heat pipe working in the vertical position with the evaporator at the bottom and the condenser at the top. It can be observed that the heat transport capacity increased from about 10 W to about 110 W when the difference in temperature increased from 25°C to 240°C. The data represented by the stars symbols correspond to the results with the heat pipe in the horizontal position. Results shows that the heat transport increased from 10 W to about 40 W when the temperature difference changed from 25°C to 255°C.

Since the temperature in the evaporator reached a value close to the limit of the testing apparatus, it was not possible to test the heat pipe at higher temperatures. Nevertheless, the value of 40 W in the horizontal position was clearly insufficient to achieve the conditions needed in this investigation, which was calculated at about 100 W per tube.

E.2 Heat pipe performance. Predictions from the computer program.

Prediction for the commercial heat pipe

In order to understand the limitations of the heat pipe tested, a computer code was developed in Pascal language. A print of the code is given at the end of this appendix. Table E.1 shows the parameters used in the simulation and the computer code results for the heat pipe tested.

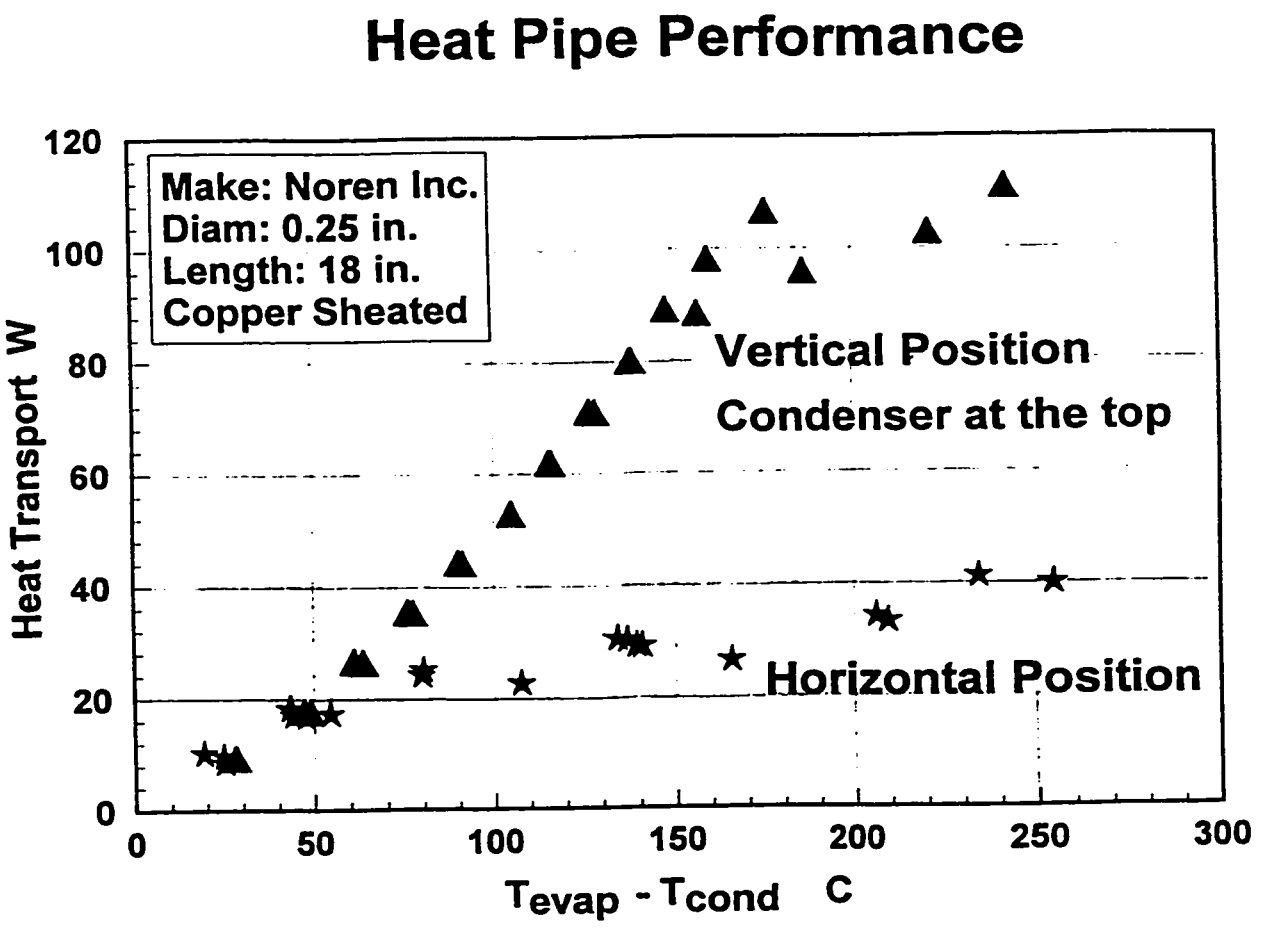

Figure E.1 Performance of a commercial heat pipe for vertical and horizontal position.

Type of heat pipe	Noren Inc.	Prototype
End conditions	AB	AB
Original estimate of heat transport [W]	100	200
Type of wick	Screen	Grooves
Wire diameter [m] or Grooves depth [m]	$9.5 \cdot 10^{-5}$	$3.556 \cdot 10^{-4}$
Wire mesh pitch [m] or Grooves width [m]	$2.59 \cdot 10^{-4}$	$3.759 \cdot 10^{-4}$
Thermal conductivity of working fluid (water) [W/m^2K]	0.68	0.68
Thermal conductivity of wick material [W/m^2K]	111 (Copper)	111 (Brass)
Total thickness of the wick [m] or Groove angle [°]	$5.00 \cdot 10^{-4}$	22.5
Length of adiabatic section [m]	0	0.1016
Length of evaporator section [m]	0.1524	0.0508
Length of condenser section [m]	0.305	0.305
Outside diameter of heat pipe [m]	$6.35 \cdot 10^{-3}$	$6.35 \cdot 10^{-3}$
Inside diameter of heat pipe [m]	$4.74 \cdot 10^{-3}$	$5.28 \cdot 10^{-3}$
Diameter of vapor core [m]	$3.74 \cdot 10^{-3}$	$4.57 \cdot 10^{-3}$
Pipe wall thickness [m]	$8.05 \cdot 10^{-4}$	$5.334 \cdot 10^{-4}$
Number of heat pipes in the tube bundle	1	1
Vapor density [kg/m^3]	0.58	0.58
Latent heat of vaporization [J/kg]	$2.256 \cdot 10^{6}$	$2.256 \cdot 10^{6}$
Vapour dynamic viscosity [kg/m s]	$1.28 \cdot 10^{-5}$	$1.28 \cdot 10^{-5}$
Thermal conductivity of pipe material [W/m^2K]	379	111
Absolute vapour temperature [K]	373	373
Temperature of external fluid at condenser [K]	298	298
Working fluid density [kg/m^3]	958	958
Working fluid dynamic viscosity [kg/m s]	$2.82 \cdot 10^{-4}$	$2.82 \cdot 10^{-4}$

Surface tension of working fluid [N/m]	$5.9 \cdot 10^{-2}$	$5.9 \cdot 10^{-2}$
Vapor specific heat ratio	1.33	1.33
External fluid density [kg/m^3]	1480	1480
External fluid thermal conductivity [W/m^2K]	0.089	0.089
Groove fin thickness [m]	N/A	$1.016 \cdot 10^{-4}$
Molecular weight of the vapour	18	18
Heat capacity of external fluid [J/kg K]	884	884
Dynamic viscosity of external fluid [kg/m s]	$4.2 \cdot 10^{-4}$	$4.2 \cdot 10^{-4}$
Average velocity of the external fluid [m/s]	0.058	0.058
Flow mass of the external fluid [kg/s]	0.833	0.833
Total blocked/open area ratio in the tube bundle	1.667	1.667
Computer code results		
Capillary limitation [W]	37.6	219.3
Sonic limitation [W]	3347	4716
Entrainment limitation [W]	358	249.7
Boiling limitation [W]	746	6939
Mach number	0.0435	0.027
Pipe overall thermal conductivity [W/m^2K]	107,327	630,682
Theoretical heat transport rate [W]	314	277

Table E.1 Computer code predictions for a commercial and a prototype heat pipe.

As it is seen in the table, the results for the heat pipe with a screen wick indicate that the capillary limitation is about 37.6 W, which is in agreement with the experimental results from the tests. This agreement indicated that the performance obtainable from the commercial heat pipe was limited by capillarity and that the design requirements for this investigation could not be met by this heat pipe when used in the horizontal position.

Predictions for a prototype based on a grooved wick.

In order to find a solution to the limitation of the heat pipe acquired from Noren Inc., an alternative heat pipe was designed. The design was based on a grooved wick, with water as working fluid. Dimensions of the cross section of the design are presented en figure E.2. The computer code was used to predict the performance of this heat pipe. In table E.1 under the column labeled " prototype", the main parameters of this design are presented as well as the predicted performance parameters.

The results from the computer program showed a substantially improved performance. In these results, the critical lowest limitation which was due to capillarity increased to 219 W. Motivated by these results, efforts were directed to the objective of manufacturing a prototype with which a experimental confirmation of the predicted performance could be obtained.

A copper tube, 0.25 inches in diameter and 18 inches long was selected. Attempts were made by the technician in the department of Mechanical Engineering to broach the internal axial grooves using high precision cutters. However, all attempts were unsuccessful as the friction and cutting forces generated in the broaching operation always exceeded the maximum yielding stress of the pulling rod of the broach tool. This condition derived in the consequence that the rod failed and ruptured before the objective was achieved. Changing the rod material or any other technique of this broaching operation did not produce a better result. After several months of trials, efforts were abandoned.

It is important to state that based on this study, there is the belief that better heat pipes can be designed and manufacture, provided that more resources are dedicated. Is in this regard and with the intention to give some guidance to anyone attempting this objective that this appendix has been included in this thesis.

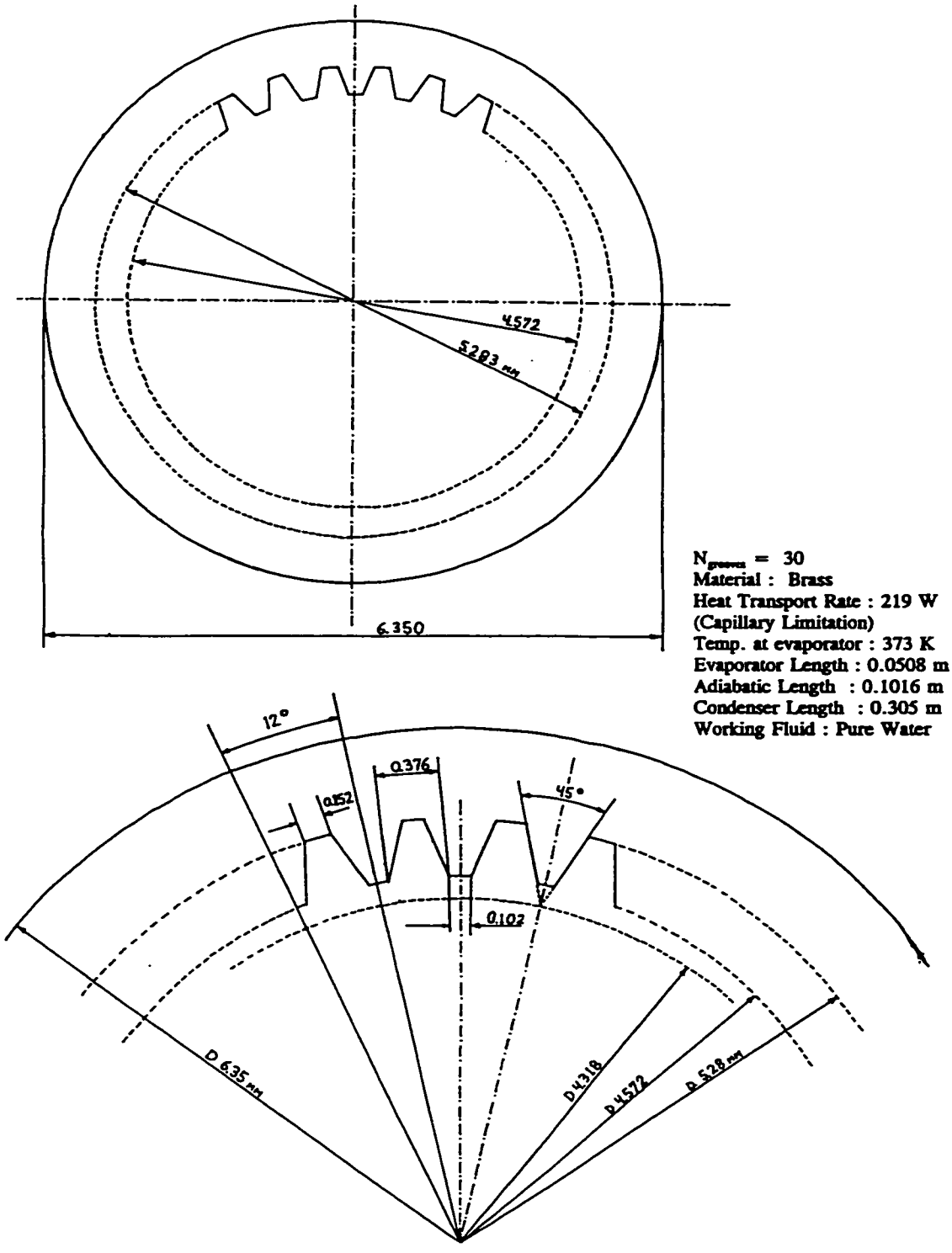

Figure E.2 Cross section of the heat pipe prototype.

```
PROGRAM HEAT PIPE;
uses crt;
var Q, Qa, Qb, Qc : real;
   Qsmax, Qe : real;   {VARIABLES FOR HEAT FLOW}
   Mv, Rev : real;     {MASS AND REYNOLD'S # FOR VAPOUR FLOW}
   Tpe : real;         {AVE. PIPE SURFACE TEMP AT EVAPORATOR}
   Tpc : real;         {AVE. PIPE SURFACE TEMP AT CONDENSER}
   Tpwc : real;        {TEMP AT PIPE-WICK INTERFACE AT CONDENSER}
   Tvc : real;         {TEMP OF VAPOUR AT CONDENSER}
   Tve : real;         {TEMP OF VAPOUR AT EVAPORATOR}
   Tpwe : real;        {TEMP AT PIPE-WICK INTERFACE AT EVAPORATOR}
   Tv : real;          {ABSOLUTE VAPOUR TEMP}
   Ap, Av : real;      {AREAS FOR PIPE AND VAPOUR FLOW}
   T2e : real;         {OUTLET AIR OR WATER TEMP AT EVAPORATOR}
   T2c : real;         {OUTLET AIR OR WATER TEMP AT CONDENSER}
   Rwe : real;         {THERMAL RESISTANCE OF WICK AT EVAPORATOR}
   Rv  : real;         {THERMAL RESISTANCE OF VAPOUR}
   Rwc : real;         {THERMAL RESISTANCE OF WICK AT CONDENSER}
   Rpc : real;         {THERMAL RESISTANCE OF PIPE AT CONDENSER}
   Rpe : real;         {THERMAL RESISTANCE OF PIPE AT EVAPORATOR}
   kee : real;         {EFFECTIVE THERMAL CONDUCTIVITY OF LIQUID-}
                       {SATURATED WICK AT EVAPORATOR}
   kec : real;         {EFFECTIVE THERMAL CONDUCTIVITY OF LIQUID-}
                       {SATURATED WICK AT CONDENSER}
   ke : real;          {EFFECTIVE THERMAL CONDUCTIVITY }
   Ref: real;          {REYNOLD'S # OF FLUID FLOW}
   Fv : real;          {FRICTIONAL COEFFICIENT FOR VAPOUR FLOW}
   hc, he, h : real;   {INTERFACE HEAT TRANSFER COEFFICIENTS}
   Vfmax : real;       {MAXIMUM VELOCITY ACROSS TUBE BANKS}
   E : real;           {WICK POROSITY}
   ng : real;          {VALUE IN CALCULATING GROOVE WICK POROSITY}
   Uhp : real;         {OVERALL THERMAL RESISTANCE}
   me, mc : real;      {MASS FLOW RATES OVER ENDS}
   Cpf : real;         {SPECIFIC HEAT OF FLUID}
   Tsi, Tso : real;    {MEAN SINK AND SOURCE TEMPS}
   T1e, T1c : real;    {INLET TEMPS AT ENDS}
   Di, Dout, Dv : real; {INSIDE, OUTSIDE, VAPOUR DIAMETERS OF PIPE}
   Le, Lc, La : real;  {LENGTHS OF EVAP., ADIABATIC, COND.}
   kp, kl, kw : real;  {THERMAL CONDUCTIVITY OF PIPE, LIQUID, & WICK}
   d : real;           {WIRE DIAMETER}
```

```
  p : real;              {WIRE MESH PITCH}
  wf : real;             {GROOVE FIN THICKNESS}
  w, w1 :real;           {GROOVE WIDTH}
  Beta : real;           {GROOVE HALF ANGLE}
  DEL, tp : real;        {GROOVE DEPTH AND PIPE THICKNESS}
  rm : real;             {MEAN RADIUS OF LIQUID FLOW PASSAGE}
  RHOv, RHOf : real;     {VAPOUR AND FLUID DENSITIES}
  LAMB : real;           {LATENT HEAT OF VAPOURIZATION}
  MUv, MUf : real;       {VAPOUR AND FLUID DYNAMIC VISCOSITIES}
  kf : real;             {THERMAL CONDUCTIVITY OF FLUID}
  C : real;              {FACTOR DEPENDING ON # OF BANKS}
  Prf : real;            {PRANDTL # OF FLUID}
  Va : real;             {FREE STREAM AVE. VELOCITY IN DUCT}
  Rat : real;            {DUCT AREA TO PIPE AREA RATIO}
  SigmaP, SigmaEC : real;      {STRESSES OCCURING IN PIPE}
  tw : real;             {Thickness of the screen wick}
  Rvs: real;             {Universal Gas constant/molecular weight}
  yv :real;              {Vapour Specific Heat Ratio}
  M  : real;             {Molecular Weight of the Vapour}
  o  : real;             {Surface tension of fluid}

  n : integer;           {LOOP COUNTER VARIABLE}
  endvalue : integer;    {TO SPECIFY END EFFECT}
  SI : integer;          {VARIABLE TO SPECIFY METRIC OR IMPERIAL}
  status : char;         {TO SPECIFY PASS OR FAIL LIMITATIONS}
  choice, endcap : char;     {CHOOSE BETWEEN OPTIONS VARIABLE}
  Np : integer;          {# OF PIPES}
  Y, flag  : char;

const S = 1.05;          {MECHANICAL EQUIVALENT OF HEAT}
    J = 777.66;          {CRIMPING FACTOR}
    R = 8314;            {Universal Gas Constant J/kg-mol-K}

{Functions definition}
{ Function to calculate effective thermal conductivity of liquid }
{ -saturated wick. (wrapped screen) }
function keF(E,kl,kw: real): real;
  var x,y: real;
    begin
      x := kl*((kl + kw) - (1 - E)*(kl - kw));
```

```
      y := (kl + kw) + (1 - E)*(kl - kw);
      keF := x/y;
    end;

{ Function to calculate effective thermal conductivity of wick }
{ at the evaporator end. (grooved)}
function keeF(wf,kl,kw,DEL,w: real): real;
  var x,y: real;
    begin
      x := (wf*kl*kw*DEL) + w*kl*(0.185*wf*kw + DEL*kl);
      y := (w + wf)*(0.185*wf*kw + DEL*kl);
      keeF := x/y;
    end;

{ Function to calculate effective thermal conductivity of wick }
{ at the condenser end. (grooved)}
function kecF(w,kl,wf,kw: real): real;
    begin
      kecF := (w*kl + wf*kw)/(w+wf);
    end;

{ function to evaluate wick porosity. }
function EF(d,p: real): real;
  begin
    EF := 1 - (pi * 1.05 * d)/(4*p);
  end;

{ This function evaluates the thermal resistance of the pipe }
{ wall at the evaporator end.}
function RpeF(Dout,tp,Le,kp: real): real;
  begin
    RpeF :=(sqr(Dout/2)*Ln(Dout/Di))/(2*Le*kp);
  end;

{ Function to evaluate the thermal resistance of wick at evaporator.}
function RweF(Dout,tw,Di,Le,kee: real): real;
  var x,y : real;
    begin
     RweF := (sqr(Dout/2)*Ln(Di/Dv))/(2*Le*kee);
    end;
```

```
{ Function to evaluate thermal resistance of vapor.}
function RvF(Dout,Fv,Tv,Le,La,Lc,RHOv,LAMB: real): real;
  var x,y: real;
    begin
      x := pi*sqr(Dout/2)*Fv*Tv*(Le/6 + La + Lc/6);
      y := RHOv*LAMB;
      RvF := x / y;
    end;

{ Function to evaluate thermal resistance of wick at condenser.}
function RwcF(Dout,tw,Di,Lc,kec: real): real;
  begin
    RwcF := (sqr(Dout/2)*Ln(Di/Dv))/(2*Lc*kec);
  end;

{ Function to calculate thermal resistance of pipe wall at condenser.}
function RpcF(Dout,tp,Lc,kp: real): real;
  begin
    RpcF := (sqr(Dout/2)*Ln(Dout/Di))/(2*Lc*kp);
  end;

{ Function to calculate vapor flow area. }
function AvF(Dv: real): real;
  begin
    AvF := pi*sqr(Dv)/4;
  end;

{The following function calculates the frictional coeff. for vapor flow.}
function FvF(RHOv,LAMB,Av,Dv,MUv: real): real;
  var x,y: real;
    begin
      x := 16*MUv;
      y := 2*sqr(Dv/2)*Av*RHOv*LAMB*(sqr(3600)*32.2/144);
      FvF := x/y;
    end;

procedure gwick(var kec,kee: real);      {calculates effective thermal}
                                  {conductivities for grooved wick}
  begin
    clrscr;
```

```
    writeln('      INPUTTED VALUES FOR GROOVED WICK:');
    writeln; writeln;
    write('i)  Groove depth  (inches, metres)         = ');readln(DEL);
    write('ii)  Groove width  (inches, metres)        = ');readln(w1);
    write('iii) Groove fin thickness  (inches, metres)  = ');readln(wf);
    write('iv) Groove half angle (90 for square groove, degrees)  = '); readln(Beta);
    w := w1;
    write('iv) Thermal Conduct.of working fluid (BTU/(ft*hr*F), W/m*K) = ');
        readln(kl);
    write('v)  Thermal conductivity of wick  (BTU/(ft*hr*F), W/m*K) = '); readln(kw);

    if SI=1 then begin            {CONVERSION}
      DEL := DEL*39.37;
      w := w*39.37;
      wf := wf*39.37;
      kl := kl*0.578;
      kw := kw*0.578;
     end;
    kee := keeF(wf,kl,kw,DEL,w);
    kec := kecF(w,kl,wf,kw);
  end;

procedure swick(var kec,kee: real);  {calculates thermal conductivities}
                          {for screen wick}
  begin
    clrscr;
    writeln('      INPUTTED VALUES FOR A WRAPPED SCREEN WICK');
    writeln; writeln;
    write('i)   Wire diameter  (inches, metres)     = ');readln(d);
    write('ii)  Wire mesh pitch  (inches, metres)    = ');readln(p);
    write('iii)  Thermal conduct.of working fluid  (BTU/(hr*ft*F), W/m*K)= ');
    readln(kl);
    write('iv)  Thermal conduct.of wick (BTU/(hr*ft*F), W/m*K) = ');readln(kw);
    write('v)   Thickness of the wick (inches, metres)  = '); readln(tw);

    if SI=1 then begin            {CONVERSION}
      d := d*39.37;
      p := p*39.37;
      kl := kl * 0.578;
      kw := kw * 0.578;
```

```
      tw := tw * 39.37;
    end;
    E := EF(d,p);
    ke := keF(E,kl,kw);
    kec := ke;
    kee := ke;
  end;

{This procedure asks general design parameters needed in the calculations}
procedure prompts(var La,Le,Lc,Dout,Di,Dv,RHOv,LAMB,MUv,kp,Tv,tp: real;  var Np:
integer);
  begin
    clrscr;
    writeln('     SPECIFICATIONS FOR HEAT PIPE');
    writeln; writeln;
    write('(1)  Length of adiabatic section (inches, metres)  = ');readln(La);
    write('(2)  Length of evaporator end    (inches, metres)  = ');readln(Le);
    write('(3)  Length of condenser end     (inches, metres)  = ');readln(Lc);
    write('(4)  Outside diam. of heat pipe (inches, metres )  = ');readln(Dout);
    write('(5)  Inside diameter of heat pipe (inches, metres) = ');readln(Di);
    write('(6)  Diameter of vapor core      (inches, metres)  = ');readln(Dv);
    write('(7)  Pipe wall thickness         (inches, metres)  = ');readln(tp);
    write('(8)  Number of heat pipes in the bank              = ');readln(Np);
    write('(9)  Vapor Density          (lbm/ft^3, kg/m^3)     = ');readln(RHOv);
    write('(10) Latent heat of vaporization (BTU/lbm,J/kg)    = ');readln(LAMB);
    write('(11) Vapor dynamic viscosity (lb/(ft*hr),kg/m3s)   = ');readln(MUv);
    write('(12) Thermal conduct.of pipe mat.(BTU/(ft*hr*F),W/m*K) = ');readln(kp);
    write('(13) Absolute vapor temperature  (degrees R, K)    = ');readln(Tv);

    if SI = 1 then begin     {CONVERSION}
      La := La*39.37;
      Le := Le*39.37;
      Lc := Lc*39.37;
      Dout := Dout* 39.37;
      Di := Di*39.37;
      Dv := Dv*39.37;
      tp := tp*39.37;
      RHOv := RHOv*0.062422;
      LAMB := LAMB*0.0004303;
      MUv := MUv*2421.3;
```

```
      kp := kp*0.578;
      Tv := Tv*5/9;
      writeln;
    end;
  end;

Procedure interfaceh(var h: real);   {Calculates the heat transfer coeff.(h)}
  var Ref,Vfmax : real;
  begin
    write('(1) Density of external fluid (lbm/ft3,kg/m3) = ');readln(RHOf);
    write('(2) Dynamic viscosity ext. fluid (lbm/ft*hr,kg/ms) = ');readln(MUf);
    write('(3) Free stream average veloc. in the duct (ft/s,m/s) = ');readln(Va);
    write('(4) Ratio of duct area to area between pipes      = ');readln(Rat);
    write('(5) Prandtl number for this external fluid        = ');readln(Prf);
    write('(6) Factor for number of tube banks (Table 1)     = ');readln(C);
    write('(7) Thermal conduct. of ext.fluid (BTU/(ft*hr*F),W/m*K)) = ');readln(kf);

    if SI=1 then begin              {CONVERSION}
      RHOf := RHOf*0.062428;
      MUf := MUf*2421.3;
      Va := Va*3.2808;
      kf := kf*0.57782;
    end;
    Vfmax := Va * Rat;
    Ref:= Dout * Vfmax * RHOf / MUf;
    h  := 0.33*C*kf / Dout * exp(0.6*ln(Ref)) * exp(0.33333*ln(Prf));
    write('The heat transfer coefficient at the condenser is: ');
    writeln(h:7:2,' W/m2 C');
  end;

Procedure pickwick(var Uhp: real);   {asks user to choose kind of wick}
                          {and then calls appropriate procedure}
  begin
    clrscr;
    writeln('Now the appropriate wick type must be chosen.');
    writeln('Enter an "S" if a screen wick is appropriate, "G"');
    writeln('if a grooved wick is appropriate.');writeln;
    write('Appropriate wick type is: ');readln(choice);
      case (choice) of
        'S': swick(kee,kec);
```

```
        'G': gwick(kee,kec);
      end;
    prompts(La,Le,Lc,Dout,Di,Dv,RHOv,LAMB,MUv,kp,Tv,tp,Np);

    Av  := AvF(Dv);
    Fv  := 16*Muv/(2*sqr(dv/2)*Av*RHOv*LAMB);
    Rpe := RpeF(Dout,tp,Le,kp);
    Rwe := RweF(Dout,tw,Di,Le,kee);
    Rv  := RvF(Dout,Fv,Tv,Le,La,Lc,RHOv,LAMB);
    Rwc := RwcF(Dout,tw,Di,Lc,kec);
    Rpc := RpcF(Dout,tp,Lc,kp);
    Uhp := 1/(Rpe+Rwe+Rv+Rwc+Rpc);
    writeln;
    writeln('Fv  =  ',Fv:7:2);
    writeln('Rpe =  ',Rpe:9:7);
    writeln('Rwe =  ',Rwe:9:7);
    writeln('Rv  =  ',Rv:9:7);
    writeln('Rwc =  ',Rwc:9:7);
    writeln('Rpc =  ',Rpc:9:7);
    writeln('Uhp =  ',Uhp:7:5);
  end;
Procedure AA(var Q: real);   {this procedure receives specific data}
                             {needed to calculate Q for AA end effect and}
                             {performs first iteration}
  begin
    clrscr;
    writeln('This heat pipe is exposed to end effects of type A ');
    writeln('at both the condenser and evaporator ends.');
    writeln;
    write('i) The temp. of the outside surface @ condenser end is (R,K): ');
    readln(Tpc);
    write('ii) The temp. of the outside surface @ evaporator end is (R,K): ');
    readln(Tpe);

    if SI=1 then begin              {CONVERSION}
      Tpc := Tpc*5/9;
      Tpe := Tpe*5/9;
    end;
    Q := Np*pi*sqr(Dout)*(Tpe - Tpc)*Uhp/(4);   {first iteration}
  end;
```

```
procedure AB(var Q: real);       {this procedure prompts for specific data}
                                 {for calculating Q for AB end effect and}
                                 {performs the first iteration}
  begin
    clrscr;
    writeln('This heat pipe is exposed to end effects of type A at ');
    writeln('the evaporator end and type B at the condenser end.');
    writeln;
    writeln('The interface heat transfer coefficient will now be calculated.');
    writeln('The following input data are required of the condenser end: ');
    writeln;
    interfaceh(h);  writeln;
    writeln('The amount of heat this heat pipe is capable of carrying will be');
    writeln('calculated. This requires the following information of the fluid');
    writeln('in contact at the condenser end: ');  writeln;
    write('(1) Inlet temperature       (degrees F, C)     = ');readln(T1c);
    write('(2) Specific heat          (BTU/(lbm*F), J/kg*K) = ');readln(Cpf);
    write('(3) Mass flow rate through the sink (lbm/hr, kg/s) = ');readln(mc);
    writeln;
    writeln('For the evaporator end : '); writeln;
    write('(4) Temperature of source at evaporator end (F,C) = ');readln(Tpe);

    if SI=1 then begin              {CONVERSION}
      T1c := (T1c+273.15)*5/9-459.67;
      Tpe := (Tpe+273.15)*5/9-459.67;
      mc := mc*7936.6;
      Cpf := Cpf*0.00023886;
    end;
    T2c := T1c + Qa/(Cpf*mc);
    hc  :=h;
    Tpc := Qa/(hc*pi*Dout*Np*Lc)* + (0.5)*(T2c + T1c);
    Q   := pi*Np*sqr(Dout)*Uhp*(Tpe-Tpc)/4;    {first iteration}

  end;

Procedure BA(var Q: real);       {this procedure prompts for data specific}
                                 {for type BA end effect and performs}
                                 {first iteration}
  begin
    clrscr;
```

```
    writeln('This heat pipe is exposed to end effects type B @ evaporator end ');
    writeln('and type A at the condenser end.');
    writeln;
    writeln('The interface heat transfer coefficient will now be calculated.');
    writeln('The following input data are required for the evaporator end:');
    writeln;
    interfaceh(h); writeln;
    writeln('Now the amount of heat that this heat pipe is capable of carrying ');
    writeln('is to be calculated.');
    writeln('This requires the following information for the fluid in contact ');
    writeln('at the evaporator end.');   writeln;
    write('Inlet temperature   (degrees F)       = ');readln(T1e);
    write('Specific heat       (BTU/(lbm*F))     = ');readln(Cpf);
    write('Mass flow rate through source (lbm/hr)  = ');readln(me);  writeln;
    writeln('For the condenser end : ');  writeln;
    write('Temperature of solid sink at the condenser end (F) = ');readln(Tpc);

    he  := h;
    T2e := T1e + Qa/(Cpf*me);
    Tpe := 0.5*(T1e + T2e) - Qa/144*(he*pi*Le*Np*Dout);
    Q   := pi*Np*sqr(Dout)*Uhp*(Tpe-Tpc)/(4);   {first iteration}

  end;

Procedure BB(var Q: real);      {this procedure prompts for specific data}
                        {needed to calculate Q for BB end effect}
                        {and performs first iteration}
  begin
    clrscr;
    writeln('This heat pipe has type B end effects at both ends.'); writeln;
    writeln('The following data are required for the fluid at the evaporator end in');
    writeln('order to calculate the interface heat transfer coefficient. '); writeln;
    interfaceh(h); writeln;
    writeln('Further data are required to calculate the amount of heat that this heat pipe');
    writeln('is capable of carrying.  These also pertain to the contact fluid at the');
    writeln('evaporator end.');   writeln;
    write('Inlet temperature       (degrees F)  = ');readln(T1e);
    write('Specific heat           (BTU/(lbm*F) = ');readln(Cpf);
    write('Mass flow rate of source  (lbm/hr)     = ');readln(me);  writeln;
```

```
    he  := h;
    T2e := T1e + Qa/(Cpf + me);
    Tpe := 0.5*(T1e + T2e) - Qa/(he*pi*Dout*Le*Np) * (144);

    clrscr;
    writeln;writeln;
    writeln('The data pertaining to the condensor end also must be inputted');
    writeln('in order to calculate the heat transfer coefficient');
    writeln('at the condensor end.');writeln;
    interfaceh(h);  writeln;writeln;
    writeln('Additional information regarding the condensor end properties');
    writeln('must also be inputted in order to calculate the heat transfer');
    writeln('possible. (Q)');   writeln;
    writeln('Inlet temperature      (degrees F)   = ');readln(T1c);
    writeln('Specific heat         (BTU/(lbm*F)) =  ');readln(Cpf);
    writeln('Mass flow rate of sink              =  ');readln(mc); writeln;

    hc := h;
    T2c := T1c - Qa/(mc*Cpf);
    Tpc := Qa/(hc*pi*Dout*Lc*Np)*144 + 0.5*(T2c + T1c);
    Q := Np*pi*sqr(Dout)*Uhp*(Tpe-Tpc)/(4);   {first iteration}
  end;

procedure CB(var Q : real); { This procedure will determine the temperatures}
                    { at the evaporator and condenser ends.}
begin
   clrscr;
   writeln('This heatpipe is exposed to end effects of type C at the ');
   writeln('evaporator end and type B at the condenser end.'); writeln;
   writeln('The interface heat transfer coefficient will now be calculated');
   writeln('The following input data are required of the condenser end: ');
   writeln;
   interfaceh(h); writeln;
   writeln('Now, the relevant temperatures will be calculated.');
   writeln('This requires the following information for the condenser end:');
   writeln;
   write('(1) Inlet temperature    (K)     = ');readln(T1c);
   write('(2) Specific heat       (J/kg K)   = ');readln(Cpf);
   write('(3) Mass flow rate through the sink (kg/s)  = ');readln(mc);
   writeln;
```

```
    if SI=1 then begin
      Qa:=Qa/0.29306;
    end;
    T2c := T1c + Qa/(Cpf*mc);
    Tpc := Qa/(h*pi*Dout*Lc*Np) + (T2c + T1c)/2;
    Tpe := Qa/(Np*pi*sqr(Dout)*Uhp) + Tpc;

    write('Pipe temperature at the evaporator is : ');writeln(Tpe:7:2, ' K');
    write('Pipe temperature at the condenser is : ');writeln(Tpc:7:2,' K');
    write('Fluid temp. at the condenser exit is : ');writeln(T2c:7:2,' K');
end;

procedure CA(var Tpe: real);
 begin
  write('Enter temperature of the pipe at the condenser : ');readln(Tpc);
  Tpe:= 4*Q/(Uhp*Np*pi*sqr(Dout)) + Tpc;
  writeln;
  write('The temperature of the pipe at the evaporator is :');writeln(Tpe:7:2,' F');
  writeln;
  writeln('Q  =  ', Q:7:2);
  writeln('Uhp = ', Uhp:7:2);
  writeln('Np  = ', Np:7);
  writeln('Dout  = ',Dout:7:2);
  writeln('Tpc = ', Tpc:7:2);
end;

procedure AAloop(var Q : real);     {performs successive iterations}
 begin
   Q := Np*pi*sqr(Dout)*Uhp*(Tpe-Tpc)/(4*144);
 end;
procedure ABloop(var Q : real);     {performs successive iterations}
 begin
   T2c := T1c + Qa/(mc*Cpf);
   Tpc := Qa/(hc*pi*Dout*Lc*Np) + 0.5*(T2c+T1c);
   Q := Np*pi*sqr(Dout)*Uhp*(Tpe-Tpc)/4;
 end;
procedure BAloop( var Q : real);    {performs successive iterations}
 begin
   T2e := T1e + Qa/(me*Cpf);
   Tpe := 0.5*(T1e+T2e) - Qa/(he*pi*Dout*Le*Np)*144;
```

```
    Q := Np*pi*sqr(Dout)*Uhp*(Tpe-Tpc)/(4*144);
  end;
procedure BBloop( var Q : real);    {performs successive iterations}
  begin
    T2e := T1e + Qa/(me*Cpf);
    Tpe := 0.5*(T1e-T2e) - Qa/(he*pi*Dout*Le*Np)*144;
    T2c := T1c - Qa/(mc*Cpf);
    Tpc := Qa/(hc*pi*Dout*Lc*Np)*144 + 0.5*(T2c+T1c);
    Q := Np*pi*sqr(Dout)*Uhp*(Tpe-Tpc)/(4*144);
  end;
procedure CBloop(var Q: real);
  begin
     clrscr;
     writeln('Now the appropriate wick type must be chosen.');
     writeln('Enter an "S" if a screen wick is appropriate, "G"');
     writeln('if a grooved wick is appropriate.'); writeln;
     write('Appropriate wick type is: ');readln(choice);
       case (choice) of
         'S': swick(kee,kec);
         'G': gwick(kee,kec);
       end;

     write('(9)  Vapor Density                (lbm/ft^3, kg/m^3)     = ');readln(RHOv);
     write('(11)  Vapor dynamic viscosity   (lbm/(ft*hr), kg/m^3*sec)   = '); readln(MUv);
     write('(12)  Thermal conductivity of pipe material (BTU/(ft*hr*F), W/m*K) = ');
     readln(kp);

      if SI=1 then begin
        RHOv:= RHOv*0.062422;
        MUv:= Muv*2421.3;
        kp:= kp*0.578;
      end;
     Av  := AvF(Dv);
     Fv  := 16*MUv/(2*sqr(Dv/24)*Av*RHOv*LAMB*(3600*32.2/144));
     Rpe := RpeF(Dout,tp,Le,kp);
     Rwe := RweF(Dout,tw,Di,Le,kee);
     Rv  := RvF(Dout,Fv,Tv,Le,La,Lc,RHOv,LAMB);
     Rwc := RwcF(Dout,tw,Di,Lc,kec);
     Rpc := RpcF(Dout,tp,Lc,kp);
     Uhp := 1/(Rpe+Rwe+Rv+Rwc+Rpc);
```

```
   CB(Q);
end;

{this procedure will return updated values used in the checks}
procedure overcheck( var Tpwc, Tvc, Tve, Tpwe, Tpe : real);

  var Apipe : real;
  begin
   Apipe := pi*sqr(Dout)/4;
   Tpwc := Tpc + (Q*Rpc)/(Apipe*Np);
   Tvc := Tpwc + (Q*Rwc)/(Apipe*Np);
   Tve := Tvc + (Q*Rv)/(Apipe*Np);
   Tpwe := Tve + (Q*Rwe)/(Apipe*Np);
   Tpe := Tpwe + (Q*Rpe)/(Apipe*Np);
   writeln;
   writeln('Intermediate temperatures are:          (Kelvin)');
   writeln('Temp. of outside wick at condenser   : ', Tpwc:7:2);
   writeln('Temp. of vapour  at condenser   : ', Tvc:7:2);
   writeln('Temp. of vapour  at evaporator  : ', Tve:7:2);
   writeln('Temp. of outside wick at evaporator  : ', Tpwe:7:2);
   writeln('Temp. of pipe at evaporator     : ', Tpe:7:2); writeln;
  end;

procedure checkscr( var Qc : real);   {Gives maximum Q allowed by the capillary}
                          {limitation for a screen wick}
  var rc, Pn, Lt, K, Aw, Fl, Ql : real;
      pl, MUf, si, LAMB2, Pt, g : real;
  begin
    clrscr;
    writeln('Calculation for capillary limitation require additional inputs.');
    writeln;writeln;
    write('working fluid density      lbm/ft^3, kg/m^3)  = ');readln(pl);
    write('working fluid dynamic viscosity (lbm/(ft*hr),Kg/m s) = ');readln(MUf);
    write('surface tension          (lbf/ft, N/m)      = ');readln(o);
    write('angle of heatpipe        (radians)          = ');readln(si);

    if SI=1 then begin              {CONVERSION}
      pl := pl*0.062428;
      MUf := MUf * 2124.3;
      o := o*0.67197;
```

```
    end;
     g := 9.8;
    rc := (p+d)/2;
    Pn := pl*g*Dv*cos(si);
    Lt :=(Le+La+Lc);
    Pt := pl*g*Lt*sin(si);
    writeln;writeln(' sin(si)  =  ',sin(si):7:2);
    K := sqr(d)*E*E*E/(122*sqr(1-E));
    Aw := pi*(sqr(Di)-sqr(Dv))/4;
    Fl := MUf/(K*Aw*pl*LAMB);

    Ql := Np*(2*o/rc - Pn - Pt)/(Fv + Fl);
    Qc := Ql/(0.5*Le + La + 0.5*Lc);
    writeln('rc  ', rc:9:7);
    writeln('Pt  ', Pt:9:7);
    writeln('K  ', K:9:7);
    writeln('Aw  ', Aw:9:7);
    writeln('Ql  ', Ql:9:7);
    writeln('Fl  ', Fl:9:7);
    writeln('Fv  ', Fv:9:7);
    writeln(' o  ', o:9:7);
  end;

procedure checkgroove( var Qc : real);  {Returns the max. Q allowed by
                                {capillary limitation in grooved wick}
  var rc, Pn, Lt, K, Aw, Fl, Ql : real;
     pl, MUf, si, flrel, rm : real;
     ng, rhl, LAMB2 : real;
  begin
    clrscr;
    writeln('The calculation for capillary limitations requires some');
    writeln('additional inputs.'); writeln; writeln;
    write('working fluid density          (lbm/ft^3, kg/m^3)     = ');readln(pl);
    write('working fluid dynamic viscosity (lbm/(ft*hr), N*s/m^2) = ');readln(MUf);
    write('surface tension                (lbf/ft, kg/m)         = ');readln(o);
    write('pipe friction coeff. for flow  (Table 2)              = ');readln(flrel);
    write('angle of heatpipe              (radians)              = ');readln(si);

    if SI=1 then begin                {CONVERSION}
      pl := pl*0.062428;
```

```
    MUf := MUf * 2124.3;
    o := o*0.67197;
  end;

  Lt := (Le + La + Lc);
  rc := w/cos(Beta/57.296);
  rm := (Dv + DEL)/2;
  Pn := 0;
  ng := pi*Dv/(w1 + wf);
  rhl := 2*w*DEL/(w+2*DEL);
  E := ng*w/(2*pi*rm);
  K := 2*E*sqr(rhl)/flrel;
  Aw := pi*(sqr(Di) - sqr(Dv))/4;
  Fl := MUf/(K*Aw*pl*LAMB);

  Ql := Np*(2*o/rc-pl*Lt*sin(si))/(Fl+Fv);
  Qc := Ql/(0.5*Le + La + 0.5*Lc);
  writeln('Di  ', Di:9:7);
  writeln('w  ', w:9:7);
  writeln('wf  ', wf:9:7);
  writeln('rm  ', rm:9:7);
  writeln('pl  ', pl:9:7);
  writeln('MUf  ', MUf:9:7);
  writeln('o  ', o:9:7);
  writeln('ng  ', ng:9:7);
  writeln('rhl  ', rhl:9:7);
  writeln('E  ', E:9:7);
  writeln('K  ', K:9:7);
  writeln('Aw  ', Aw:9:7);
  writeln('DEL  ', DEL:9:7);
  writeln('Fl  ', Fl:9:7);
  writeln('Dv  ', Dv:9:7);
  writeln('Fv  ', Fv:9:7);
  writeln('Ql  ', Ql:9:7);
end;

procedure checkstress(var sigmaP, sigmaEC : real);   {returns stress value}
                                                     {developed in the pipe}
 var  atm, t, Pv,x,y : real;
  begin
```

```
    clrscr;
    writeln('The calculations for the pipe stress limitation require');
    writeln('some additional inputs.'); writeln;writeln;
    write('atmospheric pressure for design (psi, Pa)        = ');readln(atm);
    write('end cap thickness              (inches, metres)  = ');readln(t);
    write('vapour pressure at evaporator temp. (psi, Pa)    = ');readln(Pv);
    write('Please choose type of end cap the design will use.'); writeln;
    writeln('Enter [H]  for hemispherical end cap ');
    writeln('Enter [F]  for flat end cap ');
    readln(endcap); writeln;

    if SI=1 then begin              {CONVERSION}
      atm := atm*0.000145137;
      t := t* 39.37;
      Pv := Pv * 0.000145137;
    end;

    sigmaP := (Pv-atm)*(sqr(Dout) + sqr(Di))/ (sqr(Dout)-sqr(Di));
      if (endcap = 'H')
        then
          begin
            x :=(Pv - atm)*(Dout*Dout*Dout + 2*Di*Di*Di);
            y :=2*(Dout*Dout*Dout-Di*Di*Di);
            sigmaEC := x/y;
          end
        else sigmaEC := (Pv-atm)*sqr(Dout)/(8*sqr(t));
  end;

procedure checklam(var Mv,Rev:real); {procedure will determine if flow}
                                     {in pipe is laminar}
  begin
    clrscr;
    writeln(' INPUTS REQUIRED TO CHECK FOR LAMINAR FLOW '); writeln;
        writeln;
    write('i)  The vapor specific heat ratio is          : ');readln(yv);
    write('ii) The molecular weight of the vapor is (amu) : ');readln(M);

    Rvs := R / M;
    Tv := (Tvc + Tve) / 2;
```

```
    Rev  := 4*Q / (pi*Dv*MUv*LAMB*Np);
    Mv   := Q / (Av*RHOv*LAMB*Np * sqrt(yv*Rvs*Tv) );
  end;

Procedure soniclimits(var Qsmax: real);   {will return the maximum Q}
                              {allowed by sonic limitations}
  begin
    clrscr;
    Qsmax := Av*RHOv*LAMB*sqrt( (yv*Rvs*Tve) / (2*(yv+1)) );
  end;

procedure endeffect(var Q : real);  {chooses end types and assigns}
                          {appropriate solving procedures}
   begin
    writeln;
    writeln('There are three possible end effects.  These being ');
    writeln('types A, B and C.');  writeln;
    writeln('The first letter signifies evaporator end type.');
    writeln('The second letter signifies condensor end type.');
    writeln;
    writeln('          [1]     type AA');
    writeln('          [2]     type AB');
    writeln('          [3]     type BA');
    writeln('          [4]     type BB');
    writeln('          [5]     type CB');
    writeln('          [6]     type CA');
    writeln;
    writeln('Please choose the corresponding number to the end effects');
    writeln('specific to your application.   ');
    readln(endvalue);

      case (endvalue) of
         1: AA(Q);
         2: AB(Q);
         3: BA(Q);
         4: BB(Q);
         5: CB(Q);
         6: CA(Tpe);
      end;
end;
```

```
procedure entrainmentlimit(var Qc: real);  {Returns maximum Q allowed by }
                                {Entrainment Limitation}
   var rhs : real;
 begin
   clrscr;
   if SI=1 then begin                {CONVERSION}
     o := o * 0.67197;
   end;
    case (choice) of
      'S' :  rhs := (p-d)/2;
      'G' :  rhs := w;
    end;
       Qc := Av*LAMB*sqrt((o*RHOv)/(2*rhs));

     writeln(' Av  ', Av:9:7);
     writeln(' LAMB  ', LAMB:9:7);
     writeln(' o  ', o:9:7);
     writeln(' RHOv  ', RHOv:9:7);
     writeln(' rhs  ', rhs:9:7);
 end;

procedure boilcheck( var Qc: real);  {will return maximum Q allowed by}
                              {boiling limitation}
   var rn, rc, x, y : real;
   begin
    clrscr;

   if SI=1 then begin                {CONVERSION}
     o := o * 0.67197;
   end;
    rn := 0.000000254;
     case (choice) of
       'S' : rc := (p+d)/2;
       'G' : rc := w;
     end;

    x := 2*pi*Le*kee*Tv*2*o*(1/rn -1/rc);
    y := LAMB*RHOv*ln(Di/Dv);
    Qc := x/y;
   end;
```

```
begin      {main program}
clrscr;
writeln('This program will calculate the heat tranfer rate (Q)');
writeln('of a specified heat pipe.'); writeln;
writeln('This program will allow you to input the heat pipe characteristics');
writeln('in both Imperial and Metric forms.');
writeln('Please indicate whether you wish to use :');
writeln;
writeln('          Imperial (enter 1) ');
writeln('          Metric   (enter 0) '); readln(SI);
writeln;
write('What is the original estimate for Q (in BTU/hr, Watts) ? ');readln(Q);
Qa := Q;

pickwick(Uhp);     {will choose between groove and screen}
endeffect(Q);      {will return a value for Q}
Qb := Q;

writeln('These are the values calculated for Q, T2c, Tpc. ');
writeln;
writeln('  Q (BTU/hr)   T2c (~F)     Tpc (~F)     Tpe (~F)');
writeln('    (Watts)      (°C)         (°C)         (°C)');
n := 0;

repeat       {iteration loop}
     n := n + 1;
     if SI=1 then begin
       Qb := Qb *  0.29306;
     end;
     writeln(Qb:10:2,'   : ', T2c:6:2,'     : ', Tpc:6:2,'     : ', Tpe:6:2);

     Qa := Qa + 0.1*(Qb-Qa);   {a better approximation for Q}
     Q := Qa;
     if endvalue = 1 then n :=50;
     if endvalue = 2 then ABloop(Q);
     if endvalue = 3 then BAloop(Q);
     if endvalue = 4 then BBloop(Q);
     if endvalue = 5 then n := 50;
     if endvalue = 6 then n := 50;
     Qb := Q;
```

```
until  n = 50;
overcheck(Tpwc,Tvc,Tve,Tpwe,Tpe);
Tv:= (Tvc+Tve)/2;
writeln;
writeln('Vapour Temperature (Tv) has been updated to ',Tv:7:2,' F');writeln;
writeln('Do you want to perform full procedure using new Tv (Y/N) ? ');readln(flag);

 if flag = 'Y' then CBloop(Q);

{The following code calls up the check procedures to determine if heatpipe}
{can carry the above calculated heat transfer rate}

Qc := 0;
writeln('Hit any key to continue');readln;
writeln;writeln('Some factors limit the performance of the heat pipe.');
writeln('These factors shall be accounted for now.');

overcheck(Tpwc, Tvc, Tve, Tpwe, Tpe);
status := 'P';

case (choice) of
  'S' : checkscr(Qc);
  'G' : checkgroove(Qc);
end;
writeln;
writeln('Capillary action limits the heat tranfer rate to  ',Qc:7:2,' Watts');
 if (Qc > Qb)
    then writeln('The design satisfies this limitation.')
    else
      begin
        writeln('The design does not satisfy this condition.');
        status := 'F';
      end;
    readln;

checklam(Mv, Rev);
writeln; writeln('The Reynolds number associated with this design is ',Rev);
if (Rev < 2300)
  then writeln('The flow is laminar and this limitation does not apply.')
  else
```

```
    begin
      writeln;
      writeln('The flow is turbulent therefore the design does not satisfy');
      writeln('the laminar condition.');writeln;
      status := 'F';
    end;
writeln;
writeln('The Mach no. associated with this design is ',Mv);
if (Mv < 0.2)
  then begin writeln('The flow is not sonic therefore the design satisfies this');
         writeln('limitation.');
       end
  else
    begin
      writeln('The design does not satisfy the Mach no. limitation.');
      status := 'F';
    end;
    readln;

soniclimits(Qsmax);
writeln;
writeln('The heat transfer rate is limitted by sonic effects to ',Qsmax:7:2, ' Watts');
if (Qb < Qsmax)
  then writeln('The design is within sonic limitations.')
  else
    begin
      writeln('The design does not satisfy sonic limitations.');
      status := 'F';
    end;
writeln;
readln;

checkstress(sigmaP, sigmaEC);
writeln;
writeln('Stesses placed on pipe and end cap cannot exceed 1/4 of ultimate stress.');
writeln;
writeln('The stress experienced at the pipe walls is ',sigmaP:7:2, ' psi');
writeln('The stress experienced at the end cap is ',sigmaEC:7:2, ' psi');writeln;
if (sigmaP < 7500)
   then writeln('The design satisfies this criteria for the pipe wall.')
```

```
    else
     begin
       writeln('The design does not satisfy this criteria for the pipe wall.');
       status := 'F';
     end;
writeln;
if (sigmaEC < 7500)
    then writeln('The design satisfies this criteria for the end cap.')
    else
     begin
       writeln('The design does not satisfy this criteria for the end cap.');
       status := 'F';
     end;writeln;
     readln;

entrainmentlimit(Qc);
writeln('The heat transfer rate is limited by entrainment of the fluid ');
writeln('in the vapour to  ',Qc:7:2,' Watts'); writeln;
if (Qc > Qb)
  then writeln('The design satisfies the entrainment limitation.')
  else
   begin
     writeln('The design is limitted  by the entrainment condition.');
     status := 'F';
   end;
writeln;
readln;

boilcheck(Qc);
writeln('The heat tranfer rate is limitted by boiling of the fluid to ',Qc,' Watts');
writeln;
if (Qc > Qb)
  then writeln('The design satisfies the boiling limitation.')
  else
   begin
     writeln('The design does not satisfy the boiling limitation.');
     status := 'F';
   end;writeln;
writeln;
readln;
```

```
writeln('The limitations have now all been accounted for.');writeln;
if (status = 'F')
   then writeln('-----The heatpipe has FAILED to comply with limitations.-----')
   else writeln('-----The heatpipe will perform within limitations.-----');
writeln; write('Press enter to end program.');readln;

end. {main program}
```